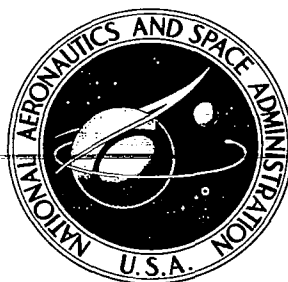


**NASA CONTRACTOR  
REPORT**



**NASA CR-7**

0061150

TECH LIBRARY KAFB, NM

**NASA CR-2064**

LOAN COPY: RETURN TO  
AFWL (DOUL)  
KIRTLAND AFB, N. M.

**INTEGRATION OF  
NASA-SPONSORED STUDIES  
ON ALUMINUM WELDING**

*by Koichi Masubuchi*

*Prepared by*  
MASSACHUSETTS INSTITUTE OF TECHNOLOGY  
Cambridge, Mass.  
*for George C. Marshall Space Flight Center*

NATIONAL AERONAUTICS AND SPACE ADMINISTRATION • WASHINGTON, D. C. • JUNE 1972



0061150

## TECHNICAL REP

1. REPORT NO. NASA CR-2064		2. GOVERNMENT ACCESSION NO.		3. RECIPIENT'S CATALOG NO.	
4. TITLE AND SUBTITLE INTEGRATION OF NASA-SPONSORED STUDIES ON ALUMINUM WELDING				5. REPORT DATE June 1972	
				6. PERFORMING ORGANIZATION CODE	
7. AUTHOR(S) Koichi Masubuchi				8. PERFORMING ORGANIZATION REPORT #	
9. PERFORMING ORGANIZATION NAME AND ADDRESS Massachusetts Institute of Technology Dept. of Ocean Engineering Cambridge, Massachusetts				10. WORK UNIT, NO.	
				11. CONTRACT OR GRANT NO. NAS 8-24364	
12. SPONSORING AGENCY NAME AND ADDRESS National Aeronautics and Space Administration Washington, D. C. 20546				13. TYPE OF REPORT & PERIOD COVERED Low Series Contractor Report	
				14. SPONSORING AGENCY CODE	
15. SUPPLEMENTARY NOTES					
16. ABSTRACT    Gas tungsten-arc and gas metal-arc processes are used extensively in the fabrication of huge fuel and oxidizer tanks of the Saturn V spacecraft used in the Apollo lunar missions. The building of these tanks has raised problems related to welding of high-strength, heat-treated aluminum alloys and have revealed a need for basic research leading to the development of new techniques; both of which will be of benefit to the general industry.  This is the second edition of the report of a study to integrate results obtained in nineteen individual studies sponsored by NASA on welding aluminum. Subjects covered include: Effects of porosity on weld-joint performance Sources of porosity Weld thermal effects Residual stresses and distortion Manufacturing process system control.					
17. KEY WORDS Welding Aluminum Alloys Porosity Thermal Effects			18. DISTRIBUTION STATEMENT		
19. SECURITY CLASSIF. (of this report) Unclassified		20. SECURITY CLASSIF. (of this page) Unclassified		21. NO. OF PAGES 322	
				22. PRICE \$6.00	



## FOREWORD

This report is the documentation of the results of a program to analyze and integrate data generated from NASA-sponsored studies on welding aluminum alloys, especially 2014 and 2219 alloys. Earlier work on this was published as NASA CR-61261, from George C. Marshall Space Flight Center, Marshall Space Flight Center, Alabama 35812. The earlier work was funded under a Department of Army grant, DA-01-021-AMC-14693(Z). The present work was performed under NAS 8-24364 contract.





## TABLE OF CONTENTS

	<u>Page</u>
CHAPTER 1 Introduction	1-1
CHAPTER 2 Welding Fabrication of Fuel and Oxidizer Tanks of Saturn V	2-1
2.1 Saturn V and It's Fuel and Oxidizer Tanks	2-1
2.2 Selection of Materials for Fuel and Oxidizer Tanks	2-3
Brief History Prior to Saturn V	2-3
Alloy 2219 for Saturn S1-C	2-4
Alloy 2014 for Second and Third Stages	2-6
Characteristics of 2014 and 2219 Alloys	2-6
2.3 Welding Fabrication	2-9
Welding Techniques	2-9
Requirements for Welds	2-11
Weld Defects, Especially Porosity	2-11
Jigging	2-14
Requirements for Joint Mismatch	2-17
CHAPTER 3 Welding Problems and Research Efforts	3-1
3.1 NASA-Sponsored Studies on Welding Aluminum	3-1
3.2 Welding Problems and Outline of NASA-Sponsored Studies	3-7
Porosity	3-7
Thermal Effects	3-7
Materials and Welding Processes Studied	3-11

	<u>Page</u>
CHAPTER 4    Effects of Porosity on Weld-Joint Performance	4-1
4.1    General Discussions on the Effects of Weld Defects on the Performance of Welded Structures	4-1
Stress Concentrations around Defects	4-2
Ductile Fracture	4-5
Unstable Brittle Fracture	4-8
4.2    Porosity Effects on Weld-Joint Performance under Static Loading	4-11
Results of Some Experiments Similar to NASA Studies	4-11
Research Procedures of the Martin Study	4-13
Experimental Results	4-16
Analysis and Evaluation of the Martin Study on Porosity Effects on Weld Strength	4-21
4.3    Porosity Effects on Fatigue Strength	4-25
4.4    Effect of Repair Welds	4-28
CHAPTER 5    Weld Porosity, Its Sources and Control	5-1
5.1    Mechanisms of Porosity	5-2
Role of Hydrogen	5-2
Effects of Shielding Gas Dewpoint and Welding Parameters on Porosity	5-4
Nucleation and Growth of Porosity	5-6
5.2    Shielding-Gas Contamination	5-10
The Boeing Study on Effects of Individual Gas Contaminants	5-11
5.3    Surface Contamination	5-17
Characteristics of Surface of Practical Joints	5-17
Surface Adsorption	5-20

	<u>Page</u>
Surface Topography	5-23
Procedures of the IITRI Study	5-27
Results of the IITRI Study	5-32
5.4 Composition of Base Plate and Filler Metal	5-47
5.5 Methods for Controlling and Eliminating Porosity	5-50
Surface Hydrogen Analysis	5-50
Tack Welds As a Source of Surface Contamination	5-63
Surface Preparation	5-68
Monitoring Shielding Gas Purity	5-75
Other Possible Means	5-88
CHAPTER 6 Weld Thermal Effects	
6.1 Time-Temperature Effect	6-3
Strength vs Welding Energy	6-10
6.2 Welding with High Density Power Sources	6-11
Experiments to Increase GTA Power Density	6-11
Electron Beam Welding	6-16
Nonvacuum Electron Beam Welding	6-19
Plasma Electron Beam Welding	6-22
6.3 Time-Temperature Control by Cryogenic Cooling	6-26
Experimental Procedures	6-26
Experimental Results	6-28
CHAPTER 7 Residual Stresses and Distortion	7-1
7.1 Analysis of Thermal Stresses during Welding	7-2
Technical Background on Analysis and Control of Weld Distortion	7-2
Development of Techniques for Analyzing Thermal Stresses and Metal Movement	7-6

	<u>Page</u>
Examples of Analytical Results	7-11
Effects of Welding Parameters	7-15
Effects of Material Properties on Residual Stress Distributions	7-23
Experimental Investigation	7-27
7.2 Reduction of Warpage and Residual Stresses by Controlling Thermal Pattern during Welding	7-33
Background and Phases of Study	7-33
Analytical Study	7-34
Experimental Work	7-34
Typical Thermal Patterns	7-37
Experimental Results	7-43
Discussion of Results	7-46
7.3 Development of Nondestructive Methods for Determining Residual Stresses	7-48
Ultrasonic Stress Measuring Techniques	7-49
Investigation on Welded Plates	7-54
Application Technique Considerations	7-58
Detection of Fatigue Damage	7-61
Summary	7-62
CHAPTER 8 Manufacturing Process System Control	8-1
8.1 Transferability of Welding Parameters	8-2
Phases and Experimental Design	8-3
Welding Test Procedure	8-6
Welding Parameter Control Development	8-7
Statistical Analysis of Effects on Welding Parameters on Weld Qualities	8-11
Analysis and Evaluation of the Lockheed Study on Transferability of Setup Parameters	8-20

	<u>Page</u>
8.2 Development of Welding Process Control Systems	8-26
Prevention of Porosity by Monitoring Shielding-Gas Purity and Surface Cleanliness	8-26
Computer Simulation of Welding Processes to Predict Thermal Effects	8-27
CHAPTER 9 Summary and Practical Recommendations	9-1
REFERENCES	10-1

## CHAPTER 1

### Introduction

Space exploration is not accomplished by wishful thinking and intense desire alone. Artifacts, tools, and transportation vehicles are brought about by scientific and technological activity. As in other escapades of curiosity, man derives by-products of knowledge in technology that are beneficial in respect to peaceful coexistence and biosocial well-being. The welding techniques and equipment that are used to produce space vehicles of high structural reliability can also be used to make better and more economical products, necessary in our more mundane existence.

During the fabrication of the Saturn V space vehicles used for the Apollo lunar missions, an extensive research program on aluminum welding was conducted by the Welding Development Branch in the Manufacturing Engineering Laboratory of the G. C. Marshall Space Flight Center, NASA. As a part of the program, a study was conducted at the Massachusetts Institute of Technology under Contract No. NAS 8-24364 to integrate NASA-sponsored studies on aluminum welding.

Results discussed in these reports are associated with welding fabrication of the Saturn V. However, they should be applicable to the welding of aluminum alloys used in future space vehicles and aerospace structures. Basic principles described here can be also applicable to structures in non-space industries.

Although this report is concerned with the welding of aluminum structures, it is important to understand that this is only one phase of the fabrication of a complex structure such as the Saturn V space vehicle, and must eventually be related to a much greater whole. The Saturn V requires a very

complex system of design and fabrication composed of many phases. These phases include design, material selection, stress analysis, cutting, machining, forming, joining, and inspection. Each phase is closely related to and dependent upon the others. For example, the material selection must be made not only on the basis of mechanical properties but also with regard to forming and joining the material. The design must be made so that a structure with sufficient reliability can be fabricated with a tolerable dimensional accuracy. There are also many factors within each phase of design and fabrication. For example, the quality of a weld depends upon such factors as the cleanliness of the metal surface, purity of the shielding gas, and the welding conditions. To improve the structural reliability of a space vehicle, we must know more about each phase, the relationship of factors within it, the relationship of any one phase to other phases, and ultimately, the importance of each phase to the final product. With this knowledge, time and money can be spent most effectively to improve the product.

Welding has been used extensively in the fabrication of the Saturn V space vehicles. NASA has selected high-strength aluminum alloys, primarily 2014 and 2219, as the major structural materials for the huge fuel and oxidizer tanks. Gas tungsten-arc (GTA) and gas metal-arc (GMA) processes have been used for fabricating these tanks. However, fusion welding of high-strength heat-treated aluminum alloys presents the following reliability problems:

- 1) The possibility of obtaining defects in welds
- 2) Undesirable thermal effects due to welding heat

Aluminum alloys are subject to certain types of weld defects, especially porosity. Every attempt should be made to minimize porosity, but it has become especially important because of the limited effectiveness of presently available



inspection techniques. Among various nondestructive inspection techniques, visual and X-ray (and sometimes ultrasonic) inspections are used to examine structural welds. However, none of these techniques is completely satisfactory. The usefulness of visual inspection is limited. X-ray inspection is usually two-dimensional, and three-dimensional distributions of defects are not determined.

The intense heat generated by the welding arc causes various undesirable thermal effects. Metallurgical structures of the weld metal and the heat-affected zone differ from those of the original base metal. A welded joint is composed of many zones with different structures and mechanical properties. It is known that the ultimate tensile strength of a welded joint in high-strength heat-treated aluminum alloy decreases with increasing heat input, that is, the amount of heat energy supplied per inch of weld length. Welding heat also causes residual stresses and distortion. Because there is no reliable nondestructive technique to determine the strength of a welded structure, it is essential to control the manufacturing process so that the fluctuation in behavior of welded structures can be minimized and limited to a certain range.

The ultimate purpose of the NASA welding research program is to improve the performance and reliability of space vehicles. This can be done by investigating each of the problems involved and then determining how best to utilize the information obtained. Results obtained in some of the investigations may be contradictory; for example, a welding process using a certain set of parameters found to be very effective in reducing porosity may be undesirable because of large thermal effects. It is important, therefore, to integrate results obtained in the individual investigations. Such integration of data will provide a basis of recommendations for design and fabrication of space vehicles.

The welding process is a dynamic whole, an entirety. It is a series of interrelated, interdependent events. We are not able to minutely analyze the dynamic whole, but must arbitrarily select restricted areas for study, which might be considered fragments of the map of welding. The studies listed herein are such fragments which collectively represent a major portion of welding technology. The time comes, however, when the fragments must be integrated and the whole map constructed, if we are to understand welding and if we are to formulate process control. The present report is a first step in the integration of individual, independent studies.

Process control is the final objective: quantitative limits of the major variables which can be expressed in manufacturing specifications. Such specifications will supplement inspection in the assurance of weld-joint reliability.

## CHAPTER 2

### Welding Fabrication of Fuel and Oxidizer Tanks of Saturn V

#### 2.1 Saturn V and It's Fuel and Oxidizer Tanks

Figure 2-1 is a simple illustration of the Saturn V. It stands 363 feet high with its Apollo spacecraft in place, and its maximum diameter is 33 feet. (1,2)

The first stage, which is called S-IC, is powered by five F-1 engines. The five engines, which burn kerosene and liquid oxygen at the rate of 15 tons per second for about 2 1/2 minutes, boost the Apollo astronauts to an altitude of 40 miles.

The second stage, S-II, is powered by five J-2 engines, which burn liquid hydrogen and liquid oxygen. The third stage, S-IVB, is powered by a single J-2 engine. The third stage accelerates the spacecraft to the velocity needed to overcome the earth's gravity.

As far as the weight is concerned, the Saturn V may be considered as an assembly of huge fuel and oxidizer tanks. The Saturn V filled with fuel and liquid oxygen weighs about 2,700 tons, while its emptied weight is only 170 tons.

The G. C. Marshall Space Flight Center was responsible for the overall design and fabrication of the Saturn V, and many contractors have participated in the fabrication of different components. The Boeing Aircraft Company, North American Rockwell Corporation, and McDonnell Douglas Aircraft Company, have built the first, second, and third stages, respectively.

Because of the gigantic task of the lunar mission and the involvement of astronauts, every effort was made to build the spacecraft with maximum reliability and minimum weight.

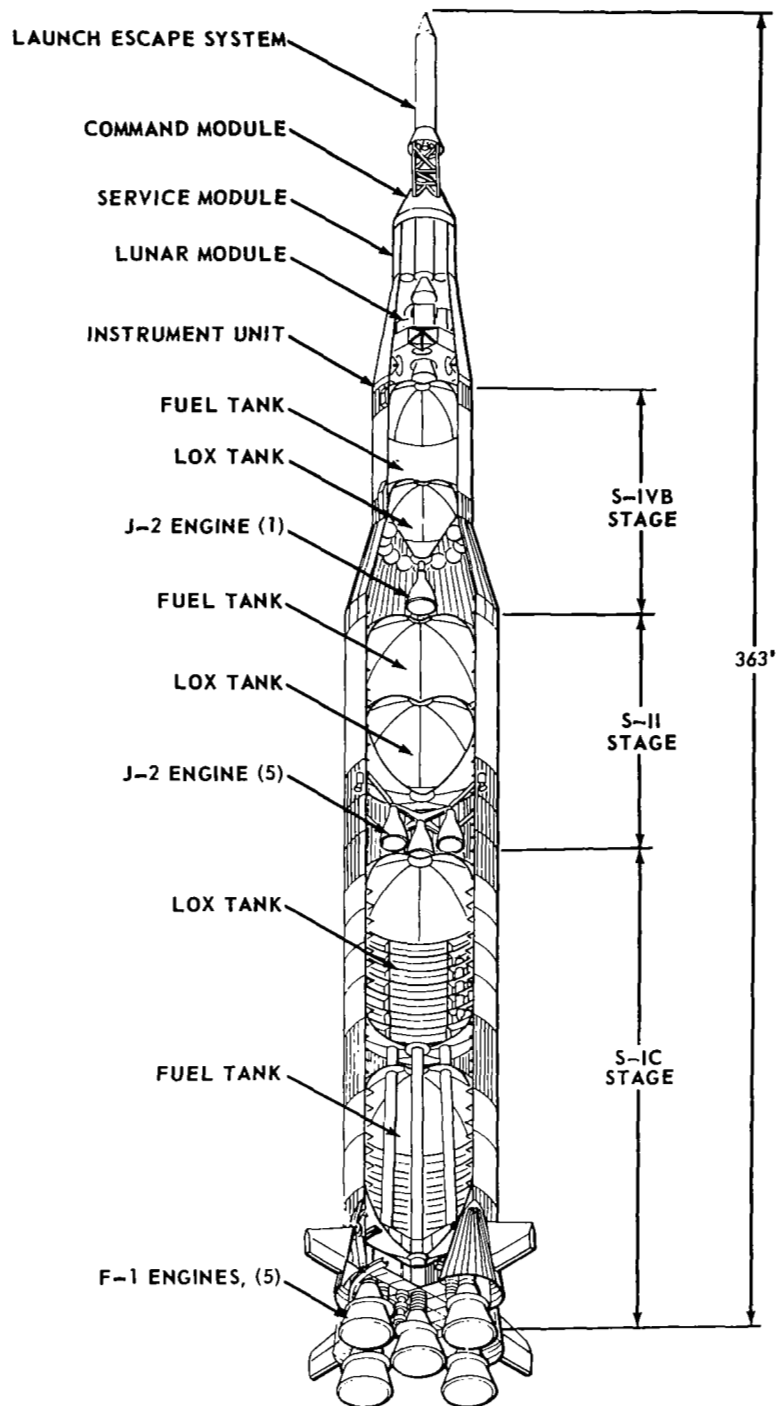


Figure 2-1. Saturn V Space Vehicle

## 2.2 Selection of Materials for Fuel and Oxidizer Tanks

NASA has selected high-strength aluminum alloys 2014 and 2219 as primary structural alloys for fuel and oxidizer tanks because of their attractive strength-to-weight ratios in the range of temperatures to be encountered. <sup>(3)</sup>

### Brief History Prior to Saturn V

The use of aluminum alloys in the Saturn V vehicles evolved from long term usage in Redstone, Jupiter, and Saturn I vehicles. A report by Hasemeyer <sup>(4)</sup> covers the history of the use of aluminum alloys in various space vehicles, which is summarized in the following pages.

An aluminum alloy similar to 5052 was used by the Germans in their World War II missiles, because of its low density, good strength at room temperature, and excellent strength at the temperature of liquid oxygen.

The U. S. Army (predecessor of MSFC) used alloy 5052 in the 70" diameter Redstone missile. Tanks were welded into short cylinders and then joined into full-length containers. Ring stiffeners were 6061-T6 aluminum and were resistance welded to the inside of the tanks. For the 105" diameter Jupiter missile, the U. S. Army used alloy 5086 and 5456 in work hardened tempers. These alloys were higher strength than 5052 and were easily welded. When the Saturn I vehicle was constructed by NASA, tooling and fabrication procedures were simplified by clustering eight Redstone missiles around one Jupiter. The same materials and welding techniques were used here as on the individual Redstone and Jupiter missiles.

When the Saturn V was to be fabricated, several changes from the Redstone and Jupiter were found to be necessary. The first and second stages were designed to be 33' in diameter.

The aluminum walls for a portion of the S-IC first stage were almost one inch thick. Re-evaluation of the alloys to be used was required because of the considerable increase in thickness over the 1/4" 5456 in the Saturn I.

#### Alloy 2219 for Saturn SI-C<sup>(4)</sup>

A test program to compare certain properties of alloys 5456-H343 and 2219-T87 was conducted at MSFC to select the material most suitable for the major structure of the Saturn SI-C launch vehicle. The Boeing Company proposal for the SI-C considered 2219 as the major structural alloy. After an intensive study, NASA decided to use 2219 alloy for the Saturn SI-C.

The choice of a structural alloy for the SI-C vehicle was based on several factors. A summary of these considerations is presented in Table 2-1.

It was determined that the length of welds necessary for the 2219 material would be approximately 300 feet less than for 5456 due to the availability of 2219 in greater plate widths. Approximately 3,000 lbs. of weight could be saved in the propellant tanks by the use of 2219 over 5456.

Alloy 2219 has a decided advantage where mating structural components, such as extrusions, tubing and forgings are concerned. These forms can be obtained in the same alloy, whereas they could not be with the 5456; thus, dissimilar welds would not be necessary with 2219. No 2219 castings were to be used in the SI-C structure.

An additional consideration in favor of 2219 is the elevated temperature properties of the alloy. The alloy was developed originally as a high temperature alloy and has the best elevated temperature properties of any aluminum alloy above the 400° F range.

TABLE 2-1. SUMMARY COMPARISON OF 5456-H343 AND 2219-T87

2219-T87				5456-H343		
MECHANICAL PROPERTIES	U.T.S.(KSI)	Y.S.(KSI)	ELON.(%)	U.T.S.(KSI)	Y.S.(KSI)	ELON.(%)
PARENT METAL – GUARANTEED MINIMUM	64.0	52.0	–	53.0	41.0	–
– TYPICAL ROOM TEMP.	68.0	56.3	12.0	56.1	44.4	10.2
– LOX TEMP.	84.6	68.2	16.3	72.1	52.3	13.9
WELD – TIG/MIG – ROOM TEMP.	43.1/41.4	26.7/26.1	4.3/3.6	41.6/39.1	26.3/25.6	6.5/4.5
– LOX TEMP.	58.5/55.7	30.8/31.9	4.9/4.0	51.1/46.3	31.0/30.5	5.5/4.9
PARENT METAL NOTCHED / UNNOTCHED			1.03/0.92		0.95/0.85	
TENSILE STRENGTH RATIO ROOM TEMP. / LOX						
OTHER CONSIDERATIONS						
LENGTH OF WELD (FT.)	~ 2500			~ 2800		
VEHICLE WT. BASED ON 100% 5456-H343	98 (3000 LB. SAVING)			100		
SIZE AND QUALITY	132" WIDE			84" WIDE		

Alloy 2219 has been successfully used by MSFC and Boeing Company in fabricating the 33 ft diameter Saturn V. Its weldability has been proven, plates can be provided in sizes up to 132 inches wide and mechanical strength and other properties are well known.

Alloy 2219 also has been used for the 120-inch Multiple Docking Adapter for the Skylab vehicle and it is favorably considered by MSFC for the Space Shuttle.

#### Alloy 2014 for the Second and Third Stages<sup>(4)</sup>

When materials were to be selected for the second and third stages of the Saturn V, the favorable experience by the two contractors involved weighed heavily in favor of alloy 2014. This alloy had been used by Douglas for the Thor missile. Also Martin-Denver had successfully used alloy 2014 in the Titan missile. There were certain advantages in processing 2014 vs 2219. Alloy 2014 can be softened by quenching in water, formed as desired, then aged to the T6 temper. For its strength in the T87 temper, alloy 2219 relies on 8 to 10% cold work. If solution heat treatment were performed by the customer, the original T87 strength would be lost. As a result alloy 2014 was selected and successfully used for the second and third stages of the Saturn V. Differences in welding of 2219 and 2014 did not prove to be greatly different. In this report, most comments on welding of 2219 can be accepted as also applying to 2014.

#### Characteristics of 2014 and 2219 Alloys

Tables 2-2 and 2-3 list some characteristics of 2014 and 2219 aluminum alloys, respectively.<sup>(5)</sup>



TABLE 2-2. CHARACTERISTICS OF 2014 ALUMINUM ALLOY (5)

Type	Wrought, heat treatable aluminum alloy	
Nominal Composition	Al-4.4Cu-0.8Mn-0.8Si-0.4Mg	
Availability	Bare and clad sheet and plate, rod, bar, wire, tube, extruded shapes, forgings and forging stock	
Typical physical properties	Density	2.815 g/cm <sup>3</sup> at RT
	Thermal conductivity	0.46 cal/cm sec °C (O temper) 0.37 cal/cm sec °C (T6 temper)
	Thermal expansion	(20-100°C, 22.5 × 10 <sup>-6</sup> in/in/°C
	Specific heat	0.23 cal/g cm at 100°C
	Electrical resistivity	3.45 μ ohm-cm at RT (O temper) 4.31 μ ohm-cm at RT (T6 temper)
Typical mechanical properties	Ultimate tensile strength	27,000 psi (O temper) 70,000 psi (T6 temper)
	0.2% tensile yield strength	14,000 psi (O temper) 60,000 psi (T6 temper)
	Elongation (2-in)	18% (O temper) 13% (T6 temper)
	Modulus of elasticity (tension)	10.6 × 10 <sup>6</sup> psi
Fabrication characteristics	Weldability	Good (fusion and resistance methods) if proper procedures are used
	Formability	Good in the annealed condition difficult to form in T6 temper
	Machinability	Good in the T6 temper
Comments	A high-strength aluminum alloy which is often used for heavy-duty structures	

TABLE 2-3. CHARACTERISTICS OF 2219 ALUMINUM ALLOY (5)

Type	Wrought, heat treatable aluminum alloy	
Nominal Composition	Al-6.3Cu-0.3Mn-0.18Zr-0.1V-0.06Ti	
Availability	Bare and clad sheet, plate, forgings, extrusions, drawn tube, rod and bar	
Typical physical properties	Density	2.82 g/cm <sup>3</sup> at RT
	Thermal conductivity	0.41 cal/cm sec °C (O temper) 0.30 cal/cm sec °C (T62 temper)
	Thermal expansion	(20-100°C), 22.3 in/in/°C
	Electrical resistivity	3.90 μ ohm-cm at RT (O temper) 5.23 μ ohm-cm at RT (T62 temper)
Typical mechanical properties	Ultimate tensile strength	25,000 psi (O temper) 69,000 psi (T87 temper)
	0.2% tensile yield strength	11,000 psi (O temper) 57,000 psi (T87 temper)
	Elongation (2-in)	18% (O temper) 10% (T87 temper)
	Modulus of elasticity	10.6 × 10 <sup>6</sup> psi
Fabrication characteristics	Weldability	Excellent (fusion and resistance methods)
	Formability	Slightly superior to 2014 alloy
	Machinability	Good in annealed condition
Comments	Alloy has good mechanical properties at cryogenic temperatures and at elevated temperatures up to 600°F. Recommended for applications requiring high-strength weldments.	

## 2.3 Welding Fabrication (6,7)

Because of the gigantic size of the Saturn V many of the major structural components need to be fabricated by joining smaller parts or segments. Gas tungsten-arc (GTA) and gas metal-arc (GMA) processes have been used extensively for the fabrication of fuel and oxidizer tanks. For example, one S-IC vehicle has over 3,000 feet of welds.

It became necessary to erect the fuel and oxidizer tanks with the longitudinal axis in the vertical position. Welding techniques had to be extended to horizontal and vertical modes, seldom used in high quality aluminum welding. The size of Saturn V has created unique jiggling and distortion control problems.

### Welding Techniques

Joint thicknesses of fuel and oxidizer tanks range from 1/8 to 1 inch. Welding was done with gas tungsten-arc and gas metal-arc processes using helium and argon respectively as the shielding gases. Type 4043 and 2319 filler wires 1/16 inch in diameter were used for welding 2014-T6 and 2219-T87 bare plate, respectively.

Tanks were constructed by attaching skin cylinders to upper and lower head assemblies by means of a Y-shaped transition ring. The unit serves as a transition piece between bulkheads and skins and between the thrust structure and forward skirt. This design is illustrated in Figure 2-2.

Welding between the transition ring and cylindrical section is probably the most critical on the S-IC stage. Three vertical joints are automatically gas metal-arc welded to join three forged and rolled billets. During final assembly of the tanks, the transition ring is joined to the cylindrical section by a gas metal-arc or gas tungsten-arc weld made from both sides in the horizontal position.

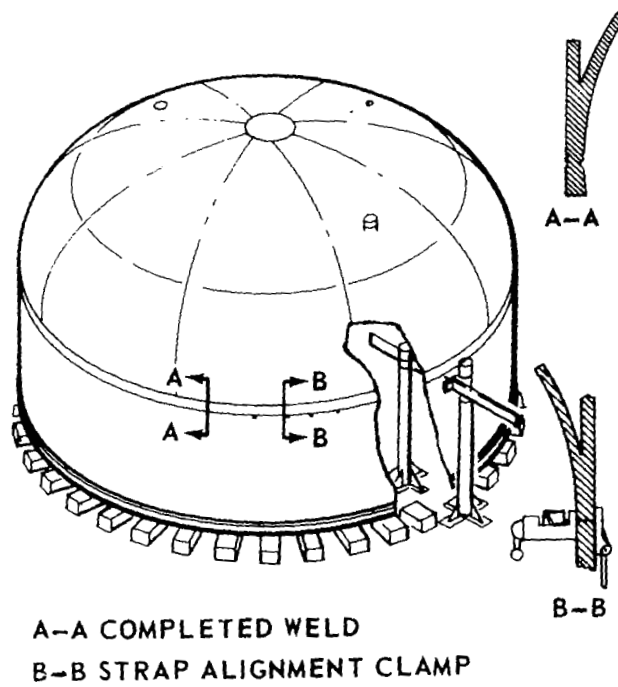


Figure 2-2. Welding of the Transition Ring

## Requirements for Welds

Table 2-4 summarizes important quality requirements for welds in aluminum oxidizer and fuel tanks of the Saturn V.

Minimum ultimate tensile strengths of butt welds were set to be 35,000 psi for alloy 2219-T87 and 38,000 psi for alloy 2014-T6.

All butt welds were 100% inspected radiographically with 2% sensitivity. Table 2-4 includes acceptable criteria for cracks (none accepted), single pore, incomplete penetration, undercutting, linear porosity, and scattered porosity.

Table 2-4 also includes criteria for dimensional and visual qualities. The maximum acceptable misalignment or offset was 5% of the plate thickness. Lack of fill, skips, or other visible irregularities are unacceptable.

## Weld Defects, Especially Porosity

If flaws are detected, and unfortunately they often were, repairs are made either manually or by mechanized equipment. Table 2-5 shows defect frequency observed in 144,000 inches of welds made on four Saturn V first stages. If defects were dispersed equally, only 0.023 of a defect would have occurred per inch of weld. Of these defects, porosity accounted for 79 percent of the total number of defects. Cracks ranked second at 9 percent. All welds containing defects were repaired.

The table clearly shows that weld porosity is one of the major problems which have faced engineers in the fabrication of the spacecraft. High-strength aluminum alloys are highly susceptible to weld porosity, and hydrogen has been considered to be a prime source of weld porosity.

TABLE 2-4. SUMMARY OF WELD QUALITY REQUIREMENTS FOR SATURN V.

---

1. Minimum Ultimate Tensile Strength of Butt Welds

Alloy 2219-T87	35,000 psi
Alloy 2014-T6	38,000 psi

2. Radiographic Quality (100% Inspection with 2% film sensitivity)

Cracks (transverse, longitudinal, or crater): None acceptable

Single pore size: 1/2 thickness (maximum)

Incomplete penetration: Not acceptable

Undercutting: 1/10 thickness (maximum)

Linear porosity: Acceptable limits, average diameters between  
3/64" and 1/16" maximum within 3 linear inches  
of weld (thickness over 0.250")

Scattered porosity: Reference radiographs

3. Dimensional and Visual Qualities

Misalignment or offset: 1/20 thickness (maximum)

Lack of fill, skips, or other visible irregularities: Unacceptable

---

TABLE 2-5. DEFECT FREQUENCY.

<u>Type of Defect</u>	<u>Number of Defects</u>	<u>Percentage of Total</u>
Arc burn	5	0.15%
Underfill	15	0.46%
Inclusion	46	1.40%
Miscellaneous	117	3.57%
Mismatch	206	6.28%
Crack	287	8.75%
Porosity	2604	79.40%

Total Defects = 3280

$\frac{\text{Total Defects}}{\text{Inches of Weld}} = .023$

Several of NASA-sponsored studies listed in Table 1 are aimed at studying various subjects related to weld porosity.

### Jigging

Figure 2-3 shows a jigging system most often used for the fabrication of a thin-walled cylindrical vessel. The jig, which has a round-cut ring and rigid clamping members, serves a two-fold purpose: to support the molten weld puddle (often to control solidification), and to forcefully maintain alignment of the parts being welded.

However, there is a limit to the size of welded tank to which this conventional approach can be applied easily and economically. The sizes of fuel and oxidizer tanks of the Saturn V were obviously greater than the limit. Since the number of Saturn V space vehicles to be built was rather small, it was not economically justifiable to build a large and strong clamping system. The fixture in Figure 2-3 is an indirect way of mating components, that is, the cylinders are first forced into roundness. The requirements for welding, however, are that the two parts assume similar shape.

NASA and aerospace companies employed what is called a soft jigging system. Although we do not discuss in this paper the details of the system actually used, it is essentially as shown in Figure 2-4. A number of strap clamps are applied at intervals around two cylinders to be joined.

A simple compressive mechanical device, with the two basic parts located on opposite sides of a welded joint, is drawn together by tightening the thin band until the work pieces are aligned. Alignment is maintained during welding by tack welds, made before removing the strap clamps. The combination of strap-clamps, tack welds, and precision weld



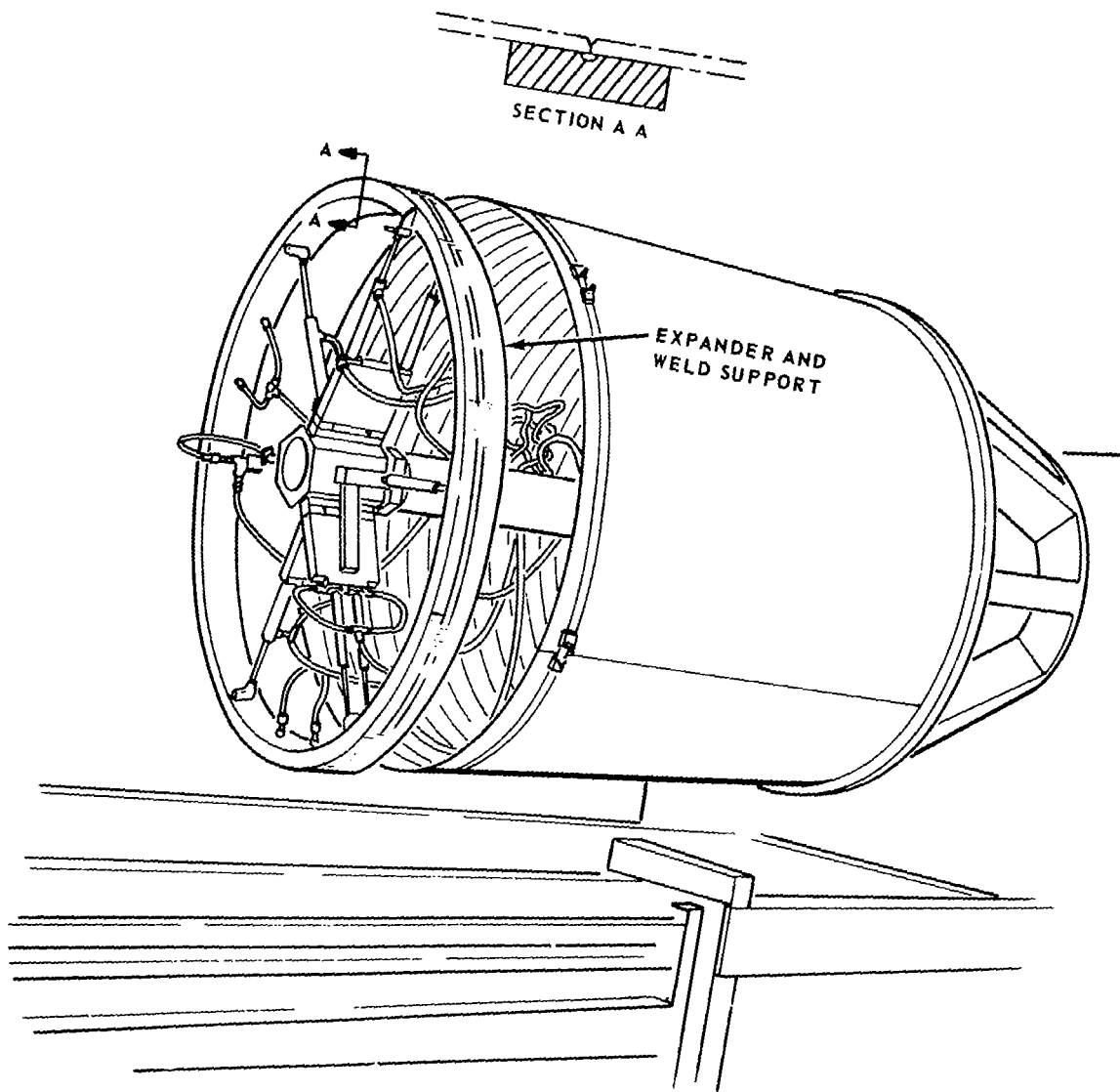


Figure 2-3. Conventional weld-jigging.

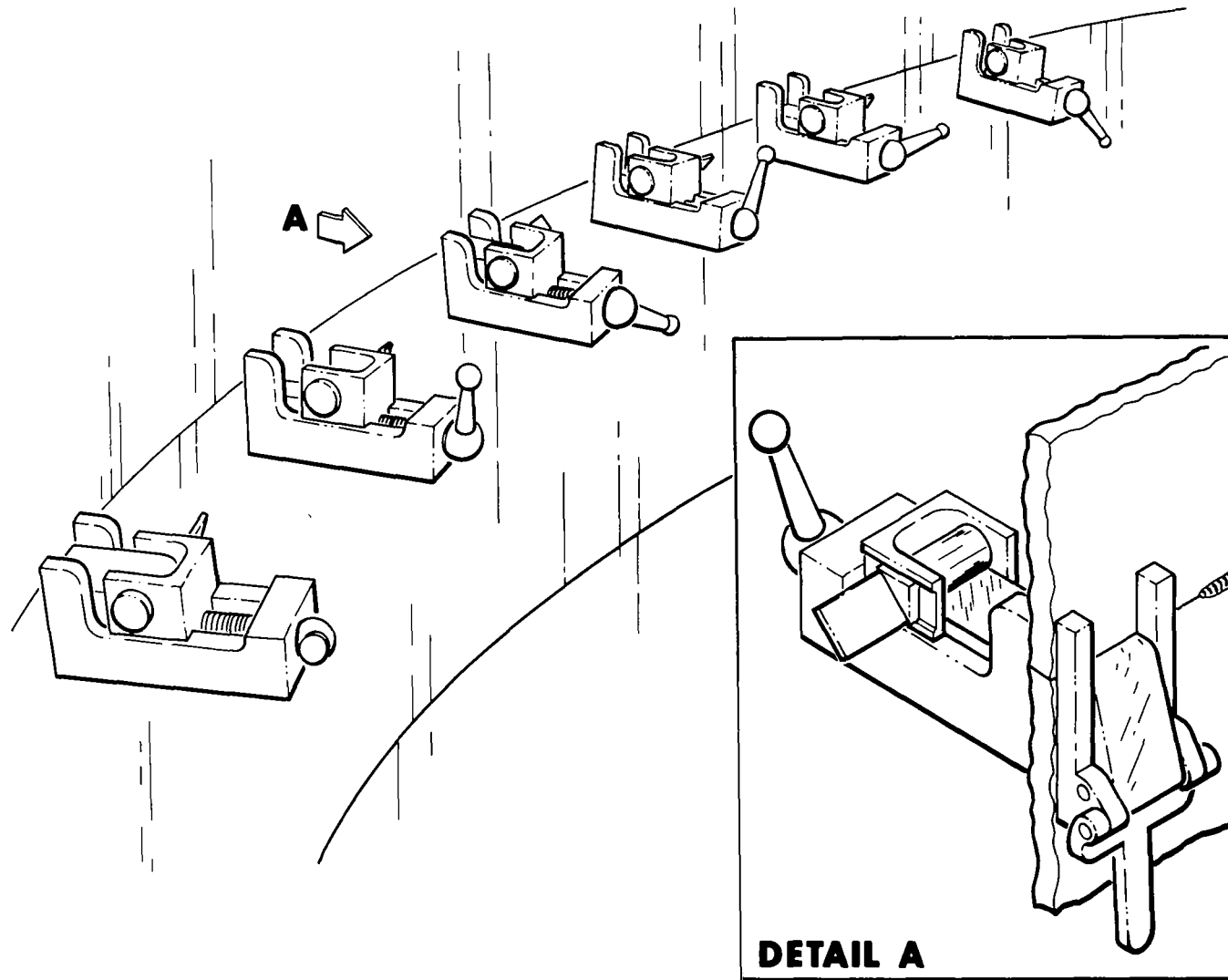


Figure 2-4. Strap Clamps.

equipment constitutes a joining method that is economical, versatile, and accurate.

#### Requirements for Joint Mismatch

The following is an example of requirements for joint offset. When welding is performed in stationary rigid type tooling, utilizing continuous length hold-down clamps and backup bars, the offset between parts of a butt joint shall not exceed 0.020 inch or 10 percent of the thinnest member for a 3 inch length to each side of that area subsequently to become a butt intersection.



## CHAPTER 3

### Welding Problems and Research Efforts

#### 3.1 NASA-Sponsored Studies on Welding Aluminum

Although the Saturn V has performed successfully during recent lunar missions, it does not mean that there were no problems in the fabrication of the spacecraft. The building of spacecraft structures has raised problems relating to the quality of welds and the reliability of the structure. Major problems include:

- 1) Weld defects, especially porosity
- 2) Undesirable thermal effects due to welding heat.

To minimize the effect of these problems, a group of process control measures were developed and used during fabrication. These measures cover the cleaning of the surfaces of base metal and filler wire, chemical compositions of base metal and filler wire, and purity of the shielding gas, jiggling and fixture, etc.

These problems also revealed a need for basic research to rationally establish weld-quality requirements and production-control measures. The Marshall Space Flight Center initiated a research program involving a wide variety of studies on welding aluminum. Some studies were conducted at M.S.F.C., while other studies were conducted for the M.S.F.C. by aerospace companies, research institutions, and universities.

Each study attacked a different aspect of or took a different approach to these problems. Different tasks were assigned to different organizations by contract, as shown in Table 3-1.

The ultimate purpose of NASA welding research is to improve the performance and reliability of space vehicles. This can be done by investigating each of the problems involved and then integrating results obtained in the individual investigations. Such integration of results provides a basis for recommendations for design and fabrication of space vehicles.

Battelle Memorial Institute, Columbus Laboratories, was assigned the task of integrating the results of the nine studies listed in Part 1 of Table 3-1. Dr. Koichi Masubuchi, who was then at Battelle, was responsible for the integration study. The final report of the Battelle integration study has been published from the Redstone Scientific Information Center as RSIC-670.<sup>(5)</sup> The RSIC-670 covers results included in reports available before February 15, 1967. These reports are listed as References (8) through (19).

The continuation of the integration study has been conducted since May, 1969, at the Massachusetts Institute of Technology under the supervision of Professor Koichi Masubuchi of the Department of Naval Architecture and Marine Engineering. The M.I.T. integration study covers all of the 19 studies listed in Parts 1 and 2 of Table 3-1. Final reports of these studies are listed as References (8) through (30).

TABLE 3-1. NASA-SPONSORED STUDIES OF WELDING ALUMINUM

Part 1 Studies Covered in the First Integration Study

No.	Title	Contractor	Objective
1	Gas Analysis Study	Boeing Aircraft Company	To study the role of gas contaminants as a source of defects in welds.
2	Base and Filler Metal Study	Battelle Memorial Institute Columbus Laboratories	To study effects of chemistry, internal and external impurities, and hydrogen content of base metal on porosity in welds.
3	Mechanisms of Porosity	McDonnell Douglas Aircraft Company	An effort to find methods of porosity arrest and inhibition through a study of how porosity nucleates and grows.
4	Gas Scavenger Study	Southern Research Institute	A study seeking an element with affinity for porosity-forming gases that would tie them up in a harmless way or wash them out of the molten pool.
5	Defect vs Joint Performance	Martin Marietta Company	To formulate realistic weld quality standards by quantitatively analyzing the effect of defects on weld strength.

TABLE 3-1. (Continued)

## Part 1 Studies Covered in the First Integration Study

No.	Title	Contractor	Objective
6	Time-Temperature Control	Harvey Aluminum, Inc.	To formulate methods of producing and controlling time-temperature gradients during fusion welding that will yield optimum properties, that is, ultimate strength, elongation, X-ray quality, etc.
7	Data Transfer	Lockheed Company	To (1) arrange welding variables in order of their importance and (2) devise instrumentation and control to accurately transfer the findings from laboratory to production.
8	Arc Shapes and Molten Puddle Stirrer	Air Reduction Company	To increase power density of the GTA arc and agitation of the molten puddle.
9	Material Preparation	Illinois Institute of Technology Research Institute	To (1) identify contaminants on the surface of material to be welded, that is, organic material, hydrogen, etc., (2) determine the best methods of surface preparation for welding.



TABLE 3-1. (Continued)

## Part 2 Studies Added in the Second Integration Study

No.	Title	Contractor	Objective
10	Welding Power Supply Output Wave Shape Effect on Weld Joint Performance	Air Reduction Company	To study effects of AC, DC, and a combination of AC and DC, and various wave shapes and frequencies on the weld joint.
11	Nonvacuum Electron- Beam Welding	Westinghouse Electric Corporation	Analysis of welding parameters, energy input, and shielding gas with defect level and mechanical properties as major responses.
12	Surface Cleaning	Illinois Institute of Technology Research Institute	To establish the significance of material preparation and surface property effects on porosity.
13	Reduction of Distortion by Cryogenic Cooling	Harvey Aluminum, Inc.	To determine feasibility of using cryogenic cooling for controlling distortion and residual stress.
14	Power Density Study	Lockheed Palo Alto Research Laboratory	To analyze and characterize the gas-tungsten arc and perform experiments to in- crease GTA power density.

TABLE 3-1. (Continued)

## Part 2 Studies Added in the Second Integration Study

No.	Title	Contractor	Objective
15	Plasma Welding	General Electric Company	To study feasibility of developing a miniaturized, battery powered plasma electron beam system for use in an earth orbiting vehicle.
16	Residual Stress Study	Benson Associates	To develop non-destructive methods for determining residual stresses and fatigue damage in metals.
17	Gas Shielding	Boeing Aircraft Company	To quantitatively define porosity and weld quality resulting from variations in joint and torch configuration.
18	Analysis of Thermal Stress and Metal Movement, I	Battelle Memorial Institute Columbus Laboratories	(1) Literature survey on thermal stresses during welding and buckling after welding, and (2) develop computer programs to calculate thermal stresses during welding.
19	Analysis of Thermal Stress and Metal Movement, II	Massachusetts Institute of Technology	To (1) improve computer programs developed at Battelle, and (2) compare experimental results with analytical results.

## 3.2 Welding Problems and Outline of NASA-Sponsored Studies

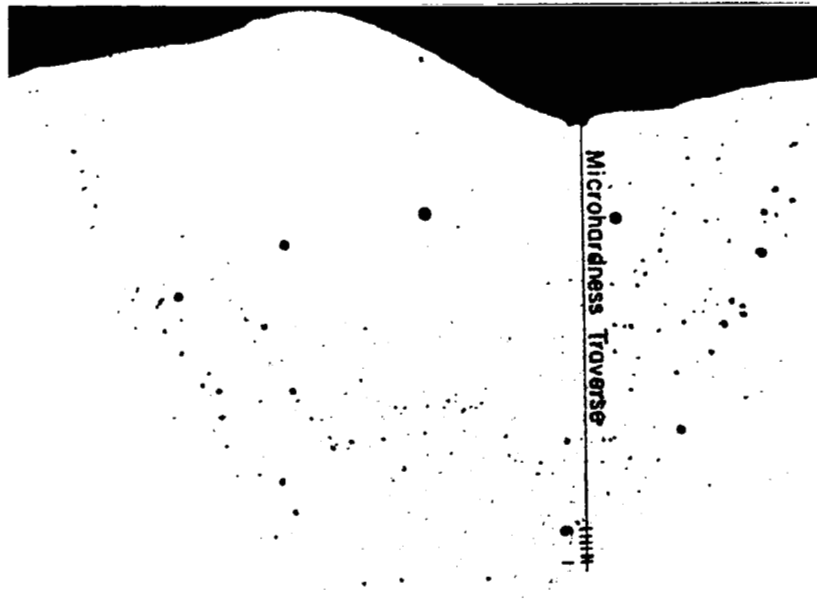
### Porosity

High-strength aluminum alloys are highly susceptible to weld porosity, which adversely affects their strength.

Figure 3-1 illustrates the porosity that may develop in an aluminum weld. Figure 3-1a shows a transverse section through a bead-on-plate weld and Figure 3-1b shows a longitudinal section through the same weld. Although various non-destructive techniques including visual, X-ray, and sometimes ultrasonic are used to detect porosity in structural welds, none of these techniques are entirely satisfactory. Because porosity cannot always be detected, it is necessary to be completely certain that the welding process is not creating it. This means finding the factors in the welding process that affect porosity and then finding ways of modifying these factors to reduce or eliminate porosity. Studies to accomplish these ends comprised a large part of the NASA research effort. Factors studied for their effect on porosity included shielding gas, surface conditions, base-metal and filler-metal composition, and welding parameters. Other studies investigated ways of reducing the effects of these factors.

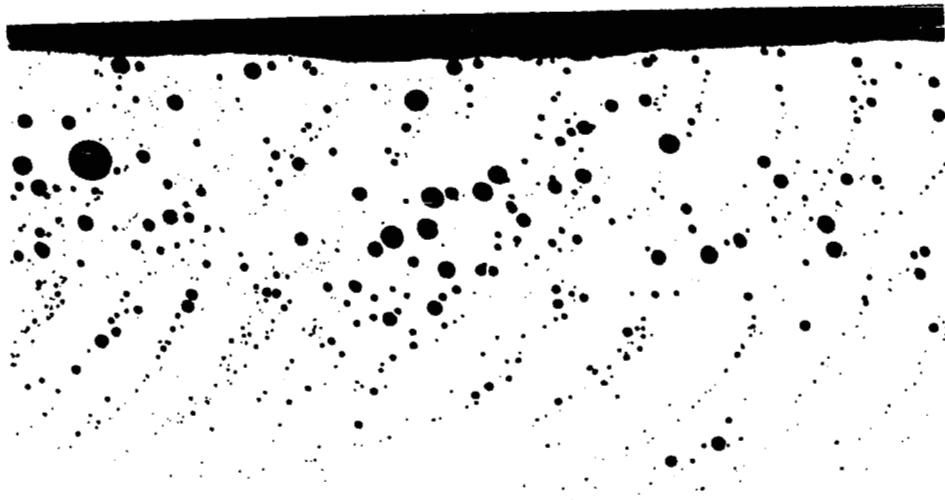
### Thermal Effects

The Manufacturing Engineering Laboratory of MSFC conducted a research program on the effects of welding heat input on the mechanical properties of aluminum welds.<sup>(31)</sup> Figure 3-2 summarizes the test results and shows the relationship between the following two variables:



20X

Transverse Section



20X

Longitudinal Section

Figure 3-1. Illustration of porosity in an aluminum weld (3).

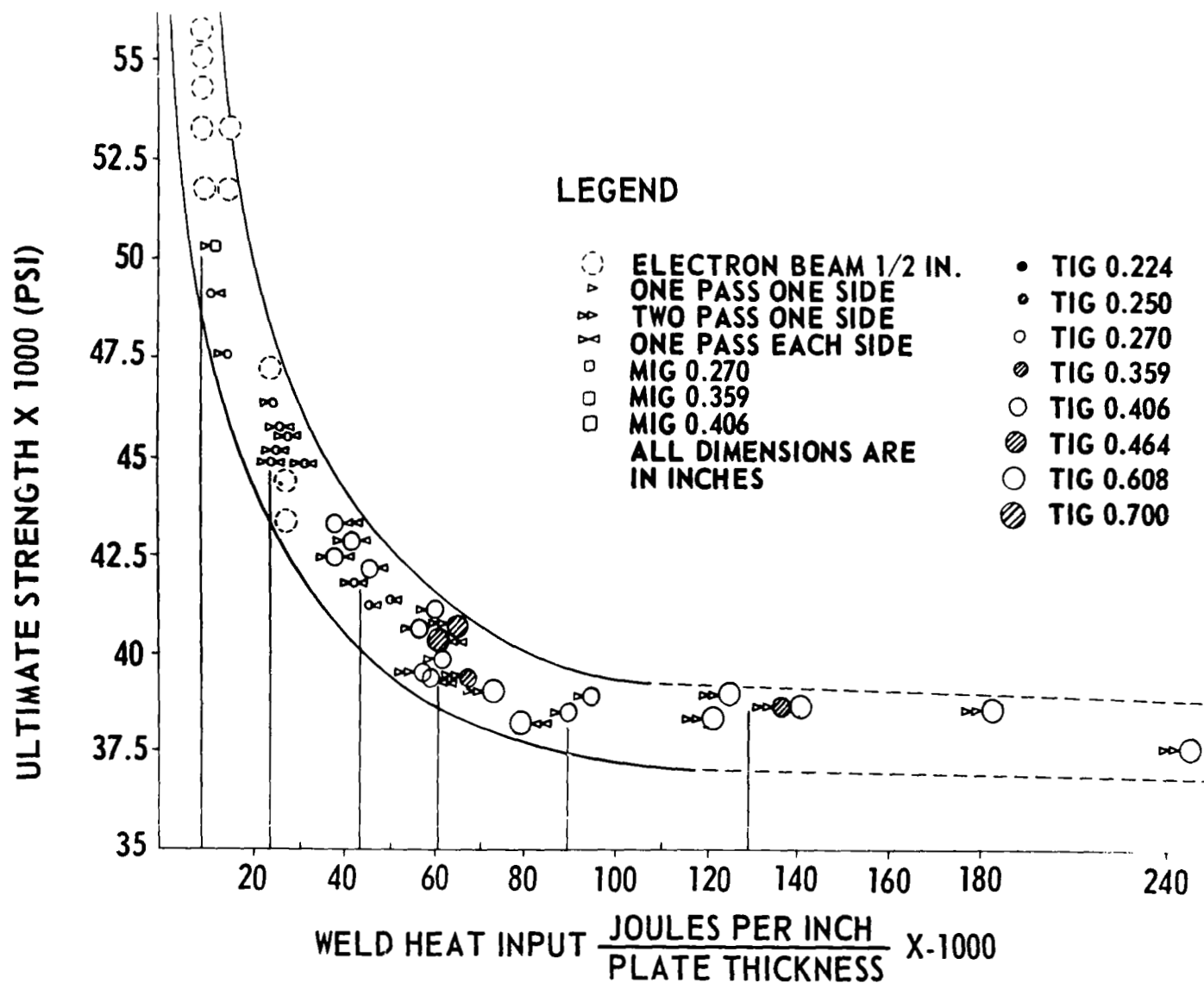


Figure 3-2. Effects of welding heat input on the ultimate tensile strength of transverse weld specimens of 2219-T87 and T81 aluminum alloys.

(1) Welding heat input per unit plate thickness

$$\frac{V \times I \times 60}{s \times T} = \text{joules/in}^2$$

when:

V = arc voltage, v

I = welding current, amp

s = arc travel speed, ipm

T = plate thickness, in.

- (2) Ultimate tensile strength of transverse weld specimens prepared from weldments in 2219-T81 and 2219-T87 alloys 0.224 to 0.700 in. thick made by the GTA, GMA, and electron-beam welding processes.

Figure 3-2 indicates that higher weld strengths were obtained by using lower heat input. This held true regardless of the material thickness or welding process used. The Marshall investigators felt this was caused by (1) a reduced thermal effect, and (2) the favorable geometry of a narrow weld. When heat input is reduced, a higher-strength metallurgical structure in the heat-affected zone results. A joint with a heat-affected zone that has lower strength than the base metal, but with a very narrow weld-metal area, can still have nearly the same ultimate tensile strength as the base metal. This is because surrounding base metal restricts plastic deformation in the weld metal and the heat-affected zone. NASA is conducting further research to determine the mechanisms by which weld-joint strength increases as heat input decreases.

MSFC has also conducted a limited investigation on electron-beam welding as a means of improving weld strength. Satisfactory electron-beam welds in aluminum alloys require much lower heat input than do GMA and GTA welds. Consequently,

much higher ultimate strengths are attainable. However, since electron-beam welds must be made in a vacuum, the process is restricted to small components. Westinghouse Electric Corporation conducted a NASA program to develop a nonvacuum electron-beam-welding unit capable of penetrating 1-inch thick 2219 aluminum alloy, which would make the process versatile as well as efficient.

The effect of welding heat on residual stresses and distortion is another important problem. Distortion and mismatch have plagued the fabrication of Saturn V fuel and oxidizer tanks. (See Table 3-1)

### Materials and Welding Processes Studied

The primary materials and processes used in the NASA-sponsored studies were:

- (1) Base Plate: 2014-T6 and 2219-T87 supplied by NASA-MSFC
- (2) Plate Thickness: 1/4, 1/2, and 3/4 inch
- (3) Welding Process: GTA processes, D-C, straight polarity
- (4) Filler Wire (when used): 4043 for welding 2014-T6 and 2319 for welding 2219-T87; 1/16 inch in diameter
- (5) Shielding Gas: helium.





## CHAPTER 4

### Effects of Porosity on Weld-Joint Performance

Considerable efforts were made to determine effects of weld porosity on weld-joint performance. The major efforts were placed on porosity effects on static strength, while limited studies were made on fatigue strength. Discussions in this chapter covers:

- (1) General discussion on the effects of weld defects on the performance of welded structures
- (2) Porosity effects on weld-joint performance under static loading
- (3) Porosity effects on fatigue strength
- (4) Effects of repair welds.

#### 4.1 General Discussions on the Effects of Weld Defects on the Performance of Welded Structures

Weld defects such as porosity, slag inclusions, incomplete penetration, and cracks cause reduction in mechanical properties of welded joints for two reasons. First, the presence of the defects causes decreases in sectional areas. Second, stress concentrations take place around the defects. The extent to which weld defects affect the strength of structures depends upon the following factors:

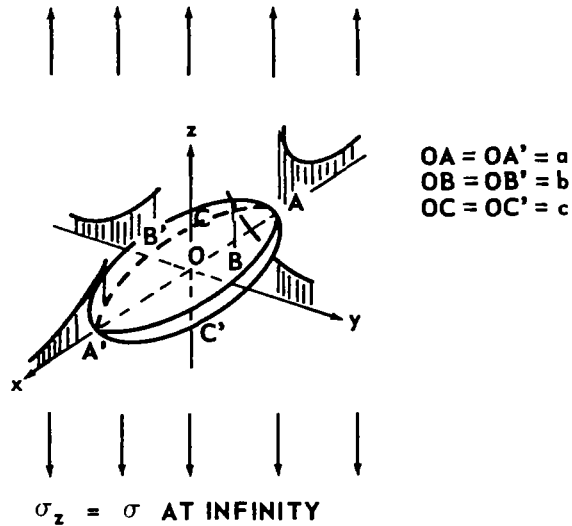
- 1) Nature and extent of defects. Sharp cracks that cause severe stress concentrations have more significant effects than do porosity or slag inclusions which cause rather minor stress concentrations. The effect of the defects on the strength becomes more severe as the size and number of defects increase.

- 2) Properties of the material. The properties of a material are significant factors that determine the effects of weld defects on the strength of welded structures. When a material is ductile, the reduction of strength is approximately proportional to the reduction of cross-sectional area, as described later. For less ductile materials, the effects of defects become more serious. When the material is brittle, the absolute size of a defect is important. When the defect size exceeds the critical size, unstable fracture can take place from the defect.
- 3) Type of loading. When the structure is subjected to impact or repeated loading, the effects of defects on the strength become more serious than when the structure is subjected to static loading.

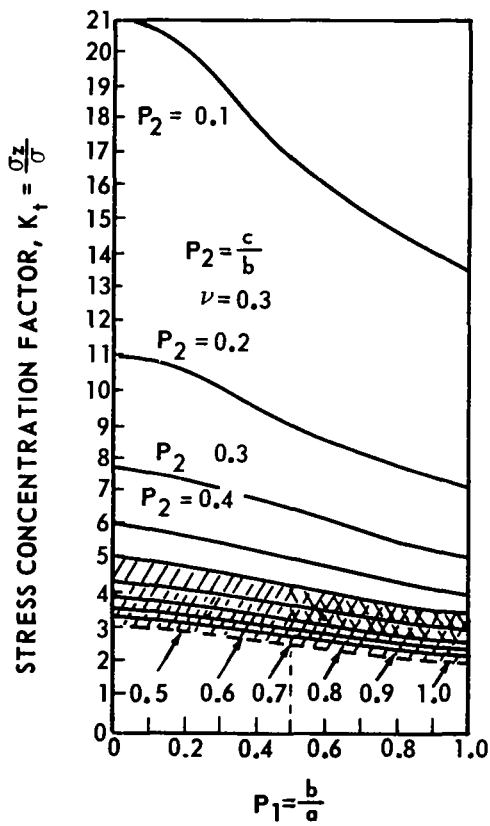
#### Stress Concentrations Around Defects

The shape of a defect and its orientation to the direction of loading significantly affect stress concentrations around the defect. (32,33)

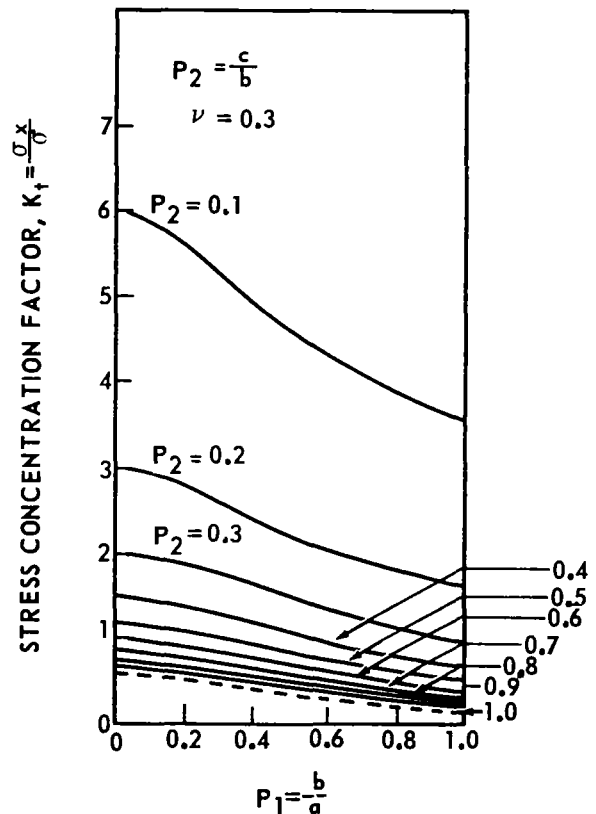
Figure 4-1a, b, and c show stress distributions around a general tri-axial, ellipsoidal cavity in a homogeneous, isotropic, elastic body of infinite length which is under a uniform tensile stress,  $\sigma$ , at infinity. It is assumed that the stress at infinity is acting parallel to one of the major axes of the cavity (z-axis), as shown in Figure 4-1a. The important stress concentrations occur along the "equator" ABA'B'A. The curves in Figure 4-1a show how rapidly the tensile stresses drop to the average value  $\sigma$  within the material.



a. ELLIPSOIDAL CAVITY IN AN INFINITE BODY UNDER UNIAXIAL TENSILE STRESS



b.  $\sigma_z$  AT POINT B



c.  $\sigma_x$  AT POINT B

Figure 4-1. Stress concentrations around an ellipsoidal cavity in an infinite body under uniaxial tensile stress.

The severity of stress concentration is expressed frequently in terms of the stress-concentration factor,  $K_t$ , which is defined as the ratio of the stress at a point concerned and the stress at infinity,  $\sigma$ . Figures 4-1b and 4-1c show values of  $\frac{\sigma_z}{\sigma}$  and  $\frac{\sigma_x}{\sigma}$  ( $\sigma_y = 0$  at Point B) as a function of the shape ratios  $\rho_1 = b/a$  and  $\rho_2 = c/b$ .<sup>(33)</sup> The value of Poisson's ratio is assumed to be 0.3.

The curves for  $\rho_2 = 1$  apply to cavity in the shape of a prolate spheroid (cigar-shaped cavity). The limiting case of  $\rho_1 = 0$ ,  $\rho_2 = 1$  can be interpreted geometrically in two ways. If  $b$  is fixed and approaches infinity, the shape of the cavity approaches that of a circular cylinder of infinite length; if  $a$  is fixed and  $b$  and  $c$  approach zero, the cavity approaches a line crack. The curves for  $\rho_1 = 1$  apply to a cavity in the shape of an oblate spheroid (button-shaped cavity). The case of  $\rho_1 = \rho_2 = 1$  applies to a spherical cavity. As shown in Figures 4-1b and 4-1c, the stress concentrations are mild for cigar-shaped cavities, the value of  $\frac{\sigma_z}{\sigma}$  ranging between 2.05 (for a spherical cavity) and 3 (for a long cylindrical cavity). On the other hand, high stress concentrations occur around a thin, button-shaped cavity having its surface perpendicular to the direction of loading.

Porosity in weld metals in aluminum alloys is spherical in many cases, as shown in Figure 3-1. The porosity may be worm shaped; elongated in the direction of weld metal solidification. Weld porosity with the shape of an oblate spheroid is rarely found; porosity rarely contains sharp notches. Consequently, stress concentrations around weld porosity usually are not very severe. The values of stress-concentration factors around porosity appear to be in the cross-hatched

areas ( $\rho_2 > 0.5$ ) or more often in the double cross-hatched areas ( $\rho_1 > 0.5, \rho_2 > 0.5$ ).

### Ductile Fracture

Let us consider a case in which a flat plate (width,  $B$ , and thickness,  $t$ ) containing a circular hole of diameter,  $d$ , is under a tensile load,  $P$ , as shown in Figure 4-2. The average stress,  $\bar{\sigma}$ , and the net stress,  $\sigma_{\text{net}}$ , are defined as follows:

$$\bar{\sigma} = \frac{P}{A_0}, \quad \sigma_{\text{net}} = \frac{P}{A_{\text{net}}} = \frac{A_0}{A_{\text{net}}} \bar{\sigma} \quad (4-1)$$

where

$A_0 = Bt$  is the original section area

$A_{\text{net}} = (B - d)t$  is the net section area.

When  $B/d$  is sufficiently large, the leastic stress-concentration factor,  $K_t$ , is close to 3.  $S_y$  and  $S_u$  are the yield strength and the ultimate tensile strength of the materials, respectively.

Curve 1 shows the distribution along line Af at the stress level  $\bar{\sigma} = \frac{S_y}{K_t}$ . The magnitude of stress at Point A reaches the yeild strength of the material. If the magnitude of applied stress exceeds  $\frac{S_y}{K_t}$ , plastic deformation takes place in the highly stressed regions as shown by the cross-hatched areas in Figure 4-2, and finally fracture occurs. <sup>(34)</sup>

It would be quite unrealistic to assume that fracture occurs at an average stress of  $\frac{S_u}{K_t}$ . When the average stress is  $\frac{S_u}{K_t}$ , the stress distribution would be as shown by Curve 2

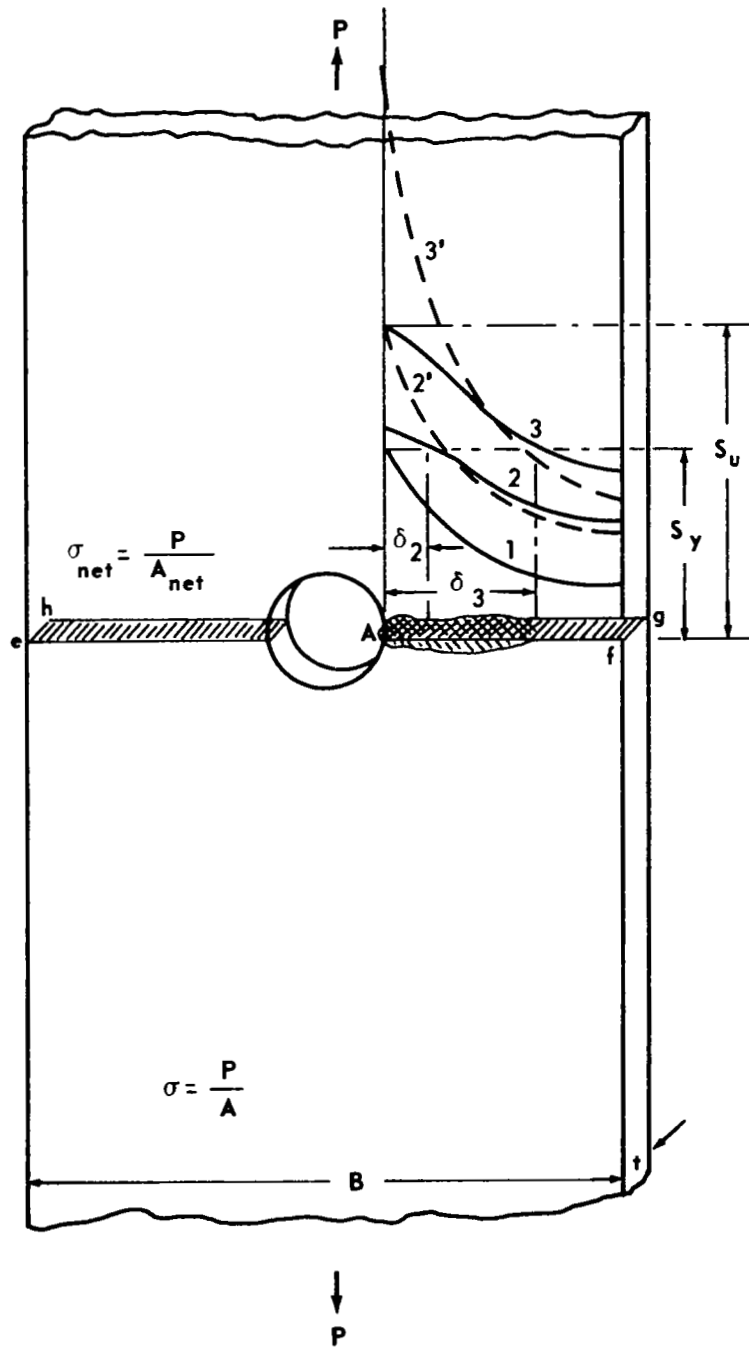


Figure 4-2. Effect of defect on behavior of ductile material under tensile loading.

instead of being shown by Curve 2', elastic stress distribution.<sup>(35)</sup> The stresses in the plastic region (depth,  $\delta_2$ ) are in the neighborhood of the yield stress,  $S_y$ , and considerably lower than  $S_u$ .

The stress distribution at fracture would be as shown by Curve 3, average stress at fracture being  $\bar{\sigma}_f$ . The plastic region extends to a depth of  $\delta_3$ . Curve 3' is the imaginary elastic stress distribution at the average stress of  $\bar{\sigma}_f$ . The maximum stress at Point A,  $K_t \bar{\sigma}_f$ , is much higher than  $S_u$ .

If the material is ductile (undergoes large plastic deformation before fracture occurs), the plastic regions extend and the stress concentrations around the defect are reduced.

However, since the section area along Plane efgh is less than the original section area, fracture usually occurs when the net stress approaches  $S_u$ . In other words, the average fracture stress  $\bar{\sigma}_f$  is:

$$\bar{\sigma}_f = \frac{A_{net}}{A_0} S_u \quad (4-2)$$

The average fracture stress of a specimen with a hole,  $\bar{\sigma}_f$ , is obviously lower than the average fracture stress of a specimen with a hole, or defect,  $S_u$ . The percentage loss in strength due to a hole is:

$$\begin{aligned} \frac{S_u - \bar{\sigma}_f}{S_u} &= 1 - \frac{\bar{\sigma}_f}{S_u} \\ &= 1 - \frac{A_{net}}{A_0} \\ &= 1 - \frac{A_0 - A_{net}}{A_0} \end{aligned} \quad (4-3)$$

The loss of strength due to a hole or a defect is proportional to the reduction of a sectional area.

### Unstable Brittle Fracture\*

Unstable rapid propagation of fracture has been experienced in a number of welded structures.<sup>(38,39)</sup> The fracture mechanics theory developed by Irwin<sup>(40,41)</sup> and other investigators has been applied to the study of unstable fractures, especially of those in high-strength materials for aerospace applications.<sup>(42,43)</sup>

Figure 4-3 illustrates typical behavior when a sheet containing a transverse central crack is subjected to uniform tensile loading. For small cracks, fracture strength exceeds yield strength. Gross yielding is observed in the load-deflection diagram, and extensive plastic deformation is observed in the fracture surface. However, fracture from long cracks occurs abruptly with negligible plastic deformation. The observed fracture stress decreases with increasing crack length. Unstable fracture occurs when the stress-intensity factor,  $K$ , reaches a value,  $K_C$ , which is characteristic for the material.

$$K \equiv \sigma \cdot \sqrt{\pi a} = K_C, \quad (4-4)$$

where

$\sigma$  = average fracture stress

$a$  = half crack length.

$K_C$  is called the critical stress intensity factor or fracture toughness of the material. The critical crack length,  $l_C$ ,

---

\*The effect of weld defect on unstable fracture is a complex subject and the discussion here only covers the importance of the crack size on unstable fracture. Detailed discussions of the effects of defects on brittle fracture of welded structures are given in References (36) and (37).



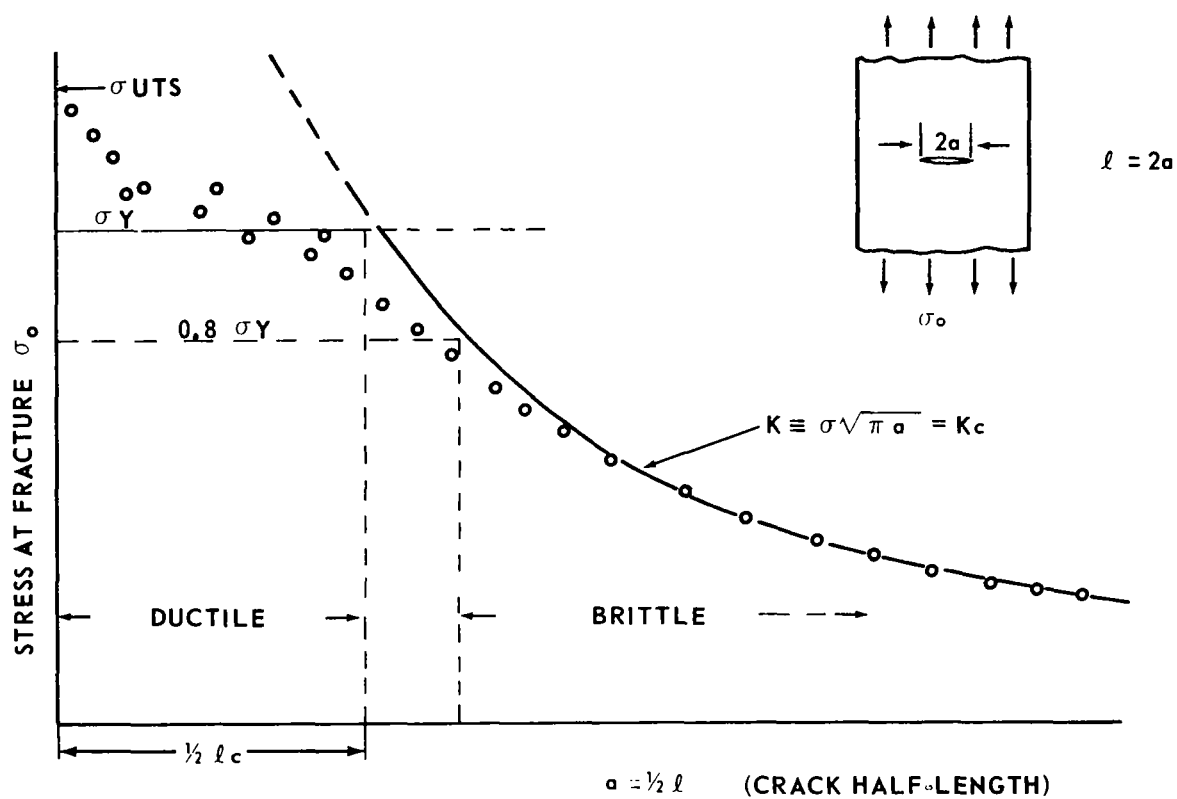


Figure 4-3. Unstable fracture, high-strength materials containing a central crack—effect of crack length on stress at fracture.

also may be used to characterize the brittle behavior of the material; when the preexisting crack is shorter than  $l_c$ , fracture stress,  $\sigma$ , exceeds the yield stress and fracture is ductile. The ASTM Committee on Fracture Testing of High-Strength Sheet Materials<sup>(42)</sup> has described methods of measuring fracture toughness of high-strength sheet metals (ferrous and nonferrous materials having a strength-to-density ratio of more than 700,000 psi/lb/in<sup>3</sup>).  $K_c$  can be determined by fracture tests of notched specimens.

An important consideration in unstable fracture is that the absolute size of a flaw is the controlling factor. If the material contains a crack larger than the critical size, the crack can grow under low applied stress even though the loss of sectional area due to the crack is minor.

It is known that metals with a body-centered cubic lattice, such as steels and titanium alloys, are sensitive to unstable fracture, while metals with a face-centered cubic lattice, such as aluminum alloys and austenitic stainless steels, are not. Unstable fracture is not a major problem for structures made in 2014-T6 and 2219-T87 alloys unless they are subjected to cryogenic temperatures.

## 4.2 Porosity Effects on Weld-Joint Performance under Static Loading

In the NASA research program on welding aluminum, effects of porosity on weld-joint performance under static loading were investigated in Study 5 at the Martin Company.<sup>(14)</sup> This subject was also investigated to a limited extent in Study 1 at the Boeing Company.<sup>(8)</sup>

Since a number of research programs have been carried out to determine experimentally the effects of defects on the static strength of weldments in various materials, the following pages first present results of some experiments similar to the NASA studies. Then discussions will be given on results obtained in the NASA research program.

### Results of Some Experiments Similar to NASA Studies

Theoretically speaking, the reduction of strength in a ductile material due to porosity should be approximately proportional to the reduction of cross-sectional area, as discussed in Chapter 4-1. This general trend has been confirmed by a number of investigators.

For example, Kihara, et al.<sup>(44)</sup> have summarized experimental results obtained from a large number of specimens to show the general tendency of the effects of weld defects on the static tensile strength of aluminum welds (Figure 4-4). The ultimate strength did not decrease appreciably when the reduction of sectional area due to defects was less than about 10 percent. From that point the strength decreased gradually as the reduction of sectional area increased. For example, a 40 percent decrease in sectional area caused between about 20 and 40 percent decrease in the ultimate tensile strength.

### Chemical Composition of the Aluminum Alloy

Chemical Composition (%)									
Specification	Cu	Fe	Si	Mn	Mg	Zu	Cr	Ti	Al
ANP-O	0.03	0.16	0.09	0.56	4.3	0.02	0.19	Nil.	Bal.

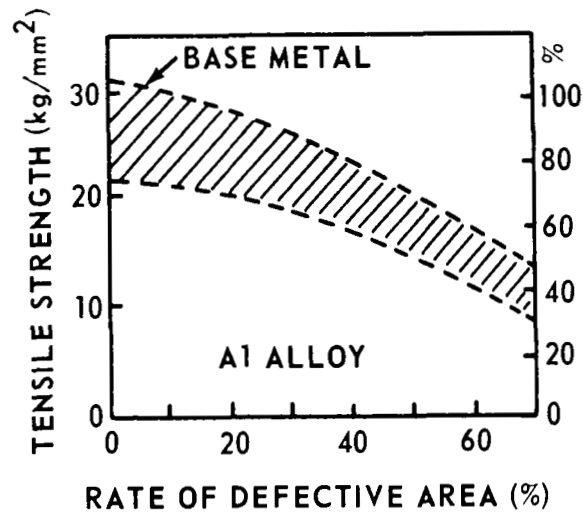


Figure 4-4. Relationship between rate of defective area and ultimate tensile strength butt welds in aluminum alloy.

Welding Research Council Bulletin 152 prepared by Pense and Stout<sup>(37)</sup> is an interpretive report on influence of weld defects on the mechanical properties of aluminum alloy weldments. It covers influence on mechanical properties of porosity and other defects.

Figure 4-5 shows results obtained by Shore<sup>(38)</sup> who studied porosity effects in 1/2-inch thick 7039-T6151 alloy welded with 5039 filler wire by the GMA process. Tensile specimens had no weld reinforcement, and pores as small as 1/250 inch in diameter were counted. Tensile strength of a weld decreased linearly with increasing loss of sectional area. Shore observed about 18% loss in strength for 10% porosity.

#### Research Procedures of the Martin Study<sup>(5,14)</sup>

Experimental welds were made by adding moisture or hydrogen to the shielding gas to produce porosity of the desired level.

Production of Defective Welds. Welds were made in two materials (2219-T87 and 2014-T6), two thicknesses (1/4 and 3/4 inch), and three welding positions (flat, horizontal, and vertical). Filler wire used was 2319 with the 2219-T87 material, and 4043 with the 2014-T6 material. Arc welding was GTA, D-C, straight polarity with helium shielding. Welds had to be intentionally contaminated to produce porosity. This was done by metering additions of hydrogen and/or moisture to the shielding gas in the tungsten torch. However, extensive additions of hydrogen tended to form a large number of very fine pores, relative to typical porosity size-frequency distribution in production welding. In some instances, the porosity was so fine that the X-rays would have been

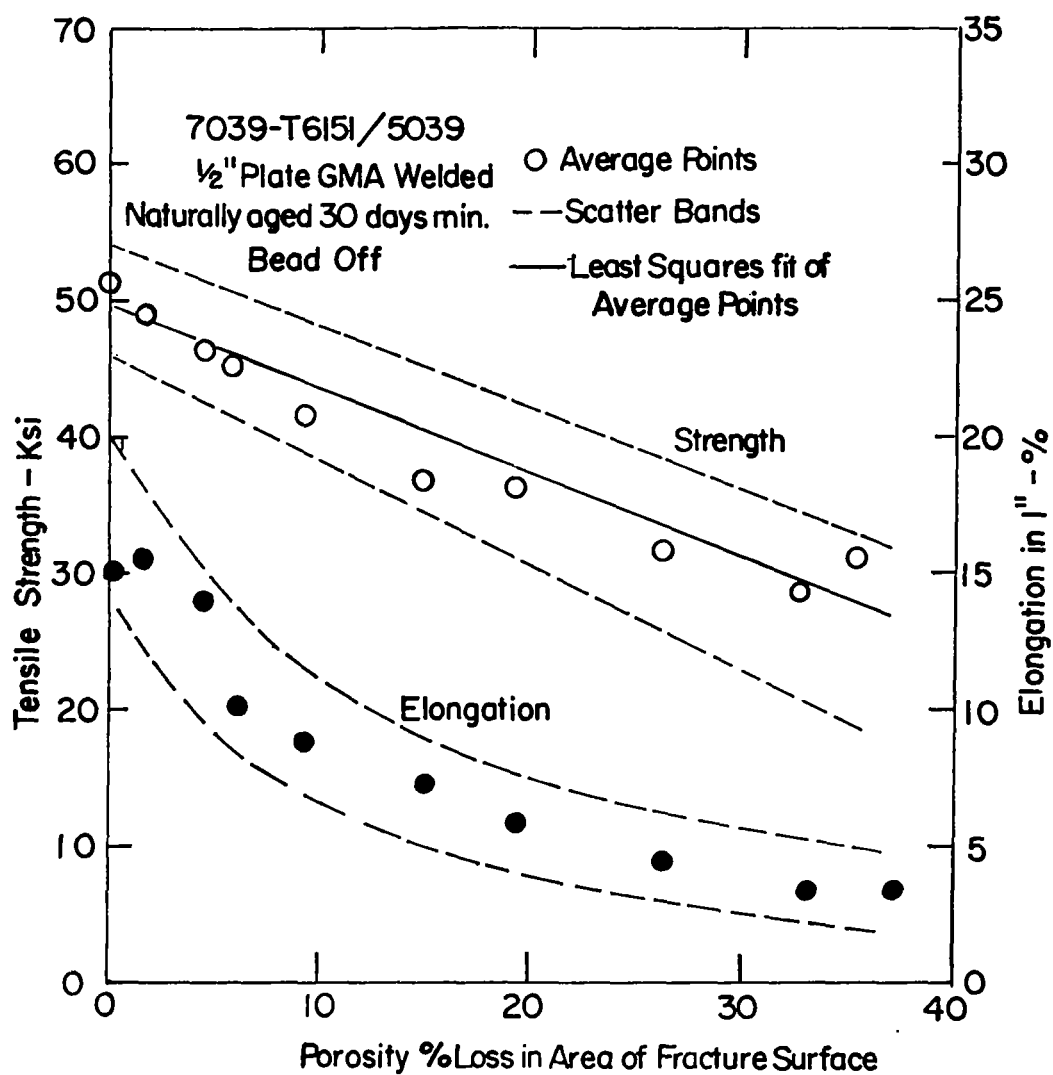


Figure 4-5. Loss of tensile strength and percent elongation in 1-inch gage due to porosity in high-strength aluminum welds (46).

acceptable by most current standards; and yet the strength of these welds was appreciably reduced.

Another difficulty was changes in the electrical characteristics of the arc which were induced by contamination of the arc atmosphere. Specimens welded with heavy contamination had poor or nontypical bead geometry.

Defect Classification System. Classification of defects was performed both before and after destructive testing of the specimen. Nonspecific and arbitrary level of porosity were assigned by comparison with an adopted series of standards. Five levels, 0 through 4, from water clear to quite bad, were adopted as target porosity levels for specimen production purposes.

Mechanical Property Evaluation. The defective welds were evaluated by longitudinal and transverse tensile testing and by transverse fatigue testing. The specimen width of the transverse tensile test was the standard 1-inch wide specimen for the 1/4-inch stock, and 1 1/2-inch wide for the 3/4-inch stock. The dimensions for the longitudinal specimen were chosen to insure that weld metal, heat-affected zone, and parent metal were included in the load-carrying cross section of the specimen. The objective was to simulate the stress picture which a weld sees in the girth orientation of a pressure vessel. In this orientation, the base plate adjacent to the weld is capable of carrying the larger part of the load, as long as the (possibly defective) weld metal is able to elongate and transfer this load to the adjacent base metal. Fatigue specimens were chosen according to a Martin Company standard (0.3 inch wide in the weld).

## Experimental Results

Static Tensile Tests on Transverse Welds. Figure 4-6 shows relationships between the porosity level and mechanical properties of transverse-weld specimens.<sup>(14)</sup> Shown in the ordinate are the high, medium, and low values for each porosity level, and the "2 minimum" values of the following:

- 1) Ultimate tensile strength
- 2) Yield strength
- 3) Elongation for 0.4-, 1-, and 2-inch gage length.

Different curves are shown for data obtained with specimens with and without weld reinforcement.

Figure 4-6 shows that the ultimate strength decreased markedly as porosity increased.<sup>(5,14)</sup> Elongation, especially with a short gage length, also was affected by the porosity level. The porosity level had the least effect on the yield strength.<sup>\*\*</sup>

Attempts were then made to determine quantitative relationships between the porosity level and the ultimate strength. After specimens were fractured, fracture surfaces

---

<sup>\*\*</sup> Similar results were obtained in Study 1 at the Boeing Company.<sup>(8)</sup> A statistical analysis was made of the effects of shielding-gas contamination levels on mechanical properties of welds. Among the six properties analyzed, the ultimate strength of transverse welds had the most significant correlation with the contamination level. The following lists the six properties with the most significant to the least significant correlation:

- 1) Most significant: Transverse-weld ultimate tensile strength
- 2) Transverse-weld elongation
- 3) Longitudinal-weld elongation
- 4) Longitudinal-weld ultimate tensile strength
- 5) Longitudinal-weld yield strength
- 6) Transverse-weld yield strength.

The yield strength was least affected by the contamination level.



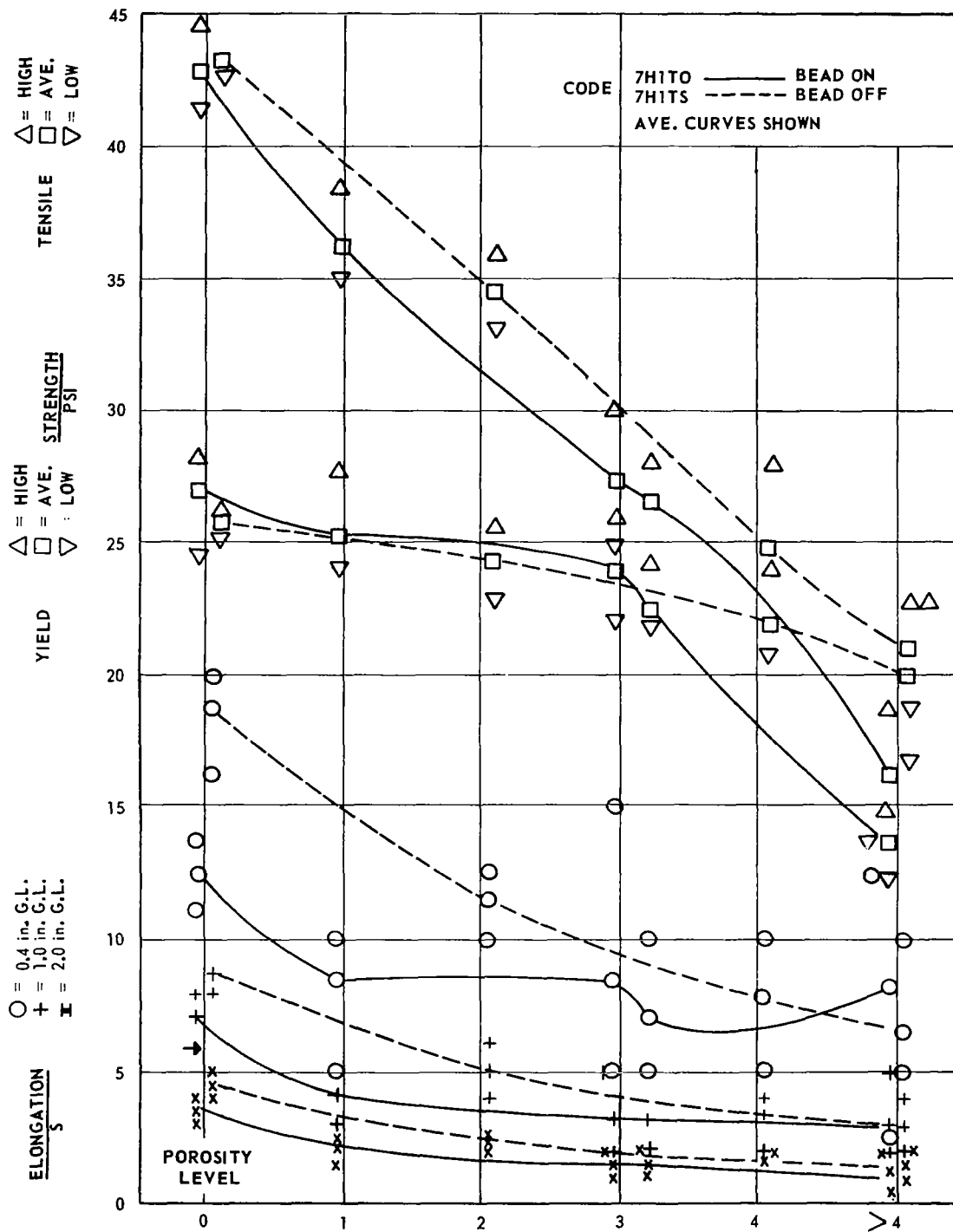


Figure 4-6. Mechanical Properties of 2219-T87, 1/4-in. aluminum alloy containing increasing levels of porosity, transverse horizontal position, D-C GTA weld 2319 Filler Metal.

were examined to determine the loss of sectional area due to porosity. All pores larger than 1/64 inch in diameter were counted to determine the loss of sectional area.

Figure 4-7 shows data for 1/4-inch thick transverse welds in 2219-T87 (horizontal position). Data for specimens with and without weld reinforcement are shown. Shown in the abscissa are the total pore areas in terms of equivalent numbers of 1/64-inch diameter pores and the reduction of sectional area in percent.\*\*\* Good correlations were obtained between the reduction of sectional area and the loss of strength. Marked decreases in the strength were observed on specimens with small loss of cross-sectional area. The Martin investigators stated that most specimens that showed significant loss of strength had many fine pores but pores smaller than 1/64 inch in diameter were not counted.

A study also was made of how existing aerospace industry specifications rate as instruments for predicting mechanical properties. Figure 4-8 illustrates ranges of ultimate strength found within welds of given classification levels according to the ABMA-PD-R-27A, in 2219 and 2014 weldments, respectively. (5,14) A large amount of scatter in data is noticed. The very low values under Class I were all taken from samples which contained large numbers of very fine pores.

Longitudinal Welds. The tensile strength of longitudinal specimens decreased as loss in cross-sectional areas due to increased porosity. Since a specimen contained the weld metal and the base plate, the porosity caused rather minor reduction in sectional area. Even specimens containing extensive porosity maintained strength over 40,000 psi. The effect of porosity on elongation and yield strength were minor.

---

\*\*\* For example, one pore with 1/32 inch diameter and one with 1/16 inch diameter are considered to be equivalent to 4 and 16, respectively, of 1/64-inch-diameter pores.

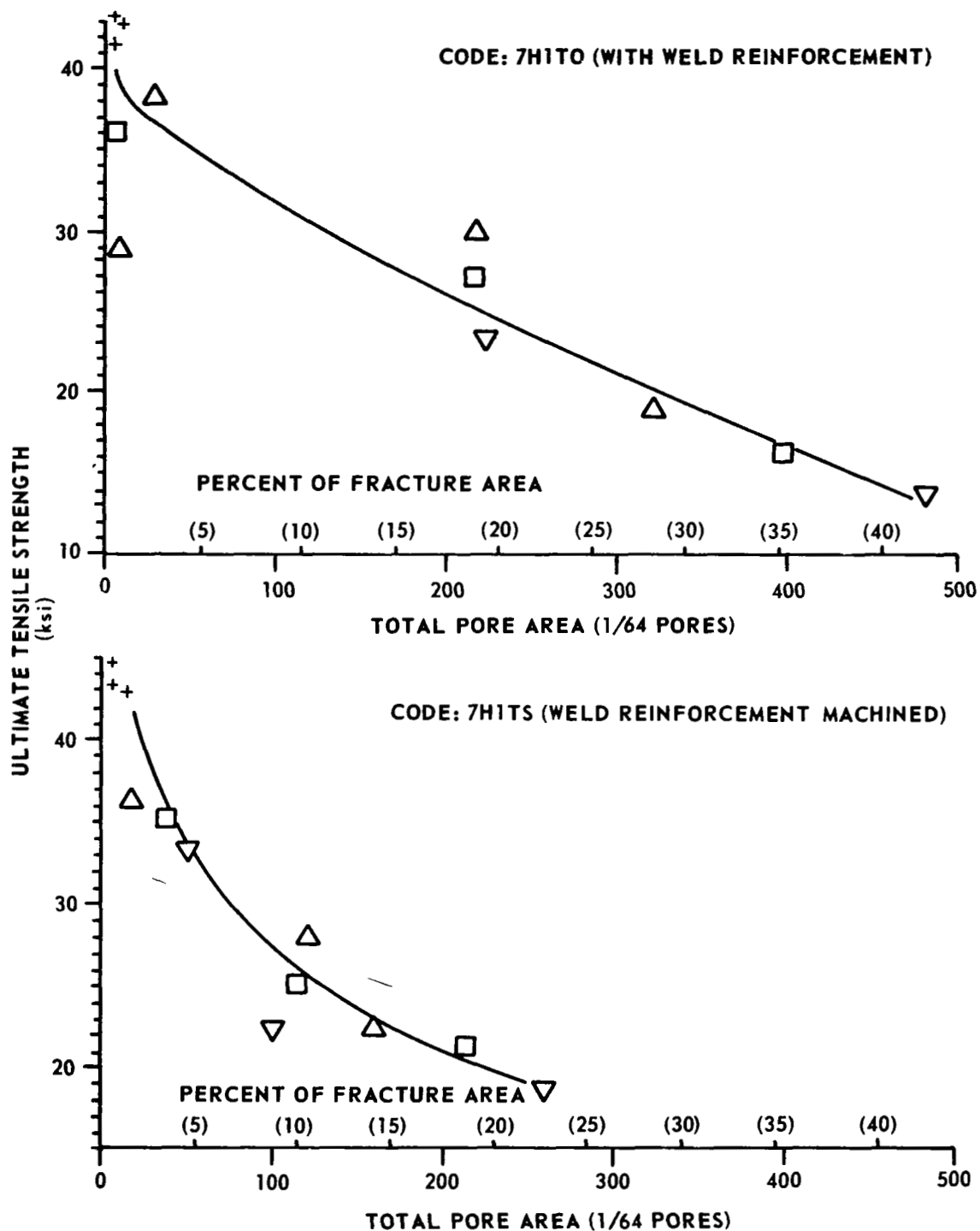


Figure 4-7. Strength Versus Pore Area, 2219-T87, horizontal weld, 1/4 in. Transverse Test.

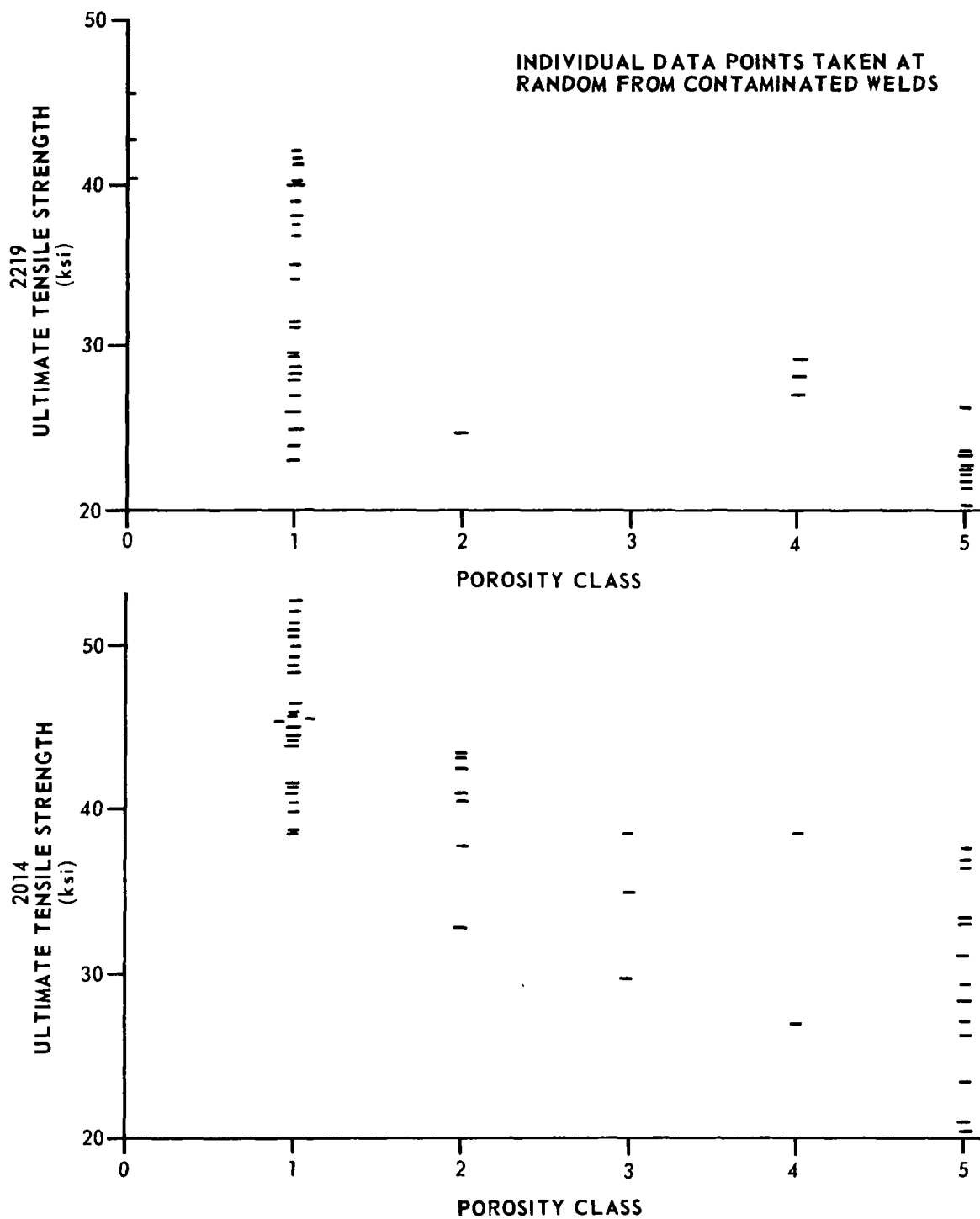


Figure 4-8. Transverse tensile strength Versus ABMA scattered porosity classification, 1/4 in., bead on and bead off, mixed together.

## Analysis and Evaluation of the Martin Study on Porosity Effects on Weld Strength

An important finding obtained in the Martin study is the significance of small pores. If the reduction of strength due to a pore is determined by its cross-sectional area, a pore size which gives the least ratio of cross-sectional area to volume is to be desired. For a spherical void, the ratio of cross-sectional area to volume,  $\alpha$ , is

$$\alpha = \frac{\pi R^2}{\frac{4}{3} \pi R^3} = \frac{3}{4} \frac{1}{R} \quad (4-5)$$

The value of  $\alpha$  increases when  $R$  decreases. Thus, a given volume of contaminant gas in a freezing puddle can cause more damage in the form of small pores than large pores. Experimental results showed that small pores did cause significant reduction in strength.

However, the reduction of strength due to a small amount of pores observed during the Martin study was very great, as shown in Figure 4-7. The results caused a considerable attention during the integration study. Two possible reasons for the drastic reduction in strength are:

- 1) The specimens contained many fine pores which were not counted
- 2) The intensional contamination of shielding gas adopted in the experiment caused some metallurgical degradation of the material.

In an effort to clasify the relationship of porosity to tensile strength of a weld, Martin-Denver conducted an additional to create artificial defects. It was found that the actual change in strength of drilled welds was slightly less than predicted on a linear basis, as indicated by Equation (4-3)

Further attempts were made to improve the technique for counting pores. It was found that very good correlation could be obtained when porosity area fraction was determined by the grid intercept method. The grid intercept method is illustrated in Figure 4-9 showing 10 X photographs of fracture surfaces of a seriously contaminated specimen. Superimposed on these fracture surfaces is a rough grid, with 36 interceptions between lines A to F and 1 to 6 for Figure 4-9a, and 42 (A to F, 1 to 7) for Figure 4-9b. The number of intercepts which fall over a pore (obvious example, D-4 in Figure 4-9a), divided by the number of total possible intercepts, is the porosity area fraction. Careful counting gave 20 pore intercepts for (a) and 18 for (b). Converting to porosity, reductions of sectional area are:

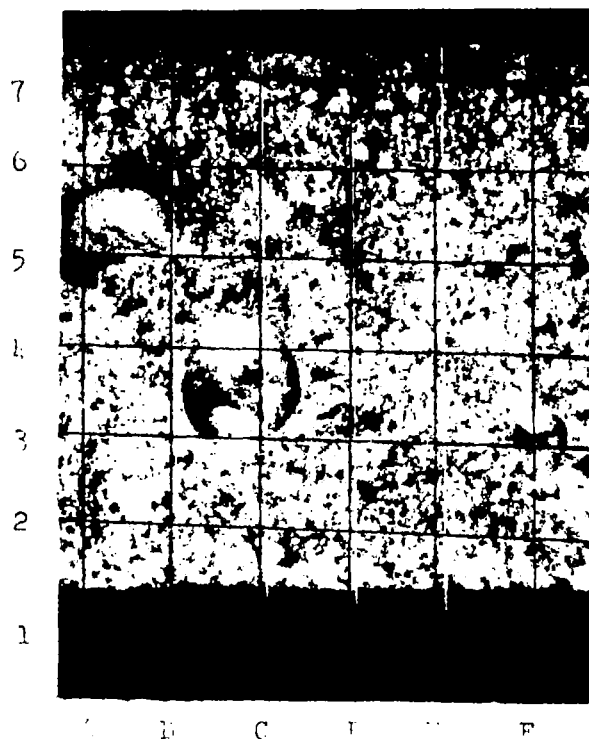
$20/36 = 57\%$  for the section shown in Figure 4-9a

$18/42 = 43\%$  for the section shown in Figure 4-9b.

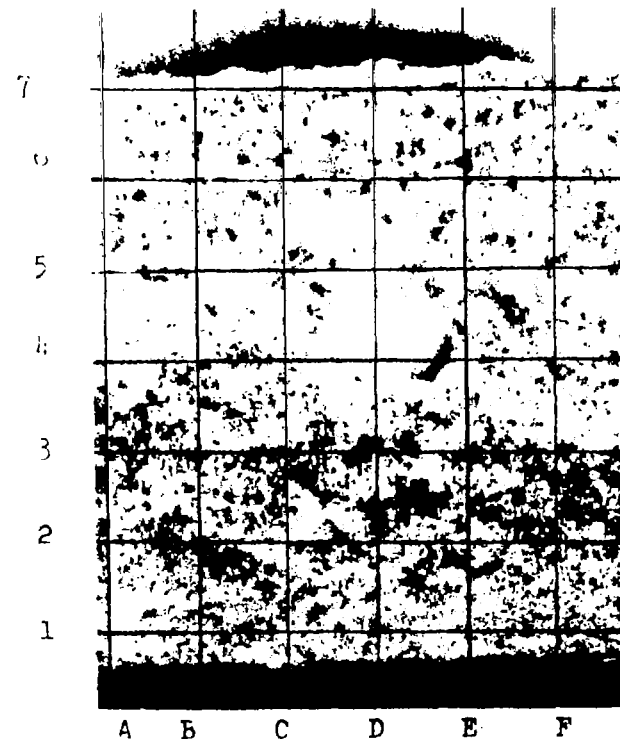
Figure 4-10 shows data for transverse tests of 2014-T6 welds in 1/4 inch plates prepared in the flat (downhand) position. The figure shows two sets of values for the loss of sectional area due to porosity:

- 1) Counting pores larger than 1/64 inch in diameter
- 2) Counting all pores by the grid intercept method.

The points X and Y in Figure 4-10 represent examples shown in Figures 4-9a and 4-9b, respectively. Figure 4-10 shows that the loss of strength due to porosity in aluminum welds was proportional to the reduction of sectional area as long as all pores were counted.



(a) FRACTURE SURFACE,  
POINT x, FIGURE 7  
57%



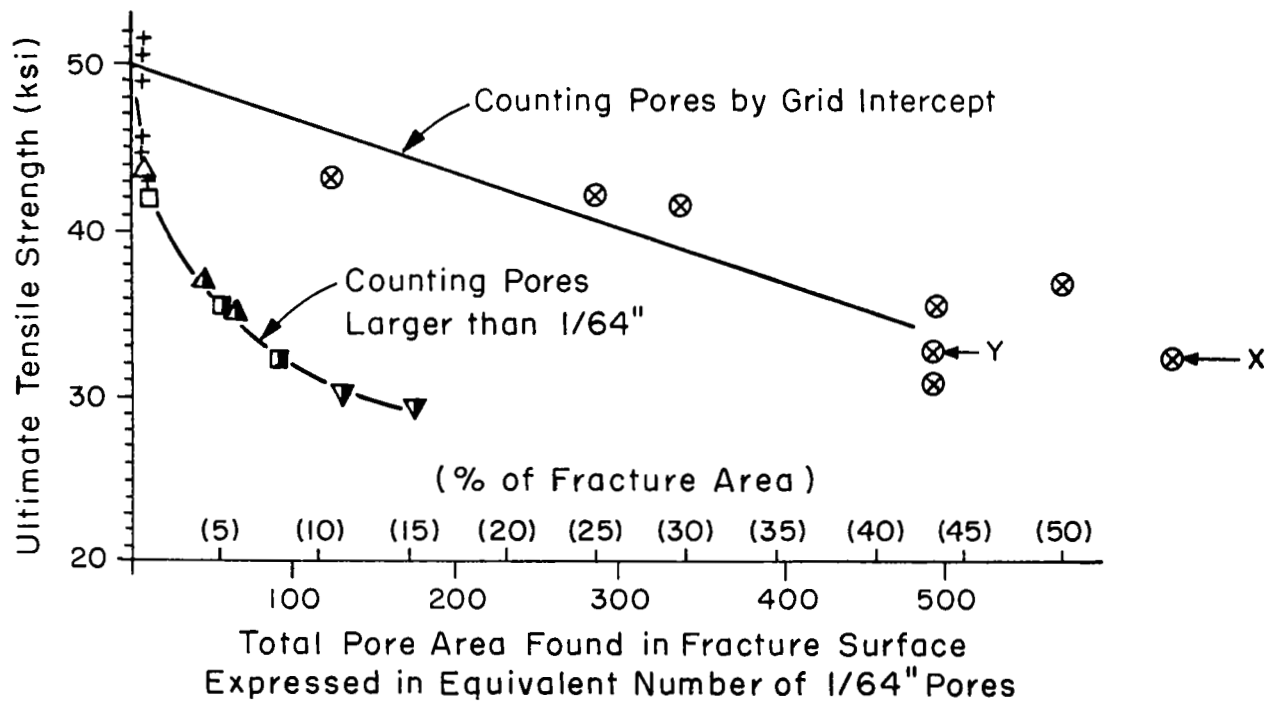
(b) FRACTURE SURFACE,  
POINT y, FIGURE 7  
43%

NOTE: GRID IS SUPERIMPOSED TO ALLOW MEASURE  
OF PORE AREA PERCENT USING

$$\frac{\text{PORE INTERCEPTS}}{\text{TOTAL INTERCEPTS}}$$

$\times 100 = \text{PORE AREA PERCENT.}$

Figure 4-9. Fracture surfaces of porous welds.



NOTE: TESTED WITH REINFORCEMENT.

Figure 4-10. Strength Vs Pore Area for 2014-T6, Flat Welds, 1/4 inch Transverse Test.



### 4.3 Porosity Effects on Fatigue Strength

In the NASA research program on welding aluminum, limited efforts were made on the porosity effects on fatigue strength. (14,8)

Figure 4-11 summarizes results obtained at the Martin Company. (14,45) Shown here are relationships between reduction of sectional area due to porosity and cycles to failure of welded joints in 2219 and 2014 alloy plates 1/4 inch thick. The reinforcement was removed, and the specimens were cycled in axial tension (zero to a given value, or  $R = 0$ ). Figure 4-11 shows cycles to failure under three stress levels: 10, 15, and 20 ksi.

The results shown in Figure 4-11 can be interpreted in several ways. For example, 10% porosity causes:

- 1) Reduction in fatigue strength for 100,000 cycle life from over 20 ksi to 12 ksi (about 1/8 that of sound weld)
- 2) Reduction in the number of cycles to failure under 20 ksi: from over  $10^4$  to around  $10^3$  (1/10 that of the sound weld)  
under 10 ksi: from over  $10^6$  to around  $5 \times 10^4$  (1/20 that of the sound weld).

Figure 4-12 shows similar results obtained at the Ohio State University. (46) Although this study was not a part of the NASA-sponsored studies included in this integration study, the results are presented here for comparison. Welds were made in 7039-T6151 plates 1/2 inch thick using 5039 filler wire. The reinforcement was removed, and the specimens were cycled to 25 ksi ( $R = 0$ ).

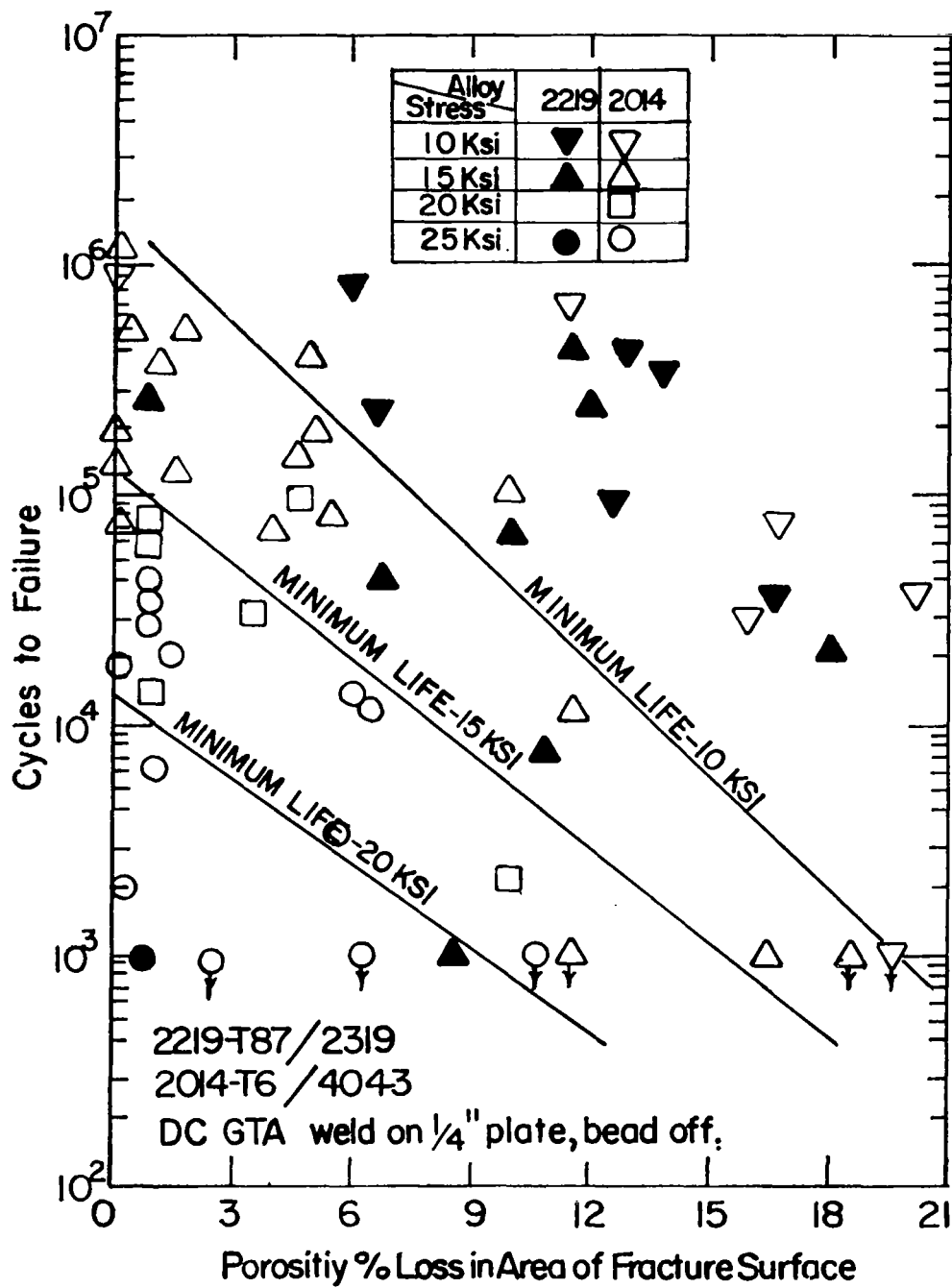


Figure 4-11. Fatigue Life Versus Fracture Pore Count for 1/4 inch thick 2219 and 2014 (14, 45).

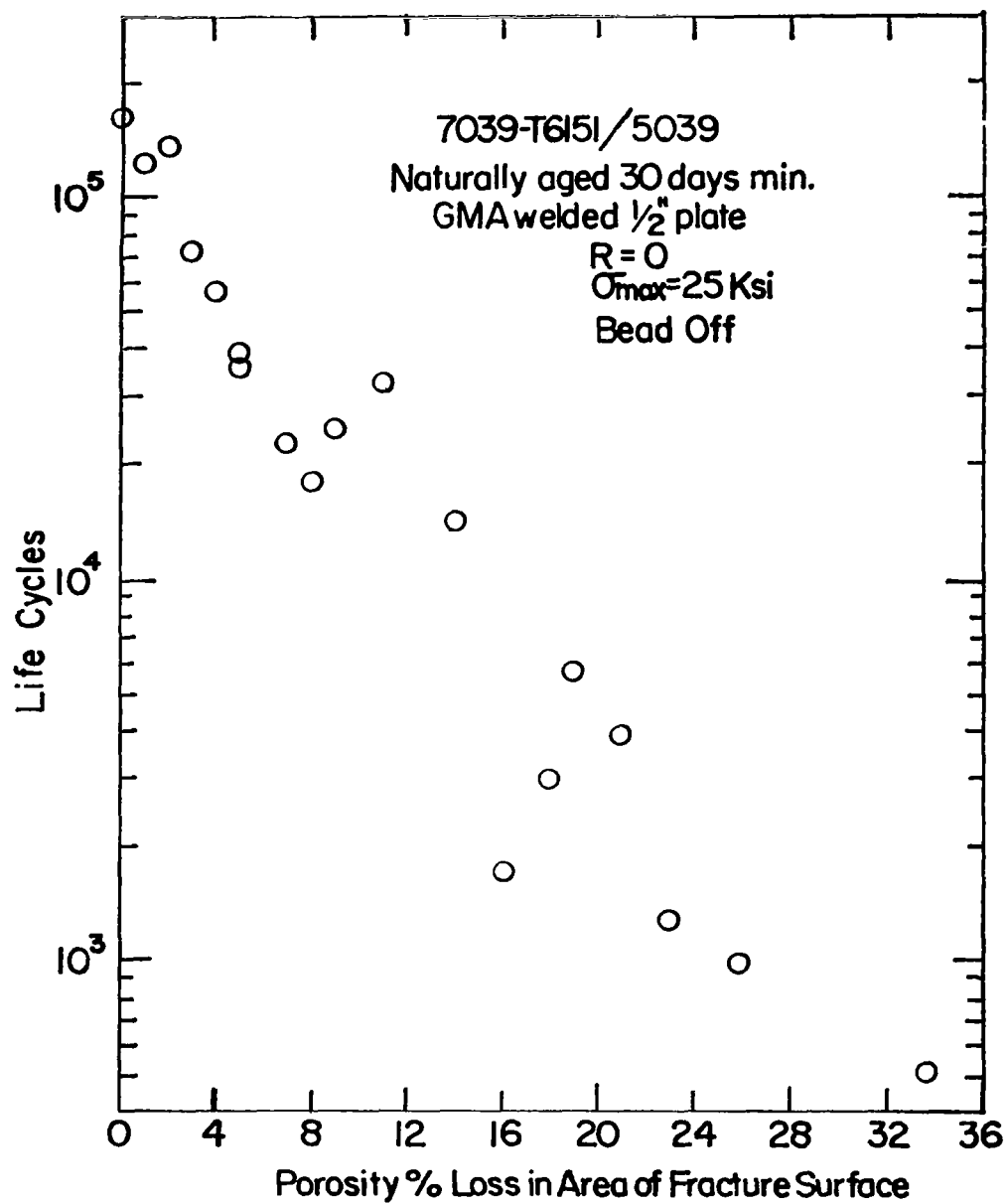


Figure 4-12. Tension-Tension fatigue life cycles Versus Porosity in 7039/5039<sup>(46)</sup>.

The results obtained in the two studies were quite similar. In the both studies 10% porosity reduces the fatigue life by an order of magnitude, that is, to 1/10 that of the sound weld.

#### 4.4 Effect of Repair Welds<sup>(4)</sup>

In considering the data which related expected mechanical properties to the porosity in aluminum welds, it is necessary to recognize that the alternative to accepting the porous weld is either repair or scrap. The scrappage alternative becomes less attractive, if not statistically close to impossible, as launch vehicle tankage increases in size.

Figure 4-13 is a plot of reduction in tensile strength with increasing number of repairs in 2014-T6 welds.<sup>(4)</sup> It is necessary to consider the probability of multiple repairs because repair welding is not always successful the first time. Recent production experience indicates that 1/4 of first repairs are unacceptable and must be repaired again; 1/2 of these second repairs are unacceptable, and approximately 2/3 of the third repairs are unacceptable. Thus, there is considerable risk that the repaired welds will ultimately be lower in mechanical properties than the defective weld which was initially rejected. It is interesting to note that a third repair (Figure 4-13 - typical strength of 36 ksi) has the mechanical properties equivalent to a weld which has sufficient porosity to be well outside of standards of acceptability, that is, to a weld containing 25 to 35 area % porosity. Thus more damage may be done by repair than is repaired by it.

Another aspect of practical application of the general rule of percent strength loss equaling percent area loss, is

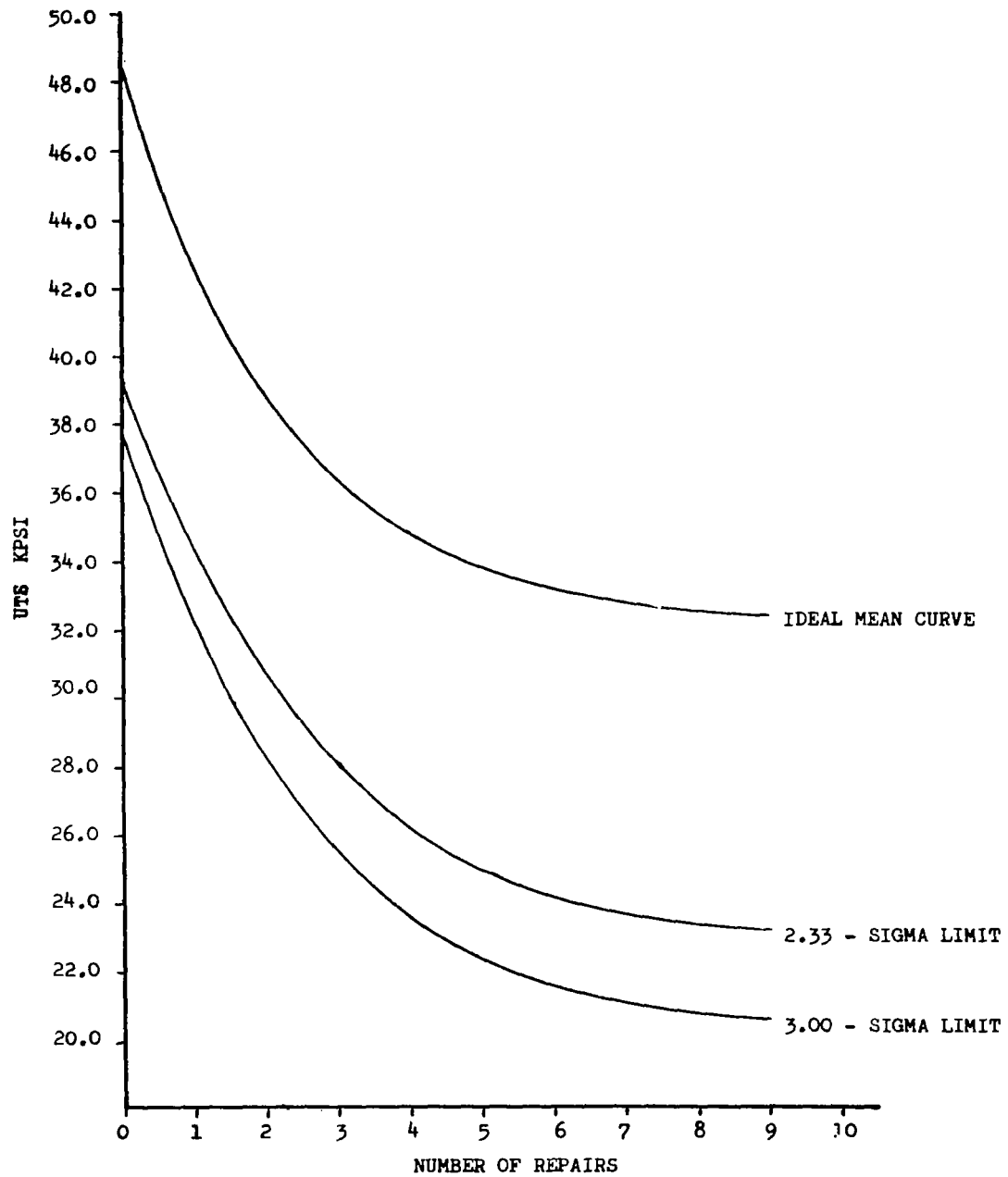


Figure 4-13. Weld Strength Versus Number of Repairs on 2014-T6 aluminum, 1/4 inch thick stock (4).

consideration of the denominator in the area loss fraction. In a uniaxial tensile specimen the denominator is simply the area of the tensile specimen. In a real pressure vessel the incremental or base line area is not so straight-forwardly assigned. Thus direct use of strength loss predictions should be verified on real parts, or simulated part destructive tests, prior to use.

## CHAPTER 5

### Weld Porosity, Its Sources and Control

It has been known for sometimes that hydrogen is the primary cause of porosity in aluminum welds. Research on porosity in aluminum casting provided some insight into the mechanisms of porosity in welds, which are essentially small-scale castings. However, the problem of eliminating or minimizing porosity in welds is far from solved. There are a number of possible sources of hydrogen in welding, and the thermodynamics of welding reactions are more complex than casting.

In the NASA-sponsored studies on welding aluminum, considerable efforts were made to identify sources of hydrogen causing porosity. Studies were made of effects on porosity of:

- 1) Shielding-gas contaminations
- 2) Surface cleanliness
- 3) Base metal and filler-metal compositions and internal hydrogen.

Efforts were also made on developing methods for controlling and eliminating porosity.

The following pages discuss:

- 5.1 Mechanisms of porosity
- 5.2 Shielding-gas contamination
- 5.3 Surface contamination
- 5.4 Composition of base plate and filler metal
- 5.5 Methods of controlling and eliminating porosity

## 5.1 Mechanisms of Porosity<sup>(47)</sup>

Hydrogen in the weld metal has been attributed to a number of possible sources. In fact, the many possible sources of hydrogen are one of the reasons for the confusion and controversy over the mechanisms of porosity formation in welds. Investigators have postulated certain mechanisms of formation based on controlling some variables but not others. The importance of certain variables may be underestimated.

The lack of knowledge of the kinetics of reactions in the weld environment is another major reason why the porosity mechanism is not well understood.

### Role of Hydrogen<sup>(4)</sup>

Table 5-1 shows the solubility of hydrogen at one atmospheric pressure in 99.9985% aluminum.<sup>(48)</sup> The solubility of hydrogen in solid aluminum is very low, about 0.036 cc/100gr or  $8.1 \times 10^{-6}$  atomic percent just below the melting point. At 660° C, the solubility of hydrogen in molten aluminum increases 60 times to about 0.7 cc/100gr or  $1.55 \times 10^{-6}$  atomic percent. The solubility further increases with increasing temperatures.

As the molten weld metal solidifies, excess hydrogen, above the solubility limit, is rejected as tiny pores of hydrogen gas scattered through the aluminum. As time permits, these nuclei will join or coalesce to form large pores. If permitted, hydrogen might grow so large that some porosity will float out of the molten aluminum.



TABLE 5-1. SOLUBILITY OF HYDROGEN AT ONE ATMOSPHERIC PRESSURE  
IN 99.9985 % ALUMINUM<sup>(48)</sup>

Solid state			Liquid state		
Temperature, °C	cc/100 g	At. %	Temperature °C	cc/100 g	At. %
300	0.001	$2.2 \times 10^{-7}$	660	0.69	$1.55 \times 10^{-4}$
400	0.005	$1.1 \times 10^{-6}$	700	0.92	$2.07 \times 10^{-4}$
500	0.0125	$2.8 \times 10^{-6}$	725	1.07	$2.40 \times 10^{-4}$
600	0.026	$5.85 \times 10^{-6}$	750	1.23	$2.77 \times 10^{-4}$
660	0.036	$8.1 \times 10^{-6}$	800	1.67	$3.76 \times 10^{-4}$
			850	2.15	$4.84 \times 10^{-4}$

## Effects of Shielding-Gas Dewpoint and Welding Parameters on Porosity

Saperstein, et al<sup>(49)</sup> investigated effects on porosity of various factors including moisture content of helium-argon shielding gas, travel speed, and arc length. Bead-on-plate welds were made on plates in type 3003 alloy by the GMA process.

Figure 5-1 shows the effect of shielding-gas dewpoint on porosity formation, as determined in this study.<sup>(49)</sup> Each data point represents a single test weld, except where otherwise noted. The dewpoint threshold for porosity formation was approximately -40° F for both travel speeds. Porosity content seemed to increase exponentially as the dewpoint increased above -40° F.

An effort was made to correlate welding parameters to porosity. The mathematical analysis of heat flow in weldments developed by Rosenthal<sup>(50)</sup> and Adams<sup>(51)</sup> was used. Adams developed expressions for weld-cooling rates in the case of two-dimensional heat flow from a point heat source moving linearly with constant velocity in a flat plate. The cooling rate at the fusion interface (on the solid side) is given by the following expression:

$$P = \text{cooling rate parameter} = \left( \frac{10^3 Vt}{EI} \right)^2 \left( \frac{\text{in}^2}{w, \text{ min}} \right) \quad (5-1)$$

The cooling rate on the solid side of the fusion-line interface is directly proportional to the solidification time per unit volume on the liquid side. (Solidification time is the elapsed time between the liquidus and solidus temperature). Since pores form during solidification, the cooling-rate parameter represents a convenient measure of porosity.

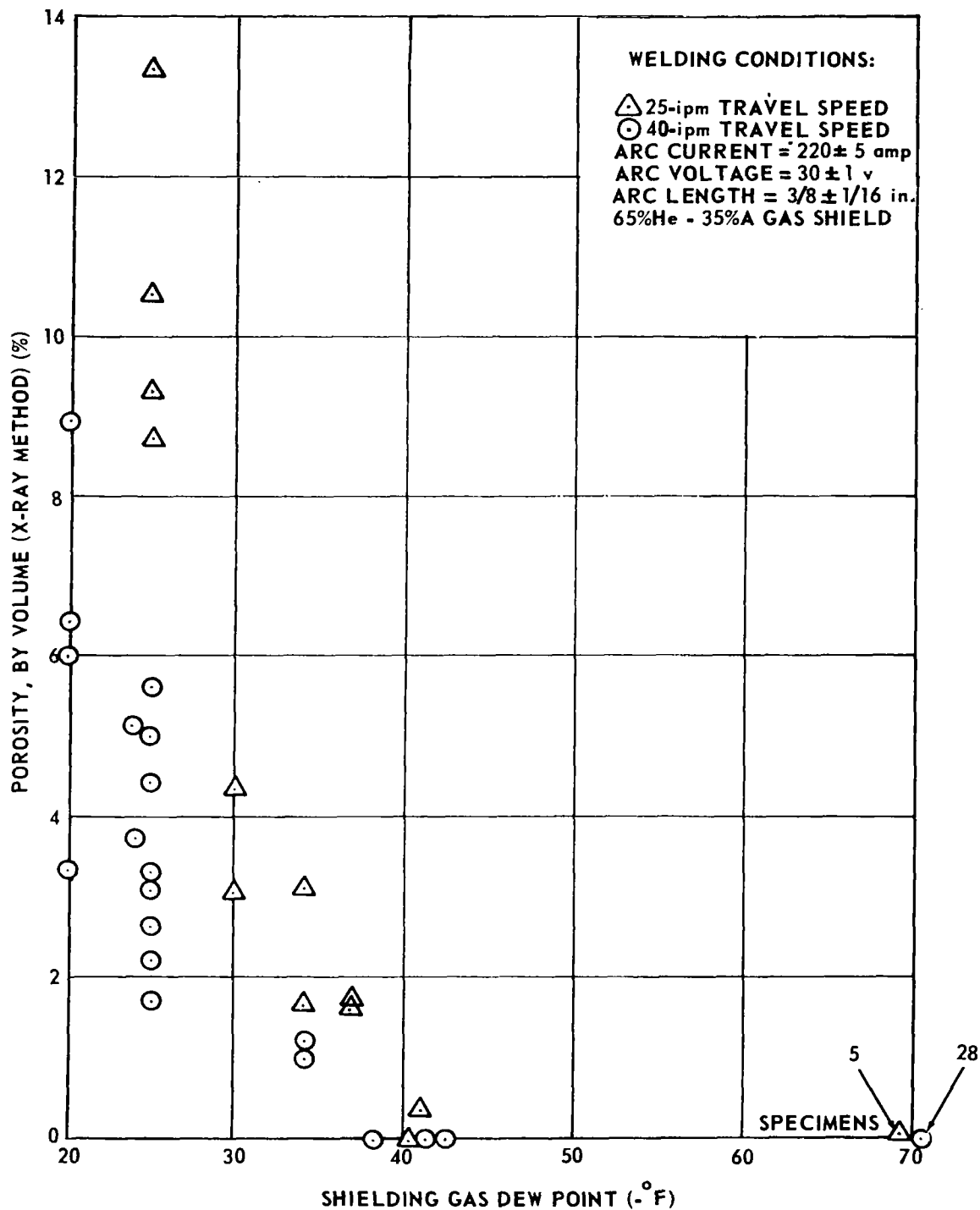


Figure 5-1. Effect of shielding-gas dewpoint on porosity formation.

Many test welds were made to establish a correlation between the cooling-rate parameter and porosity. Figure 5-2 shows a typical dependence between percent porosity and the cooling-rate parameter. (49)

At low values of the parameter (long solidification time), the porosity level is low. The few pores present in the weld are large. At high values of the parameter, or with brief solidification times, the porosity level is also low, and the pores tend to be very fine. Between these two extremes, the porosity level reaches a maximum, exceeding 25 percent. Pore sizes at the maximum level range from medium to large.

### Nucleation and Growth of Porosity

The experimental results shown in Figure 5-2 can be explained in terms of the nucleation and growth processes. After nucleation, time is required for hydrogen to diffuse into pores and for subsequent coalescence to occur. Thus, a rapidly cooling weld is essentially free of porosity, or it contains only micro-porosity or hydrogen in super-saturated solid solution. A slower cooling weld, containing the same hydrogen concentration, exhibits severe porosity. However, once maximum porosity is reached, the level again decreases as the cooling rate decreases. Very slow cooling rates evidently allow enough time for out-gassing of the hydrogen contained in the pores.

In the NASA research program on welding aluminum, an attempt was made to study the nucleation and growth mechanisms of porosity in aluminum welds. In Study 3 at the McDonnell Douglas Aircraft Company, efforts were made to investigate the mechanisms responsible for porosity in aluminum welds in terms of metallurgical phenomena as well as welding parameters.

Figure 5-2. Dependence of porosity formation on cooling-rate parameter, Helium/Argon welds.

Research Procedures of the Douglas Study. Experiments were made in two phases. In Phase I, an arc was produced for a predetermined period at the center of a 2-inch diameter disk. In Phase II, a weld bead was laid on a rectangular specimen 4 by 18 inches. The specimens in Phase I and II were prepared in 2219-T87 and 2014-T6 alloys 1/4- and 3/4-inch thick.

Welds were made by the GTA process, DC straight polarity in the flat position. Specimens were welded in a controlled atmosphere in a specially designed double chamber.

Temperature changes in areas in or close to the weld puddle were measured using thermocouples. After welding, the porosity level was determined in three ways: radiographic, pore counting, and gravimetric techniques.

Statistical analyses were used extensively in the design of experimental programs and the analyses of experimental data. The following model was used for stepwise regression analysis:

$$\begin{aligned}
 Y_i = & b_0 + b_1x_1 + b_2x_2 + \dots + b_nx_n \\
 & + b_{12}x_1x_2 + \dots + b_{(n-1)n}x_{n-1}x_n \\
 & + b_{11}x_1^2 + \dots + b_{nn}x_n^2
 \end{aligned}
 \tag{5-2}$$

where,

$x_1, x_2, \dots, x_n$  = independent variables

$Y_i$  = dependent variables.

Independent variables investigated include atmosphere contaminant level, welding current, arc voltage, arc time (or travel speed), and material thickness. Dependent variables investigated include porosity, hydrogen content in the weld metal, and the solidification time of a weld.

During the course of the integration study, however, questions were raised about the way conclusions were drawn from experimental data. Apparently the mechanisms of porosity formation and effects of welding parameters are more complex than those anticipated by the investigators.

## 5.2 Shielding-Gas Contamination

It has been known that moisture in the shielding gas is a major cause of porosity. Collins<sup>(52)</sup> stated that shielding-gas contamination is especially likely when the arc is unsteady.<sup>(47)</sup>

Saperstein<sup>(49)</sup> showed that welds deposited using shielding gas with dew points below  $-40^{\circ}$  F were virtually free from porosity (Figure 5-2), while porosity concentration increased exponentially with increasing dew-point temperature above  $-40^{\circ}$  F.

Among the NASA-sponsored studies listed in Table 3-1, Studies 1, 2, 3, and 5 covered effects of shielding-gas contamination on porosity. In all of these programs, it was found that the shielding-gas contamination had a much more significant effect on porosity than did the other factors investigated.

It has been found that shielding-gas contamination can be one of the major sources of porosity in aluminum weldments. However, it also has been found that commercial shielding gas is normally acceptably pure as received. In the NASA-sponsored programs conducted at Boeing,<sup>(8)</sup> Battelle,<sup>(9,10)</sup> Douglas,<sup>(11)</sup> and Martin,<sup>(14)</sup> investigators reported that it was always necessary to intentionally contaminate the shielding gas to produce an appreciable amount of porosity. Welds made in the laboratory did not contain appreciable amounts of porosity when they were made with proper procedures, that is, when plates were cleaned properly and commercially pure shielding gas was used.



## The Boeing Study on Effects of Individual Gas Contaminants

The effects of individual gas contaminants were studied by making welds in an atmospheric-control chamber containing various levels of gas contamination. The study was performed in two phases:

Phase I: Determination of the ranges for which a relationship exists between contaminants ( $O_2$ ,  $N_2$ ,  $H_2$ , and  $H_2O$ ) in arc-shielding helium and weldment defects.

Phase II: A quantitative determination of the shielding-gas contamination effects on porosity, mechanical properties, and metallurgical characteristics of 2219-T87 aluminum weldments.

Welding Procedures. The metal studied was 1/4-inch thick 2219-T87 aluminum alloy. Welds were made in the horizontal position by the GTA process, DC straight polarity using 2319 aluminum-alloy filler wire. The chamber was vacuum-purged and then filled with helium containing predetermined amounts of contaminant gases.

Weldment Evaluation. Following radiographic analysis, each weldment panel was machined to obtain two gravimetric, two tensile, and three fatigue samples and one metallographic sample.

Statistical Analyses. Statistical analyses were used extensively in the design of experimental programs and the analysis of experimental data. The  $2^4$  factorial analysis was used to design experimental programs for studying effects of the four contaminating gases (oxygen, hydrogen, nitrogen, and water vapor). Experimental results were analyzed on the

basis of the factorial analysis. The data were then analyzed to obtain regression equations relating the levels of contamination to each measure of weld quality.

Findings. The following results were obtained:

- 1) Increasing hydrogen concentration increased porosity.
- 2) Increasing water vapor increased porosity.
- 3) Increasing oxygen did not increase porosity; in some cases, a slight decrease in porosity was observed.
- 4) Increasing nitrogen had little effect on porosity.

The Boeing investigators presented Figure 5-3 as a guide for controlling shielding-gas contamination.<sup>(8)</sup> The contamination levels shown indicate where occurrence of a weld-quality change is initially observed. The figure indicates that 250 ppm of either hydrogen or water vapor was necessary before significant quality changes were observed. As shown in Figure 5-3, shielding-gas contamination caused various effects including surface discoloration, undercut, and reduction in arc stability. Such phenomena also were observed in other programs.<sup>(9,10,11,14)</sup>

Figure 5-4 gives the calculated relationship, as determined by the Boeing investigators, between percent of water-saturated air in the base gas and resulting hydrogen concentration.<sup>(8)</sup> The figure indicates that at 70° F, for example, an addition of 0.6 percent saturated air to pure helium would result in 250 ppm hydrogen in the shielding gas.

On the basis of experience gained in the current programs, it is believed that there is no reason to change the present NASA specification (MSFC-364A) for shielding gas. Normal commercial gases which meet this specification are believed to have sufficient purity.

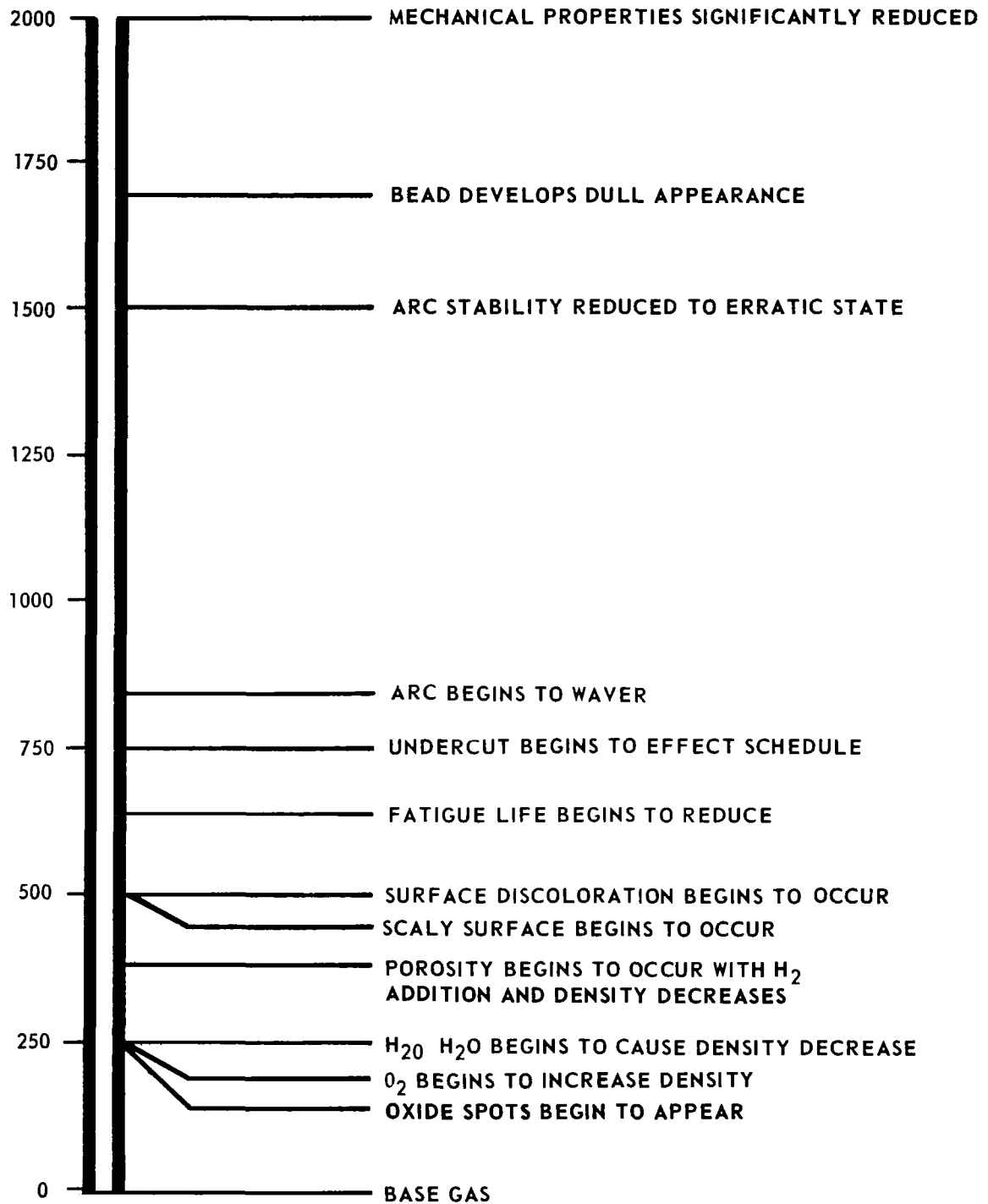


Figure 5-3. Contamination concentration levels at which significant changes occur in weld quality.

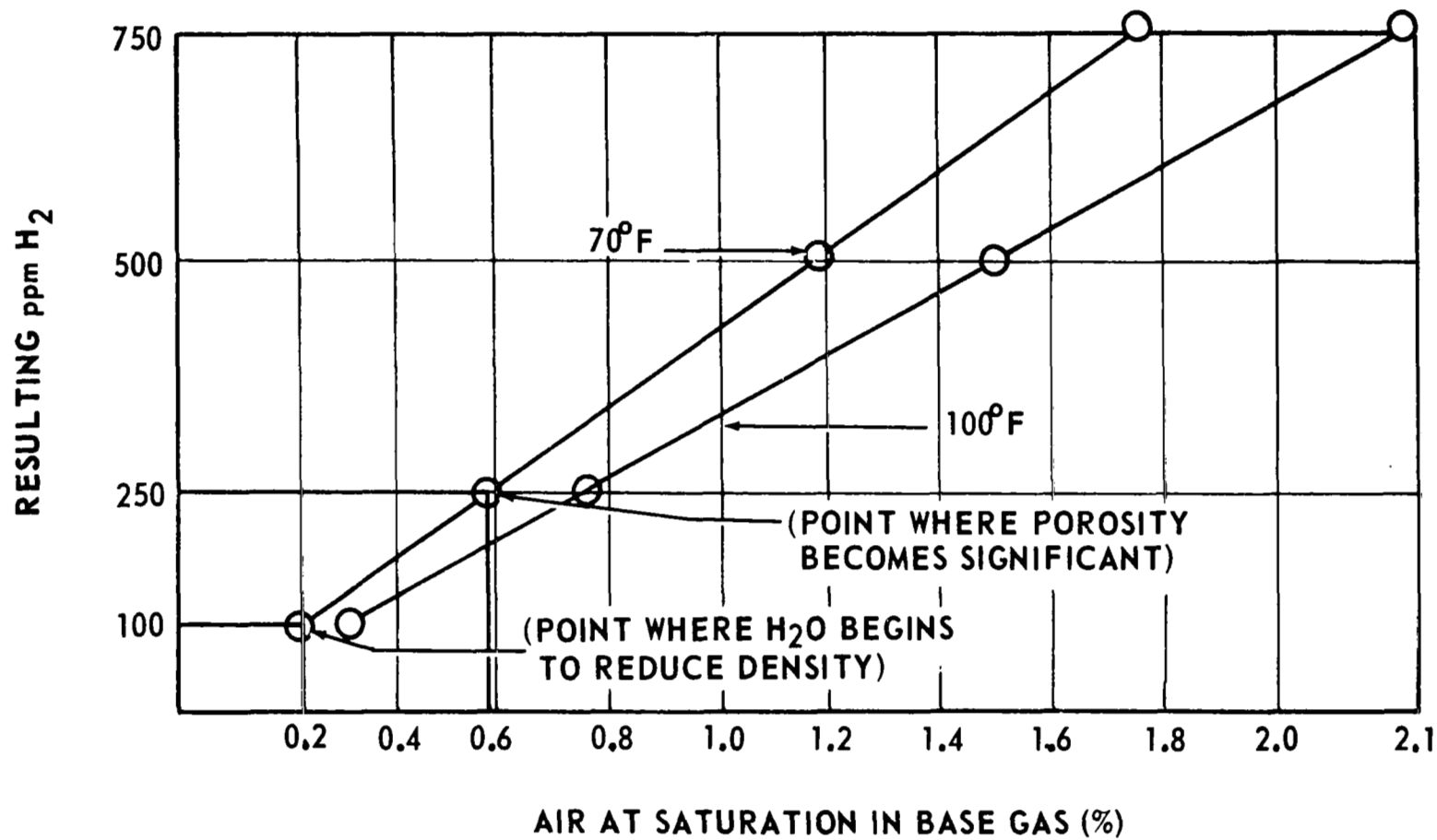


Figure 5-4. Volume of water available to weldment from saturated air contamination.

However, gas contamination can occur within the bottle, or sometimes between the bottle and the torch nozzle. Contamination could occur in a partially empty bottle, for instance. Or, it could occur due to defective connections in the tubing system. An effort was made in Study 17 to devise means of instantly checking the purity of shielding gas at the torch nozzle. This subject will be discussed in a later part of this chapter.

The Boeing investigators further extended the analysis to calculate the amount of hydrogen gas available by decomposition of hydrocarbon on the weld groove. It is assumed that hydrocarbon will decompose completely to gases by the welding arc and they will become gas contaminants.

According to their calculation, it requires less than 1 mg of hydrocarbon per inch of weld to continuously generate 250 ppm hydrogen in the shielding gas. It is estimated that a single fingerprint would result in a 750-ppm hydrogen increase in the area contaminated. By comparing Figures 5-3 and 5-5, the Boeing investigators estimated that a single fingerprint would cause a significant increase in porosity. The estimation was based on the assumption that hydrocarbons on the surface of the weld joint would have the same effect as an equivalent amount of hydrogen being introduced as a contaminant in the shielding gas.

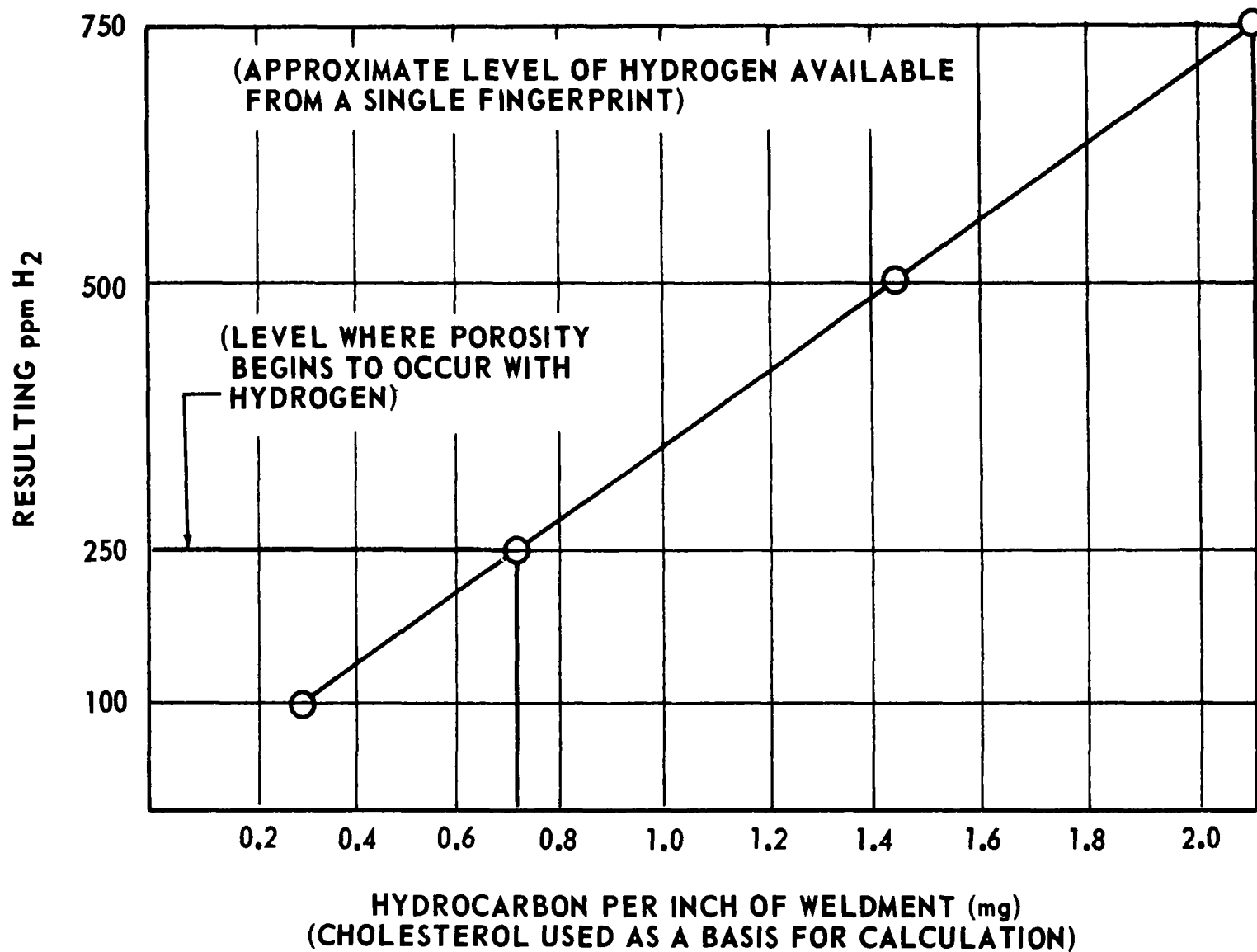


Figure 5-5. Calculated volume of hydrocarbon available to weldment from hydrocarbon contamination.

### 5.3 Surface Contamination

Many investigators believe that the surface condition of the base plate and welding wire is the most important factor contributing to porosity.<sup>(47)</sup> Aluminum oxidizes rapidly and may contain water in the adsorbed form or the chemically combined form.

The Boeing investigators, for example, reported that a single fingerprint could cause three times the minimum level of hydrogen necessary to cause porosity (Figure 5-5). A thorough evaluation of surface conditions capable of producing weld defects was undertaken in Study 9 at IITRI (Illinois Institute of Technology Research Institute).

#### Characteristics of Surfaces of Practical Joints<sup>(4,20)</sup>

From a practical standpoint, all surfaces which are prepared for welding are "contaminated" to some degree. The extent of contamination will be dependent upon a host of factors which include but are not necessarily limited to the following:

- (a) initial as-received surface condition,
- (b) machining variables,
- (c) environmental conditions,
- (d) chemical treatments,
- (e) solvent treatments,
- (f) storage durations.

The effects of these factors may be generalized in terms of more directly measurable surface factors which include the following:

- (a) surface topography,
- (b) surface plastic deformation,
- (c) oxide thickness,
- (d) oxide crystalline structure,

- (e) adsorbed gases, vapors, or liquids (particularly hydrogen-bearing substances such as water organic solvents, lubricants, etc.),
- (f) foreign metallic and nonmetallic particulate matter (such as tool fragments, paper or cloth fibers, skin particles, etc.),
- (g) miscellaneous residuals (i.e., F, Cl, Na, etc., in combined or free form resulting from various preparation treatments).

The problem that confronts the aluminum welding fabricator is that of establishing surface preparation specifications which, despite the contamination, will not degrade weld quality to some unacceptable level.

Since an ideally clean surface is virtually impossible to achieve for normal welding fabrication, it is imperative to consider various factors that may determine the "real" surface condition. The ability to control such factors will ultimately determine our ability to minimize weld damage produced by surface contamination. Aluminum is such an active metal that an aluminum/air interface must of necessity include a barrier layer of some kind--usually the oxide. It is possible to produce a perfectly clean metallic surface by cleaving or fracturing a metal within an ultra high vacuum ( $10^{-10}$  torr or better). However, surface adsorption of gases occurs on the freshly fractured surfaces almost immediately after fracture. At a pressure of  $10^{-6}$  torr a monolayer of gas will form within 1 second. If it were possible to weld only freshly cleaned surfaces then the surface defect potential would be an absolute minimum. This, of course, is a virtual impossibility. However, it would appear necessary to approach this condition so as to minimize defect potential.



In a paper entitled "What is a Clean Surface?" it was pointed out that there are three common types of impurities present on a metal surface:<sup>(53)</sup>

- 1) Substances derived from the base metal, comprising generally oxides of the metal, but also including various compounds formed by corrosion or other surface reactions.
- 2) Substances not chemically associated with the base metal, such as water, oils, greases, solvents, drawing compounds, buffing and polishing compounds, and miscellaneous dirt picked up in manufacturing, handling, or shipping. Such substances may be attached very loosely or in either a physical or chemically adsorbed state. The latter condition may be most difficult to remedy.
- 3) Substances due to an altered base-metal surface layer. The surface of the base metal itself may be physically unsound because it consists of a film of stressed, distorted, broken, or disordered base metal. Alternatively, such metal may be readily converted to oxides, hydroxides, or other oxidation products of the altered metal.

In the light of the foregoing, the surface chemistry and physics of aluminum immediately after the preparation of the surface for welding may be expected to have significant effects on the structure and kinetics of formation of the oxide film which forms at room temperature. The degree of moisture adsorption, or hydration, would also probably be highly sensitive to variations in surface activity related to different methods of surface preparation for welding.

## Surface Adsorption (4,20)

Probably the most detrimental surface condition, with respect to weld-defect potential, is that related to surface adsorption. Adsorbed hydrogen-bearing contaminants would be expected to be the principal cause of porosity-type defects. The preparation of a "good" weld joint surface should be one that is relatively free of adsorbed hydrogen-bearing contaminants. The objective of this section is to describe some of the important adsorption phenomena and their relevance to this program.

Two types of surface adsorption are distinguished: physical adsorption and activated adsorption (generally termed chemisorption). Physical adsorption is characterized by the concentration of molecules on the surface of the metal at comparatively low temperatures. Physical adsorption involves the attraction of molecules to surfaces by the same forces that are responsible for the liquefaction of gases. Hence physical adsorption is essentially a rapid and reversible process because very low activation energy is required for this phenomenon. The surface concentration of the adsorbate decreases with increasing temperature, and increases with increasing partial pressure. Theoretically, physical adsorption reaches a saturation equilibrium level at or near a monomolecular layer thickness at a very rapid rate. However, in practice, especially with porous adsorbents (such as porous oxide films), considerable time may be required to establish an equilibrium saturation because of the slowness of diffusion of the adsorbate through the pores and crevices in the adsorbent. Considering the surface preparation of aluminum for welding, physical adsorption could conceivably have an important effect on subsequent weld quality. For example, if a thick fragmented oxide were produced as a result of joint

preparation, considerable water adsorption may occur during exposure in the ambient atmosphere. Moisture from the atmosphere could be "sponged" up by the porous oxide. No known data are available on the rate of physical adsorption of water (from the ambient atmosphere) on oxidized aluminum.

The second, and potentially more damaging, type of adsorption is that termed "chemisorption." In chemisorption the adsorbed molecule or molecular fragment is held to the surface or surface oxide by strong bonds characteristic of covalent, ionic, or metallic bonding. The interaction of an adsorbate with a surface is much more specific than in the case of physical adsorption where any adsorbate may be readily "sponged" up. The reason for this is the specific chemical changes that take place between the surface adsorbent and the specific adsorbate. The rate of adsorption may be slow due to the need for acquiring an activation energy before the chemisorption process can take place. But once adsorption has taken place, it is not easily reversed, and the application of comparatively high temperatures may be needed before desorption can occur. In some cases even the application of very high temperatures will not bring about a reversal of the original adsorption process because a chemical change takes place involving breakdown of the adsorption complex into new products.

The bulk  $\text{Al}_2\text{O}_3\text{-H}_2\text{O}$  system is characterized by chemisorption reactions. The trihydrate,  $\text{Al}_2\text{O}_3\cdot 3\text{H}_2\text{O}$ , is very stable up to  $280^\circ\text{ F}$  ( $140^\circ\text{ C}$ ). Above this temperature the alpha monohydrate (boehmite) is formed and is stable to approximately  $760^\circ\text{ F}$  ( $400^\circ\text{ C}$ ). Beyond this temperature alumina tends to become dehydrated if heated in an absolutely dry atmosphere. The simple desorption of physically adsorbed water can be rapidly achieved at approximately  $212^\circ\text{ F}$  ( $100^\circ\text{ C}$ ) at ambient

pressures, whereas much higher temperatures are required to desorb chemically adsorbed water. Of course, the crucial questions from a practical standpoint are: (a) to what extent does the chemisorption of water occur on an aluminum/aluminum oxide surface as a result of weld joint preparation and (b) what effect does such adsorption have on the ultimate weld quality? These questions constitute an important part of this program.

Constituents other than water (such as solvents, lubricants, etc.) may also be adsorbed on aluminum/aluminum oxide surfaces, and they may be equally or more important than water. Irreversible adsorption can occur with a large number of simple organic molecules (including benzene, ethyl alcohol, and carbon tetrachloride) on various oxide surfaces (CuO, NiO, ZnO, and MgO). In the case of ethyl alcohol there was evidence that chemisorption had occurred because various breakdown products of the molecule were formed when the surfaces were heated.

Adsorption of pure nonpolar liquid compounds (including benzene, toluene, xylene, and carbon tetrachloride) on polished surfaces of Pt, Au, Ag, Cu, Ni, W, Cr, Sn, and Cd was very pronounced. "In past investigations of cleaning, friction, adhesion, corrosion prevention, and other studies or uses of the surface properties of metals, it usually was assumed that a final solvent cleaning or degreasing of a surface was satisfactory provided that a sufficiently pure or volatile solvent was used. Our results prove that this supposition is incorrect, even if the solvent is nonpolar, and is capable of greatly confusing or interpreting the experiments. Where complete freedom from adsorbed organic material is desired, it is better to avoid using any organic solvent in the last stage of cleaning the solid surface." The implications of this conclusion as related to the surface preparation for

welding are quite obvious. The adsorption of chemical reagents, particularly those that are capable of liberating hydrogen, must also be considered. For example,  $4.4 \times 10^{-2} \text{ mm}^3$  of hydrogen may be adsorbed on  $1 \text{ cm}^2$  of aluminum surface in the form of a monatomic layer. Hydrogen evolution during chemical cleaning may, thereby, produce significant amounts of adsorbed hydrogen, which is exceedingly harmful to weld quality.

Finally, adsorption of the common gaseous constituents of air (oxygen, nitrogen, carbon dioxide, etc.) should be considered. Oxygen, of course, is abundant in the oxide form. The other gases may be adsorbed to the detriment of weld quality. However, it is probable that the adsorption of nitrogen, carbon dioxide, etc., will be of negligible importance compared to the adsorption of hydrogen-bearing constituents.

#### Surface Topography (4,20)

The topography of the aluminum/aluminum oxide surface may have important effects on weld-defect formation. Several factors must be considered. A brief discussion of some of these factors and their potential relationship to weld-defect formation is presented in the following pages.

Although a majority of surfaces appear to have random topographies and consist of many irregular, jagged protrusions, there are definite patterns which characterize a surface (Figure 5-6a). These patterns can generally be classified according to their respective wavelengths. This is possible because the surface irregularities are actually periodic in nature, although they may be complicated in waveform and difficult to interpret. The irregularities of the longest wavelength can be considered as errors of form described by Figure 5-6b. These are caused by flexure of the machine or

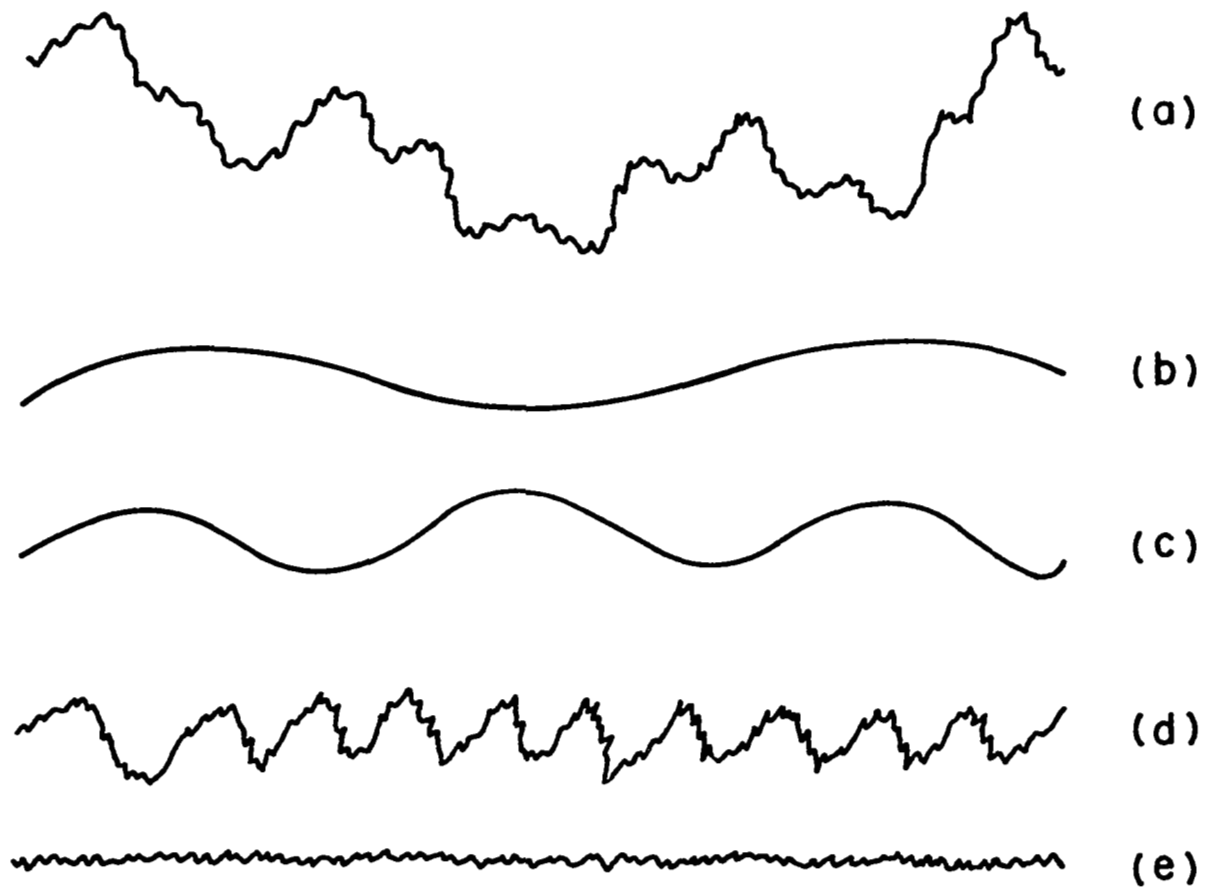


Figure 5-6. Constituents of the topography of a machined surface; (a) The general topography which includes the irregularities caused by (b) flexure or slideways, (c) vibration or bad truing, (d) the cutting tool, and (e) chip removal.

part, or by errors caused in the slideways. Superimposed upon this waveform is one of shorter wavelength described in Figure 5-6c, which is caused generally by components of vibration, or by bad truing of a grinding wheel. The next shorter wavelength wave (Figure 5-6d) is commonly referred to as surface roughness. It is the pattern formed by successive grooves or scratch marks. The shortest wavelength pattern (Figure 5-6e) is superimposed on the previous wave and results from the irregularities within each groove, which are formed by the rupturing of the material as the chip is torn from it. In many cases, these characteristics are broadly classified by designating them as either surface roughness or waviness. Roughness takes into account the finer irregularities caused by the cutting tool and the machine tool feed, while waviness is the wider spaced irregularity resulting from machine or work deflections, vibrations, or heat treatments. To distinguish between these two forms, a roughness-width cutoff is defined as a maximum width of surface to be included in the measurement of roughness height. In addition to these surface characteristics, there is a class of random irregularities called flaws. These occur at one place or at relatively infrequent intervals in a surface. Scratches, tears, ridges, holes, peaks, cracks, or checks are examples of flaws.

On even a smaller scale than surface waviness, there is a predominant direction of the surface pattern called the lay of a surface. The controlling factor in this case is the production method, which results in patterns such as parallel, perpendicular, angular, multidirectional, circular, and radial relative to some fixed reference. In general, the character of a surface depends upon the degree to which a machine is properly set up and used, the particular machine cutting apparatus, the direction of the cut, the feed and

tool shape, the crystalline structure of the material, the elastic and plastic deformations of the material, and the mechanism of material removal.

At least two possible effects of surface roughness are immediately evident. The actual area, rather than the apparent area, of a surface increases in direct proportion to its roughness. The potential amount of surface oxide and/or adsorbed contaminants would, therefore, be expected to be directly proportional to surface roughness. Consequently, surface roughness could potentially affect weld soundness by providing more or less actual surface area for adsorption of damaging contaminants.

The second possible effort of surface topography is that related to the mechanical entrapment of harmful contaminants. Folds, tears, scratches, crevices, and other such irregularities may promote the mechanical entrapment of cutting tool debris, lint, lubricants, solvents, water, and even humid air on the surface of a weld joint preparation. This type of entrapment could cause subsequent weld defects. One very important attribute of this type of mechanical entrapment could be its statistically random nature. The occurrence of weld defects is also frequently by statistically random distributions. Conceivably, such random defect distribution could be closely related to the probable random distribution of mechanically entrapped surface contaminants.

The aforementioned methods were selected for initial evaluation because they were believed to be capable of disclosing surface characteristics which could cause degradation of weld soundness. Mass spectrometry, gas chromatography, and spark emission spectroscopy were selected to determine surface absorption effects. Spectral reflectance analysis was evaluated for the purpose of pertinent oxide or surface



topography characteristics and possibly compositional differences. The evaporative rate method of analysis is a special case and was employed to determine whether or not gross surface differences could be measured.

Coincident with the preliminary surface analysis studies, a parallel evaluation of weld-defect potential was undertaken. The exploratory evaluation was performed for two reasons: (1) to develop a simple weld test which was capable of disclosing surface-induced defects and (2) to establish a tentative correlation between surface contamination level and weld-defect potential. The latter objective was considered to be vitally important since it would be futile to indiscriminately measure surface conditions which were in no way related to weld-defect potential. Furthermore, a simple weld test could in itself be a very potent screening test for the evaluation of surface preparation methods.

#### Procedures of the IITRI Study

The objective of Study 9 performed at IITRI was to establish the significance of material preparation and surface property effects on weld porosity. A three-phase program was undertaken to achieve the program objective:

- Phase I: Identification and classification of deleterious surface conditions
- Phase II: Standardization of surface condition measurements
- Phase III: Correlation of surface condition and weld quality.

Materials. Two aluminum alloys, 2014 and 2219, were supplied by the Marshall Space Flight Center, NASA, for this program. Eight sheets of 2014-T651, 48 x 144 x 0.250 inches,

and six sheets of 2219-T87, 72 x 144 x 0.359 inches were obtained. Only the 2014 material was used in the preliminary Phase I evaluations.

Surface Preparation An overwhelming number of accepted preparations for aluminum surfaces prior to welding are currently used in the aerospace industry. A systematic study of each one would have been impossible within the time and funds scope. Therefore, treatments representative of solvent degreasing, chemical cleaning, and mechanical cleaning were employed in this investigation.

Preparation of Nonmachined Specimens. Materials in the as-received condition exhibited maximum surface roughness of less than 10 inches (peak-to-peak). The surface was heavily contaminated with oils, greases, ink, and foreign particles picked up in fabrication, handling, and storage. Small blanks, approximately 1 x 1.5 x 0.250 inches, were saw-cut from the sheets of 2014 Al and individually stored in snap-top jars, about 2 inches diameter by 3 inches deep, for subsequent treatment. All further handling of specimens was by Teflon-lined tongs, disposable tissue, or plastic gloves. The jars were stored in a desiccated dry box between processing steps and until just prior to specimen analysis. The air in the dry box was maintained at -40° F dew point (about 72° F dry bulb temperature) by continuously purging with bottled dry air.

Degreasing was performed by a detergent (Tide) and/of solvent soak. The solvent was reagent grade benzene. Samples were immersed for a period of 1 minute, followed by a vigorous tissue wipe or warm (110° F) air dry using a heat gun.

The original film was removed by chemically cleaning (1-min. immersion in a 5 w/o NaOH solution at 180°-190° F).

The dark film that formed was removed (desmuted) by a short (15 seconds) dip in 50 v/o  $\text{HNO}_3$ . Agitated rinsing in deionized water and warm air drying followed.

Additional treatments were included to attempt to produce surfaces having a range of weld-defect potential. These were: boiling in water, storage over water, coating with silicone grease, anodizing, and certain combinations of these. Anodizing was done in an electrolyte of 15 w/o  $\text{H}_2\text{SO}_4$  at 72° F and a current density of 12 amp/ft<sup>2</sup> for periods ranging from 1 sec to 60 minutes. Water rinsing and warm air drying followed.

Preparation of Machined Specimens. Numerically programmed machining was done with a Sundstrand 5-axis, Om-3 Omnimil to obtain a reproducible starting surface. The omnimil used specially constructed fixturing. The specimen chamber enabled the maintenance of a controllable environment during machining. A dry air (20% relative humidity) or a moist air (90% RH) atmosphere was incorporated in the machining procedures by flushing the chamber with bottled dry air (-40° F dew point) or passing the air through a water bubbler then to the chamber. The ambient temperature and relative humidity in the Omnimil room was maintained at about 72° F and 50%, respectively, at all times.

The most valid discrimination between defective and nondefective welds (including a possible range of defect content) is ascertained by correlating the surface analysis results with actual weld results. Therefore, a simple weld test was developed and used extensively throughout the program. The test proved to be extremely useful and is in itself an excellent screening test for determining the acceptability of various surface preparations for welding.

Weld Test. A weld test was developed to disclose damage mainly produced by surface contamination. A pair of samples of a particular preparation are placed together on 1 x 1.5 in. faces and positioned in a vise between two 3 1/2 x 2 1/4 x 1 in. thick pieces of type 1100 aluminum so that the 1.5 in. edges are forward. The large pieces of aluminum served as a heat sink. The vise is tightened with a force of about 30 ft-lb. A spot is fused at the midpoint along the interface. The spot welds are made with DCSP/TIG process, using the following settings with a Sciaky S-4 power supply: constant current mode, arc current, 320 amps; arc voltage, 18 volts; arc length, 1/16 in.; gas, high-purity helium (10 ppm H<sub>2</sub>O); arc duration, 2 sec; gas preflow, 1 min; gas flow, 100 cfh; electrode, tungsten-2% thoria, 5/32 in. diameter; and tip geometry, 32° taper, 3/32 in. blunted tip. Figure 5-7 illustrates the spot weld-test specimen.

The test is extremely sensitive to the properties of the butting surfaces. The gases liberated from the surfaces by the heat of the arc are trapped by solid contact along the fusion line. The pressure of gases generated at the melting front is a function of the amount of surface contamination. At some level of contamination there is sufficient pressure built up to cause the gases to "escape" into the weld pool. Porosity is formed by the rejection of the dissolved gases during solidification and cooling. Heavily contaminated surfaces exhibit porosity throughout the fusion zone, whereas cleaner surfaces are characterized by porosity only along the fusion line or complete absence of porosity. The amount of oxide film present on the surfaces determines the fusibility and depth of penetration along the interface. Oxide inclusions are readily disclosed on the parted surfaces, at the fusion line and in the weld.

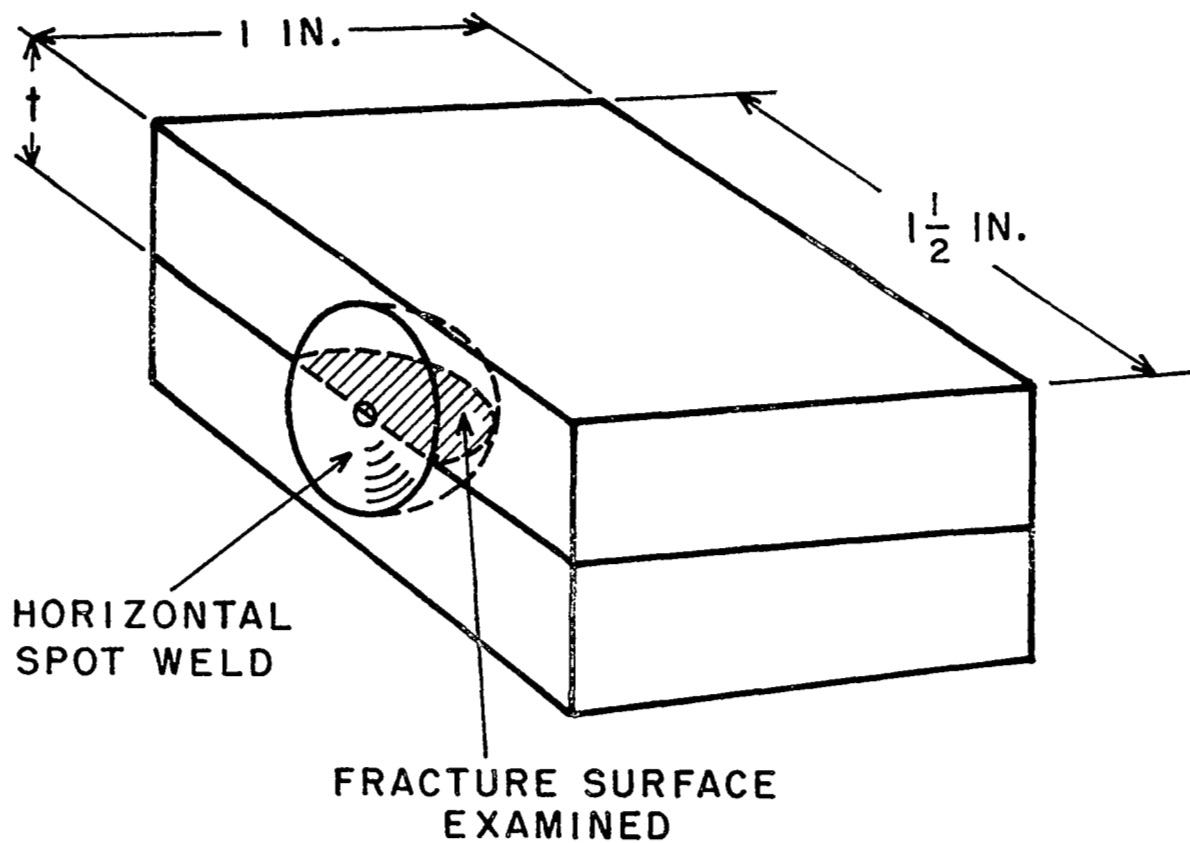


Figure 5-7. Weld test specimen for evaluating defect potential of surfaces.

The extent of weld damage is best determined by fracturing the pieces through the weld, thereby exposing the interface, fusion line, and fused weld metal. Defect content is evaluated by inspection at 25X magnification.

#### Results of the IITRI Study

Table 5-2 summarizes the surface preparations and a description of defects. All test welds contained significant porosity except the machined specimens (Figure 5-8) that received no further treatment. Figure 5-9 shows large porosity encountered when the surface was not machined but was solvent degreased. Figures 5-10, 5-11, and 5-12 show photos taken of machined surfaces with a scanning electron microscope; numerous tears and smears are present. Figure 5-13 shows a fractured specimen with a residue of thichloroethylene near the surface. Figure 5-14 shows reaction products from chemical cleaning.

Figure 5-15 presents the finding in a simple manner. Shown here are weld-defect potential of various surface preparations. Figure 5-16 is a similar presentation, but it includes the effect of storage time on defect potential. As-machined surfaces have the lowest defect potential. Characteristics of various surface preparations are as follows.

1. As-Received. This type of surface generally will be covered with an anodized or severely oxidized hydrated layer which is laden with oils, inks, grease, dirt, and other debris. The weld defect potential of as-received material is generally very high and, at best, cannot be relied upon to produce consistently good weld quality.

2. Machined. Removal of the as-received surface by an "undercutting" machining operation, such as face milling

TABLE 5-2. DESCRIPTION OF SPOT-WELD DEFECTS RELATED TO SURFACE PREPARATIONS.

Surface Preparation	Description of Defects
<u>A. Nonmachined</u>	
(a) As-received	Coarse and continuous fusion-line porosity and oxide inclusions.
(b) Benzene degreased	Cavernous porosity on fusion line and in weld. Porosity is discolored to a yellowish tint.
(c) Chemically cleaned	Large and fine pores along fusion line. Oxide inclusions in weld.
(d) Chemically cleaned and coated with silicone grease.	Cavernous, discolored porosity on fusion line. Fine pores and oxide inclusions in weld.
(e) Chemically cleaned, silicone grease coated, stored over water for several days.	Similar to (d). More porosity and oxide inclusions in weld.
(f) Chemically cleaned and stored over water for several days.	Continuous fusion line porosity and large elongated pores in weld.
(g) Anodized 1 sec to 5 min.	With increasing anodizing the porosity becomes more continuous on fusion line. Greater amounts of oxide inclusions develop until the original interface remains unfused.
(h) Anodized for 5 min or 60 min, boiled in water for 5 min.	Almost no fusion across interface. Much large porosity on surface.
<u>B. Machined</u>	
(a) As machined (all types)	Nearly free of defects. Occasionally some very fine pores on fusion line.
(b) Trichlorethylene rinsed	About 20 large pores on fusion line, some discolored.
(c) Chemically cleaned	About 30 pores on fusion line, large and small. Some large area of lack-of-fusion. Occasional oxide inclusions.

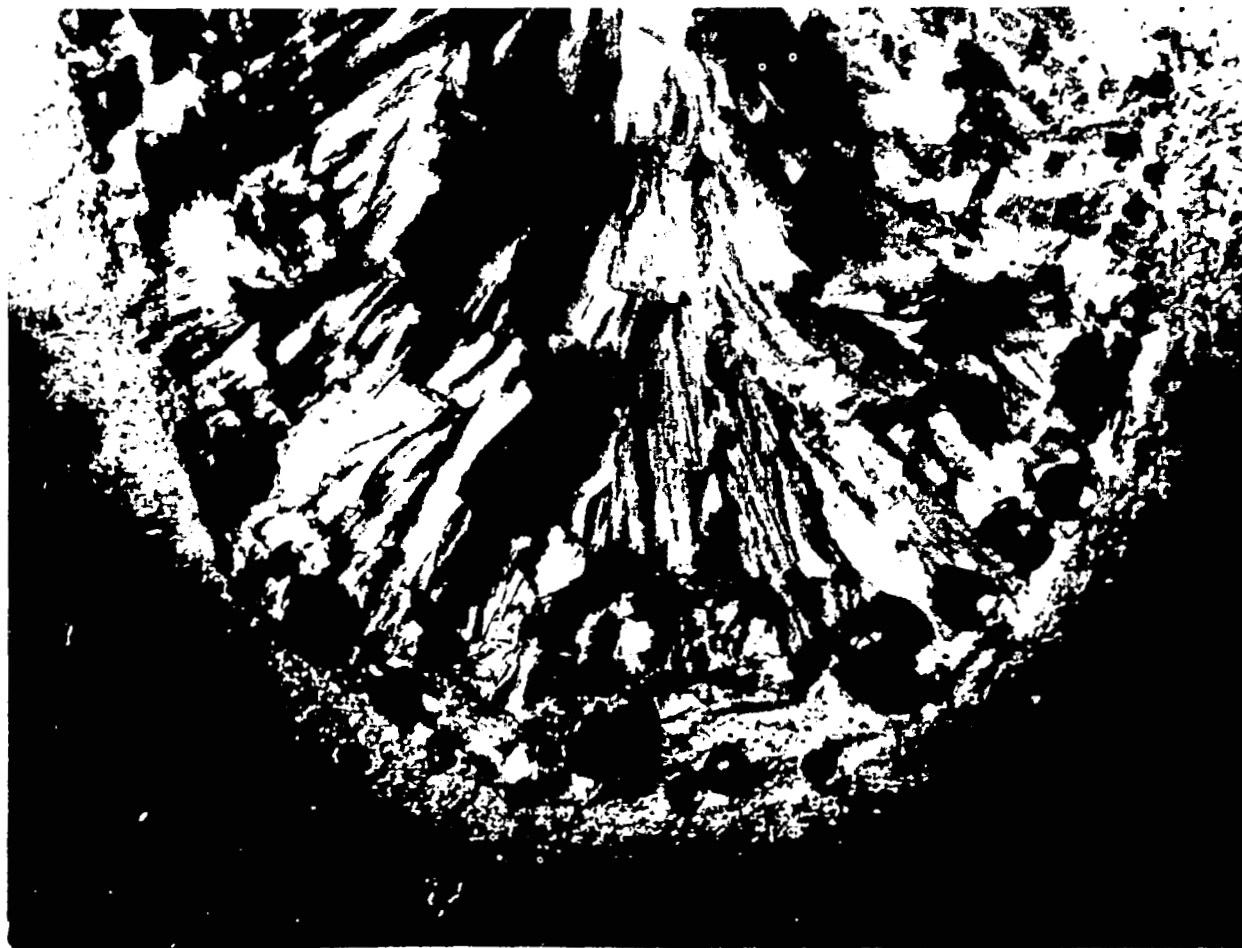


Neg. No. 32725

25X

Figure 5-8. Nil defect spot weld fracture surface typical of the as-machined surface condition.





Neg. No. 33403

25X

Figure 5-9. High defect spot weld fracture surface typical of the nonmachined and solvent degreased surface condition.

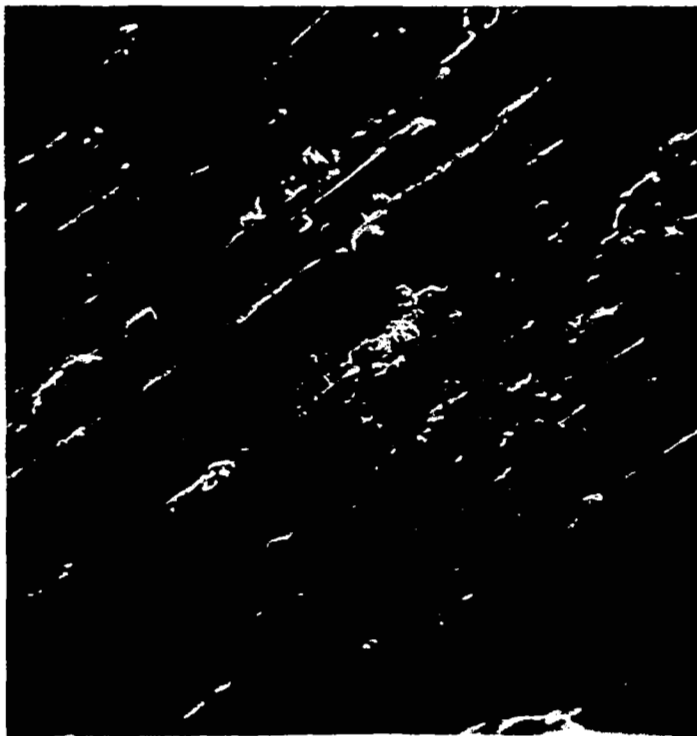
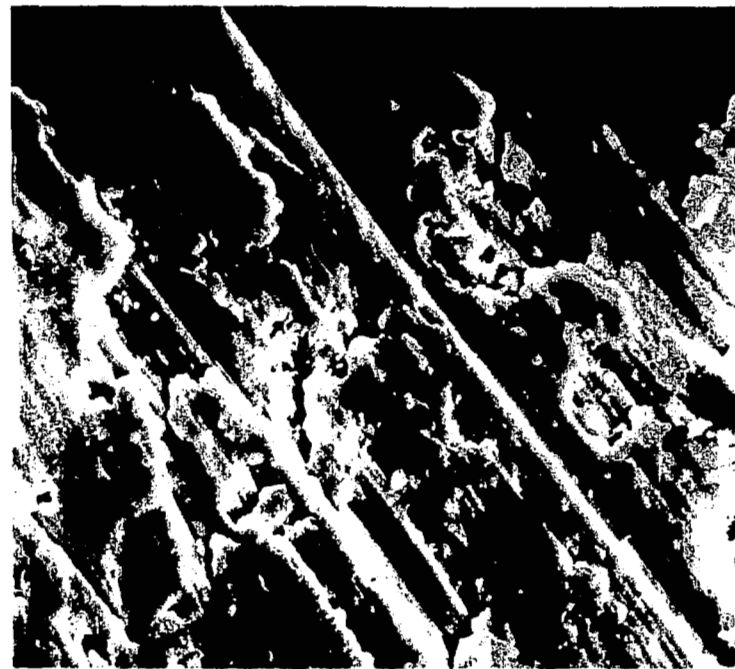
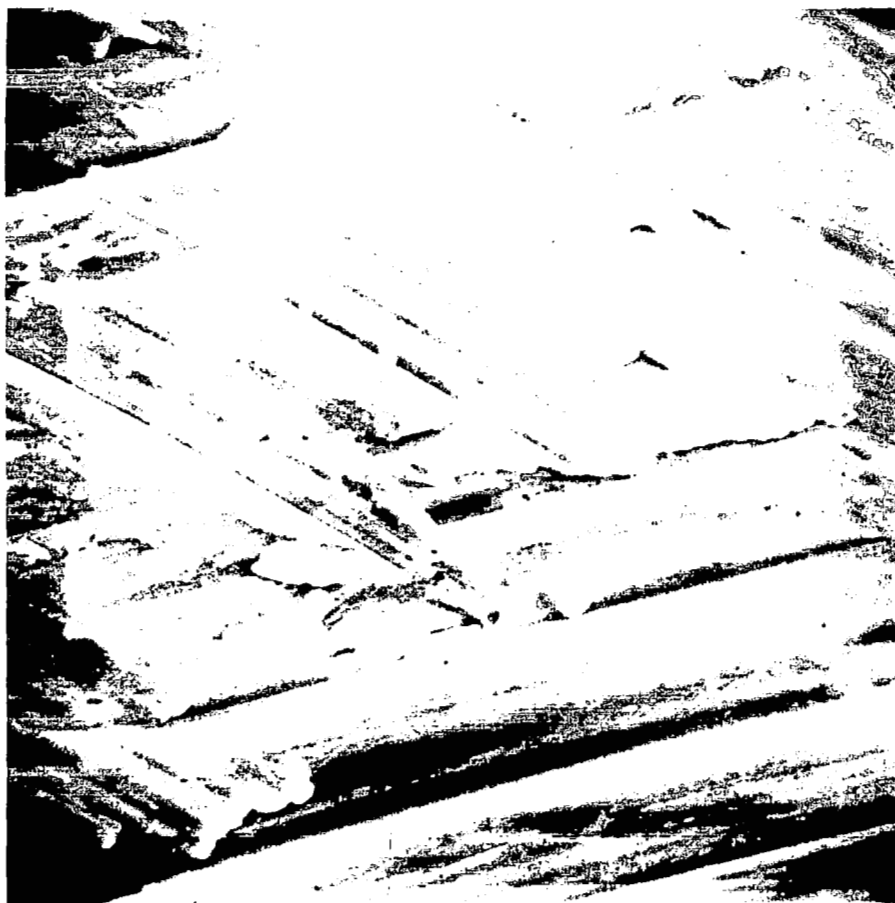
**330X**

Figure 5-10. Scanning electron micrograph of an as-machined surface.

**1100X**

NOTE: NUMEROUS TEARS AND SMEARS ARE PRESENT ON THE SURFACE.

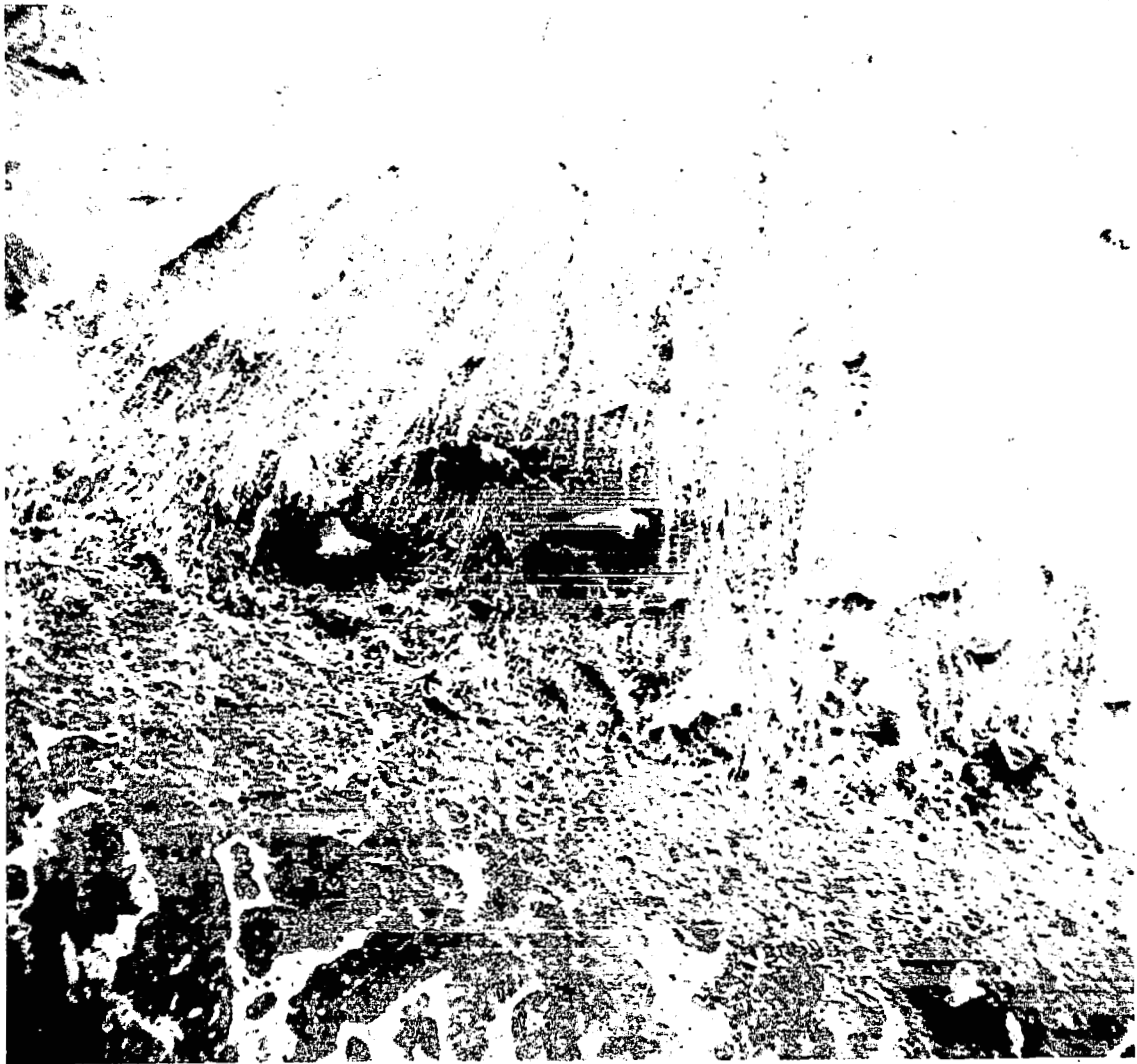
Figure 5-11. Scanning electron micrograph of an as-machined surface.



**1100X**

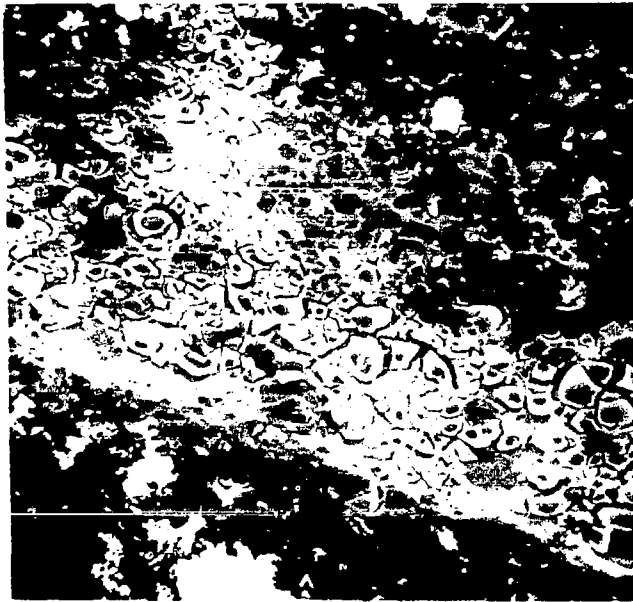
**NOTE: THIS SURFACE IS SIMILAR IN APPEARANCE TO  
THE AS-MACHINED SURFACE. CROSS MACHINING  
MARKS ARE DUE TO TOOL CHATTER.**

Figure 5-12. Scanning electron micrograph of a trichlorethylene-rinsed surface.



NOTE: NOTICE THE THIN RESIDUE AWAY FROM THE FUSION LINE WHICH IS PROBABLY A PRODUCT OF TRICHLORETHYLENE.

Figure 5-13. Scanning electron micrograph of a spot weld fracture of as-machined specimen.



340X



5500X

NOTE: NOTICE THAT PARTICLES ON SURFACE ARE MUCH DIFFERENT FROM OXIDE FLAKES.

Figure 5-14. Scanning electron micrograph of chemically cleaned surface in region of oxide spalling.

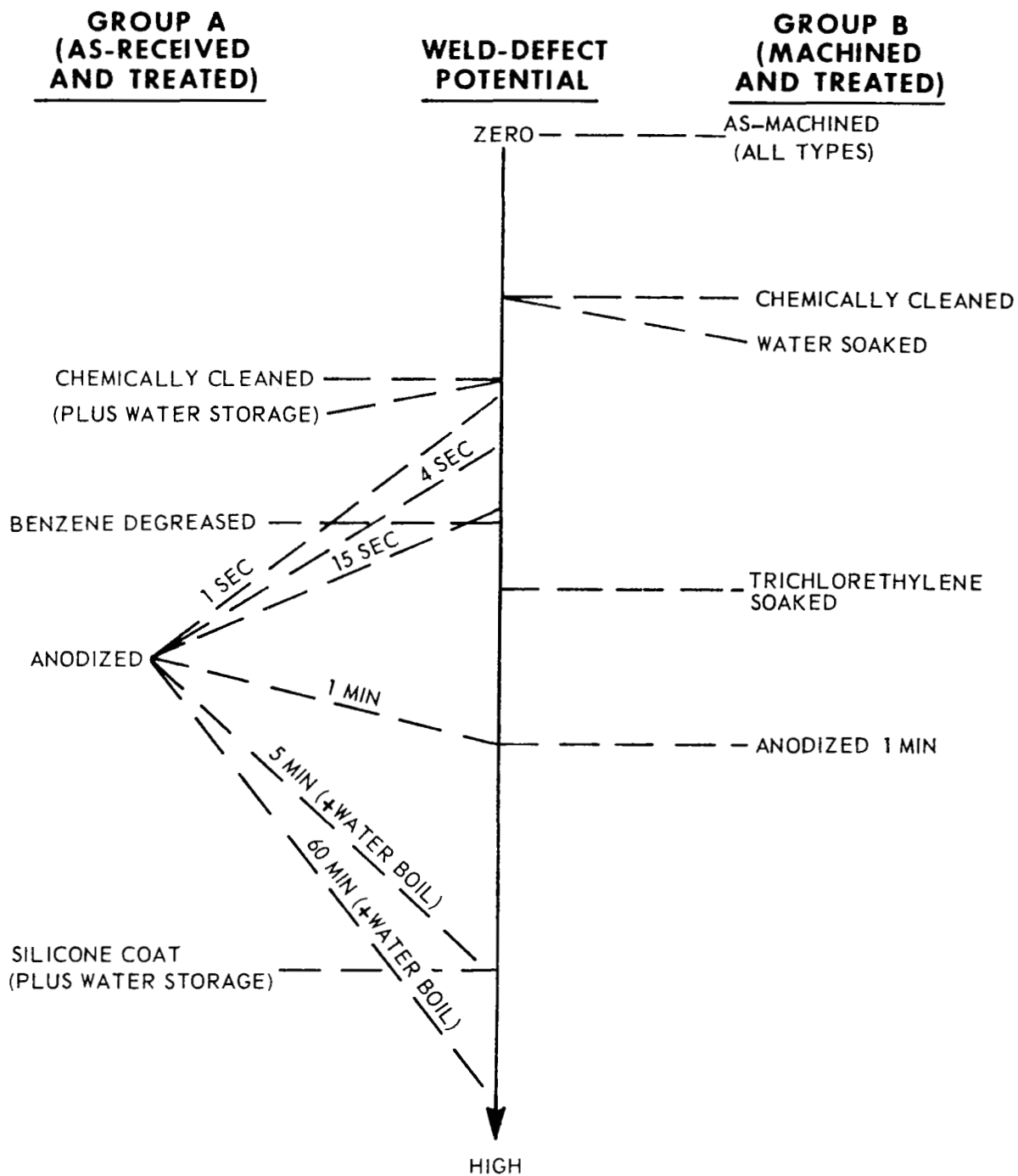


Figure 5-15. Scale of weld-defect potential of various surface preparations.

# STANDARDIZATION TESTS

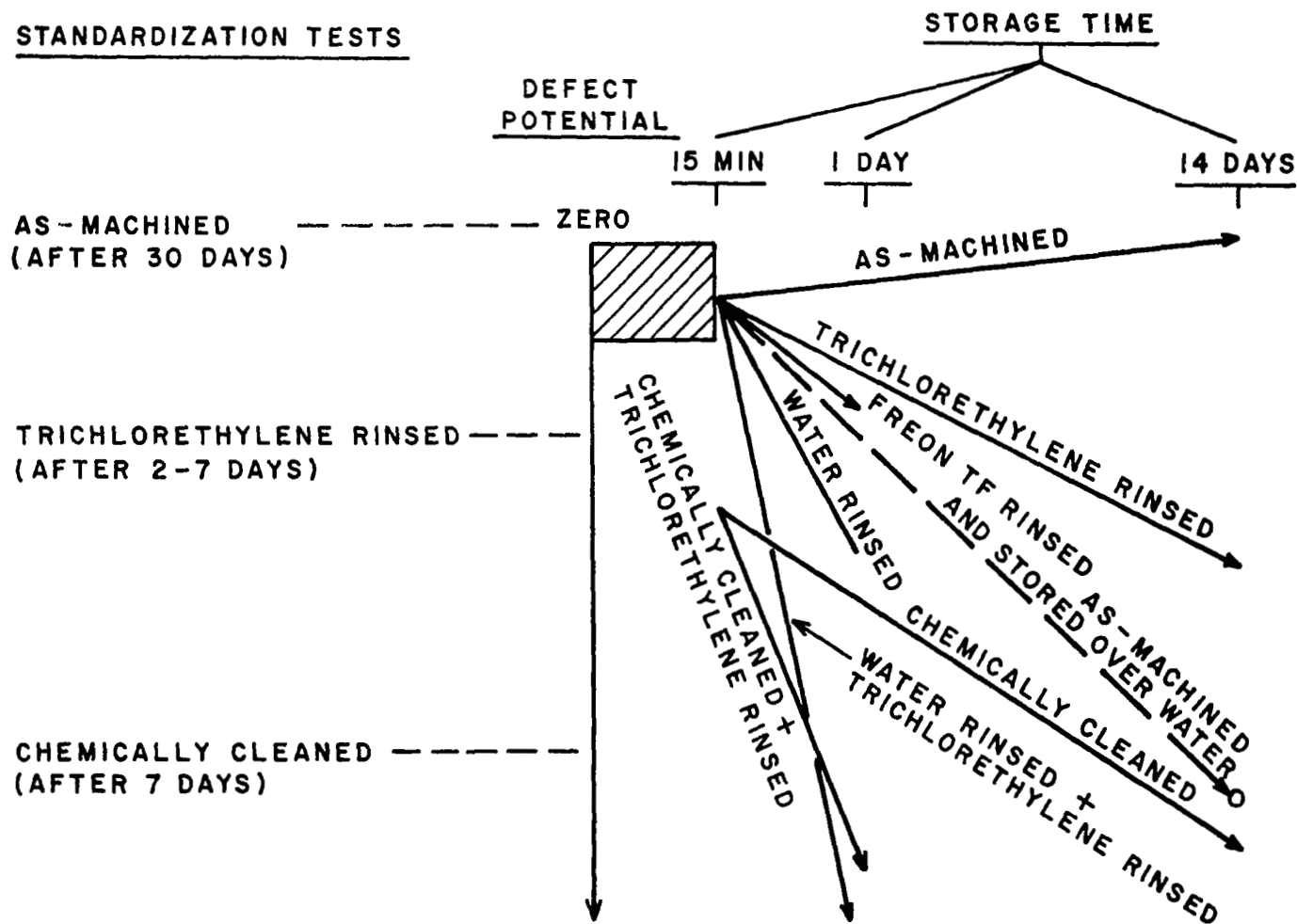


Figure 5-16. Weld-defect potential scale for both standardization and storage effects tests.

(without coolant), can produce a very low defect-potential surface. (The as-machined surface should be superficially wiped prior to machining to remove excess contamination.) This surface is characterized by the normal topographical features produced by machining (that is, tears, pits, waves) and naturally formed hydrated oxide layer (approximately 100 Å or less in thickness). Surfaces machined to 50-200  $\mu\text{in.}$  peak-to-peak finish in an ambient air atmosphere (72° F, 50-60% RH) contain at least 0.01-0.05  $\mu\text{g}/\text{cm}^2$  of water in the hydrated oxide surface layer. This level of contamination alone does not ordinarily produce significant weld defects. From a practical or technical standpoint the "machined" surface condition represents the best condition for welding.

3. Degreased Surfaces. Organic residues and debris are commonly removed by degreasing treatments prior to welding. However, the results of this program have demonstrated that the solvent itself may be adsorbed on the surface and create a significant weld-defect potential. Adsorption of trichloroethylene on 2014 surfaces can exceed 500  $\mu\text{g}/\text{cm}^2$ . Such concentrations are equivalent to at least 10 times the threshold hydrogen concentration above which porosity will form. Furthermore, trichloroethylene is chemically adsorbed and hence desorbs very slowly at ambient conditions. Upon welding trichloroethylene degreased surfaces, an irreversible desorption reaction produces solid reaction products which can become entrapped (as inclusions) within the solidified weld. Therefore, porosity and solid inclusions are caused by absorbed trichloroethylene.

Exploratory work with benzene and Freon-TF indicated that similar damaging adsorption reactions occur. Degreasing with trichloroethylene represents, at best, a process whereby one type of organic contaminant is exchanged for or diluted



with another and adsorbed on the surface. The weld-defect potential produced by the exchange or dilution will vary depending upon the composition of the adsorbed species involved. The defect potential of trichloroethylene rinsed surfaces tends to worsen as the surface ages during storage. The mechanism of degradation is unknown, although it is associated with the increased incidence of oxide inclusions and microporosity. These results show that trichloroethylene degreasing, prior to welding, should be avoided unless followed by a machine cutting operation which removes the contaminated surface. Solvents other than trichloroethylene may be more or less damaging than trichloroethylene; however, any solvent will be adsorbed to some extent and individual evaluations are necessary to determine the effects.

#### 4. Water-Rinsed Surfaces and Ambient Humidity Effects.

Water-rinsing adds to the water burden which already exists in the hydrated oxide layer or entrapped in topographical defects. At least  $0.1 \mu\text{g}/\text{cm}^2$  of water can be added by rinsing, however, natural desorption in the ambient atmosphere can cause a gradual reduction of the concentration. High humidity will retard the rate of desorption. Prolonged storage in saturated air will lead to substantial adsorption of water, and an estimated  $1.0 \mu\text{g}/\text{cm}^2$  can be adsorbed during a seven day storage period. Any added water burden naturally increases the weld-defect potential and should, therefore, be avoided. Water rinsing should not be employed as a final processing step just prior to welding, and prolonged ambient temperature storage cannot be relied upon to produce significant surface desorption.

5. Chemically Prepared Surfaces. Conventional hot sodium hydroxide-nitric acid chemical "cleaning" produces a surface which exhibits an unusually high defect potential. Both porosity and gross oxide-type inclusions are produced by this type of surface treatment. The water of hydration will exceed a measured  $0.7 \mu\text{g}/\text{cm}^2$ , and the surface itself is characterized by a relatively thick (1,000 to 10,000 Å), fragile complex refractory oxide layer. The complex oxide layer is easily fragmented and tends to become entrapped within the solidified weld or along the fusion line. Often macroporosity is associated with the entrapped oxides, apparently caused by the localized dissociation of water of hydration.

Desorption from a chemically prepared surface is a two-stage process where reversible water of hydration is desorbed at temperatures below  $750^\circ \text{F}$ . At temperatures between  $750^\circ \text{F}$  and  $970^\circ \text{F}$  irreversible desorption occurs, but the products of desorption have not been identified. Thermal desorption did not appear to improve the defect potential since the refractory oxide layer remains behind to form inclusions or lack-of-fusion defects.

The obvious conclusion from these results is that conventional sodium hydroxide-nitric acid surface preparations should not be used to prepare 2014 and 2219 aluminum alloys for welding. If used, the surface should be deoxidized before welding.

6. Anodized Surfaces. Anodized surface layers consist of porous, hydrated,  $\text{Al}_2\text{O}_3$  films. The water of hydration tends to increase in direct proportion to the film thickness such that after a 15 second sulfuric acid anodizing treatment the water concentration exceeds  $0.7 \mu\text{g}/\text{cm}^2$ ; after 1 minute the concentration exceeds  $1.0 \mu\text{g}/\text{cm}^2$ . The weld-defect potential of anodized surfaces is very high. Lack-of-fusion,

oxide inclusions, and porosity are produced by the presence of anodic layers. Complete removal of anodized surfaces is essential to achieve low-defect potential.

7. Surfaces Produced by Mechanical Wire Brushing, Scraping, and Grinding. Surface procedures which employ abrasive methods such as grinding, or wire brushing and scraping cannot be relied upon to produce a minimum defect potential condition. Surface contaminants tend to become imbedded or redistributed on the surface rather than removed. The grinding wheel, brush, or scraping blade also become loaded so that contaminants from one surface region are transferred to another. Contaminated surface layers must be cut and cleanly excised from the underlying material. Wire brushing and grinding cannot be expected to accomplish this, scraping is only partially effective.

8. Thermally Desorbed Surfaces. Surface adsorption of liquids and vapors may be partially reversed by elevated-temperature desorption treatments. However, such treatments are not entirely effective. Chemically adsorbed species may not desorb, instead they undergo irreversible surface reactions which may worsen rather than improve the weld-defect potential. This type of damaging reaction appears to occur with NaOH-treated and with trichloroethylene-rinsed surfaces. Furthermore, thermal desorption will not remove oxide layers and can instead produce thicker oxides. Consequently, thermal desorption cannot be considered as a generally beneficial treatment and must be evaluated for each individual set of conditions.

9. High-Frequency Sparked Surfaces. High-frequency sparking can be effectively used to locally desorb a surface. Surface adsorbed species are desorbed and dissociated under

a high-frequency spark and even chemisorbed species may be removed. However, refractory oxide layers are not effectively dispersed by sparking and the high defect potential due to this source of contamination will tend to remain. High-frequency sparking also produces a very irregular, spongy surface which has very high adsorption potential. The surface must be protected from vapor and liquid exposure otherwise even more severe contamination may result.

10. Surfaces Produced by Combined Treatments. Ordinarily, the preparation of precipitation-hardenable aluminum alloys for welding involves many individual processing steps. Some are planned as "cleaning" processes, whereas some are used for other reasons (e.g., heat-treatment, adhesive bonding, corrosion protection, etc.). Each process and related storage condition will produce a different surface which may possess improved or degraded defect potential compared to the prior condition. Generally, the defect potential is increased in a compounded manner. The complexity of surface reactions makes it very difficult, if not impossible, to predict or measure synergistic effects. The weld-defect potential may be assessed by means of the horizontal spot-weld test. Undoubtedly, the safest procedure to minimize weld-defect potential is to mechanically remove prior surfaces using an "undercutting" process. The low defect potential of "as-machined" surfaces may thereby be achieved.

#### 5.4 Composition of Base Plate and Filler Metal

Another possible source of porosity is some variables in the composition of base plate or filler metal. Study 2 conducted at Battelle Memorial Institute has revealed that composition of base plate and filler metal should cause little problem. (9,10)

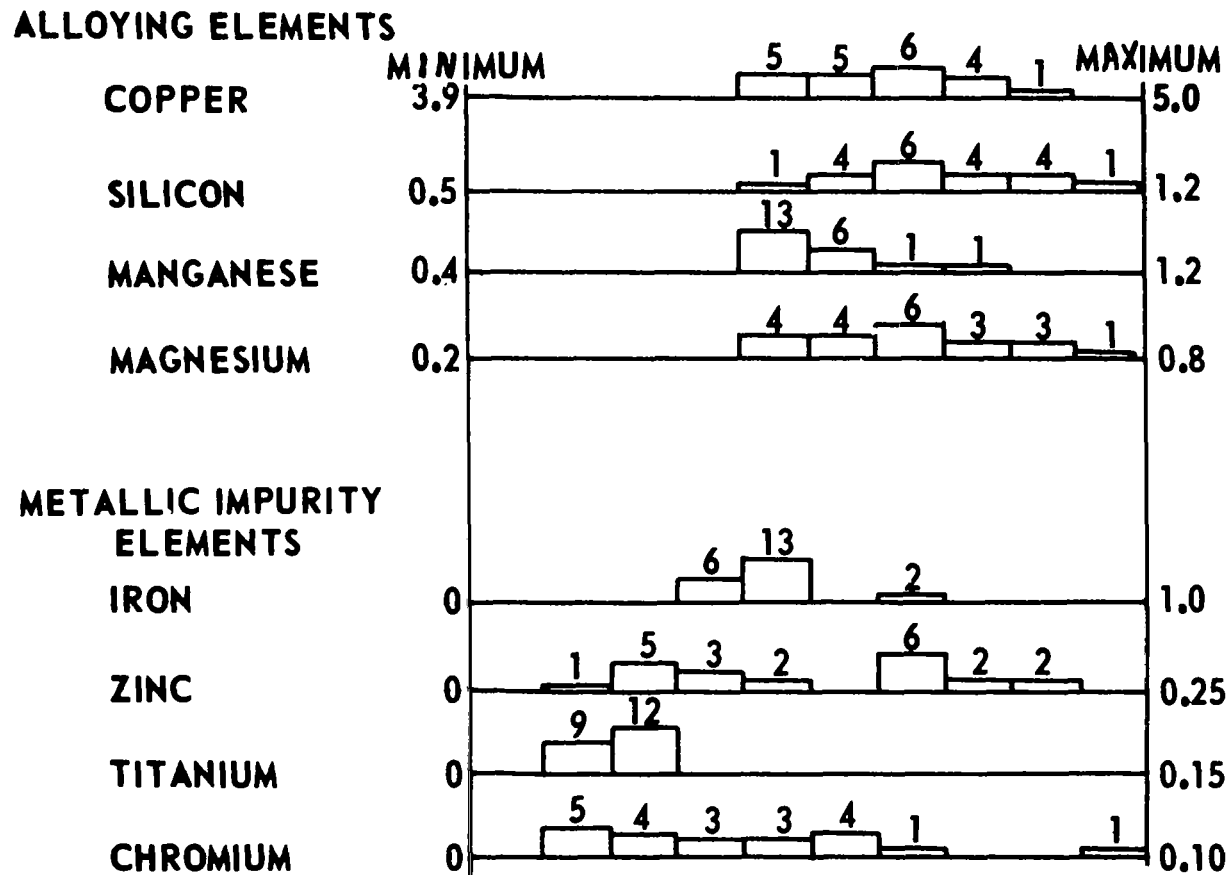
Research Procedures. The study was conducted in two phases. During the first phase, an evaluation was made of the effects on weld-defect potential of four factors:

- 1) Shielding-gas moisture content
- 2) Alloying elements
- 3) Metallic impurities
- 4) Internal hydrogen content.

Two experimental base-metal alloys, X2014-T6\* and X2219-T87 in 1/4- and 3/4-inch-thick plates, and two experimental filler wires X4043 and X2319 were used. Battelle set the alloy content at one of two levels, classified as high and low. Alloying elements at the low level were near the specified minimum and impurity elements were almost nonexistent. Battelle prepared 38 separate experimental compositions.

In the second phase, commercial-alloy base plates were used, and they were welded with experimental filler wires. Figure 5-17 shows the range of compositions for twenty-one 2014-T651 base plates.

In both phases, bead-on-plate welds were made by the GTA process in the horizontal position. Welds were made in a chamber, which had been vacuum-purged and filled with helium. With this set-up, water vapor could be added as a shielding-gas contaminant.



NOTE: NUMERAL INDICATES NUMBER OF HEATS THAT FALL WITHIN EACH INTERVAL.

Figure 5-17. Ranges of composition for 2014-T651 base plate welding <sup>(3)</sup>.

Findings. A statistical analysis was employed to study the effects of the experimental variables on weld porosity. Battelle investigators concluded that the base-plate and filler-metal compositions are not likely to be significant sources of porosity as long as (1) shielding gas and surface contamination are controlled at low levels and (2) base plates and filler metals are carefully prepared to meet the present specification with no gross hydrogen contamination. On the basis of findings, there is apparently no reason to change the present NASA specification for base-plate and filler-metal compositions.

## 5.5 Methods for Controlling and Eliminating Porosity

In the NASA research program on welding aluminum, several attempts were made to develop methods for controlling and eliminating porosity. The following pages discuss:

1. Surface hydrogen analysis
2. Surface preparation
3. Monitoring shielding gas purity
4. Other methods including (1) use of hydrogen getters, (2) magnetic arc shaper and molten metal stirrer, and (3) cryogenic cooling.

### Surface Hydrogen Analysis (4,28)

A research program was conducted at the Boeing Company to determine the level of hydrogen contamination of the metal surface.

Background. The specific problem prompting this investigation is the porosity found in the horizontal weld made when joining two sections of the 33 ft diameter Saturn Booster (Figures 5-18 and 5-19). The tooling setup is shown in Figures 5-18 and 5-19; the time required in jiggling up the entire part is about eight hours. The two parts are held by Hawthorn clamps positioned every six inches along the joint. Most of the time is spent placing and adjusting these clamps. This cut was at first a slot but then altered by tapering the edges to prevent entrapment of contamination. When the clamps are adjusted to reduce the misfit to a minimum, a tack weld is made between each clamp one after the other as the clamps are removed. After all the clamps have been removed, the joint is welded in one continuous pass, if possible, covering all the tacks and the gaps left by the clamp slots. Some



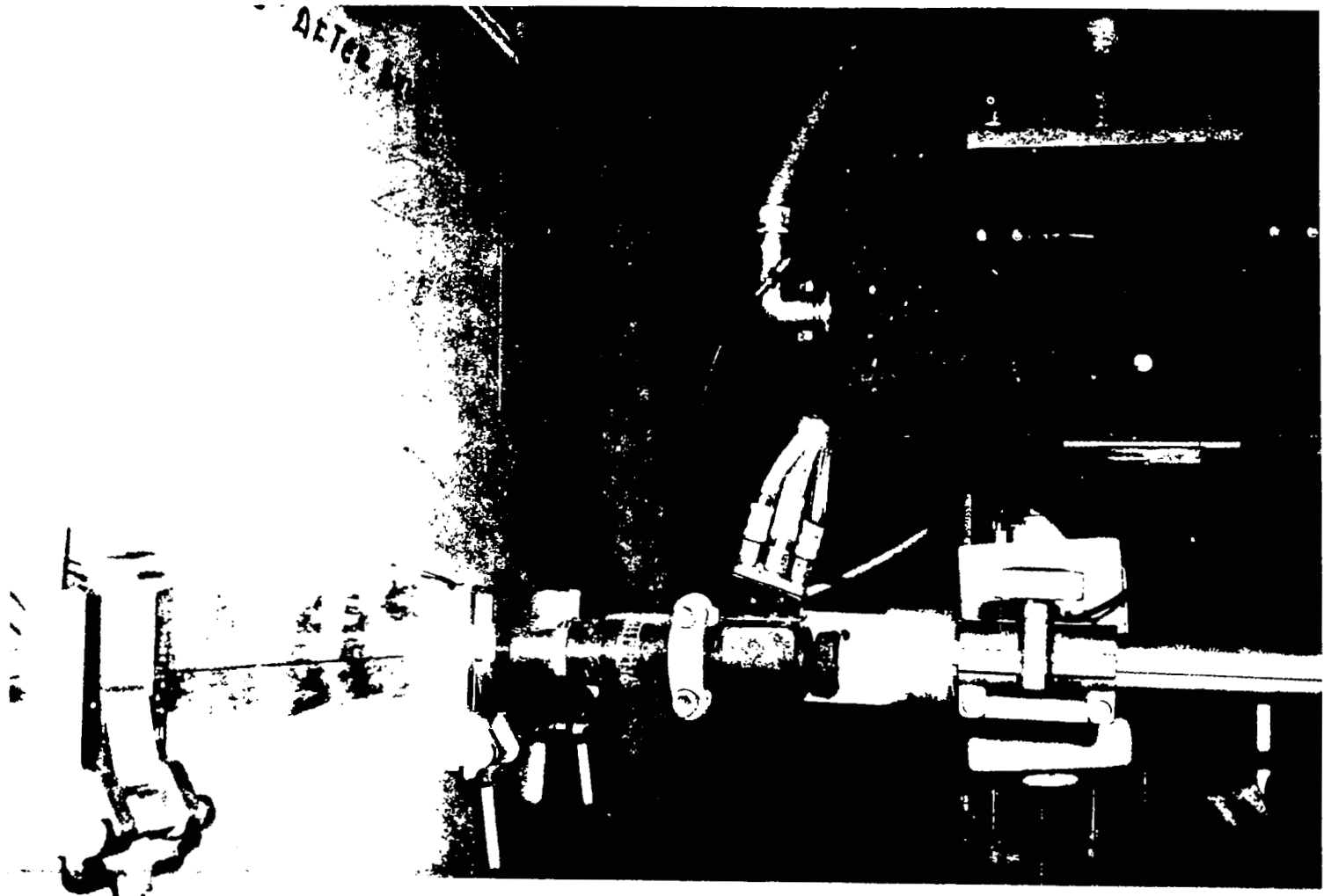


Figure 5-18. Welding head and local tooling clamps in position for making horizontal weld in 160 inch diameter tank.

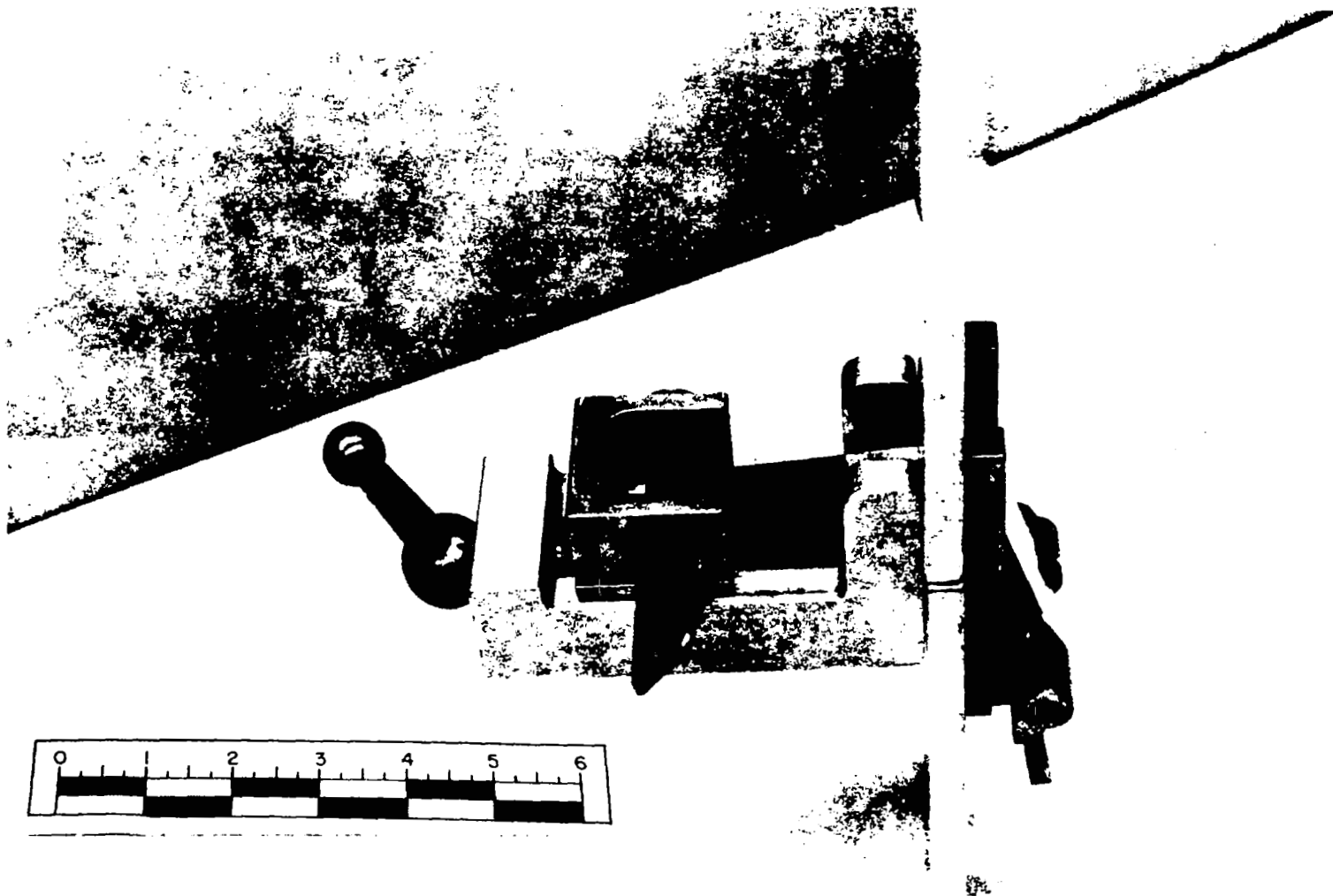


Figure 5-19. Two pieces of 1/2 inch aluminum plate aligned for welding using local tooling clamp.

welds showed considerable porosity, some of which appears to be associated with the clamp slot location.

Test welds made at NASA did not produce porosity when the same materials were used. These test welds were prepared in the same way with the exception of clamp slots, tack welds, misfit, and the lengthy handling and metal-to-metal rubbing at the joint. Thus the conclusion was reached that clamp slots, tacks, joint misfit and metal movement contribute to the observed porosity.

The significant differences between the Saturn welds exhibiting porosity and the test weld are: First, the large amount of handling of the surface in preparing Saturn weldments. Second, tack welds are known to produce surface contamination that can lead to porosity. Third, considerable rubbing and abrading of faying surfaces occurred during set-up.

These conditions result in chemical changes in the surface, changes that could involve hydrogen and, therefore, could produce porosity. Even though white gloves are worn, the time period is long enough for severe contamination to occur. Tack welds could result in porosity forming a surface deposit. Whenever two aluminum surfaces are rubbed enough to cause galling, the new metal exposed can react with water present in the air. If sufficient moisture is present, the galled metal can be pockets of high hydrogen concentration and thus lead to porosity during weldings. These considerations led to a series of tests utilizing the measurement of surface hydrogen.

Operation of Analyzer. The surface analysis was carried out using a very sensitive hydrogen detector recently developed by Das and Strobelt under Boeing funded R & D program. The instrument is capable of detecting bulk as well as surface hydrogen in metals and has a detection sensitivity of

as low as few parts per billion in a gas stream. Besides having a high sensitivity this instrument is unique from the point of view of simplicity of handling and low cost investment. It is simple enough to be used for an on-line or in-process inspection on a continuous basis in a manufacturing operation, or used for defining procedures for a specific manufacturing process.

A schematic of the surface hydrogen analyzer is shown in Figure 5-20. The plate under test is fastened securely on a spark chamber and sealed by means of an "O" ring. This apparatus is shown in Figure 5-21. The spark used to extract hydrogen is low energy, supplied by a high voltage, high impedance direct current power supply. The energy supplied (ca. 5 watts) is not enough to vaporize a measurable amount of metal. The hydrogen thus liberated is directed to an activated palladium barrier under a positive pressure of high purity argon (carrier gas). The palladium barrier lets only hydrogen permeate through it while being impermeable to argon. On the other side of the barrier is an ion pump. Thus, the palladium barrier has a high vacuum on one side of it and one atmosphere pressure on the other side. The vacuum in the ion pump chamber is measured by the current through the pump and is recorded on a strip chart recorder. Once the pump has reached its base vacuum any diffusion of hydrogen through the palladium barrier will result in an increase in current. The current through the pump is directly proportional to the pressure, which establishes a relationship between the amount of hydrogen in the gas stream and the pump current. This makes it possible to estimate the amount of hydrogen in a gas stream from an unknown source.

Calibration is performed by using an electrolysis cell to generate known amounts of hydrogen. The electrolyte used is a saturated solution of potassium hydroxide. The

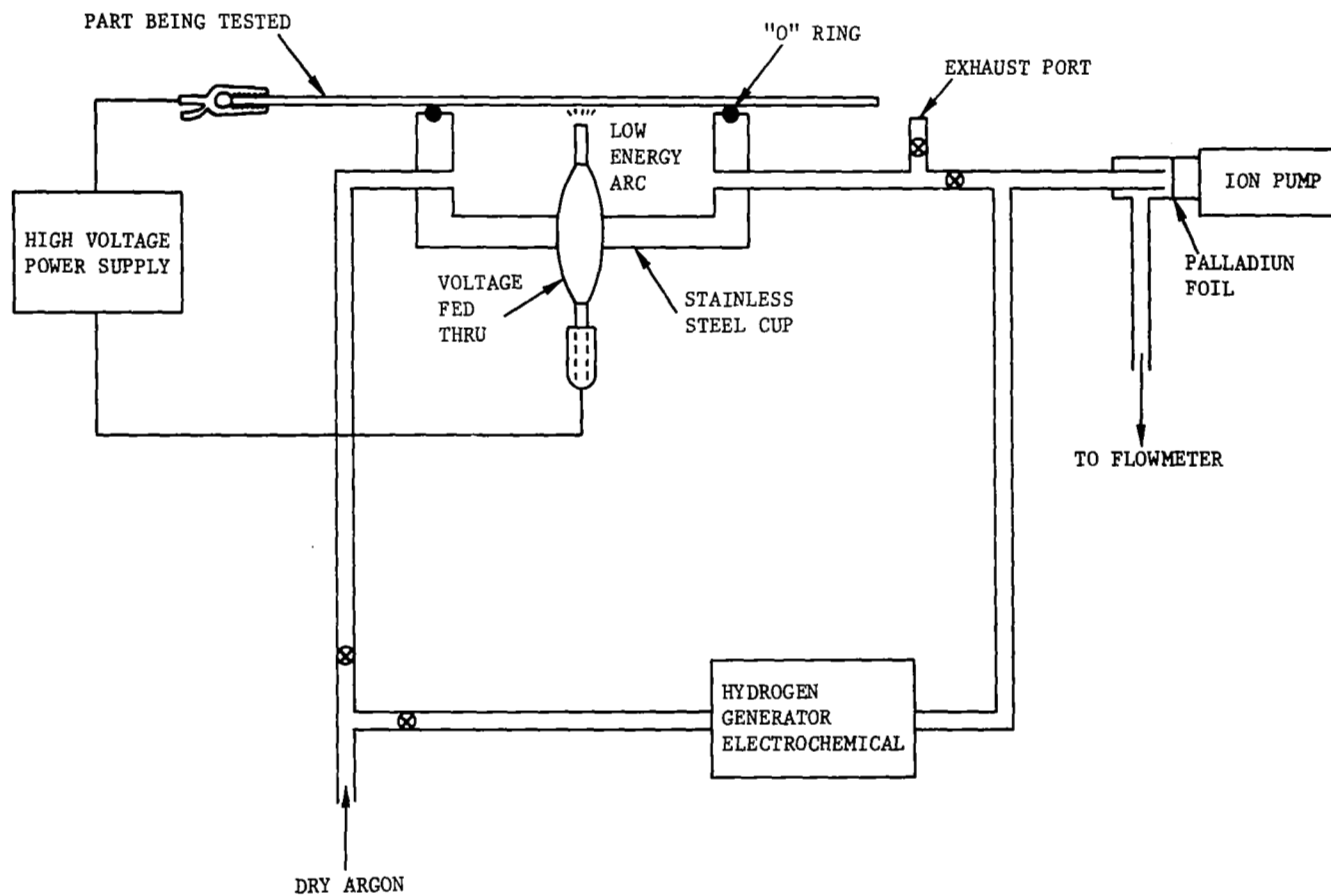


Figure 5-20. Schematic of surface hydrogen measurement equipment.

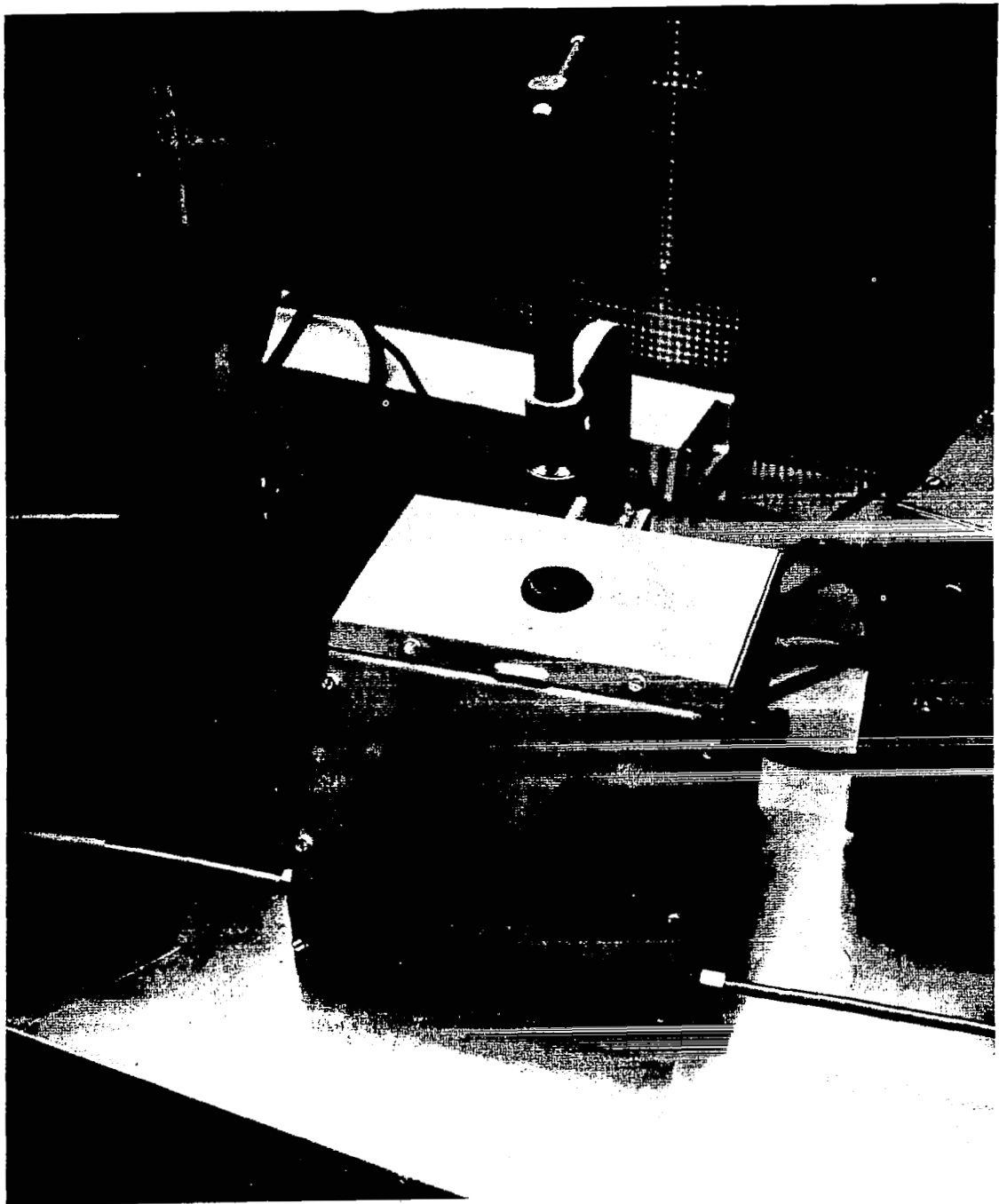


Figure 5-21. Spark chamber for surface hydrogen analysis.

hydrogen thus generated is mixed with pure argon and directed towards the palladium foil. A carrier gas flow of 100 cc/min. was used throughout these tests. The temperature of the palladium foil is maintained at about 560° C for adequate diffusion of hydrogen through the foil. By varying the current in the electrolysis cell the response of the ion pump can be calibrated. 76.5 parts per million of hydrogen are carried through in the gas stream at a flow of 100 cc/min. per d.c. milliampere through the cell. Once the detector is calibrated in this manner, it is a simple matter to estimate quantitative amounts of hydrogen in the gas stream from an unknown source.

Figure 5-22 shows the calibration curve for the detector as obtained under the conditions given below:

Total flow rate (50 cc/min. through the electrolytic cell and 50 cc/min. through the spark chamber) of argon = 100 cc/min. Palladium disc temperature -- 560° C.

The calibration curve shows the detector response in microamperes as a function of hydrogen concentration of ppm in the carrier gas stream as generated by the electrolysis cell. It is observed that below 20 ppm of hydrogen concentration in the gas stream the curve deviates slightly from linearity. This is because the efficiency of the ion pump for hydrogen at such low concentration levels is reduced. Since the data in the entire calibration range is quite repeatable, the non-linearity does not affect the surface hydrogen analysis.

Once the calibration of the detector is performed, extreme care is exercised to maintain the same conditions of palladium disc temperature and argon gas flow to insure consistent results. When surface analysis is carried out, it is necessary to have a constant background of .05 ma through the electrolytic cell (4 ppm) to maintain detector sensitivity. Argon is supplied from a bottle of high purity

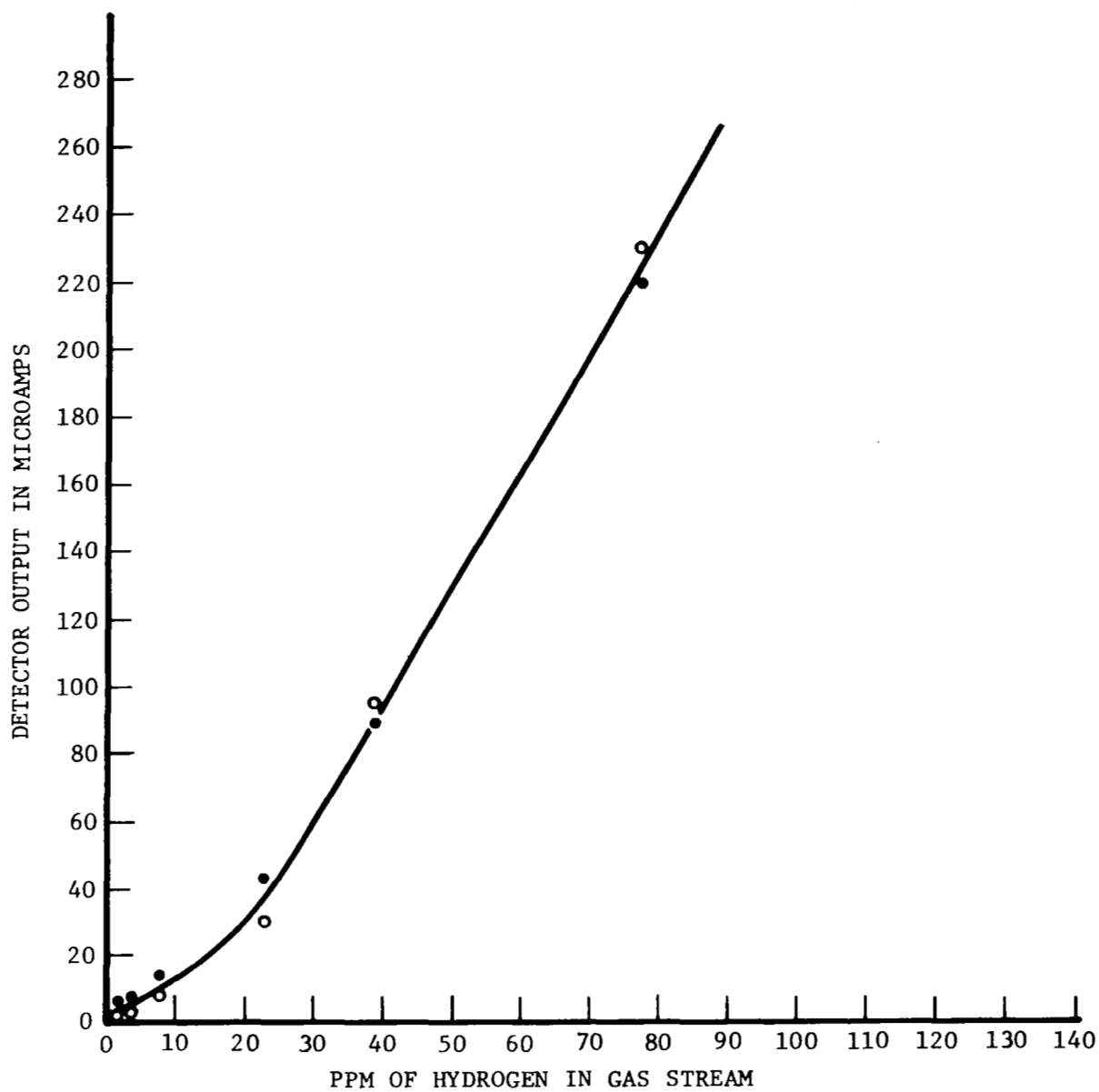


Figure 5-22. Calibration of hydrogen detector.



liquid argon. Since the temperature of liquid argon is  $-193^{\circ}\text{C}$  there is very little water present, significantly less than one part per million. All surface measurements were made on bare 7075-T6 aluminum alloy samples prepared by vapor degreasing and alkaline cleaning.

Figure 5-23 shows a typical result. Within a few seconds after turning on the power to the spark source, an initial peak is noted. After about 3 to 5 minutes of continuous arcing the curve begins to fall off. Within 30 minutes it reaches a constant level and further arcing produces no change in the curve. It is believed that the initial high hydrogen peak is due to surface contamination. The portion of the curve after the peak should then be representative of a clean surface. When the power is shut off, the signal level is observed to drop back to the original background level. If the power is subsequently turned on, no large initial increase in the hydrogen level was observed, thereby further indicating that surface contamination was removed by the initial power application. It is further observed that the signal level after the peak is considerably higher than the background level. This suggests that some hydrogen is being extracted from the interior of the metal. The difference between the peak current and the current at 30 minutes ( $\Delta I$ ) is used as a first approximation of the surface hydrogen detected. A more exact value would be obtained from the increase in area under the curve, measured on a cleaned surface.

The value of  $\Delta I$  for cleaned aluminum was found to be  $93 \pm 32$ . This is an average of 15 measurements on separate pieces of the same alloy. Although all samples were cleaned the same way at one time, there was a variation in the observed value of  $\Delta I$  from one sample to the next. This variation could be due to the complex relationship between adsorbed water and oxide film.

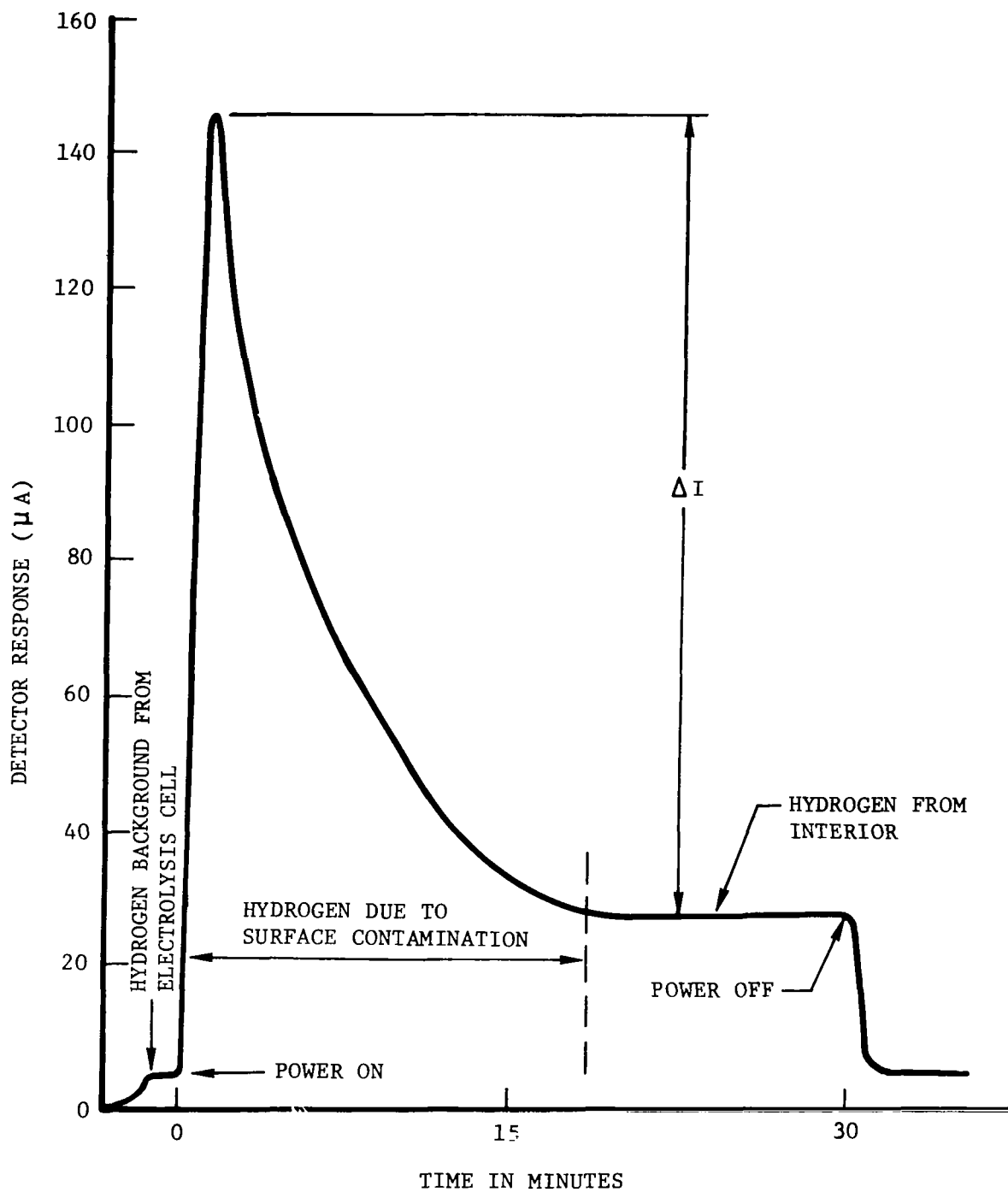


Figure 5-23. Typical result of arcing aluminum alloy surface.

All measurements were started within one minute after the test sample was mounted on the spark chamber and argon flow adjusted. This was done to prevent a change in surface due to the effect of dry argon found to occur after 30 minutes of exposure.

Surface Measurements. Figure 5-24 shows the detector response of an aluminum plate with adsorbed water. The plate was flooded with distilled water and air dried until the visible traces of water disappeared. This was accomplished in about 90 seconds. When the plate was allowed to dry for longer periods of time the value of  $\Delta I$  drops to that obtained with an untreated plate. The  $\Delta I$  value for the untreated plate was 155 while after drying in air for 1, 1.5, and 3 hours the values were 85, 60, and 170 respectively (equal within experimental error).

This series of measurements demonstrates the relative speed at which wet aluminum dries and reaches equilibrium with moisture in the air. The atmosphere of the laboratory in which these measurements were made is controlled to 50% relative humidity and 21° C temperature.

Since scraping the surface is a common method used in preparation for welding, it is necessary to measure the amount of surface water before and after scraping. The results of three different plates showed no difference between scraped and unscraped surface hydrogen levels. The  $\Delta I$  values were 119 and 135, 59 and 105, 90 and 73 representing before and after scraping respectively. These are all within experimental error of the same value.

These two experiments demonstrate the rapidity with which water adsorbed on aluminum reaches equilibrium with water in the atmosphere. These values could be affected to

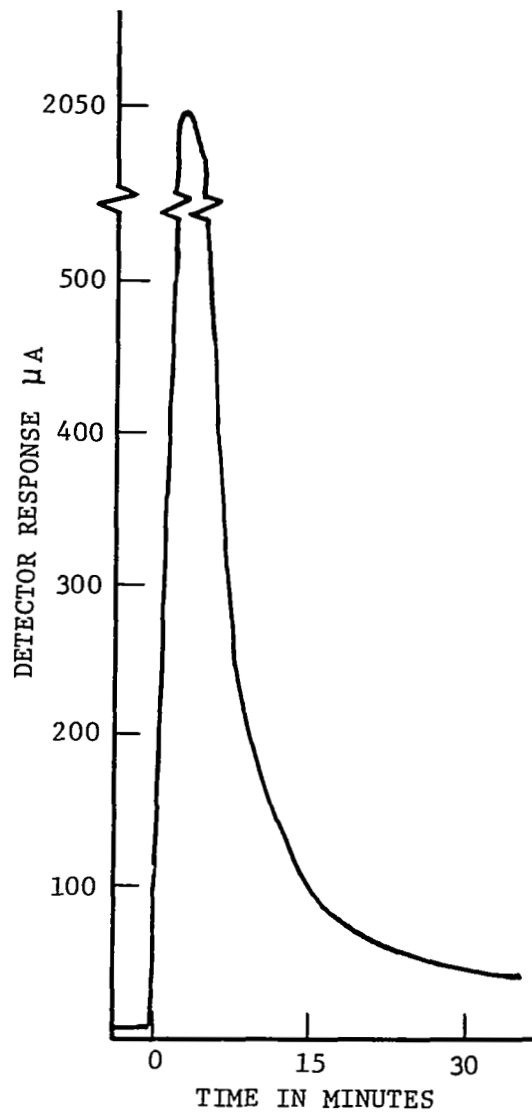


Figure 5-24. Hydrogen resulting from surface water.

a limited extent by changes in humidity, however, it appears that adsorbed water is not a potentially severe problem.

#### Tack Welds As a Source of Surface Contamination

Tack welds were prepared using a hand held torch with helium shield gas. The measurements were made 4.5 minutes after welding. The following  $\Delta I$  values were obtained:

Alternating current with filler wire	-- 195 ua
Direct current with filler wire	-- 65 ua
Direct current without filler wire	-- 80 ua
Direct repeat	-- 85 ua

The  $\Delta I$  value of 195 for an a.c. tack weld represents a contamination level above that found for an untreated surface. However, the other three values do not represent an increase in contamination. The fact that the one tack weld showed a slight increase in contamination suggests a possible problem but perhaps not a serious one under the conditions of these tests. Other conditions may produce problems but would require considerably more experimentation to determine if a problem does exist.

Handling As a Source of Surface Contamination. With the surface hydrogen detector, it is possible to measure small amounts of hydrogen or hydrogen containing material such as oil and grease deposited as a result of handling. In this series of experiments, measurements of surface contamination were made of finger prints, clean glove prints, and used glove prints.

Finger prints made by two different subjects were measured with the following results:

Subject A	$\Delta I = 1455$ ua
Subject A, repeat	$\Delta I = 1570$ ua
Subject B	$\Delta I = 975$ ua

The hands of subject A were relatively clean and dry, a normal condition, while the hands of subject B were washed with a detergent, rinsed thoroughly with distilled water, and dried with a clean towel before making the finger print.

Since the normal procedure for shop work is to use white cotton gloves when handling material for critical welds, surface contamination measurements were made of finger prints using white cotton gloves. The fingerprints were made with new clean gloves and gloves that had been worn for various lengths of time. These tests were made by subject B:

New, clean gloves, pair A	$\Delta I = 200$ ua
another pair new gloves, pair B	$\Delta I = 335$ ua
glove worn for 0.5 hours, pair C	$\Delta I = 360$ ua
glove worn for 1.0 hours, pair A	$\Delta I = 455$ ua
glove worn for 1.5 hours, pair B	$\Delta I = 435$ ua
glove worn for 2.0 hours, pair B	$\Delta I = 420$ ua
undetermined time, pair D	$\Delta I = 425$ ua

These gloves were worn in the laboratory under normal working conditions; no effort was made to either keep them especially clean or to contaminate them with grease or oil. These data clearly show that contamination cannot be avoided even through the use of white cotton gloves. While cotton gloves reduce the level of contamination by a substantial amount, the contamination level resulting from even new gloves indicates a severe potential for porosity if the faying surface has been touched. Our welding foreman stated that perhaps we would have cleaner welds if white gloves were not used. Then the mechanics would realize that they were positively not to touch the joints.

Use of Freon to Remove Contamination. Since the most likely source of surface hydrogen appears to be organic rather than absorbed water, a cleaning method involving a

solvent rinse might be in order. A likely choice for solvent is "Freon" 113 ( $C_2Cl_3F_3$ ) since it does not contain hydrogen and is a good general solvent. In order to demonstrate that no problem would be encountered in using "Freon" 113, several measurements were made of the contamination remaining after use. "Freon" used for this series of tests had been distilled to ensure no hydrocarbon contamination. The test sample was flooded with "Freon" as might be done in washing a part in preparation for welding. The "Freon" was not, however, wiped on as is sometimes done since contamination is not as easily removed by this method. Two measurements of  $\Delta I$  after washing with "Freon" 113 gave values of 35 and 60, experimentally equal to the value of  $\Delta I$  before treatment.

"Freon" 113 prepared by distillation in the same way, was used to wash weld joints (described below) prior to welding. In order to properly wash the joint a polyethylene squeeze bottle was used to direct the stream of "Freon" into the weld joint. After the bottle was in use for about a week the surface contamination was again checked. This time a  $\Delta I$  value of 3735 ua was found indicating a severely contaminated surface. It was apparent that the "Freon" had become contaminated from the polyethylene bottle even though the bottle was new. To check this conclusion the bottle was rinsed several times with "Freon" then let stand for about 4 days. This "Freon" was compared to the original "Freon" with a Beckman IR-12 infrared spectrophotometer. The original "Freon" contained no hydrocarbons while that stored in the polyethylene bottle contained 154 ppm. These data clearly demonstrate the need for careful handling of "Freon" or any other solvent for this use. A metal container with no organic parts would be required to prevent contamination of this nature.

Significance of  $\Delta I$  Values. It is possible to make an estimate of the amount of hydrogen from the observed value of  $\Delta I$ . The area under the curve is related to total amount of hydrogen removed from the surface by the following equations:

$$\frac{it}{2} \times \frac{E}{96,500} = w$$

$$\frac{W}{2} \times 22,400 = v$$

The area of a triangular peak is  $it/2$  and has the units of coulombs when  $i$  is in amperes and  $t$  in seconds. Coulombs divided by 96,500 and multiplied by equivalent weight (1.00 for hydrogen) gives weight in grams of material. When this is multiplied by  $E$ , efficiency of the pump and palladium foil (100 in this experiment) the weight of hydrogen present in the gas stream at any one instant is obtained. Dividing the weight by the molecular weight (2.00 for hydrogen) and 22,400 the volume of hydrogen in cubic centimeters at standard temperature and pressure is obtained. For a  $\Delta I$  value of 1000 this calculation gives 1.4 cc. This value of 1.4 cc depends on the shape of the current-time curve and could be much larger for the same value of  $\Delta I$ .

In a like manner the amount of hydrogen deposited from a single fingerprint while wearing a new cotton glove is 0.4 cc. This is pure hydrogen; if it were distributed through one liter, it would be 400 ppm. This calculation clearly shows that any type of handling of the weld metal whether gloves are worn or not, will produce enough contamination to result in weld porosity.

Cleaning. The results of welding after cleaning dramatically demonstrates the role of surface contamination in porosity formation and ease of removal by the proper use of



solvents. Welds were handled and then cleaned, with porosity occurring in only one of the six welds. This handling process without cleaning resulted in measurable porosity. The welds made after cleaning but not handling help substantiate the correlation between surface hydrogen measurements and porosity. Only two welds of ten showed porosity after treatment with the "Freon". Certain welds were excluded from consideration because all were cleaned with "Freon" 113 contaminated with unknown amounts of hydrocarbons from the polyethylene bottle. No statements can be made about the correlation of porosity and various factors when this over-riding factor is uncontrolled. It was demonstrated that "Freon" picked up hydrocarbons from polyethylene but no metal container was available so polyethylene was used with a rinse prior to cleaning. Polyethylene containers do not appear to be adequate. Nevertheless, the fact that five welds of six showed no porosity after cleaning, when they were treated in a manner that produced porosity, demonstrates that porosity of this nature can be avoided. These conclusions are summarized in this table.

Summary of Porosity vs Surface Hydrogen

<u>Surface Condition</u>	<u><math>\Delta I</math>, ua (<math>\pm 32</math>)</u>	<u>Porosity</u>
Untreated	93	-
Scraped	104	No porosity
Tack weld	77	No porosity
Handling with gloves	376	Measurable porosity
Hydrocarbon contamination	3735	Significant porosity

The relationship of porosity and the surface contamination index,  $\Delta I$ , can be seen. Scraped and tack welded surfaces show the same level of contamination and no porosity, while surface

contamination and porosity both increase when the surface is touched with gloved hand. This demonstrates that the surface contamination index,  $\Delta I$ , can be used to predict porosity.

Analytical techniques for analyzing surface contaminants were previously conducted at IITRI.<sup>(20)</sup> Three techniques were found to be effective in detecting hydrogen contaminants. The first one was gas chromatography. It is a readily calibratable method which could measure adsorbed surface contaminants. It does not readily lend itself to manufacturing applications since the instrumentation and sampling techniques are quite complex.

The second technique involves radioactive tracers. This method is capable of revealing the complete adsorption/desorption cycle with minimum disturbance of the surface being measured. The radioactive tracer method, however, is mainly a research tool.

The third technique was spark emission spectroscopy. It essentially heats, desorbs, dissociates, and excites certain species which exist on the surface. The method of measurement involves the quantitative determination of relative film densities produced by exposure to spark excited spectra. This spark emission method of surface analysis appears to rate surfaces in accordance with their relative hydrogen-contamination levels.

### Surface Preparation<sup>(20)</sup>

A study was conducted at IITRI to develop new techniques.

Phase I: Conceptual study to evaluate and select surface preparation techniques and systems.

Phase II: Design and fabrication study to develop and fabricate a prototype device for weld surface preparation of aluminum components.

Phase III: Evaluation study to provide an empirical evaluation of surfaces prepared with the prototype device.

The basic concept for the system was to remove contaminated surface layers from weld surfaces and completed parts. Therefore, all parts must be final, machined with reasonably smooth surfaces prior to the surface preparation operation. A number of requirements were developed for the surface preparation methods as follows:

- 1) Surfaces must include the abutting edges of the weld grooves and 25.4 mm (1 in) widths on the adjoining surfaces.
- 2) Weld edges must be on cylinders (longitudinal and circumferential surfaces) and on elliptical and hemispherical domes; welds must be in vertical, horizontal, and inclined curved positions and in combinations of these positions.
- 3) Groove geometry must include all standard configurations including square grooves, single V-grooves, double V-grooves, and single U-grooves.
- 4) Depth of metal removal will be a minimum of 0.127 mm (0.005 in).
- 5) The finished surface roughness will be a maximum of 5.08  $\mu\text{m}$  (200  $\mu\text{in}$ ) and have a minimum of smeared metal.
- 6) Thicknesses of the aluminum material should be in the range of 2.54 mm (0.100 in) to 25.4 mm (1.00 in).
- 7) No lubricants nor any manual work will be permitted.
- 8) Other geometrical characteristics will be those that permit the best welding practices, that is, minimum waviness of edge; absence of burrs; no burning, no discoloration or contamination of surfaces; and no gouges, grooves, nicks, or undercuts.

Two techniques were investigated for preparing aluminum weld surfaces: mechanical cleaning and electric discharge cleaning. Primary emphasis was on mechanical cleaning, since the effectiveness of this method was established in a previous NASA program discussed in Chapter 5.3.

Electrical discharge cleaning was evaluated as a supplementary method to be used only if the mechanically cleaned surfaces were accidentally contaminated or exposed to a humid atmosphere for a considerable time after cleaning. Under these conditions a second mechanical preparation step might not be permissible because of dimensional tolerance limits (for example, minimum thickness or gap); consequently, an electrical discharge desorption treatment could be advantageous for restoring the surface. If effective, the electrical discharge desorption treatment would employ either the same power supply and torch used for welding, or an auxiliary power supply and electrode system would be used to achieve the proper electric discharge conditions.

Mechanical Cleaning. A practical system for preparing the welding surfaces of aluminum components was developed and demonstrated. The system consists of dry milling the abutting edges and adjacent surfaces of aluminum to remove contaminated surface layers and expose a fresh surface with a low defect potential. A prototype device was designed and fabricated to demonstrate the feasibility of the system.

The prototype device is designed to straddle the edge that is being prepared and to align with the existing edge and adjacent surfaces of the component. Depth of cut is regulated from the existing surfaces. Therefore, reasonably smooth existing surfaces and a uniform thickness are required on the component that is being prepared.

The device is equipped with an electric drive unit to provide travel and three air-operated milling motors to provide the required machining operations. The drive unit provides a mechanized uniform travel speed. The milling motors are aligned to machine the abutting edges and adjacent surfaces simultaneously.

The device was used to prepare plate edges with the plates in the horizontal welding position (Figure 5-25), downhand welding position (Figure 5-26), and vertical welding position (Figure 5-27). When simulating the lower subassembly of a part in the horizontal welding position, the device maintains contact with the plate due to gravity and the operator does not need to hold the unit. With parts in position for downhand welding, manual force is adequate to hold the device in contact with the surface of the part. Likewise, the same technique is satisfactory for the vertical position with the device moving down the component.

The prototype device was used to prepare the weld surfaces of flat and curved aluminum plates with a square butt weld joint configuration. These surfaces were evaluated on the bases of gas tungsten-arc spot and seam weld soundness, Proficorder measurements, and scanning electron microscopy. Results from these evaluations proved the technique, system, and prototype device to be satisfactory for the intended application.

Electric Discharge Cleaning. Three electrical discharge conditions were investigated:

- 1) Pulsed direct-current reverse-polarity
- 2) Radiofrequency
- 3) Steady-state direct-current reverse-polarity

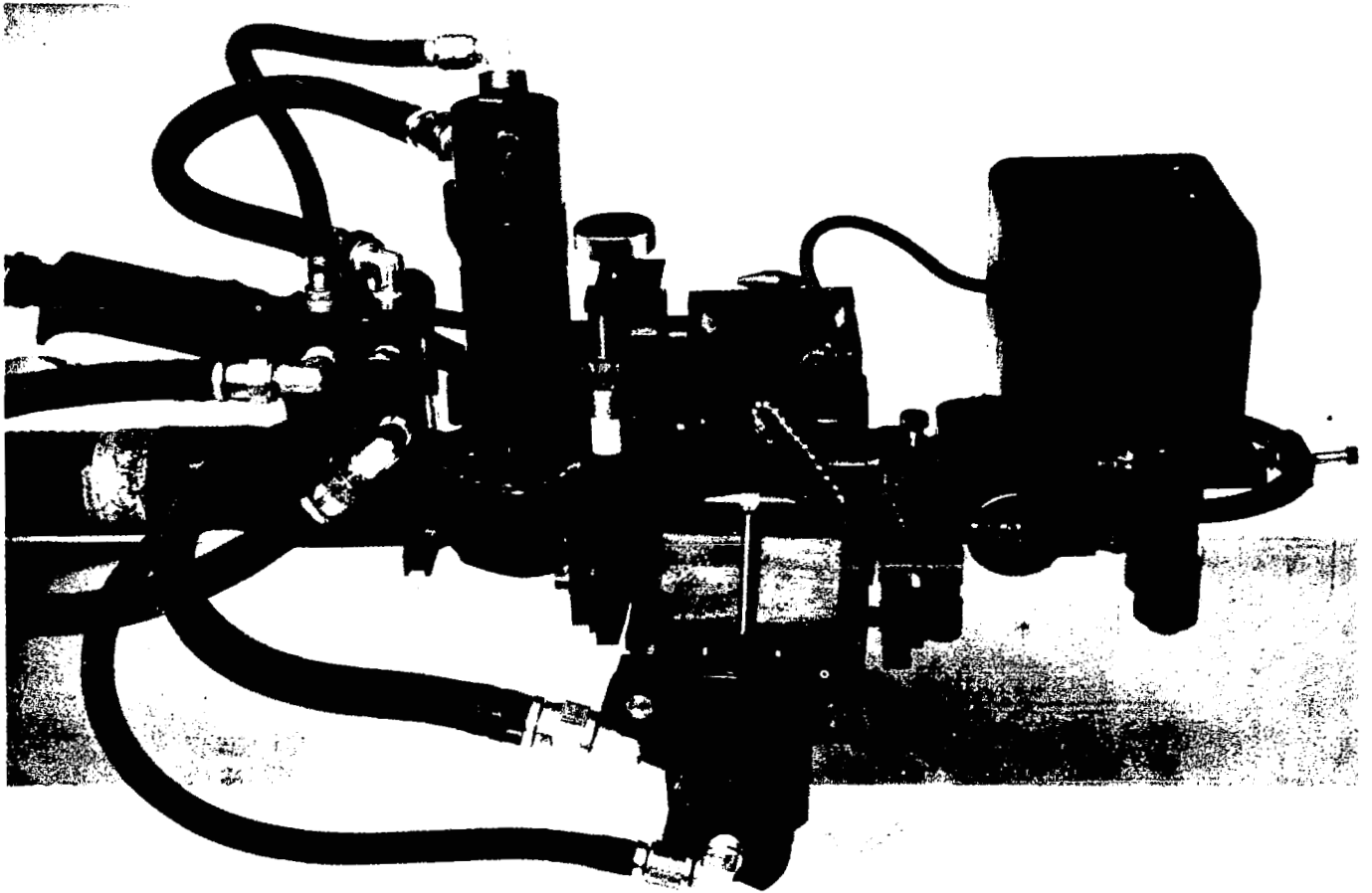


Figure 5-25. Unit in position for preparing lower part of an assembly to be welded in horizontal position.

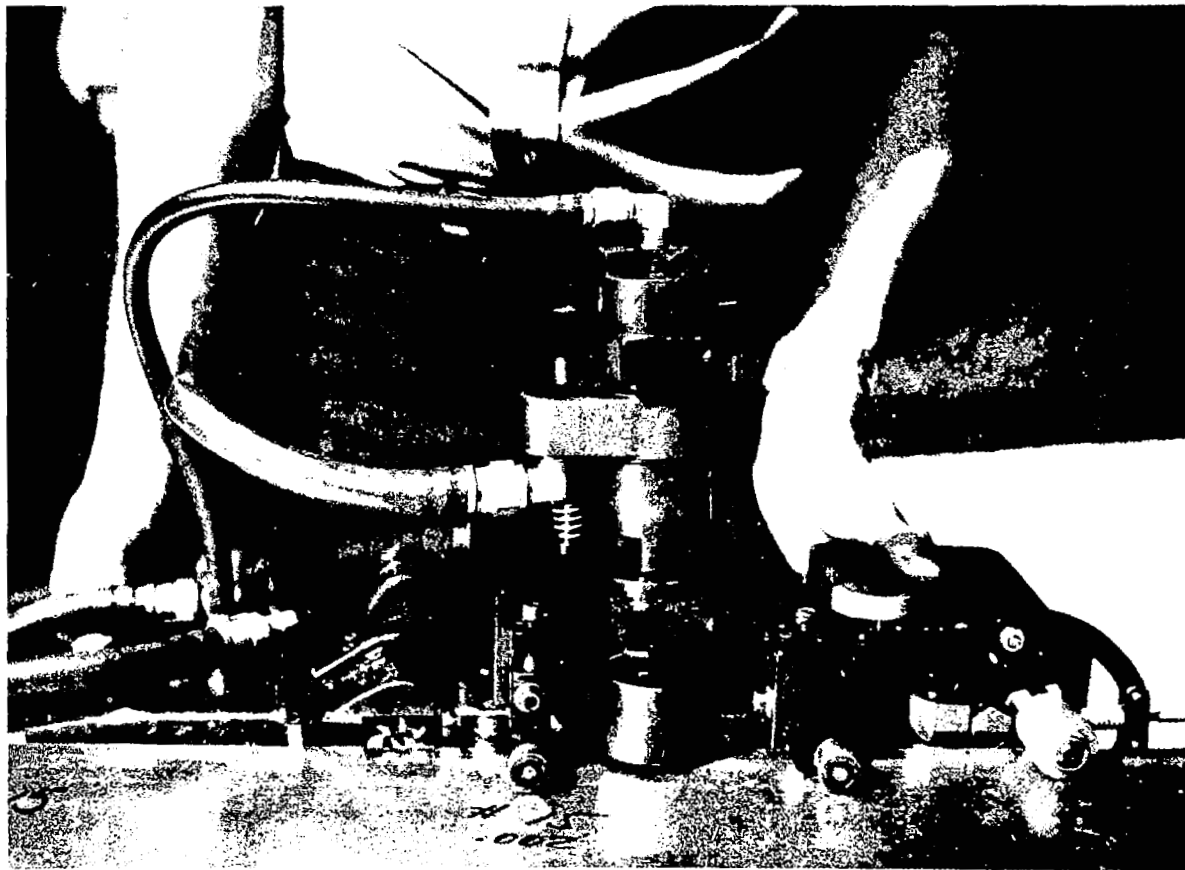


Figure 5-26. Method for holding device on plate for preparing surfaces in down-hand welding position.

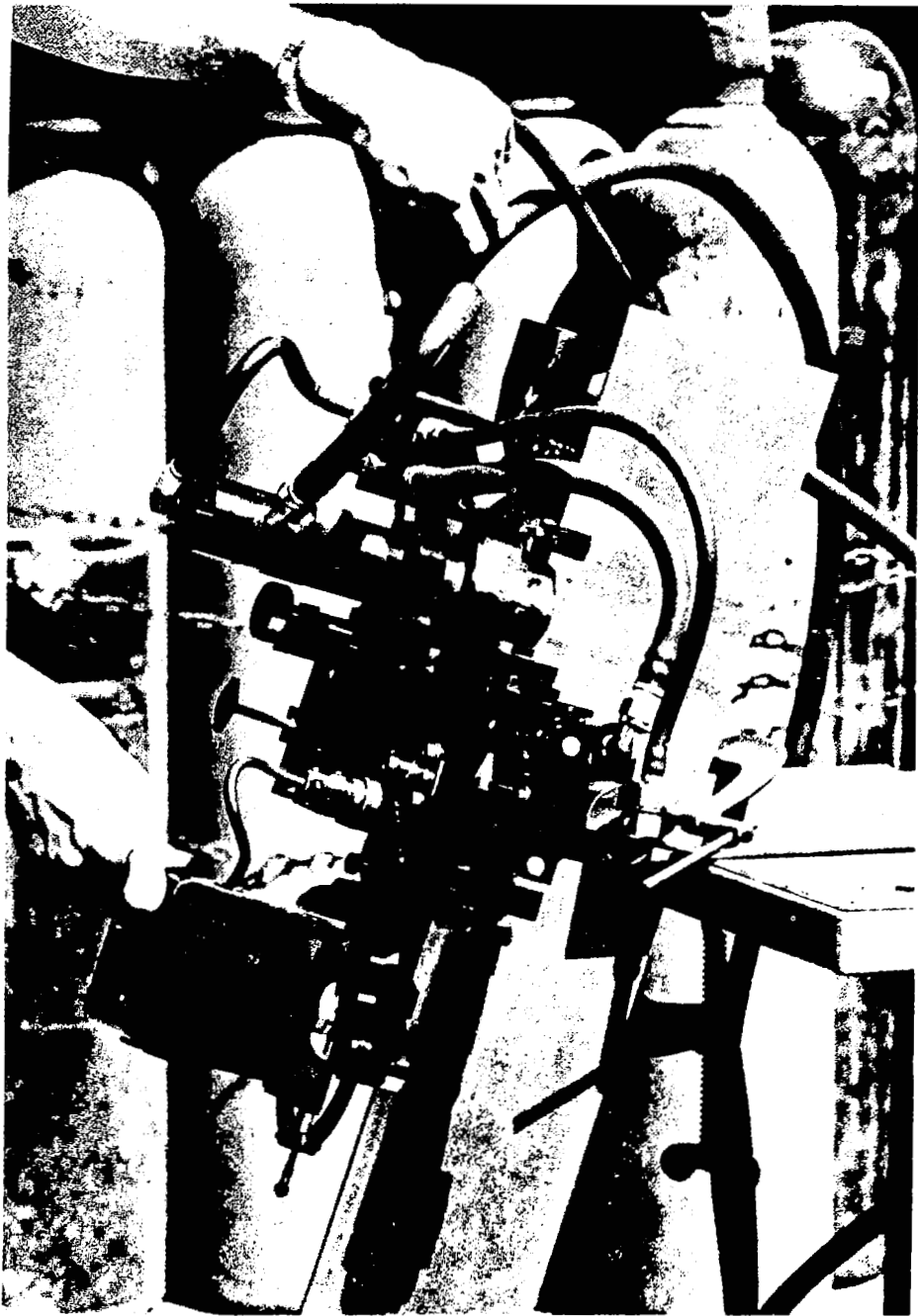


Figure 5-27. Method for supporting device in preparing surfaces in vertical welding position.



Test specimens for electrical discharge cleaning evaluations were first dry machined to produce a surface with low defect potential and then deliberately contaminated, retaining some specimens in the as-machined condition for experimental control purposes. The following surface conditions were evaluated:

- 1) As-machined and carefully stored
- 2) Alconox degreased
- 3) Chemically cleaned (1 min in 5 w/o NAOH solution at 180°-190° F, dipped in demineralized water, 15 sec dip with agitation in 50 v/o HNO<sub>3</sub> to remove smut, followed by a 1 min rinse in demineralized water)
- 4) Trichlorethylene degreased.

Cleaning was performed with conventional gas tungsten-arc welding equipment mounted on a side beam carriage and equipped with an oscillator to provide longitudinal and transverse travel over the specimen surfaces. A photograph of a cleaning operation with direct-current reverse-polarity discharge is shown in Figure 5-28.

Unfortunately, all the electrical discharge cleaning methods investigated failed to produce surfaces with low weld defect potential.

#### Monitoring Shielding Gas Purity<sup>(4,28)</sup>

As discussed earlier in Chapter 5.2, it was found during previous programs that:

- 1) Small amount of hydrogen about 250 ppm in the shielding gas is enough to produce porosity in aluminum welds

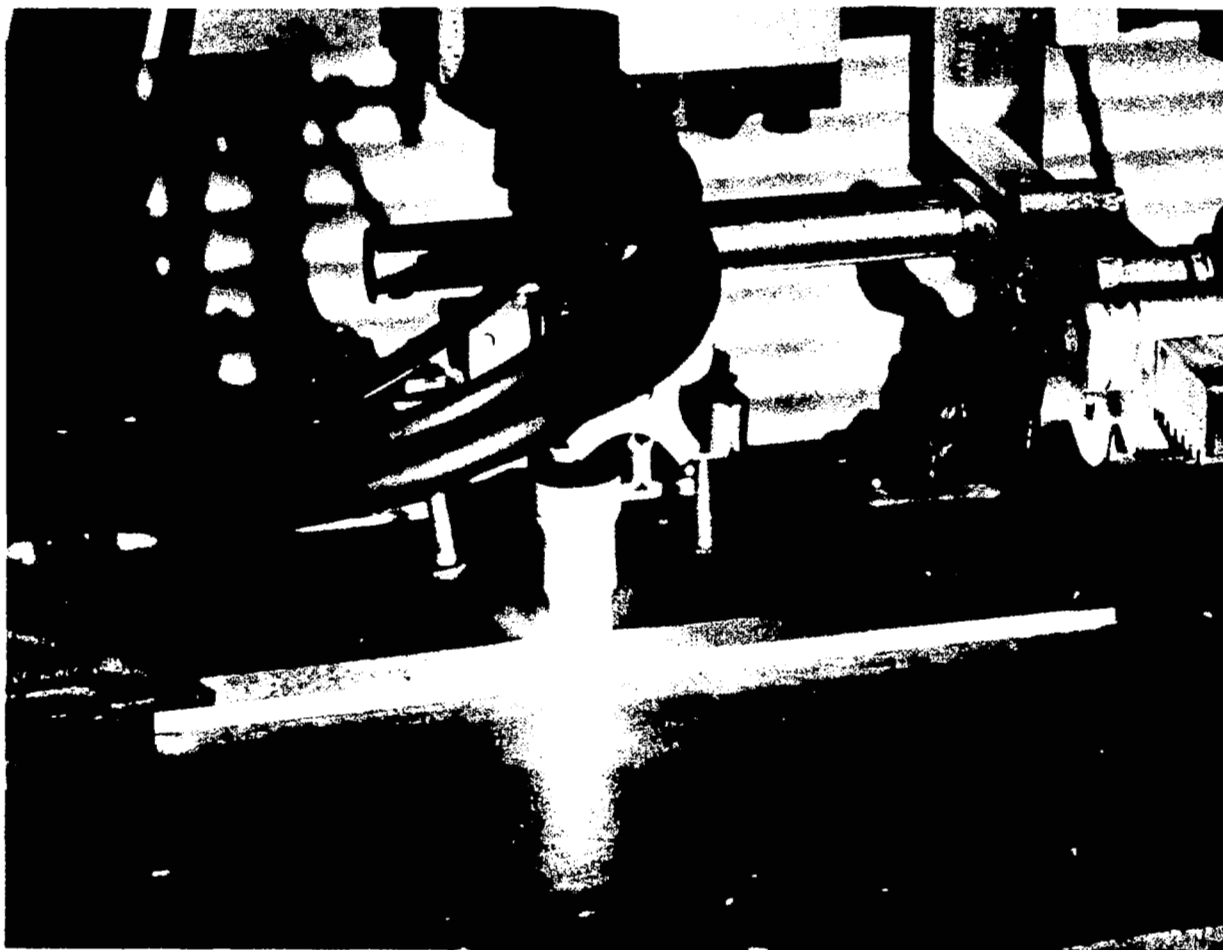


Figure 5-28. Electric discharge cleaning with direct-current reverse-polarity discharge.

- 2) Normal commercial gases which meet the current NASA specification for shielding gas are sufficiently pure.

However, gas contamination can occur within the bottle, especially when it is empty, or between the bottle and the torch nozzle. In order to successfully control welding production, it is necessary to monitor purity of shielding gas at the torch.

A study was conducted at the Boeing Company with the following objectives:

- 1) Define the shielding gas profiles of typical production weld torches
- 2) Determine the degree of contamination introduced into the arc region as a result of joint defects
- 3) Correlate the above with weld porosity.

Probe for Gas Analysis. In order to measure contamination in the shield gas a special probe was designed which could continuously sample a very small portion of the gas and deliver it to a mass spectrometer for analysis. The probe was made by silver soldering a 0.025 mm (1 mil) stainless steel capillary with 0.15 mm (6 mils) outside diameter into the end of a 0.79 mm (1/32") stainless steel tube. The tube was connected to a mass spectrometer as shown in Figure 5-29. The probe was affixed to the weld torch by means of a motor driven clamp. The probe tip and mount are shown in Figure 5-30. The motor used was a synchronous type geared down so that the probe travel was 1 cm/min. This drive speed provided a position resolution of 0.025 cm, since the response time was about one second (the time required for the gas to pass through the probe and into the mass spectrometer).

The mass spectrometer used was a Veeco Model RG-4 residual gas analyzer. Calibration of the mass spectrometer was accomplished by passing the helium gas to be analyzed past an

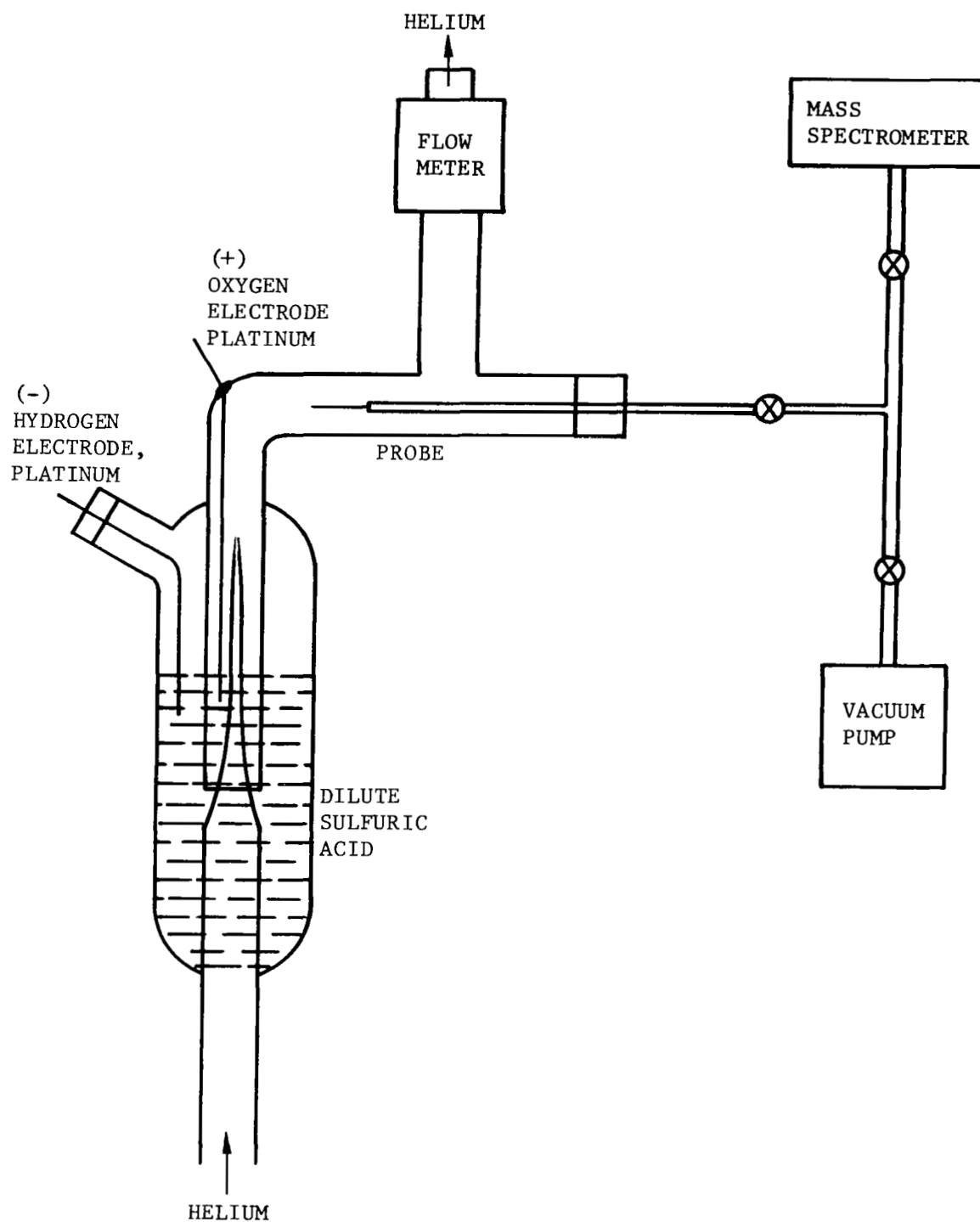
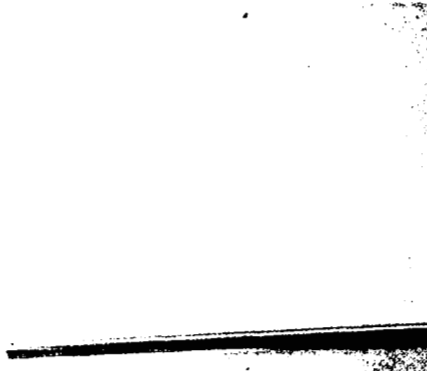
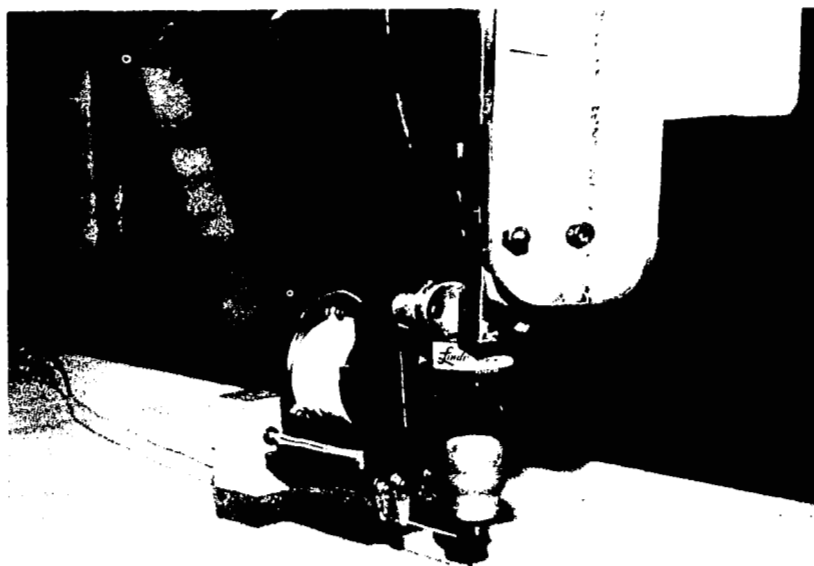


Figure 5-29. Schematic of mass spectrometer and calibration cell.



PHOTOGRAPH OF PROBE TIP  
(A)



PHOTOGRAPH OF WELD TORCH, PROBE, AND CONTROL  
(B)

Figure 5-30. Mass spectrometer probe and control.

electrochemical cell at a known flow rate. Oxygen was generated electrochemically at a platinum electrode from dilute sulfuric acid.

Under the operating conditions the sensitivity to oxygen in helium was found to be 3.15 ppm/division with an observed noise level of up to 0.3 division or an uncertainty of ca. 2 ppm oxygen.

By means of the motor driven probe it was possible to scan the gas shield and relate composition to position and to reconstruct the contamination profile. The mass spectrometer was set to continuously monitor oxygen. A typical scan is shown in Figure 5-31. From these scans the distances at which oxygen reached 10, 100, 1000, and 5000 ppm were recorded. Scans were made at several positions (up to twelve per profile) to define the nature of each profile. Four helium flow rates, 0.34, 0.44, 0.57, and 0.68 standard liters per second (43, 56, 72, and 86 standard cubic feet per hour), four torch to work distances 0.6, 1.0, 1.3, and 1.5 cm (1/4, 3/8, 1/2, and 19/32 inch), two torch positions horizontal and vertical, and two torches Linde HW-27 and HW-13 were used to prepare reference profiles. These profiles are reproduced in the appendix.

The oxygen contamination levels may be converted to water contamination levels but these depend upon temperature and humidity. Each oxygen contour can be converted to a water contour by multiplying by the ratio of the partial pressure of water to the partial pressure of oxygen.

At 100% relative humidity the partial pressure of water  $P(H_2O)$  is equal to the vapor pressure of water and can be found in standard handbooks. At 50% R.H.  $P(H_2O)$  is one-half the vapor pressure, etc. At one atmosphere pressure, dry air contains 20.95% oxygen by volume, therefore, the partial

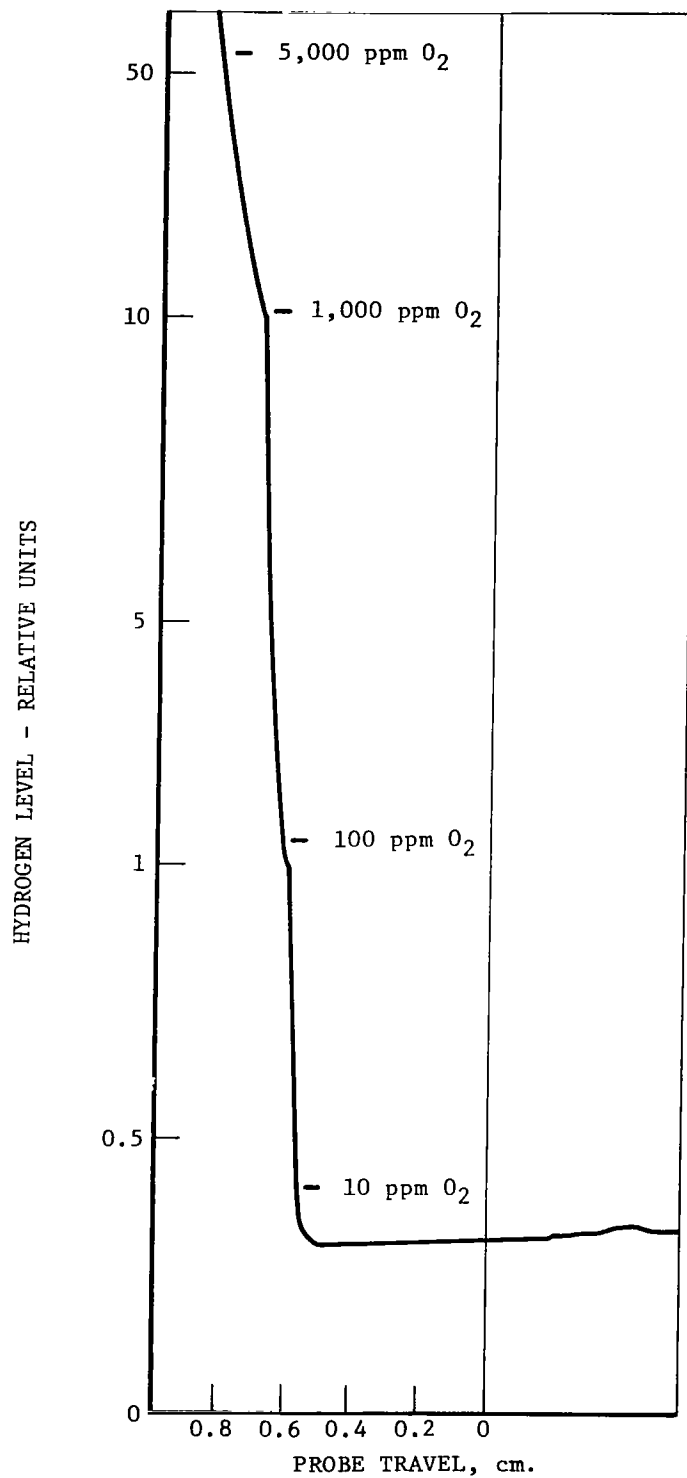


Figure 5-31 Typical scan for gas profile.

pressure of oxygen,  $P(O_2)$ , is

$$P(O_2) = 0.2095 [760 - P(H_2O)] \quad (5-3)$$

The ratio  $P(H_2O)/P(O_2)$  is given in Table 5-3 for various temperatures and humidity levels that may be encountered in a production area.

These data indicate that a ratio of 0.1 to 0.2 covers the range encountered in most shop environments. If we assume a value of 250 ppm water in the gas shield is necessary to produce significant porosity, then it is necessary to introduce a contamination level of something greater than 1000 ppm oxygen from shop air. This represents a rather large contamination level and therefore, should be easy to detect.

Joint Defects. Experiments were conducted to determine the minimum size defect that results in contamination in the critical arc zone. Gaps were selected for the first experiment. Flow rates were selected which represent minimum coverage and thus the easiest to perturb.

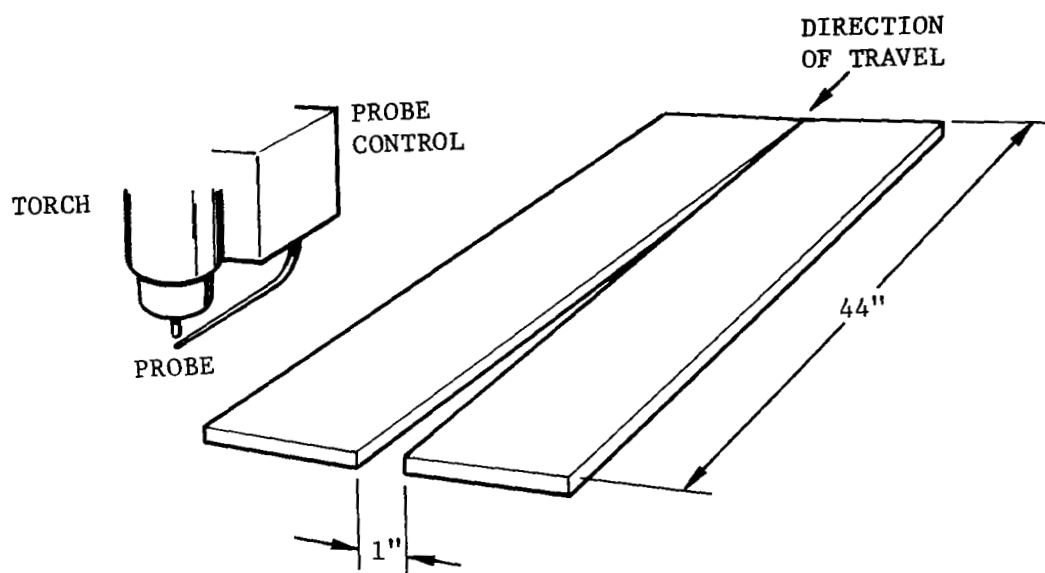
The following experiment was conducted: The mass spectrometer probe was set directly below the electrode tip at the surface of the aluminum panel. The joint was adjusted so that a gap of 2.54 cm (one inch) existed at one end and no gap at the other end. The joint was made up from two pieces of 0.63 cm (0.25 inch) by 1.118 m (44 inches) long. The weld torch was moved along the joint starting at zero gap at various speeds. (See Figure 5-32) The gap size at which the contamination level changed was recorded and is listed in Table 5-4.

These data indicate that only gaps of very large size allow contamination to enter the critical zone. The gas flow rate was lowered to the point where coverage was just barely

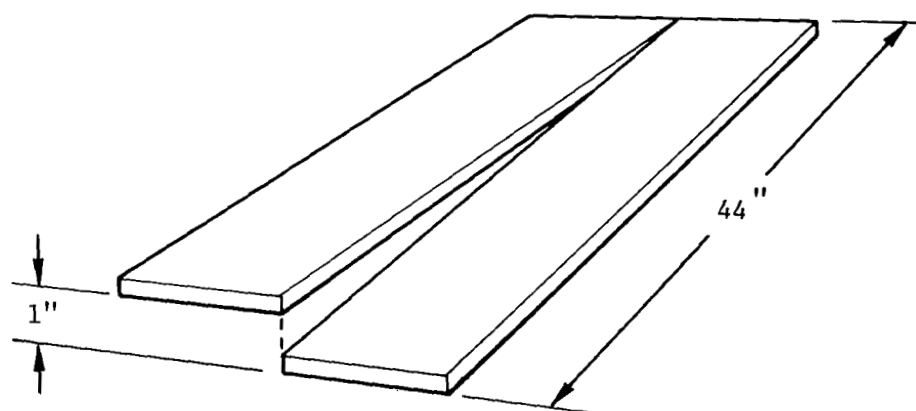


TABLE 5-3. THE RATIO  $P(H_2O) / P(O_2)$

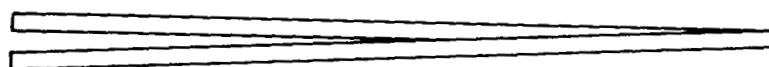
<u>Temperature</u>		<u><math>P(H_2O) / P(O_2)</math></u>	
<u>°C</u>	<u>°F</u>	<u>50% R.H.</u>	<u>100% R.H.</u>
20	68	.056	.112
25	77	.076	.154
30	86	.102	.209
35	95	.136	.280



GAPS



MISFITS



SIDE VIEW

Figure 5-32. Gaps and Misfits.

TABLE 5-4. GAP SIZE NECESSARY TO CAUSE CONTAMINATION CHANGES IN GAS SHIELD.

o Torch: Linde, HW-13

Position	Flat					
Helium Flow Rate	0.44 1/s			0.57 1/s		
Torch Travel Rate cm/min	29.5	51.6	73.1	29.5	51.6	73.1
Gap Size where contamination level changes (cm)	1.52	1.9	1.75	2.21	2.34	*

Position	Horizontal					
Helium Flow Rate	0.44 1/3			0.57 1/s		
Torch Travel Rate cm/min	29.5	51.6	73.1	29.5	51.6	73.1
Gap Size where contamination level changes (cm)	*	*	*	*	*	*

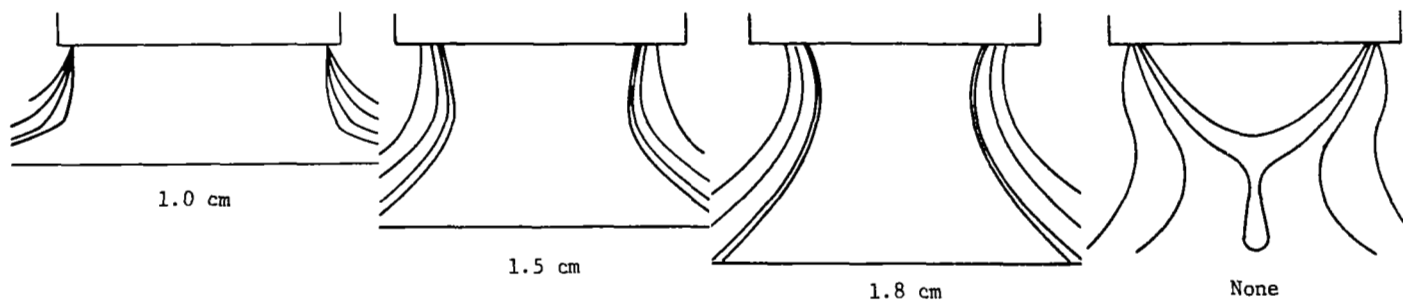
o Torch: Linde, HW-27

Position	Horizontal					
Helium Flow Rate	0.44 1/3			0.57 1/s		
Torch Travel	29.5	51.6	73.1	29.5	51.6	73.1
Gap Size	*	*	*	*	*	*

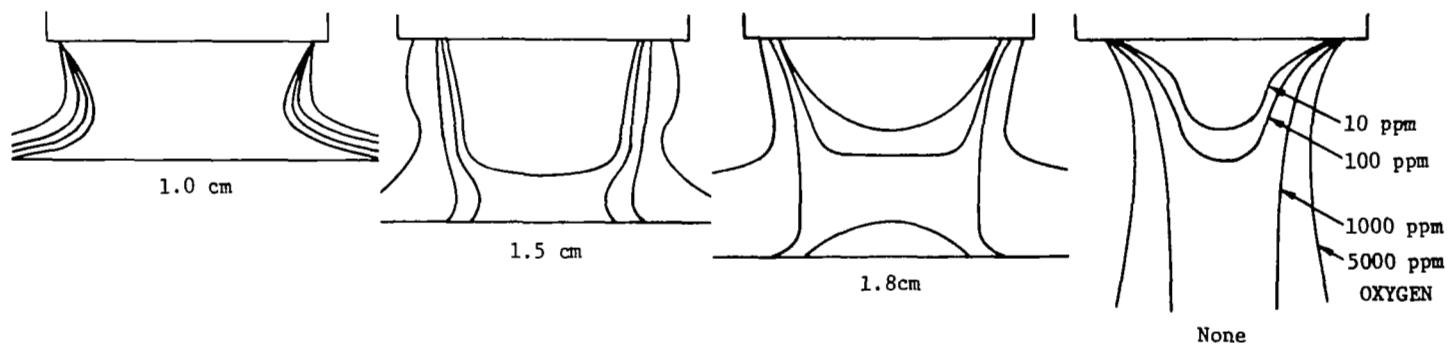
\* No change was noted in the contamination level.

adequate and the experiment repeated. With this lower flow rate it was impossible to prevent even the slightest draft from disturbing the gas shield despite extensive shielding. The movement of the torch was enough to cause contamination of the gas shield. The results of these tests may be summed up as follows: If shielding gas flow rate is adequate, gaps do not perturb the contamination profile but if flow rates are reduced to where gaps may cause contamination, then movement of the torch and other slight drafts disturb the shielding gas enough to completely overshadow any effect of the gap. This condition was also found to exist for misfits (Figure 5-32), that is, either no change in the profile was found or drafts overshadow the effect. In order to properly interpret these results, it is necessary to compare the contamination profiles for constant gas flow by changing torch to work distances. To supplement the profiles in the appendix it was necessary to determine profiles for the case of no work present. This series is shown in Figure 5-33. A helium flow rate that is adequate for short torch to work distance becomes inadequate at longer distances. When carried to extreme, the region of zero contamination decreases to a small cone. At the shorter torch to work distances, the work forces the shield gas out, thus there is adequate coverage. When a gap is encountered, the profile exhibits a transition to that observed with no work present, when the gap is large enough.

This transition is dependent upon helium flow rate. At a flow rate high enough to provide adequate coverage the transition occurs at a large gap. At lower flow rates the gas shield is unstable with respect to slight air movement and the transition cannot be seen. These data indicate that joint variations may have very little influence on shielding.



HW-27 TORCH, 0.57 1/SEC (72 SCFH) AT VARIOUS TORCH TO WORK DISTANCES, TWICE ACTUAL SIZE



HW-13 TORCH, 0.68 1/SEC (86 SCFH), AT VARIOUS TORCH TO WORK DISTANCES, TWICE ACTUAL SIZE

Figure 5-33. Effect of torch to work distance on contamination profiles.

The data obtained so far strongly suggests that mechanical joint defects do not lead to porosity. That is, mechanical joint defects do not easily produce poor shielding and if they could, atmospheric contamination, particularly moist air, cannot enter the arc region in sufficient quantities to produce porosity in aluminum even under the most adverse production conditions.

#### Other Possible Means

In the NASA research program on welding aluminum, several methods other than discussed previously were studied as possible means for reducing porosity. The methods studied include:

- 1) Use of hydrogen getters
- 2) Magnetic arc shaper and molten-puddle stirrer
- 3) Cryogenic cooling.

Even though major objective of the last two methods were not to control weld porosity, their effects on porosity were studied on a limited scale.

Use of Hydrogen Getters.<sup>(13)</sup> It has been known that certain elements will act as scavengers of hydrogen, either eliminating it or combining with it in a harmless form. The Southern Research Institute conducted a research program which consisted of two phases: (1) a literature and theoretical study, and (2) an experimental study.

On the basis of a survey of literature<sup>(54-57)</sup> hydrogen appears to be able to combine with almost every element to form binary compounds. These compounds are divided into three groups: the covalent hydrides, the saline hydrides, and the transition-metal hydrides.

The covalent hydrides are formed by the elements B, C, N, O, F, Si, P, S, Cl, Ge, As, Se, Br, Sn, Sb, Te, I, Pb, Bi, and Po. The elements Cu, Ag, Au, Zn, and Hg form an intermediate type of hydride that is neither pure ionic nor metallic bonded but tends to have the characteristics of the covalent hydrides. Therefore, this type hydride was included with the covalent hydrides for consideration in this study. In their natural state covalent hydrides are usually in either liquid or gaseous form. Since it was considered likely that liquid or gaseous hydrides would be detrimental if mixed into the weld puddle, these elements were eliminated from further consideration.

The saline hydrides are ionic in their bonding and form stoichiometric compounds. The elements included in this classification are Li, Na, Mg, Al, K, Ca, Rb, Sr, Cs, Ba, and Ra. It is probable that the rare earths are also included in the saline-hydride group.

The transition-metal hydrides are formed by Ti, Zr, Hf, Th, V, Nb, Ta, Pa, Cr, Mo, W, U, Pu, Fe, Ru, Os, Rh, Ir, Ni, Pd, Co, and Pt. These hydrides exhibit metallic bonding and nonstoichiometric compositions depending upon the exposure time to hydrogen, temperature of reaction, and past history of the element.

It was decided to select four of the promising elements for experimental investigation of their hydrogen-getting abilities, one from the saline group, two from the transition metals, and a rare earth. Calcium was chosen to represent the saline group because it was more readily available and presented less stringent handling requirements than Ba and Sr. Of the transition metals, Ti and Zr were chosen because of their availability and lower cost in comparison to Hf. Mischmetal, a mixture consisting of approximately 50 percent

cerium and other rare-earth metals (principally lanthanum and neodymium), was chosen to represent the rare earths.

Experiments were made to determine whether porosity could be reduced by applying hydrogen getters in areas near a GTA arc spot weld. The getters were prepared in powder form and applied to specimens by various techniques as outlined in the preceding discussion. None of the techniques proved to be effective for reducing porosity.

Fine powders have large surfaces compared to their volumes and are easily contaminated. Air is always present around powders, even when they are packed. As demonstrated by other investigators in the NASA program, porosity in aluminum welds can result from very slight shielding-gas impurities and very minimum contamination of the electrode or workpiece surface. Findings obtained at Boeing indicate that the existence of only 250 ppm of gas impurity, or of a single fingerprint on the metal surface, will cause porosity. At SRI, no measurement was made of the impurities around the hydrogen getters applied to specimens.

It is the integrator's opinion that SRI work has neither proved nor disproved whether porosity can be reduced by using hydrogen getters. Therefore, it may be worthwhile to try a different approach to the problem. Perhaps an approach would be the use of experimental filler wires containing hydrogen getters.

Magnetic Arc Shaper and Molten-Puddle Stirrer.<sup>(18)</sup> Another possible method of reducing porosity is the use of mechanical devices that either agitate the puddle or oscillate or shape the plasma. Both puddle stirring and plasma oscillation have proved successful in reducing the level of porosity, although the percent reduction was relatively small. However, attaining this reduction requires the addition of complicated equipment to the welding torch.



Cryogenic Cooling. <sup>(15)</sup> The results obtained at Harvey Aluminum have shown that porosity could be reduced by cryogenic cooling during welding. However, the percentage of porosity reduction was relatively small. The use of this method introduces the risk of contaminating the weld and further complicates the welding process. More study is needed before conclusive statements can be given on this subject.

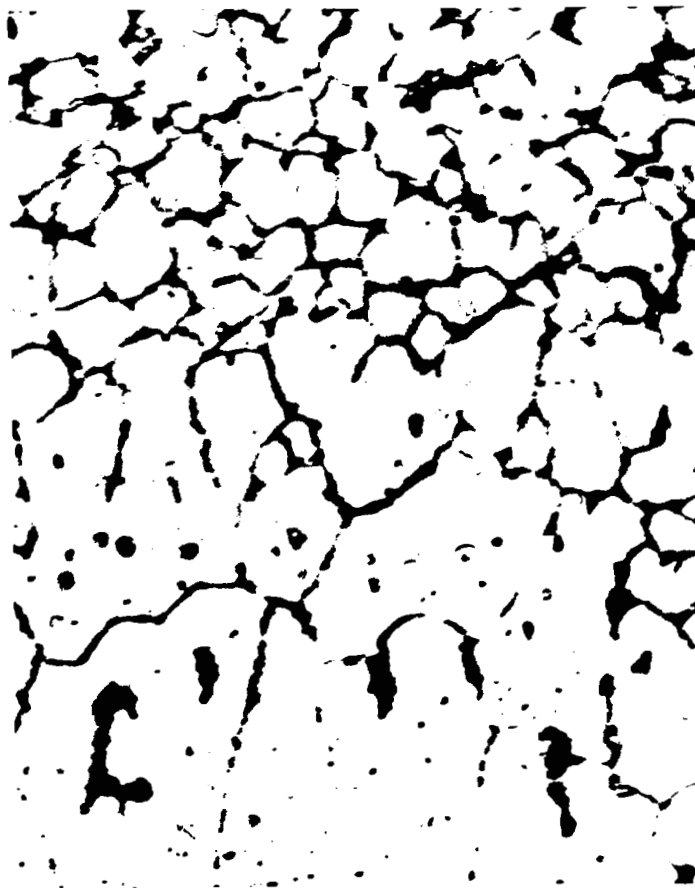


## CHAPTER 6

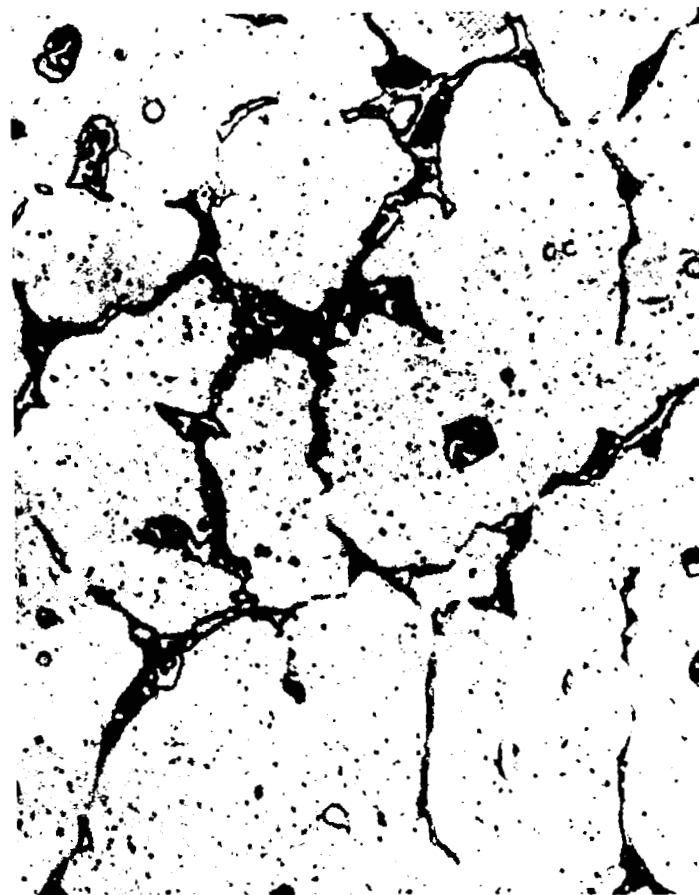
### Weld Thermal Effects

Figure 3-2 summarizes the experimental results obtained at the Marshall Space Flight Center which show the effects of welding heat input on the ultimate tensile strength of welds in 2219-T81 and 2219-T86 alloys.<sup>(4,6,7)</sup> When the weld heat input is between 40,000 and 100,000 joules/in<sup>2</sup>, the ultimate strength of a weld is between 37,500 and 42,000 psi. As the heat input decreases, the weld strength increases sharply reaching as high as 57,000 psi with a 10,000 joules/in<sup>2</sup> heat input by electron-beam process. The 2218-T87 base metal has a strength of 69,000 psi, about 10,000 psi of which strength is due to strain hardening. The strength of the alloy in the unstrained condition, T-62, is listed at 59,000 psi, nearly reached in electron-beam welds of 10,000 joules/in.<sup>2</sup>

The thermal effect is also seen metallurgically. Figure 6-1 shows typical microstructures of the heat-affected zones of welds made in two different heat inputs, 20,000 and 80,000 joules/in.<sup>2</sup> As heat input increases, there is an increase in grain size and in theta or copper aluminide agglomeration at the grain boundaries. The strength vs heat input curve has a steep slope from 30,000 to 10,000 joules/in.<sup>2</sup> This may be related to a marked decrease in the excess energy over that required for activation of copper migration.



a. 20,000 joules/m<sup>2</sup>  
(1,000 x fusion time)



b. 80,000 joules/in<sup>2</sup>  
(1,000 x fusion time)

Figure 6-1. 2219 Microstructure Versus energy.

## 6.1 Time-Temperature Effect

Jackson<sup>(57)</sup> proposed the time-temperature concept to study the effects of heat input on the strength of aluminum welds.<sup>(5)</sup> Figure 6-2 shows the temperature change during welding of a point in a weldment. Maximum temperature is defined as the peak temperature which the material being joined experiences during the welding heat cycle. Time at temperature is defined as the time that the material being joined is above the temperature that adversely affects strength properties of the base metal being joined. According to Jackson, the strength properties of 2219-T87 aluminum alloy are found to be adversely affected above 450° F.

An investigation was made to develop relationships between weld heat input and strength characteristics of 2219 aluminum welds. By the use of multivariate regression analysis of experimental data, the relationship among maximum temperature, time at temperature, and mechanical property characteristics including yield strength, ultimate tensile strength, and elongation were determined. The results are summarized as follows:<sup>(4)</sup>

- 1) Yield Strength:  $Y_1 = 5.04 + 0.19X_8^2 - 0.62X_8X_9$ ;  
Standard error of  $Y_1 = 2.65$ ; and multiple correlation coefficient = 0.79.
- 2) Ultimate Tensile Strength:  $Y_2 = 12.51 - 2.30X_8 + 0.40X_8^2 - 0.67X_8X_9$ ; Standard error of  $Y_2 = 4.70$ ;  
and Multiple correlation coefficient = 0.82.
- 3) Elongation:  $Y_3 = 2.08 - 0.30X_8 + 0.03X_8^2$ ;  
Standard error of  $Y_3 = 0.71$ ; and Multiple correlation coefficient = 0.82.

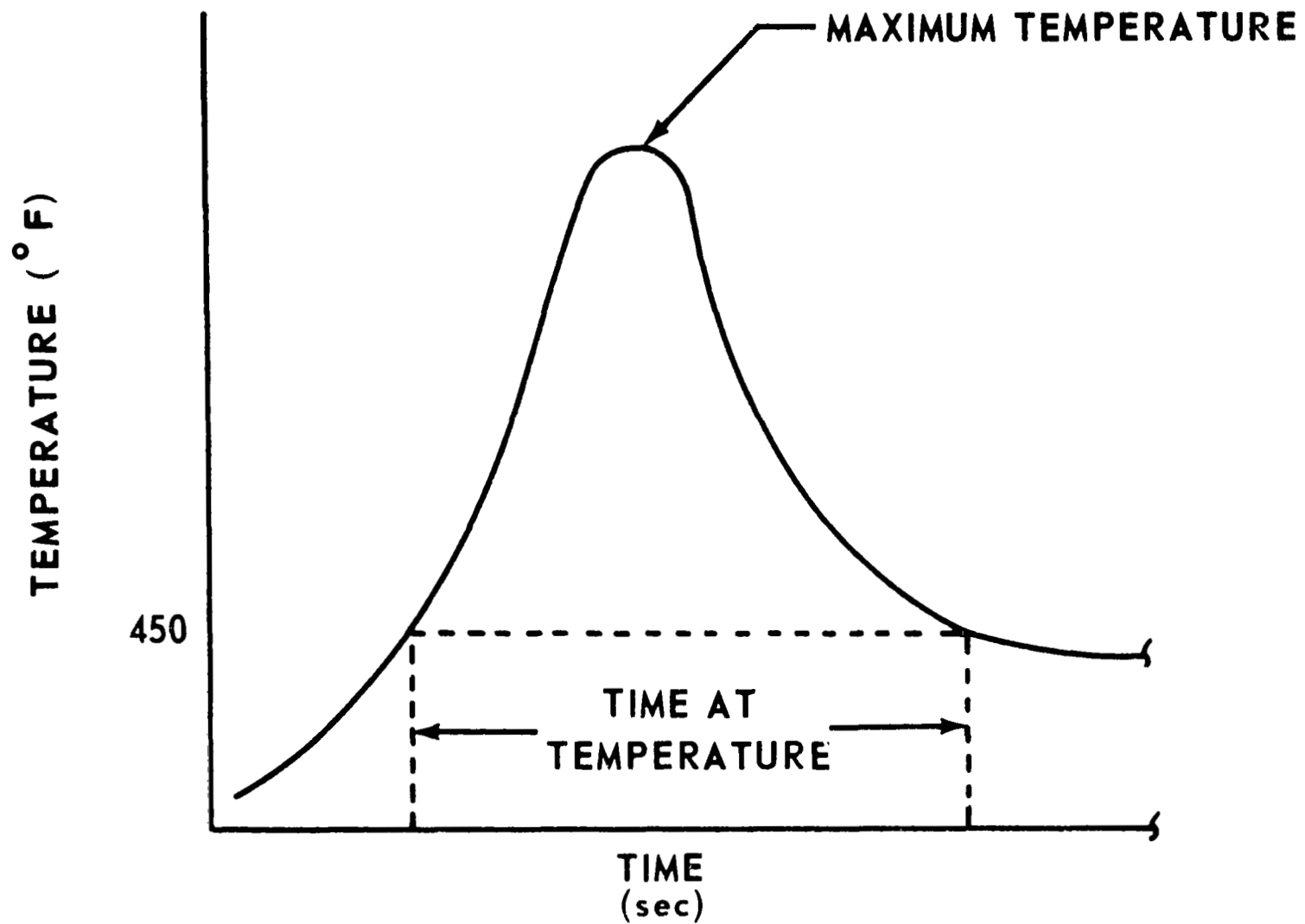


Figure 6-2. Time-temperature characteristics curve.

where,

$Y_1$  = Yield strength, ksi

$Y_2$  = Ultimate tensile strength, ksi

$Y_3$  = Elongation, percent

$X_8$  = Maximum temperature  $10^2$  °F

$X_9$  = Time at temperature, seconds

The strength characteristics, yield strength and ultimate tensile strength varied with maximum temperature and inversely with time at temperature as shown in Figures 6-3 and 6-4. Elongation varied with both maximum temperature and time at temperature, as shown in Figure 6-5, which increased the heat-affected zone. To optimize the value of yield and ultimate strength a maximum value of maximum temperature and minimum value of time at temperature is required. These values of maximum temperature and time at temperature are 1500° F and 16 seconds, respectively. To optimize the value of elongation maximum values of maximum temperature and maximum time are required. These values are 1500° F and 52 seconds. From the response surfaces shown in Figures 6-3, 6-4, and 6-5, the theoretical maximum values attainable for the strength characteristic responses are: yield strength, 35.13 ksi; ultimate strength, 54.39 ksi; elongation, 4.87%.

Maximum temperature,  $X_8$ , and time at temperature,  $X_9$ , were further expressed as follows:

4) Maximum temperature:  $X_8 = 62.97 - 0.36X_1X_2 + 0.55X_1X_3 + 1.56X_2X_7 - 0.01X_4X_6 + 5.35X_3 - 0.21X_5^2 + 0.15X_5X_7 - 29.56X_7 - 0.56X_7^2$ ; Standard error of  $X_8 = 0.96$ ; and Multiple correlation coefficient = 0.96.

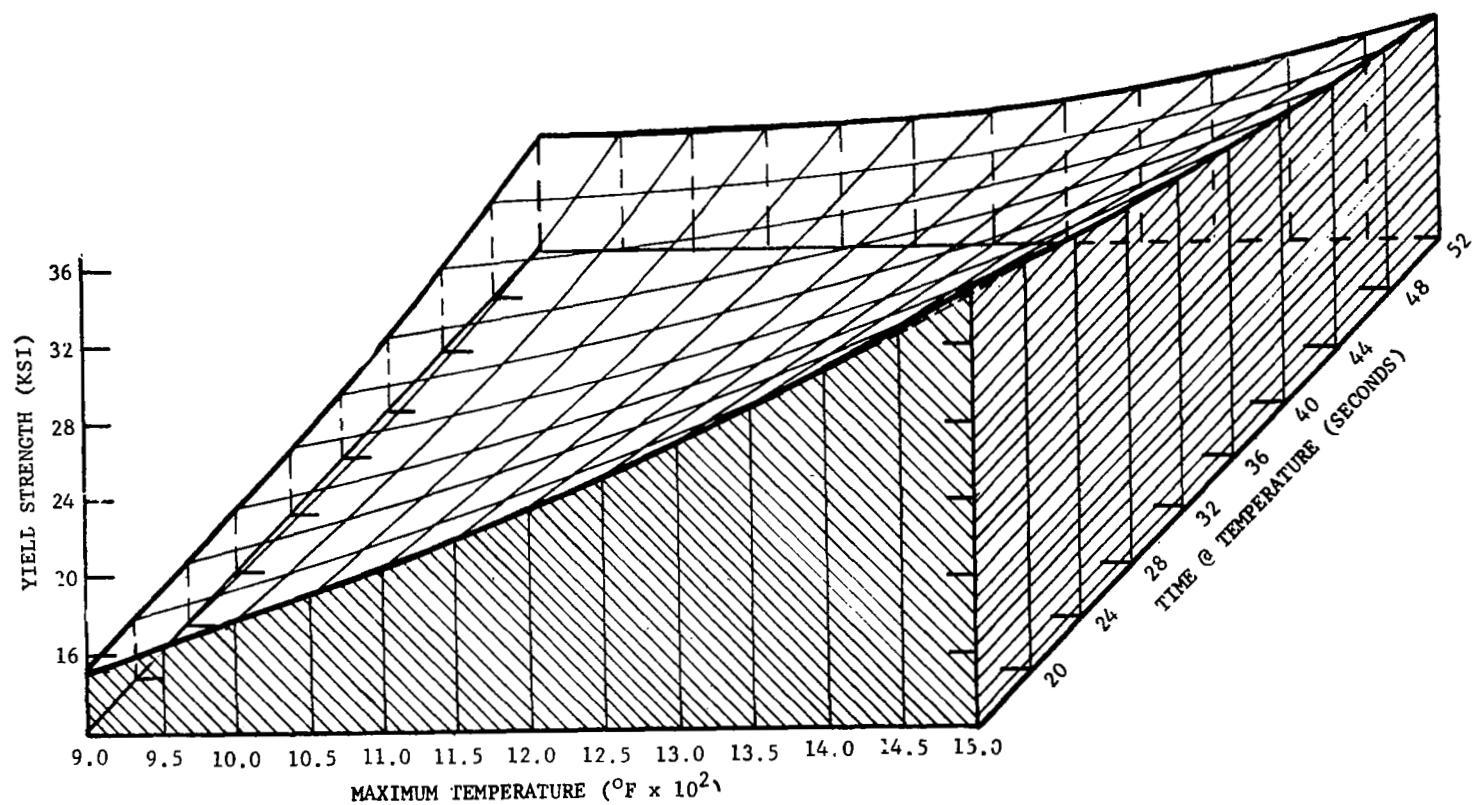


Figure 6-3. Yield strength of welds Versus maximum temperature and time at temperature.



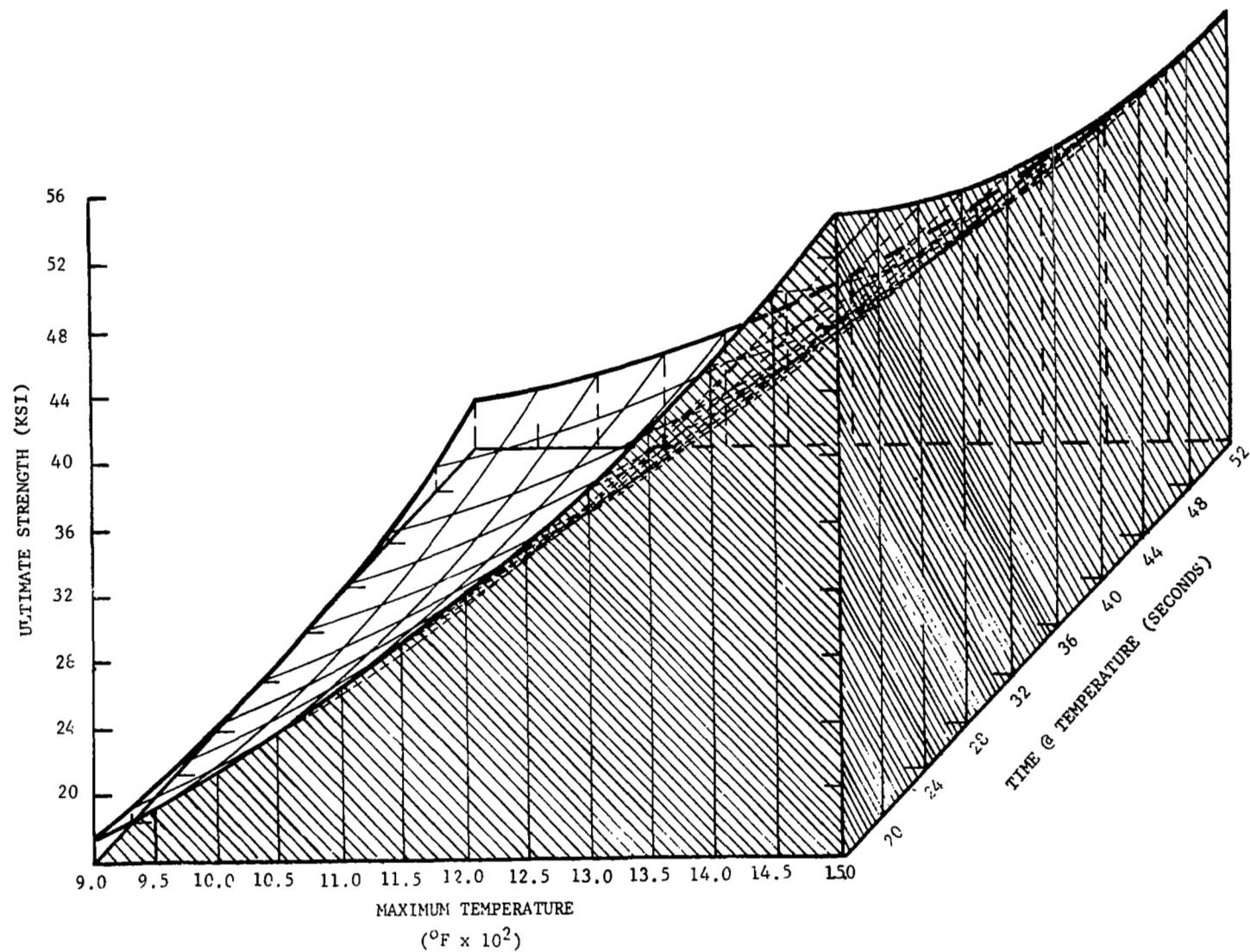


Figure 6-4. Ultimate tensile strength of welds Versus maximum temperature and time at temperature.

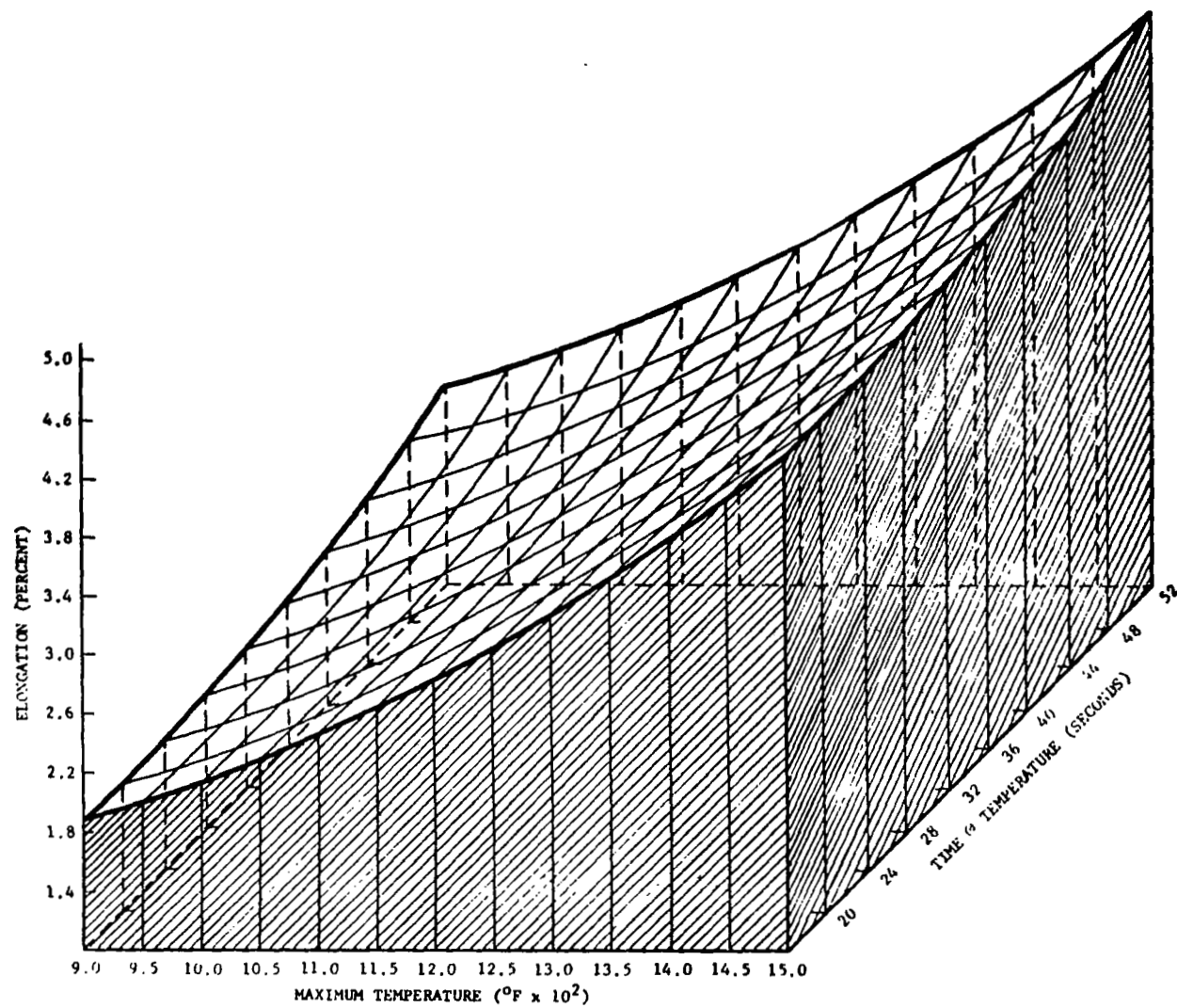


Figure 6-5. Elongation Versus maximum temperature and time at temperature.

- 5) Time at temperature:  $X_9 = -96.27 + 7.23X_2 - 33X_2X_3 + 5.35X_3$ ; Standard error of  $X_9 = 0.54$ ; and Multiple correlation coefficient = 0.95.

where,

$X_1$  = arc voltage, volts (10.5 to 11.5)

$X_2$  = welding current, amperes (160 to 180)

$X_3$  = arc travel speed, ipm (6 to 9)

$X_4$  = filler metal speed, ipm (16 to 24)

$X_5$  = electrode holder angle, degrees (2 deg lead to 4 deg lag)

$X_6$  = gas flow rate, cfh (80 to 120)

$X_7$  = tungsten length, in (3/8 to 1/2)

The independent variables were set at two levels as shown above in keeping with the  $2^7$  factorial experimental design with 1/4 replicate.

The following general conclusions were drawn as a result of this investigation.

1. Maximum temperature and time at temperature were found to be significant in measuring effective weld heat input.
2. Current and travel speed were the only controllable independent variables that significantly affected time at temperature while voltage, current and tungsten length affected maximum temperature.
3. Definite mathematical relationships can be developed describing the interactions between weld heat input and factors that require optimization.

## Strength vs Welding Energy<sup>(4)</sup>

Shortly after Jackson completed the above mentioned work, tensile data from hundreds of welding panels were plotted with reference to welding energy per inch of thickness. Various welding techniques were used such as electron-beam (EB), gas tungsten-arc (GTA), gas metal-arc (GMA), done with one pass one side, two pass one side, and one pass each side. The welding energy is expressed in joules per linear inch of travel per inch of thickness. The lowest strength was produced by welds with weld heat input greater than 80,000 joules per inch per inch, as shown in Figure 3-2. The highest strength of 57,000 psi was produced by electron beam equipment.

It is worthwhile to mention that all the welds of which data are shown in Figure 3-2 were made without back-up bars. In the past the industry had used back-up bars and they were thought to be essential. As a result of an extensive study at NASA, it has been found that back-up bars are not necessary, even on heat treated alloys.<sup>(4)</sup>

## 6.2 Welding with High Density Power Sources

As shown in Figure 3-2, higher strengths are obtained with welds made with lower energies. Expressed differently, welds made with high power densities and appropriate parameters will produce higher strengths. Attempts were made to weld with high density power sources. The following pages discuss:

- 1) Experiments to increase GTA power density
- 2) Electron Beam welding
- 3) Non-vacuum electron beam welding
- 4) Plasma electron beam welding.

### Experiments to Increase GTA Power Density

A study was conducted by Lockheed<sup>(25)</sup> to investigate possibilities to significantly increase the power density of tungsten arc welding. Modifications of gas tungsten arcs were selected which were believed to show the most promise. Each of these influences a different portion of the arc and can be classified as follows:

- a) Modification of the electrode (cathode)
- b) Modification of the anode (workpiece)
- c) Modification of the shielding gas
- d) Use of magnetic fields to constrict the arc plasma.

Modification of the electrode may include changes in the material from which it is constructed, changes in its shape, or changes in the means used to cool it. Emphasis was placed on materials with high thermionic emissivity since they could operate with a smaller cathode spot at a given current and thereby provide a narrower current--conducting path near the cathode. The reported high thermionic emission of lanthanum hexaboride together with its high melting point, 2210° C (4012° F), good electrical conductivity, and stability led to its selection as one of the materials for experimentation.

Barium-calcium-aluminate impregnated cathodes were also selected for their high thermionic emission and because of their successful application as electrodes in an arc plasma generator. Accordingly, experiments were made to study these two materials.

At the anode or workpiece in DCSP-GTA welding, there is much less latitude available in which to perform modifications to increase power density; that is, the composition only can be changed and only in very small amounts. A fourfold difference in penetration due to trace amounts of chlorine reported by Ludwig was justification for further investigation of this phenomenon in this program. Several experiments with halogen additions to the anode region were made.

The marked effect of shielding gas composition on arc voltage, power density, and thermal efficiency reported in the literature indicated a potential for significant improvement in GTA power density. Additions of the diatomic gases--hydrogen, nitrogen, oxygen, and chlorine--were selected for study as showing particular promise. It was anticipated that hydrogen and nitrogen could be studied in all concentrations whereas oxygen and chlorine, because of possible degradation of the cathode, would be limited to about 1% by volume.

An arc plasma such as used for GTA welding diverges from the cathode to the anode as the result of a form of thermal diffusion called ambipolar diffusion. This phenomenon occurs when the more mobile electrons, formed near the cathode by ionization, diffuse radially outward more rapidly than the larger, more massive positive ions. The charge separation produced results in a radial electrostatic field which retards the motion of electrons and simultaneously increases the force driving the positive ions outward. If the electrons could be restrained from their rapid outward flight, the plasma divergence could be decreased, effectively constricting the arc

in the anode region. One means of inhibiting the outward motion of electrons would be by the application of a longitudinal magnetic field through the arc. Such a field would be expected to cause small circular motions of the electrons between collisions in contrast to the interrupted linear motion that normally occurs. Longitudinal magnetic fields of the order of 20 to 50 G had been used to stabilize the gas tungsten arc and to provide "stiffness." Somewhat higher field strength (100 G) has been reported to provide a "focussing" action on the arc. Therefore, a study was conducted of longitudinal magnetic fields of up to 300 G to determine their effect on arc power density.

Experimental Results. Significant increases in arc power density, as measured by narrowing of the continuum, were noted for additions of 20 vol % hydrogen to helium or argon shielding gas. Nitrogen additions to helium also increased power density, particularly in concentrations of 40 Vol % or greater. The greatest increase measured, however, was with the addition of 0.5 vol % SF<sub>6</sub> to helium.

The improvement in weld penetration and depth-to-width ratio obtained in the bead-on-plate tests is much smaller than suggested by the continuum data; for example, an increase of about 30% compared to a tenfold increase in the continuum power density measured for the SF<sub>6</sub> addition. Moreover, nitrogen additions, actually resulted in lower depth-to-width ratios in stainless steel.

The use of materials with high thermionic emission for the electrode (cathode) shows some promise with up to a 60% increase in power density, as measured by the continuum, and about a 30% increase in depth-to-width ratios, for the tip configurations studied. Problems with thermal shock and melting of the lanthanum hexaboride tips (Figure 6-6) could

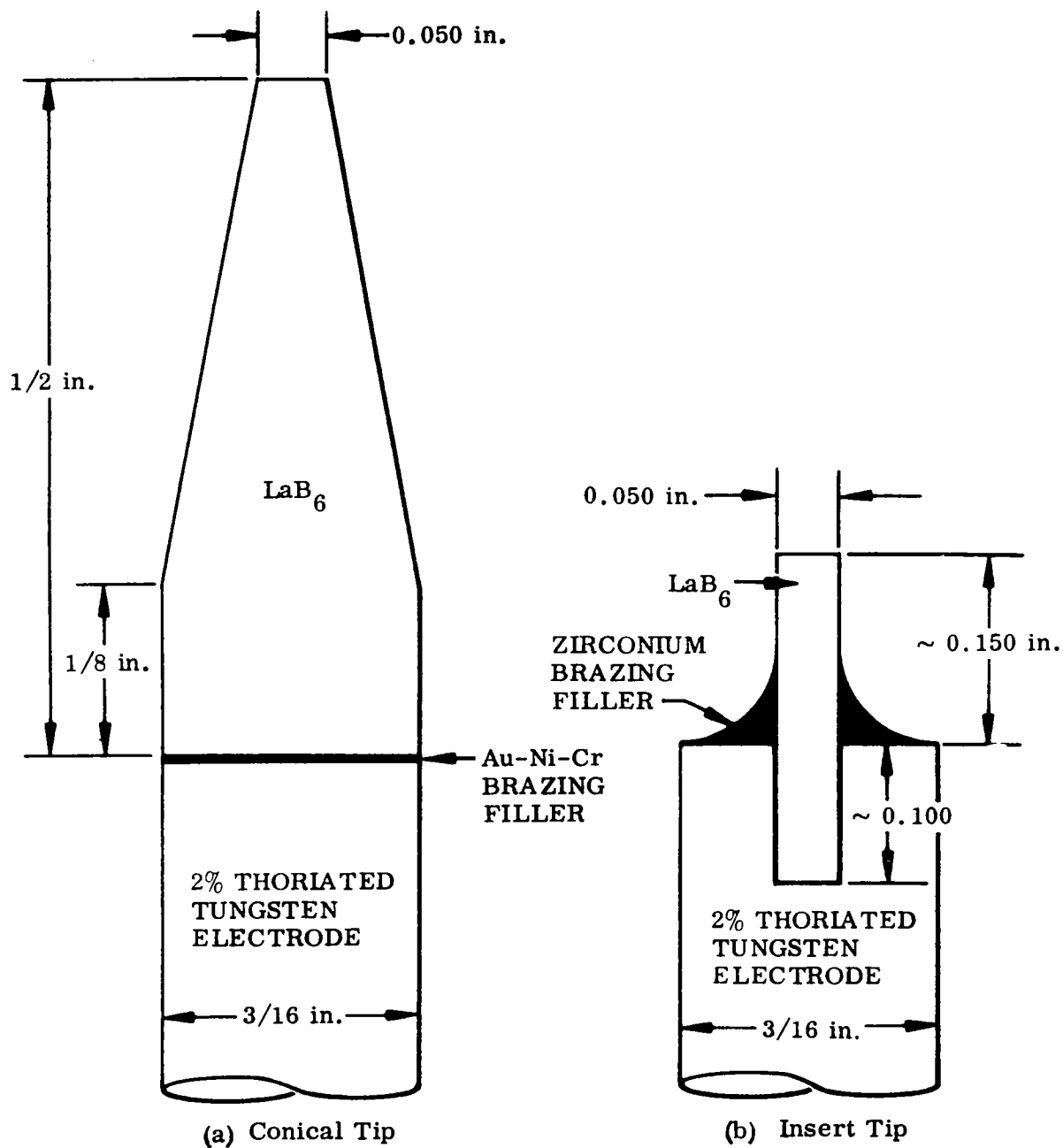


Figure 6-6. Configurations of LaB<sub>6</sub> tipped electrodes.



possibly be avoided by adding small quantities of the lanthanum to conventional thoriated tungsten electrodes. These tips would have the resistance to melting of the thoriated tungsten plus the high emissivity of the lanthanum.

The use of a longitudinal magnetic field resulted in a slight narrowing of the current width on the copper anode but caused severe distortion of the weld pool under practical welding conditions in the bead-on-plate tests.

No improvement in power density was observed in the experiments to modify the anode.

Surface melting of the water-cooled copper anode was observed in several of the continuum runs at high power density and are noted in the tables. Slight melting did not appear to interfere with the continuum measurement but in some instances small beads of copper were formed on the surface and tended to reflect light from the arc. This could result in erroneously high readings of power density. To avoid melting, all continuum runs were made at 150 A. In some cases, particularly with chlorine additions, a reaction with the copper surface was observed which could influence the measurement. The majority of the runs were made at 0.25 mm (0.010 in) above the copper anode surface but some runs were made at 0.50 mm (0.020 in) to avoid surface effects.

In general, the bead-on-plate tests were made under uniform conditions with little attempt made to optimize welding conditions for the specific arc modification under study. Therefore, the results should only be considered as showing possible trends.

The depth-to-width ratios attainable by the electron beam welding process are over ten times greater than the best GTA conditions. The total power for each process is of the order of 5 KW yet because of the difference in the

size of the heat source as it impinges on the work the maximum electron beam power density is of the order of  $10^9 \text{ W/cm}^2$  whereas for GTA the maximum power available is of the order of  $10^5 \text{ W/cm}^2$ . The results of this study decreased about 1/2 the difference of power density between the two methods but the power density of electron beam welding will still be about 100 times that of the tungsten arc process.

### Electron Beam Welding

Electron beam welding is one of the newer welding processes which is being evaluated for missile and rocket welding applications. In electron beam welding, fusion is accomplished by bombarding the workpiece with a dense stream of high-velocity electrons. The joint design for electron-beam welding is a square-butt joint with no gap. No filler metal is required. Welding usually takes place in an evacuated chamber, and this places some limitations on the size of the workpiece. This factor is one of the major limitations in the application of electron beam welding. Considerable work is being done to minimize this limitation.

In 1963, MSFC made its first effort to extend the use of an electron beam welding system.<sup>(4)</sup> A "split-chamber" concept as developed for MSFC by the Sciaky Brothers Company was used. In brief, this means that a vacuum chamber is reduced to a size that will encompass only the joints to be welded.

MSFC chose the 33-foot diameter ring that makes the transition from a bulkhead to a cylinder in the Saturn V first stage. The cross section of the ring forms a Y, as shown in Figure 6-7. Maximum thickness was about 2 1/2 inches. Only short arcs of the ring segments were in a low atmosphere (Figure 6-8). The "A" half of the chamber was stationary.

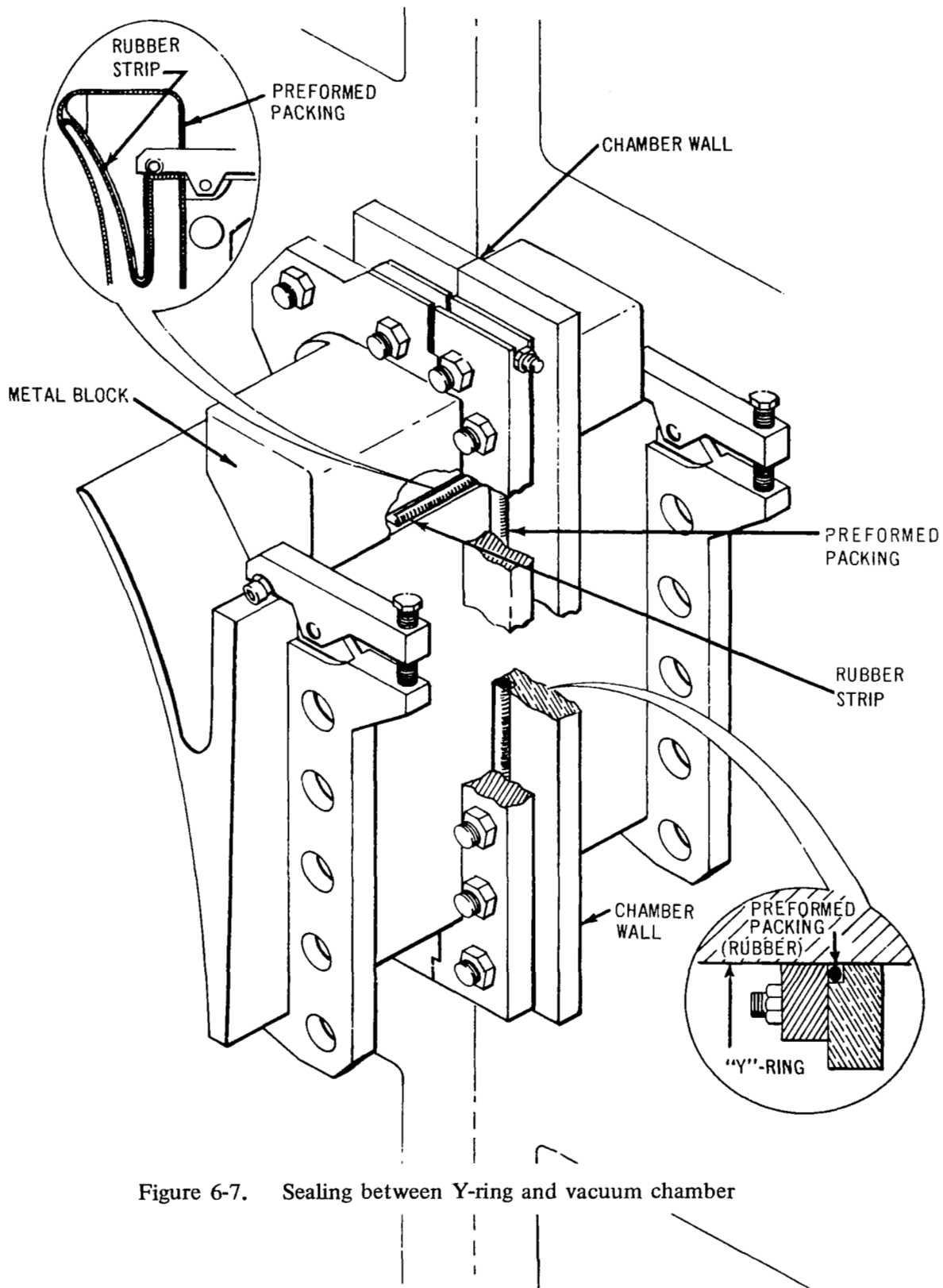


Figure 6-7. Sealing between Y-ring and vacuum chamber

- A SECTION - STATIONARY  
 B SECTION - MOVEABLE
1. SEALS ON VIEWING AND ACCESS PORTS
  2. SEALS ON THE ELECTRON GUN Y-AXIS DRIVE RODS
  3. SEALS AT THE INTERFACE OF THE CHAMBER HALVES

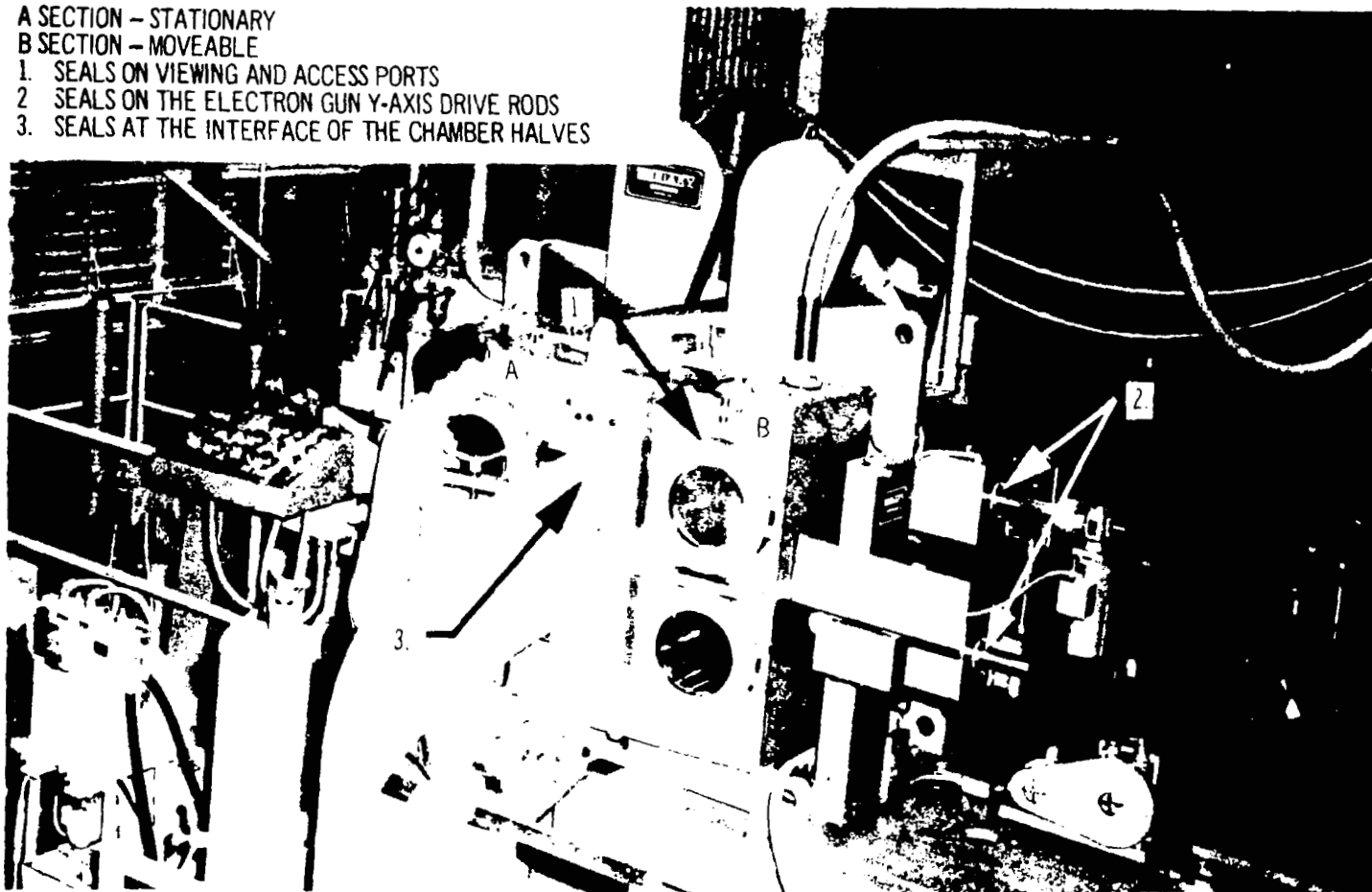


Figure 6-8. Vacuum seals on the split chamber Y-ring welding unit.

The "B" half was moveable on a pair of precisely aligned rails and was backed away to permit placement of the work-piece or to get to the electron guns.

The critical aspect of such a system is the adequacy of the seals at the interface of the chamber halves and between the Y-ring and the chamber. Sealing between the machined mating surfaces was done with Neoprene rubber strips. After the chamber halves were brought into contact, four bolts, one at each corner, were tightened to produce a tight joint. This is one area that proved to be troublesome during the Y-ring welding program. During many of the pump down cycles, it became evident that a leak existed somewhere in the system. Quite often further tightening of one or more of the bolts stopped the leak.

Sealing between the Y-ring and the chamber was done with metal blocks, rubber strips, and either preformed packing or O-rings. Again small leaks were often corrected by tightening the clamping plates, yet the exact location of leaks could not be determined.

Despite these problems, three segments were joined into a complete ring. In general, MSFC demonstrated the split-chamber to be a practical concept for joining large components.

#### Non-Vacuum Electron Beam Welding<sup>(4)</sup>

An attempt has been made for using a high-voltage non-vacuum electron beam welding system.<sup>(22)</sup> A newly developed model was delivered to MSFC in 1969 by the Westinghouse Astronuclear Laboratory. Powered by 150 KV supply, the welder is of a unique compact design. The power supply and welding gun, complete with all high vacuum pumps and accessories, are assembled into a 210-lb package that can be mounted in either the down-hand or horizontal welding position (Figure 6-9). It is mounted on a conventional side beam carriage. Flexible low vacuum lines permit the welding head

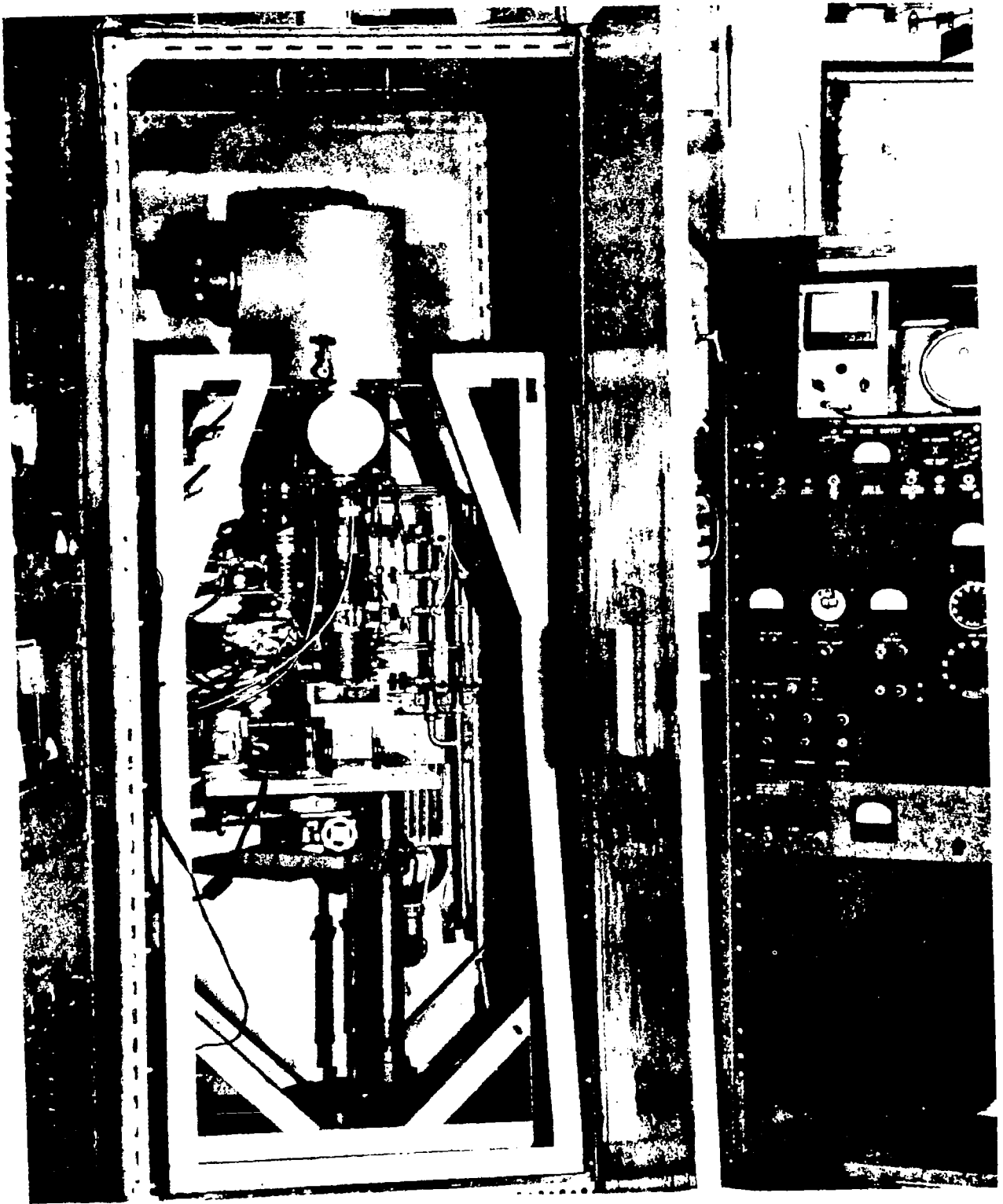


Figure 6-9. Westinghouse 15 KV laboratory welder.

to be traversed four feet in a straight line. The complete unit is enclosed in a lead shielded room.

Electron emission from an indirectly heated tungsten rod is forced through differentially pumped orifices by a combination of electrostatic and electromagnetic electron optical systems. Maximum operating power is 80 mA at 150 kV. A positive pressure is applied just below the exit orifice of the gun.

Welding has been done on 1/4-inch thick aluminum and 1/8-inch and 1/2-inch thick steel.

If material were welded in one atmosphere, an EB system would be as applicable as the gas-arc processes. But this poses no small challenge. The concentrated stream of electrons that makes low energy welding possible has from the onset of EB systems required a "low" atmospheric pressure. A low power density but versatile EB system would only be a regression, better left alone. It would be meaningful only if the welds produced were significantly superior to GTA and gas metal arc (GMA) welds. At this date, our non-vacuum system produces aluminum welds definitely inferior to hard vacuum welds, and only occasionally superior to GTA welds. Porosity is highly unpredictable.

But to obtain non-vacuum EB welds in aluminum that are similar in shape to hard vacuum welds, welding must be done at more than 200 in/min. Narrow welds made at any speed impose strict accuracy requirements. Transverse deviations of the beam from the center of the joint, and joint gaps of more than 0.005 inch can result in lack of fusion. The situation is greatly exaggerated when the gun is moving at 200 in/min. At this speed a seam tracking device would have to move the gun system laterally 0.005 inch in 3 1/3 inches of forward movement per second. Proximity of the gun to the work, less than 3/8 inch, is equally critical. Even if the

power density of the electron beam were increased so that much slower travel speed could be used, that is, 40 in/min vs 200 in/min, accuracy of parts fit-up would still be critical and seam guidance and proximity control would still be mandatory. In addition, shielding of personnel from x-rays generated by the high voltage means that remote monitoring of welding is necessary.

It is clear, that much analysis, development, and planning are necessary before the system can be considered applicable and thus versatile. In a rational approach to EB welding we must recognize and accept that the process will have limitations, just like any other joining process. EB welding is not yet a panacea.

#### Plasma Electron Beam Welding

A study was carried out by General Electric Company to develop a plasma electron beam (PEB) system.<sup>(26)</sup>

PEB is a new kind of electron beam source based on a cold hollow cathode gas discharge (Figure 6-10). With a pressure of about 10 microns of nitrogen, for example, a body of plasma fills the cathode and an electron beam formation takes place. Beam current is controlled by varying the gas pressure and consequently the influx of positive ions. The beam is focused by a magnetic lens spaced 8 or 10 inches from the end of the cathode. Capability of this equipment was demonstrated by a narrow penetration weld 1 3/4 inches deep into 5456 material. Porosity was not present at the root of the weld, indicating good electron beam stability as compared to conventional electron beam welding systems. The principle of operation is discussed in detail in the final report from General Electric. PEB offers the advantages of long cathode life and good performance under poor vacuum conditions where gaseous contaminants may be present. Parts



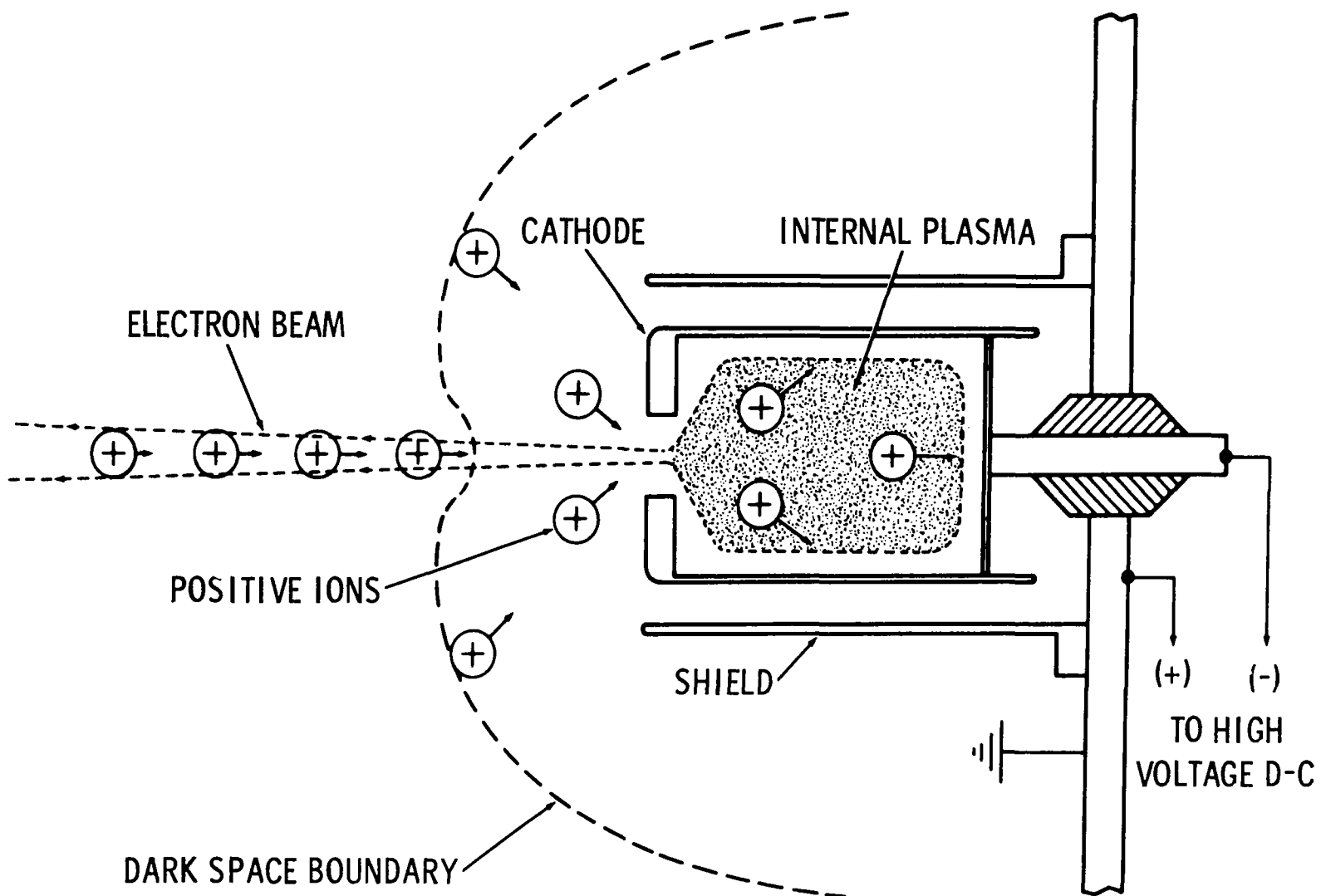


Figure 6-10. Beam formation in shielded PEB cathode.

can be welded in an atmosphere of about 75 microns. For welding structures too large to be contained in a vacuum chamber, it would seem feasible to extract the electron beam into a small chamber which moves along the weld seam maintaining a reduced pressure by means of a sliding seal. Sciaky Brothers, sponsored by the Air Force, has developed such a sliding seal for their own "partial" pressure EB system. A reliable moving chamber and the relatively simple PEB system would be a significant step toward versatility.

The plasma electron beam unit is shown in operation in Figure 6-11. The cathode at the top of the photo is emitting an electron beam through the focus coil into a Faraday cup. The photograph shows the man peering through the viewing port.



Figure 6-11. Plasma Electron Beam Unit in operation.

### 6.3 Time-Temperature Control by Cryogenic Cooling

Figures 6-2 and 6-3 suggest that the strength of a welded joint in aluminum could be increased by shortening the time at temperature. It can be achieved by the absorption of heat by forced cooling of the base plate by impingement of cryogenic liquids, such as liquid CO<sub>2</sub> and liquid nitrogen. A study was conducted at Harvey Aluminum of the effect of cryogenic cooling during welding on properties of weldments. (15)

#### Experimental Procedures (15)

Materials selected for the experimental work were aluminum alloys 2219-T87 and 2014-T6 in plate thickness of 5/16 and 1/2 inch. The welding process selected was gas tungsten arc welding, D-C, straight polarity with helium shielding gas welding done from one side in the horizontal position using 2319 filler wire for both alloys. One pass was prescribed for the 5/16-inch material and two passes for the 1/2-inch material.

Experimental equipment and procedures were developed for welding 12- by 48-inch panels with sufficient instrumentation to monitor pertinent heat input and extraction variables. Weldment temperatures were measured by thermocouples embedded in the plate. Limited investigations were conducted for measuring weld temperature by means of infrared radiometers.

Two series of welded panels were fabricated. They were bead-on-plate and square-butt welds. Table 6-1 shows typical welding parameters. Half of each series was welded without chilling and half with liquid CO<sub>2</sub> chilling, attempting to maintain comparable weld-bead dimensions. In the first series,

TABLE 6-1. TYPICAL WELDING PARAMETERS USED IN THE HARVEY ALUMINUM STUDY.

Plate Thickness (in)	Penetration Pass				Filler Pass			
	Arc Current (amp)	Voltage (v)	Travel Speed (ipm)	Wire Speed	Arc Current (amp)	Voltage (v)	Travel Speed (ipm)	Wire Speed
5/16	215-220	11	7-10	80	--	--	--	--
1/2	320-325	11	7	None	300	11	18	120

chilling was effected from the back side of the weldment using a double layer of glass tape to prevent deformation and contamination of the underbead by the liquid CO<sub>2</sub>. In the second series, weldments were chilled from the front (torch) side using a shield to prevent leakage of CO<sub>2</sub> into the arc area. Several systems of jet orifice sizes and arrangements were used for each series.

Comparable unchilled and chilled weldments for both series were examined by X-ray, fracturing, and macrosectioning. Tensile tests were performed after natural aging, artificial aging, and after reheat treating to the T-6 condition.

### Experimental Results <sup>(15)</sup>

Thermal Cycle Curves. Figure 6-12 shows examples of thermal cycle curves for points at 3/8 and 3/4 inch, respectively, from the weld centerline on 12- by 48-inch butt welds in 1/2-inch thick 2219-T87 plates. Data are compared for the unchilled weld and the weld chilled with the Jet System No. 14.\*

Macrosections. In most cases, the macrosections showed that chilling reduced the extent of the heat-affected zone, and reduced the grain size of the cast structure. For example, Figure 6-13 shows comparisons of macrosections of the unchilled and the chilled weld in 1/2-inch thick 2219-T87 plate.

Tensile Properties. Specimens were selected from chilled and unchilled weld panels of each alloy and each thickness for room-temperature tensile tests. The selection was made on the basis of X-rays which indicated less than 1 percent porosity.

---

\* Jet System No. 14 was designed for front-side chilling, using a cryogenic liquid. It utilized a traveling shield with a spring-loaded, metallic wool-and-wire brush seal and a metallic-shirt, 7-jet manifold for helium purging.

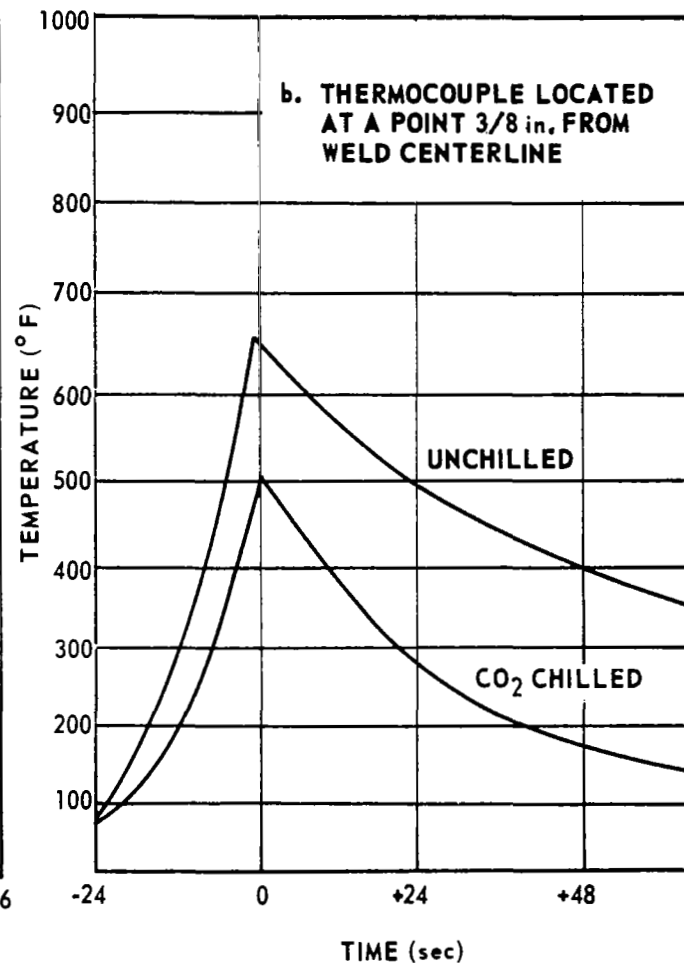
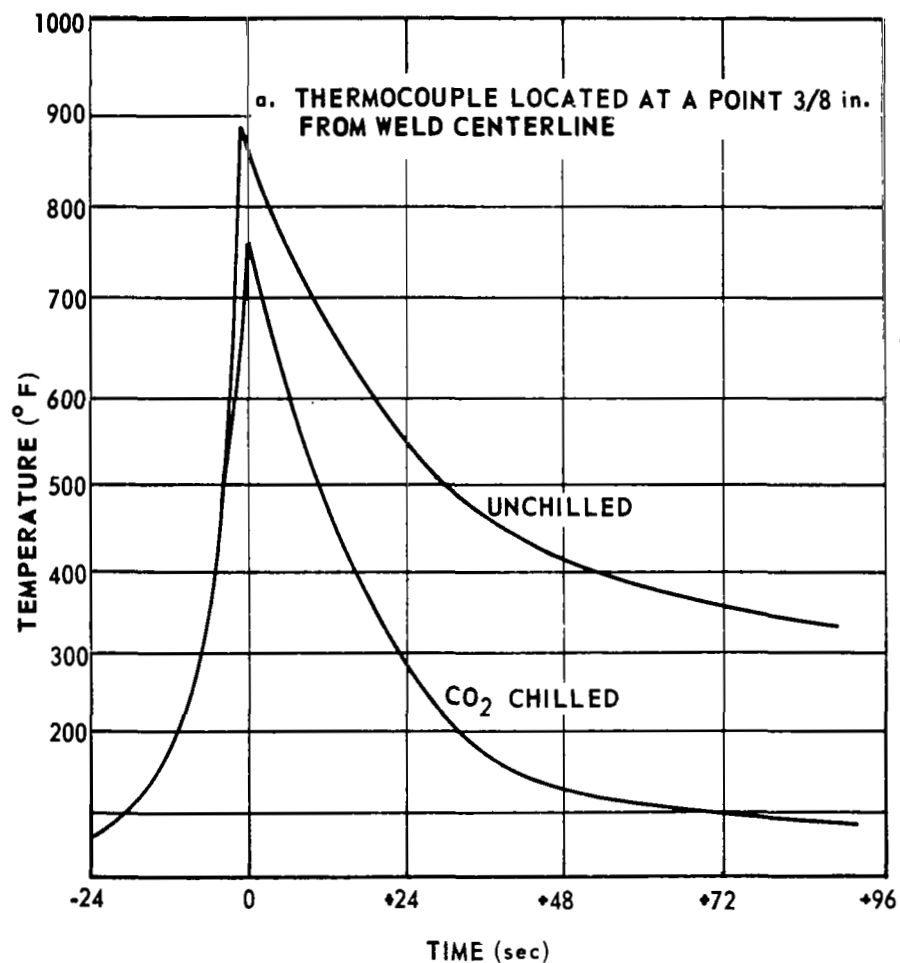


Figure 6-12. Effect of front-side chilling on thermal-cycle curves.

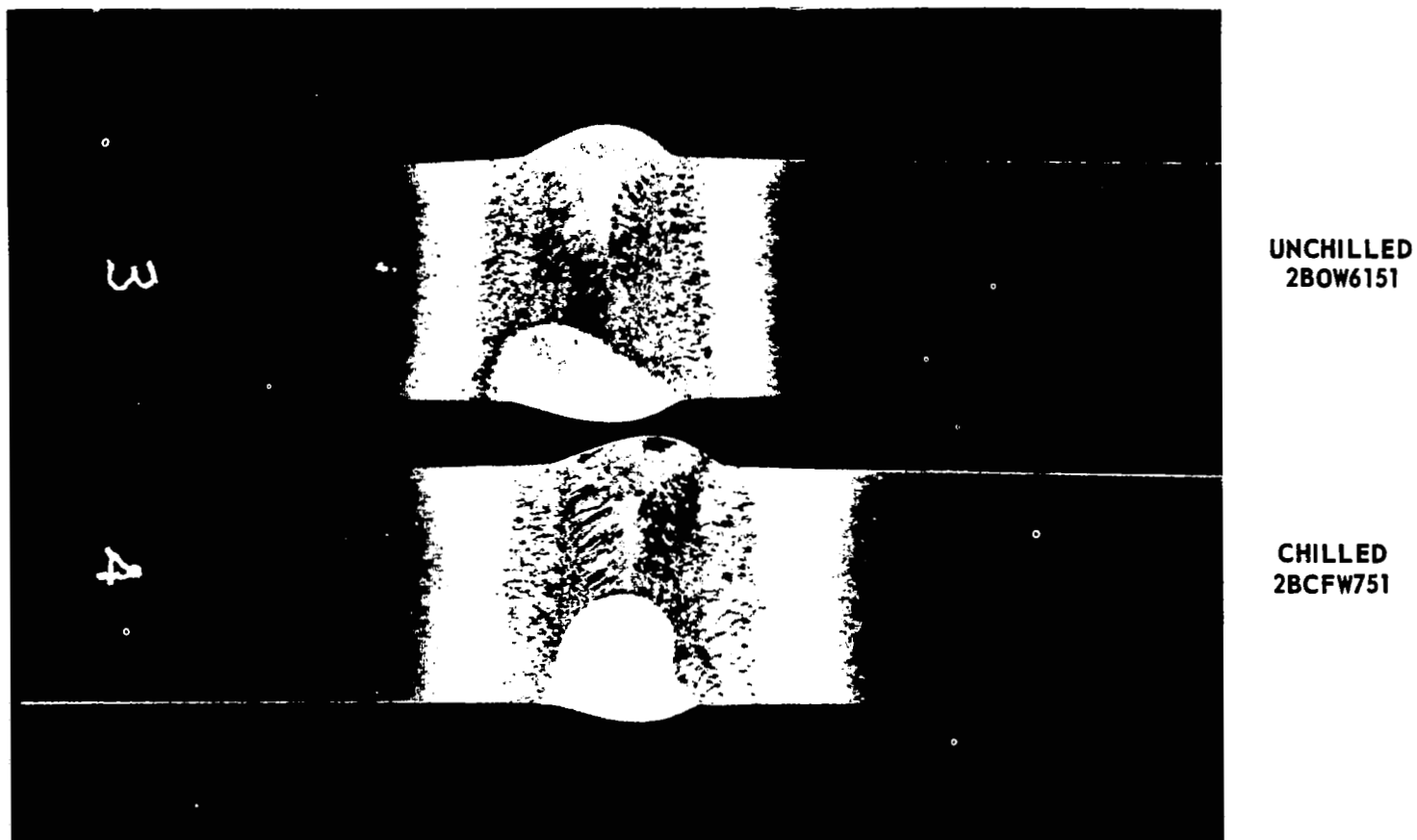


Figure 6-13. Macrosections showing effect of front-side chilling of welds.



All specimens were cut to 3/4-inch wide straight-sided bars with the weld transverse and weld bead intact. One group of specimens from each panel was artificially aged to the -T6 condition after welding. All tests were performed at room temperature.

Table 6-2 summarizes average tensile values obtained for artificially aged specimens, and Table 6-3 shows such values for naturally aged specimens.

Yield strengths are substantially increased by chilling from the front side. The greatest increase in average values was 17.8 percent for artificially aged welds in 1/2-inch 2014-T6 plate. The greatest increase in average yield strength for welds in 2219-T87 plate was 8.8 percent (for welds in 5/16-inch artificially aged specimens).

Porosity. It was found that porosity could be reduced by cryogenic cooling (refer to Chapter 5.5). Approximately 60 percent of the unchilled weld samples contained porosity ranging from 1/2 to 20 percent of the cross-sectional area, while more than 90 percent of the chilled welds were free of porosity.

Distortion. Several panels fabricated by chilling from the front side remained essentially flat after welding, exhibiting almost no longitudinal bow or peaking. Unchilled weld panels have contained a longitudinal bow up to 1 1/2 inch and peaking to 10 deg, depending upon the amount of heat input. The effectiveness of cryogenic cooling on distortion control was investigated in another contract at Harvey Aluminum. <sup>(24)</sup>

TABLE 6-2. EFFECT OF FRONT-SIDE CHILLING ON TENSILE PROPERTIES OF WELDMENTS,  
ARTIFICIAL AGING.

Weldment Material	Chill System (No.)	Average Tensile Strengths (ksi)					
		Yield			Ultimate		
		Unchilled	Chilled	Change (%)	Unchilled	Chilled	Change (%)
5/16-in. 2014-T6	18	33.9	36.9	+ 7.7	45.9	41.3	-10.0
	18	37.1	39.9	+ 7.6	49.0	48.3	- 1.4
	19	32.5	34.7	+ 6.8	44.8	42.3	- 5.6
	23	36.3	39.0	+ 7.5	48.5	47.5	+ 2.0
1/2-in. 2014-T6	18	30.9	36.4	+17.8	47.0	47.3	+ 0.6
	19	34.4	38.9	+14.4	47.2	47.6	+ 0.1
	19	34.0	38.7	+13.8	47.2	48.7	+ 3.2
5/16-in. 2219-T87	19	31.9	33.2	+ 4.2	38.4	39.0	+ 1.6
	19	35.4	38.5	+ 8.8	40.4	44.7	+10.7
	23	35.1	36.0	+ 2.6	42.5	40.7	- 4.2
1/2-in. 2219-T87	18	35.1	36.7	+ 4.6	46.8	48.1	+ 3.4
	19	34.2	36.0	+ 6.4	43.7	45.6	+ 4.3
	23	35.1	36.6	+ 4.3	45.0	46.8	+ 4.0

TABLE 6-3. EFFECT OF FRONT-SIDE CHILLING ON TENSILE PROPERTIES OF WELDMENTS, NATURAL AGING.

Weldment Material	Chill System (No.)	Average Tensile Strengths (ksi)					
		Yield			Ultimate		
		Unchilled	Chilled	Change (%)	Unchilled	Chilled	Change (%)
5/16-in. 2014-T6	18	32.7	34.5	+ 5.6	45.5	45.2	-0.6
	19	33.5	36.6	+ 9.3	40.2	40.4	+0.5
	23	33.0	35.5	+ 7.6	49.7	45.5	-8.5
1/2-in. 2014-T6	19	28.8	32.1	+11.5	47.4	48.3	+1.9
	19	28.8	33.2	+15.5	47.4	49.0	+3.4
5/16-in. 2219-T87	23	24.2	26.8	+ 2.6	37.8	40.5	+2.5
	19	25.5	25.7	+ 0.8	36.1	37.3	+3.3
1/2-in. 2219-T87	18	20.9	22.5	+ 7.7	40.4	41.5	+2.7
	19	19.7	20.2	+ 2.5	38.8	40.1	+3.8
	23	21.7	21.6	- 0.5	39.4	40.8	+3.6



## CHAPTER 7

### Residual Stresses and Distortion

An important problem facing engineers engaged in welding fabrication of aluminum structures is that residual stresses and distortion. Control of weld distortion is generally more of a problem in aluminum structures than steel structures because:

- 1) Aluminum, compared with steel, has higher heat conductivity. Therefore, the welding heat spreads in wider areas, or expansion and contraction occur in larger areas.
- 2) Aluminum has a larger coefficient of thermal expansion than steel.
- 3) Many aluminum alloys have rather low yield strengths, thus producing large plastic zones near the weld.

Due to combined effects of these factors, considerable amounts of thermal stresses are produced during welding in areas adjacent to the welding arc. These thermal stresses may cause joint mismatch, when the joint is not tightly clamped. When welding is completed, high tensile residual stresses are produced in areas near the weld which can cause considerable shrinkage and distortion.

## 7.1 Analysis of Thermal Stresses during Welding

Several aerospace companies have encountered distortion problems during fabrication of the Saturn V components including welded fuel and oxidizer tanks. Although production practices have been developed to temporarily overcome these problems, they are empirical solutions and little is known about the mechanisms causing such distortion. It is essential to understand the mechanisms in order to develop methods for minimizing distortion effects during fabrication of future vehicles.

MSFC recognized the importance of conducting research on mathematical analysis of thermal stresses and metal movement during welding and supported studies at Battelle Memorial Institute and Massachusetts Institute of Technology.\* Computer programs have been developed to calculate transient thermal stresses in areas surrounding the moving welding arc and resulting residual stresses.

### Technical Background on Analysis and Control of Weld Distortion

This section presents a brief technical background on the analysis of thermal stresses and metal movement during welding. Discussions in this section are limited to those subjects which are directly related to the studies at Battelle and M.I.T. and a number of other subjects on various types of weld distortion are not covered.

A recent Welding Research Council Bulletin No. 149 entitled "Control of Distortion and Shrinkage in Welding"

---

\* Dr. Koichi Masubuchi, who was the principal investigator of the Battelle study joined the Faculty of M.I.T. in 1968.

is an interpretive report covering the development of analytical means for predicting and controlling various types of weld distortion.<sup>(58)</sup> The material in this section is a condensation of this report.

Welding Thermal Stresses. Because a weldment is locally heated by the welding arc, the temperature distribution in the weldment is not uniform and changes as welding progresses. This non-uniform temperature distribution causes thermal stresses in the weldment, which also change as welding progresses. The major effort in the studies at Battelle and M.I.T. has been to develop computer programs to analyze such thermal stresses during welding and also the resulting residual stresses.

Figure 7-1 shows schematically how welding thermal stresses are formed. Figure 7-1a shows a bead-on-plate weld in which a weld bead is being laid at a speed  $v$ .  $O$ - $xy$  is the coordinate system; the origin,  $O$ , is on the surface underneath the welding arc, and the  $x$ -direction lies in the direction of welding.

Figure 7-1b shows temperature distribution along several cross sections. Along Section A-A, which is ahead of the welding arc, the temperature change due to welding,  $\Delta T$ , is almost zero (Figure 7-1b-1). Along Section B-B, which crosses the welding arc, the temperature distribution is very steep (Figure 7-1b-2). Along Section C-C, which is some distance behind the welding arc, the distribution of temperature change is as shown in Figure 7-1b-3. Along Section D-D, which is very far from the welding arc, the temperature change due to welding again diminishes (Figure 7-1b-4).

Figure 7-1c shows the distribution of stresses along these sections in the  $x$ -direction,  $\sigma_x$ . Stress in the

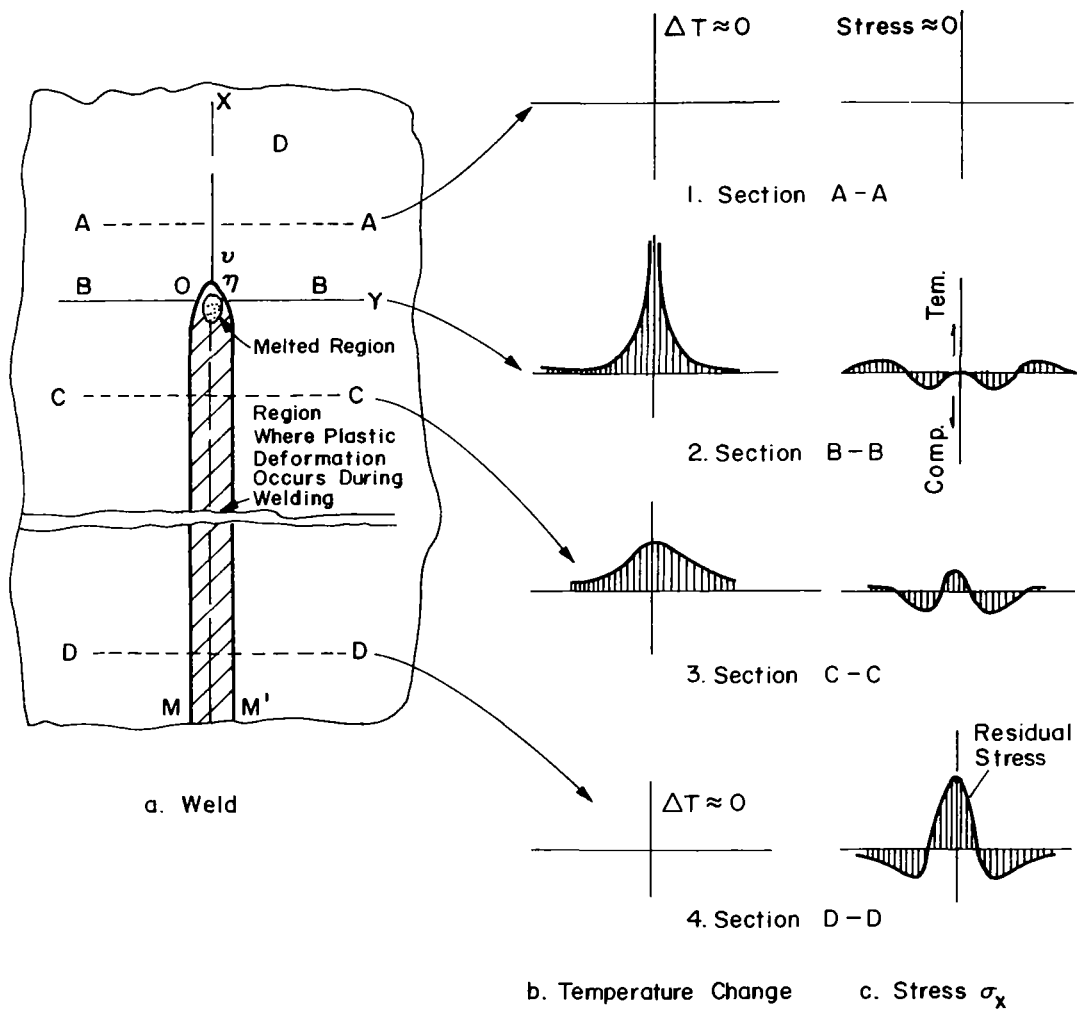


Figure 7-1. Schematic representation of changes of temperature and stresses during welding.



y-direction,  $\sigma_y$ , and shearing stress,  $\tau_{xy}$ , also exist in a two-dimensional stress field (Figure 7-1a).\*

Along Section A-A, thermal stresses due to welding are almost zero (Figure 7-1c-1). The stress distribution along Section B-B is shown in Figure 7-1c-2. Stresses in areas underneath the welding arc are close to zero, because molten metal does not support loads. Stresses in areas somewhat away from the arc are compressive, because the expansion of these areas is restrained by surrounding areas that are heated to lower temperatures. Since the temperatures of these areas are quite high and the yield strength of the material is low, stresses in these areas are as high as the yield strength of material at corresponding temperatures. The amount of compressive stress increases with increasing distance from the weld or with decreasing temperature. However, stresses in areas away from the weld are tensile and balance with compressive stresses in areas near the weld. In other words,

$$\int \sigma_x \cdot dy = 0 \quad (7-1)$$

across Section B-B.\*\* Thus, the stress distribution along Section B-B is as shown in Figure 7-1c-2.

Stresses are distributed along Section C-C as shown in Figure 7-1c-3. Since the weld-metal and base-metal regions near the weld have cooled, they try to shrink causing tensile stresses in areas close to the weld. As the distance from the weld increases, the stresses first change to compressive and then become tensile.

---

\* In a general three-dimensional stress field, six stress components,  $\sigma_x$ ,  $\sigma_y$ ,  $\sigma_z$ ,  $\tau_{xy}$ ,  $\tau_{zy}$ ,  $\tau_{zx}$  exist.

\*\* Equation (7-1) neglects the effect of  $\sigma_y$  and  $\tau_{xy}$  on the equilibrium condition.

Figure 7-1c-4 shows the stress distribution along Section D-D. High tensile stresses are produced in areas near the weld, while compressive stresses are produced in areas away from the weld. The distribution of residual stresses that remain after welding is completed as shown in the figure.

The cross-hatched area, MM', in Figure 7-1a shows the region where plastic deformation occurs during the welding thermal cycle. The ellipse near the origin O indicates the region where the metal is melted. The region outside the cross-hatched area remains elastic during the entire welding thermal cycle.

Metal Movement during Welding. Welding thermal stresses cause metal movement during welding. There are two major types of metal movement. The first type involves motion in the plane of the plate, that is opening or closing of the joint gap ahead of the weld.

The second type involves motion out of the plane of the plate, that is either bending due to temperature variations in the thickness direction or buckling due to compressive thermal stresses. This out-of-plane metal movement often causes joint mismatch.

#### Development of Techniques for Analyzing Thermal Stresses and Metal Movement

As shown in Figure 7-1, thermal stresses during welding are produced by a complex mechanism which involves plastic deformation at a wide range of temperatures from room temperature up to the melting temperature. Because of the difficulty in analyzing plastic deformation, especially at elevated temperatures, mathematical analyses conducted in the past

are limited to simple cases such as spot welding.\*\*\*

However, on the basis of recent development in computer technology, it appears that we are on the verge of technological breakthrough as far as the analysis of thermal stresses during welding are concerned. The following pages describe recent developments made at Battelle and M.I.T.

Battelle Computer Analysis. Under a recent contract for Redstone Scientific Information Center, U. S. Army Missile Command, Masubuchi, Simmons, and Monroe of Battelle Memorial Institute developed computer programs for calculating thermal stresses in bead-on-plate welding.<sup>(29)</sup> The Battelle study uses the technique which was originally developed in 1964 by Tall.<sup>(59,60)</sup>

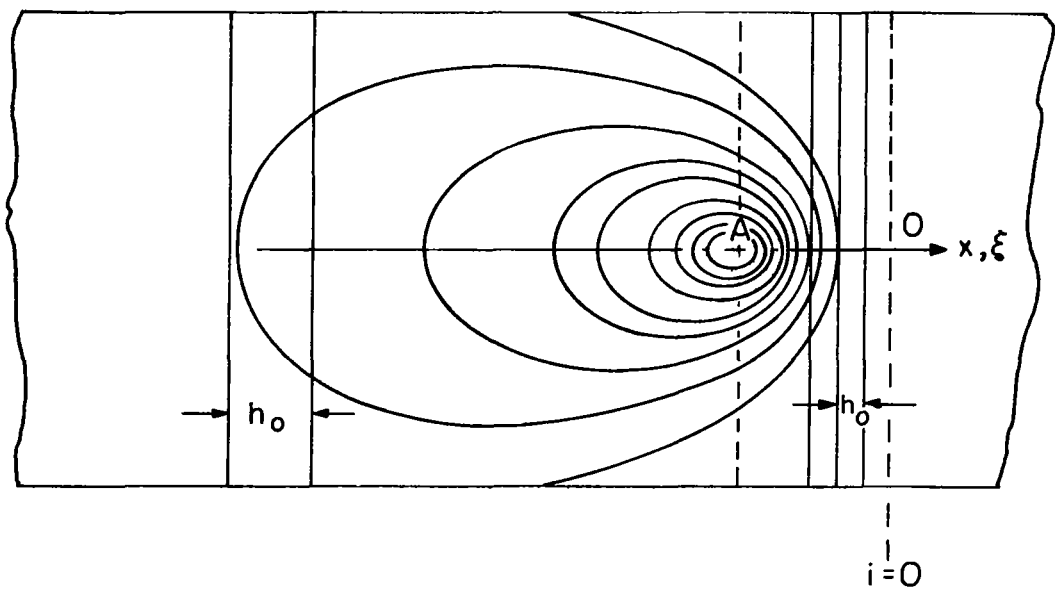
In the Battelle analysis, it was assumed that (1) the longitudinal stress,  $\sigma_x$ , is a function of  $y$  only and (2)  $\sigma_y$  and  $\tau_{xy}$  are zero (see Figure 7-1). Details of the Battelle analysis are reported in RSIC-820.

First, the temperature distribution around the moving arc is calculated. Then the stress field is divided into a set of transverse strips of width,  $h_0$ , as shown in Figure 7-2. The time intervals represented by the strip width must be short enough so that the temperature and thermal stress for each increment may be regarded as being constant. Since the greatest changes in temperature occur near the arc, narrow strips are used in areas near the arc

The calculation starts on a strip some distance ahead of the welding arc where the temperature change is negligible and stresses are purely elastic. Time zero is fixed on the strip. For example, in the calculations shown later

---

\*\*\* The Welding Research Council Bulletin 149 discusses the historical trend in the development of techniques for analyzing thermal stresses during welding and resulting residual stresses.<sup>(58)</sup>



$$\theta = \frac{q}{2\pi\lambda} e^{-\frac{\nu}{2\kappa} \xi} K_0\left(\frac{\nu}{2\kappa} r\right)$$

$$r = \sqrt{\xi^2 + y^2}$$

Figure 7-2. Dividing the stress field into transverse strips for calculating thermal and residual stresses.

(Figures 7-3 through 7-6), the heat source is located at  $T = 9$  seconds. Since the welding speed in this particular case is 0.233 ips, or 14 ipm, the calculation starts at a strip 2.1 inches ( $0.233 \times 9$ ) ahead of the arc.

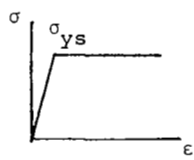
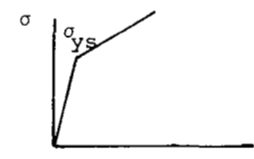
First, stresses in the strip crossing the origin, 0, are calculated based on elasticity theory. Then, stresses in the second strip are calculated by adding stresses due to the temperature increment. In this case, analysis is made whether or not any plastic deformation takes place. It is assumed that the amount of stresses at a given point does not exceed the yield stress of the material at the temperature of that point. Similar analyses are conducted step by step on the following strips. Thus the stress distribution in the entire field is determined.

The program is written in FORTRAN IV computer language for use on a Control Data Corporation (CDC) 6400 computer system including a Cal-Comp plotter. The FORTRAN language is common in computer programming and can be adapted readily to any other computer that has a FORTRAN compiler program.

M.I.T. One-Dimensional Analysis. The Battelle program was improved during a study at M.I.T. completed in October, 1970. Table 7-1 presents comparison between the Battelle program and the M.I.T. program. Although both of them are one-dimensional analyses, the M.I.T. program has several improvements over the Battelle program.

For example, strain hardening of the material is considered in the M.I.T. program, while the material is assumed to be perfectly plastic in the Battelle program. In both programs, however, the yield strength,  $\sigma_{ys}$ , changes with temperature. The M.I.T. program includes the analysis of strain which is important in comparing results of the theoretical study with experimental data. In the experimental

TABLE 7-1. COMPARISON BETWEEN THE BATTLE PROGRAM AND THE M. I. T. PROGRAMS.

	Battelle Program	M.I.T. Program
Type of Weld Analyzed	Bead-on-plate	Bead-on-plate, Edge, and Butt weld
Configuration	Flat plate with finite width	Flat plate with finite width
Stress Analysis	Longitudinal stress only $\sigma_x = f(x,y)$ $\sigma_y = \tau_{xy} = 0$	Longitudinal stress only $\sigma_x = f(x,y)$ $\sigma_y = \tau_{xy} = 0$
Material Behavior	Perfectly plastic* 	Strain hardening (linear) included* 
Analysis of Strain	Not included	Includes total strain and plastic strain
Temperature distribution	Calculated by same program	Calculated by separate program. Distributions from other sources may be used for stress calculation

\*Yield strength varies with temperature.

analysis, strains rather than stresses are commonly measured.

The M.I.T. program is written in FORTRAN IV for use on an IBM 360/65 computer.

M.I.T. Two-Dimensional Analysis. Under a current contract for MSFC, a study is being conducted at M.I.T. to develop a two-dimensional analysis of thermal stresses during welding. All three components,  $\sigma_x$ ,  $\sigma_y$ , and  $\tau_{xy}$  are analyzed as functions of x and y. The analysis uses the finite-element method.

The finite-element method is an approximate stress analysis technique which yields accurate solutions for complex problems by use of a high-speed computer. This method, which was originally developed in the aircraft industry, has been successfully applied to a wide variety of problems.

#### Examples of Analytical Results

Figures 7-3 through 7-6 shows results of an example. In this particular example, calculations are made under the following conditions:

Aluminum alloy 2014-T6, 1/4 inch thick  
Plate width: 8 inches  
Welding current: 254 amp  
Arc voltage: 10 v  
Arc travel speed: 0.233 ips (14 ipm)  
Arc efficiency:\* 80%

Except for some letters such as "Center Line," "1 inch out from " and "Edge" in Figure 7-3 and "100 F," "200 F," etc., in Figure 7-4, most lines and letters in Figure 7-3 through 7-6 are plotted by a Cal-Comp plotter. In other

---

\* It is assumed that 80% of the energy generated by the arc is transmitted to the plate.

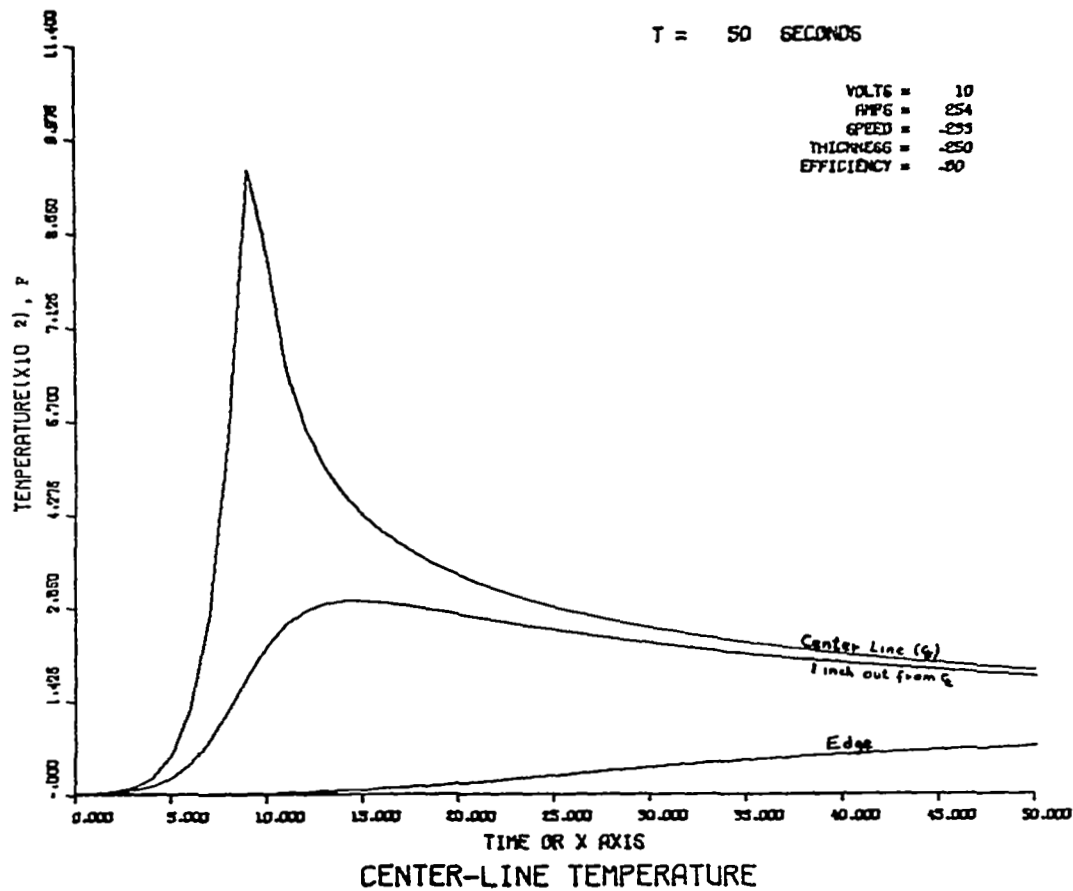


Figure 7-3. Temperature changes along three longitudinal lines.

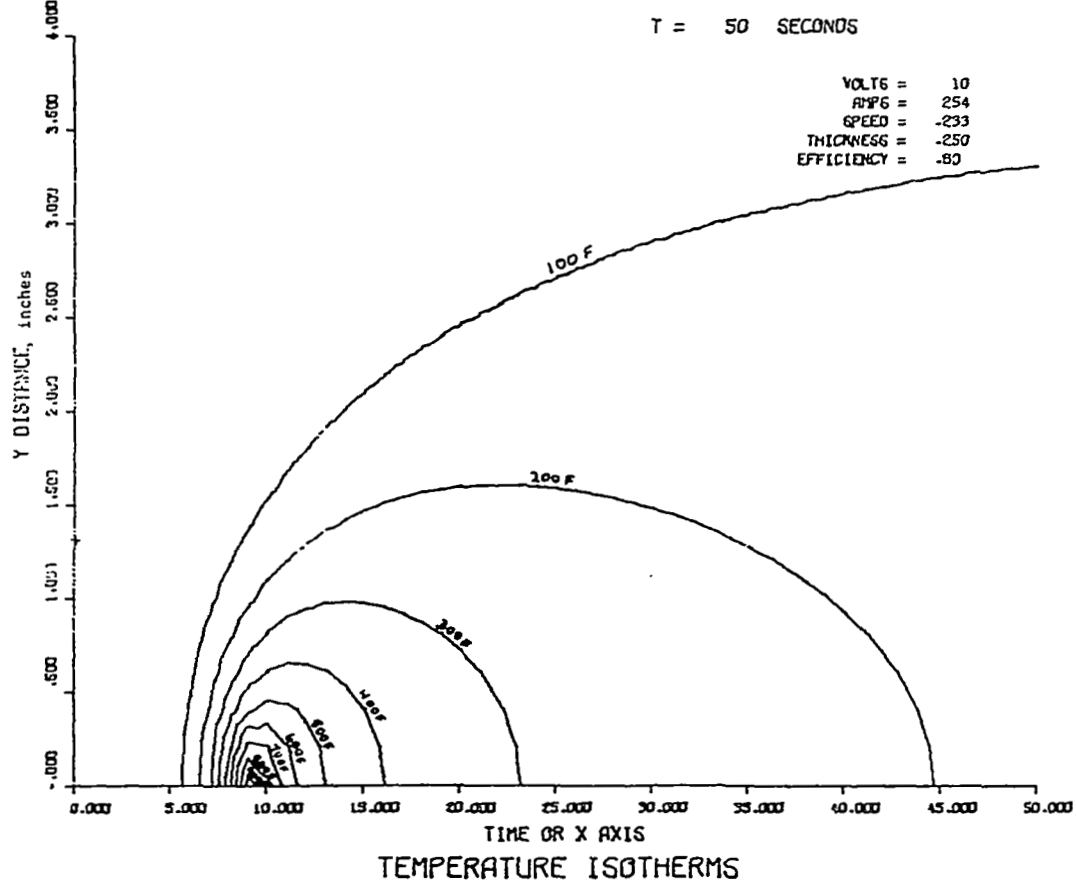


Figure 7-4. Isotherm pattern.



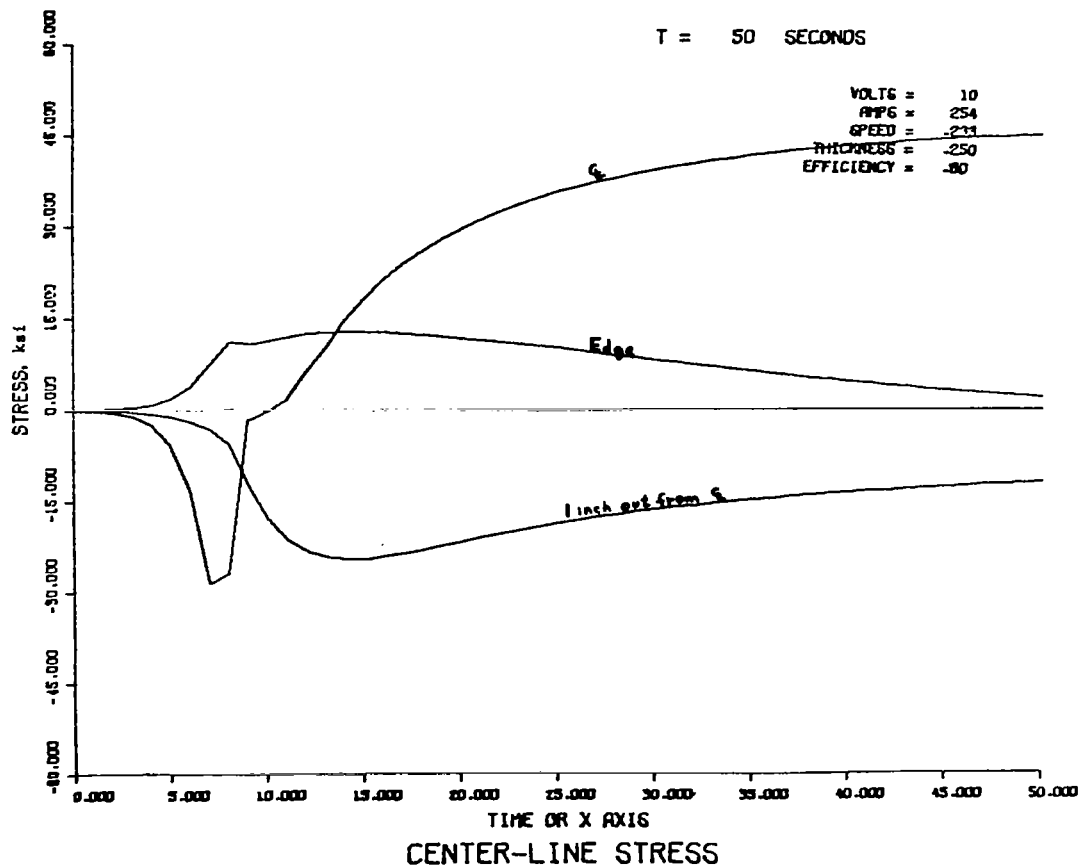


Figure 7-5. Stress changes along three longitudinal lines.

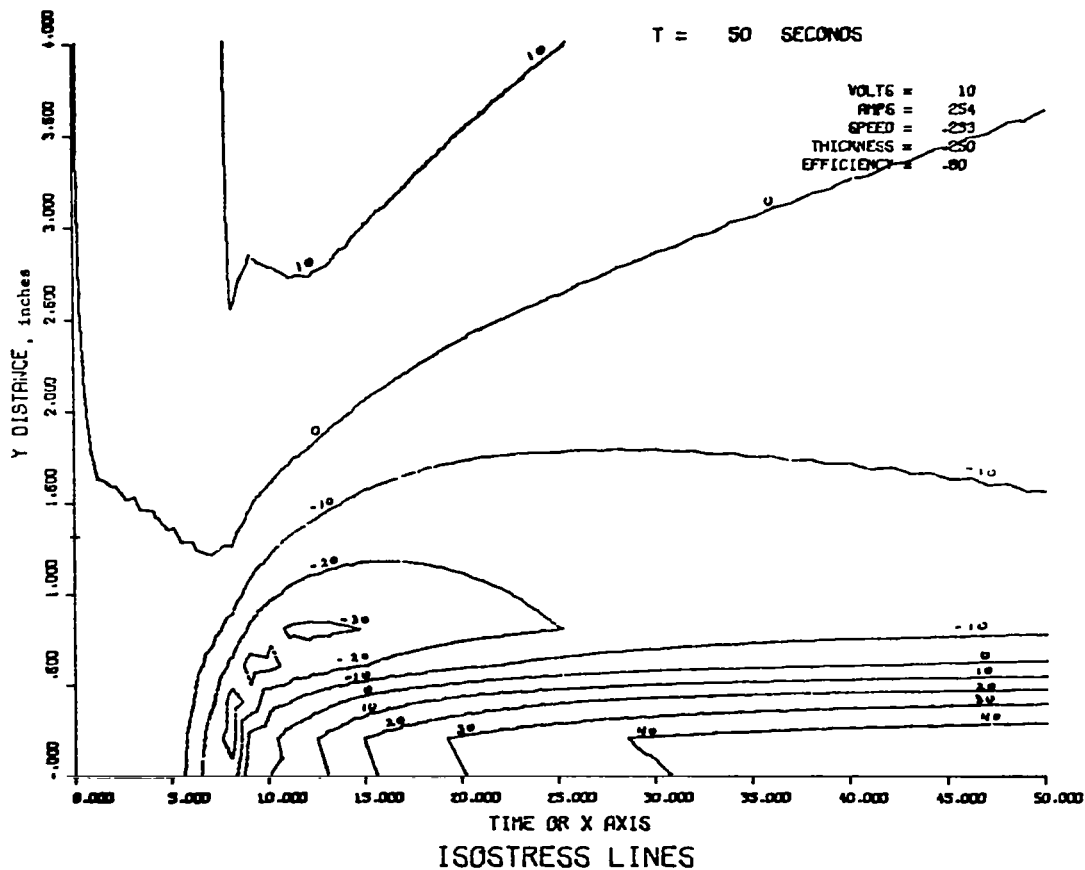


Figure 7-6. Isostress pattern.

words, a computer provides not only a print-out sheet but also figures already printed as shown in Figures 7-3 through 7-6.

Figure 7-3 shows temperature changes along the weld center line ( $y = 0$ ),  $y = 1$  inch, and  $y = 4$  inches. The abscissa is given in terms of time, and the arc is located at 9 seconds. Each curve, therefore, also can be considered as a curve showing the thermal cycle of a point some distance away from the weld.

Figure 7-4 shows the isotherm pattern around the arc. Again the time scale can be interpreted as the longitudinal coordinate  $x$ .

Figure 7-5 shows stress changes along  $y = 0$ , 1 and 4 inches. Along the weld center line ( $y = 0$ ), stresses are in compression in areas ahead of the arc. As the arc approaches the point, the absolute value of the compressive stress first increases and then decreases as the temperature increases. At the point below the arc, the stress is zero. Stresses are in tensile, in areas behind the arc, since cooling takes place in these areas.

Figure 7-6 shows the isostress pattern around the arc. There is a high compressive stress area shortly ahead of the heat source; however, values of compressive stresses are very low in high-temperature areas very close to the heat source. There is a narrow tensile-stress zone along the center line behind the heat source, and compressive-stress zone expands outwards in a horseshoe shape.

From the standpoint of metal movement in the thickness direction during welding which causes joint mismatch, the compressive stress zone appears to be of particular importance. If the plate is thin, or the compressive-stress zone is large, the plate may buckle during welding. Distortion in the thickness direction also may be caused if the temperature and

stress distributions are not uniform in the thickness direction.

### Effects of Welding Parameters

An important benefit of the computer analysis is that once the program is developed it is relatively less expensive to conduct calculations under different conditions. M.I.T. researchers studied effects of welding parameters on thermal stresses during welding of 2219-0 aluminum plates and resulting residual stresses.\*

Welding Parameters Used in the Analysis. Table 7-2 shows values of welding parameters used in the sixteen cases studied. The definitions of linear net heat input,  $h$ , and linear net heat intensity,  $q$ , are:

$$h = H/T \qquad q = Q/T \qquad H = Q/v \quad (7-1)$$

where

$Q = \eta \cdot V \cdot I$ , thermal power of heat source in watts or joules/second

$\eta$  = arc efficiency

$V$  = arc voltage

$I$  = arc current

$v$  = welding speed in inches/second

$T$  = plate thickness, inch

From the definitions,  $q$  is the intensity of a line heat source, or the average value of the intensity of heat source in the thickness direction; therefore,  $q$  is called the "linear

---

\*An experimental investigation was made on bead-on-plate welds in 2219-0 alloy as discussed later.

TABLE 7-2. WELDING PARAMETERS USED IN THE ANALYSIS

Case Number	Arc Travel Speed, v		Linear Net Heat Input, $h^*$ joules/inch <sup>2</sup>	Linear Net Heat Intensity, $q^*$ joules/sec/inch
	inches/min	inch/sec		
1	5	0.0833	10,000	833
2	5	0.0833	32,000	2,667
3	5	0.0833	56,000	4,667
4	5	0.0833	80,000	6,667
5	10	0.1667	10,000	1,667
6	10	0.1667	32,000	5,333
7	10	0.1667	56,000	9,333
8	10	0.1667	80,000	13,333
9	20	0.333	10,000	3,333
10	20	0.333	32,000	10,667
11	20	0.333	56,000	18,667
12	20	0.333	80,000	26,667
13	30	0.500	10,000	5,000
14	30	0.500	32,000	16,000
15	30	0.500	56,000	28,000
16	30	0.500	80,000	40,000

\* Values of h and q are actual values supplied to the plate.

net heat intensity." The value  $h$  is the net heat input supplied to unit plate thickness; therefore, it is called the "linear net heat input."

As shown in Table 7-2, welding speed,  $v$ , was changed in four levels 5, 10, 20, and 30 inches per minute, or 0.0833, 0.1667, 0.333, and 0.500 inches per second. Linear net heat input,  $h$ , was also changed in four levels, 10,000, 32,000, 56,000, and 80,000 joules/inch/inch. When the value of arc efficiency is 0.7, for example, these net heat input values correspond to 14,300, 45,700, 80,000, and 114,000 joules/inch/inch, respectively welding heat input.

It must be mentioned that linear net heat input,  $h$ , and welding speed,  $v$ , are not independent, as shown from Equation (7-1). For example, when  $v$  is increased to  $2v$ , while  $q$  is unchanged,  $h$  will be reduced to  $1/2 h$ . Figure 7-7 shows welding parameters used for the 16 conditions studied. The value of linear net heat intensity  $q$  is the lowest for Case 1 with low heat input and slow welding speed, while it is the highest for Case 16 with high heat input and fast welding speed.

All calculations were conducted on bead-on-plate welding along the longitudinal center line of a infinitely long strip, 18 inches wide.

Results of the Analysis. The analysis included effects of welding parameters on:

- (1) High tensile thermal stresses in areas behind the arc
- (2) Compressive thermal stresses in areas ahead of the arc
- (3) Size of plastic zone
- (4) Residual stress distributions.

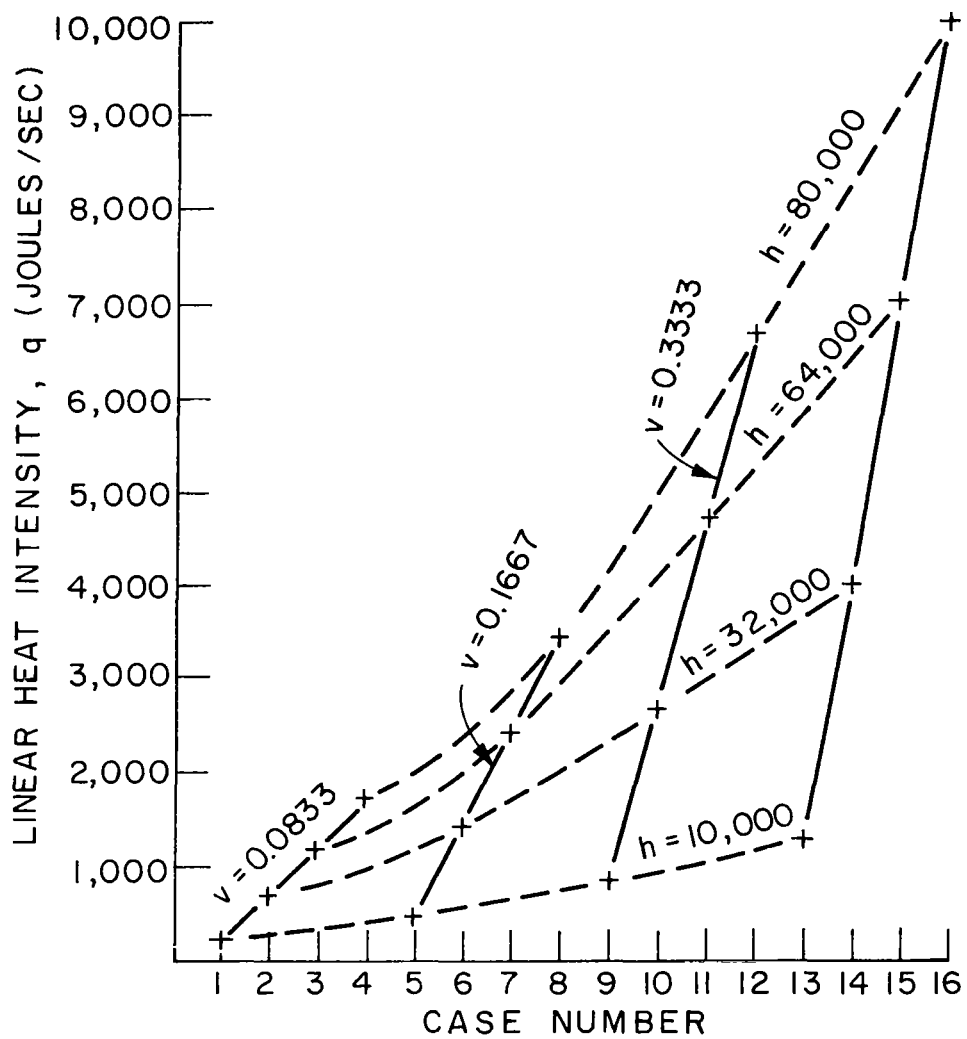


Figure 7-7. Welding parameters used for the sixteen conditions studied.

In order to keep the size of this report to a minimum, the following pages discuss only the last subject: effects on welding parameters on residual stress distributions.

Figure 7-8 shows distributions of longitudinal residual stresses for Cases 2, 6, 10, and 14 ( $h = 32,000$  joules/in<sup>2</sup>). High tensile stresses are produced in areas near the weld, while compressive stresses are produced in areas away from the weld. The maximum value of residual stress at the weld center line is about 11,000 psi, which is the yield stress level at room temperature, regardless of welding conditions.

However, the width of tensile residual stress zone is affected by welding parameters. In the cases shown in Figure 7-8, for example, the width of tensile stress zone increased as the welding speed increased, while keeping the linear heat input,  $h$ , constant.

Figure 7-9 shows the half width of tensile residual stress zone as affected by linear net heat input,  $h$ , and welding speed,  $v$ ; while Figure 7-10 shows the half width of tensile residual stress zone as affected by linear net heat intensity,  $q$ , and welding speed,  $v$ .

Figures 7-9 and 7-10 show that linear net heat input,  $h$ , is the most significant factor that affect the width of tensile residual stress zone, and it increases with increasing heat input. The effect of heat input, however, is not linear. The increase in the width of tensile residual stress zone per unit increase in heat input decreases as heat input increases.

From the practical viewpoint, the results clearly show the advantage of using low welding heat input to reduce residual stresses and distortion.

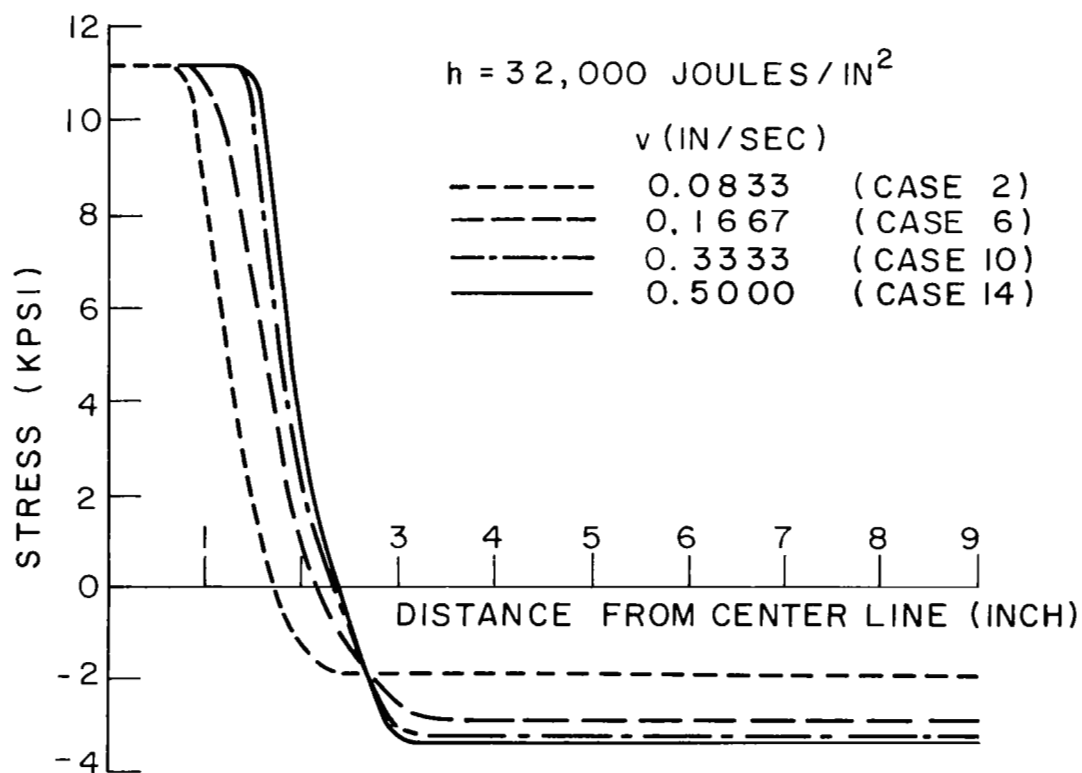


Figure 7-8. Distributions of longitudinal residual stresses for cases 2, 6, 10, and 14 ( $h = 32,000 \text{ joules/in}^2$ ).



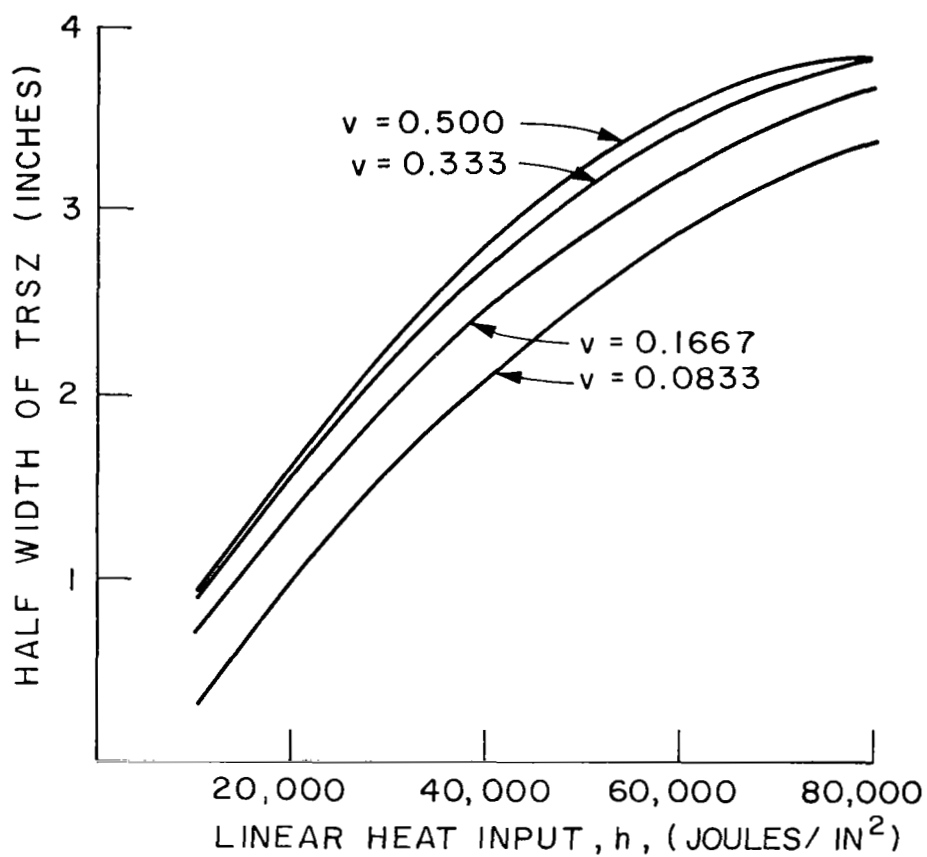


Figure 7-9. Effects of Linear Heat Input,  $h$ , and Welding Speed,  $v$ , on the Width of Tensile Residual Stress Zone.

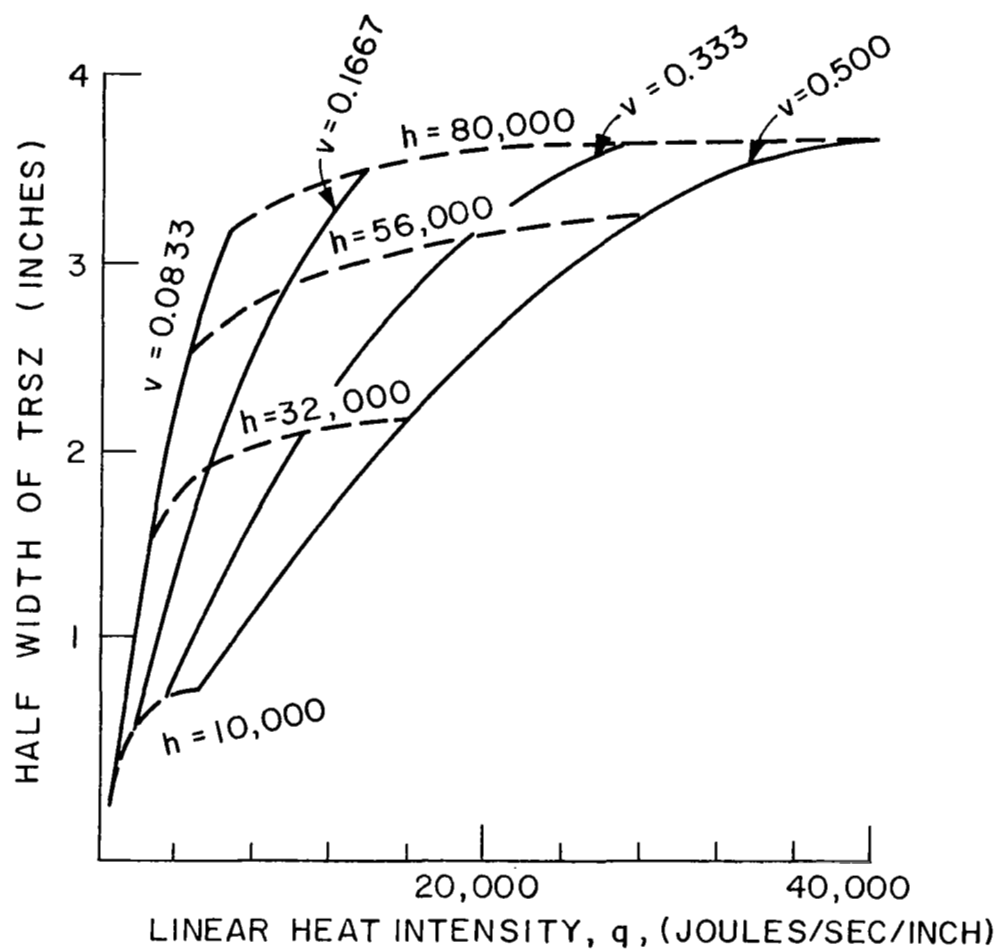


Figure 7-10. Effects of Linear Heat Intensity,  $q$ , and Welding Speed,  $v$ , on the Width of Tensile Residual Stress Zone.

## Effects of Material Properties on Residual Stress Distributions

An analysis was made of effects of material properties on residual stresses. Figure 7-11 shows yield stress vs temperature curves for several materials including high-strength aluminum (with which the current study is primarily concerned), low carbon steel, ultrahigh strength steel, columbium, and tantalum.

The yield strength of ultrahigh-strength steel is very high at room temperature, but it decreases rather rapidly with increasing temperature. Columbium and tantalum, which were included by the request from MSFC, are characterized by low yield stresses at room temperature and relatively high yield stresses at high temperature.

Figure 7-12 shows residual stress distributions for low carbon steel and ultrahigh-strength steel. In both cases, maximum tensile stresses at the weld center are as high as the yield stresses of these steels. The width of tensile residual stress for ultrahigh-strength is very narrow. This is primarily due to the fact that only a very narrow zone undergoes plastic deformation during welding.

Figure 7-13 shows residual stress distributions for columbium and tantalum. The widths of tensile residual stress zones are very large. Since both columbium and tantalum have relatively low yield stresses at a wide temperature range, very large areas of plastic deformation occur during welding.

Figure 7-13 suggests that residual stresses and distortion can be quite a problem during welding some refractory metals including columbium and tantalum. It was informed from the MSFC that some distortion problems have been experienced in welding these metals.

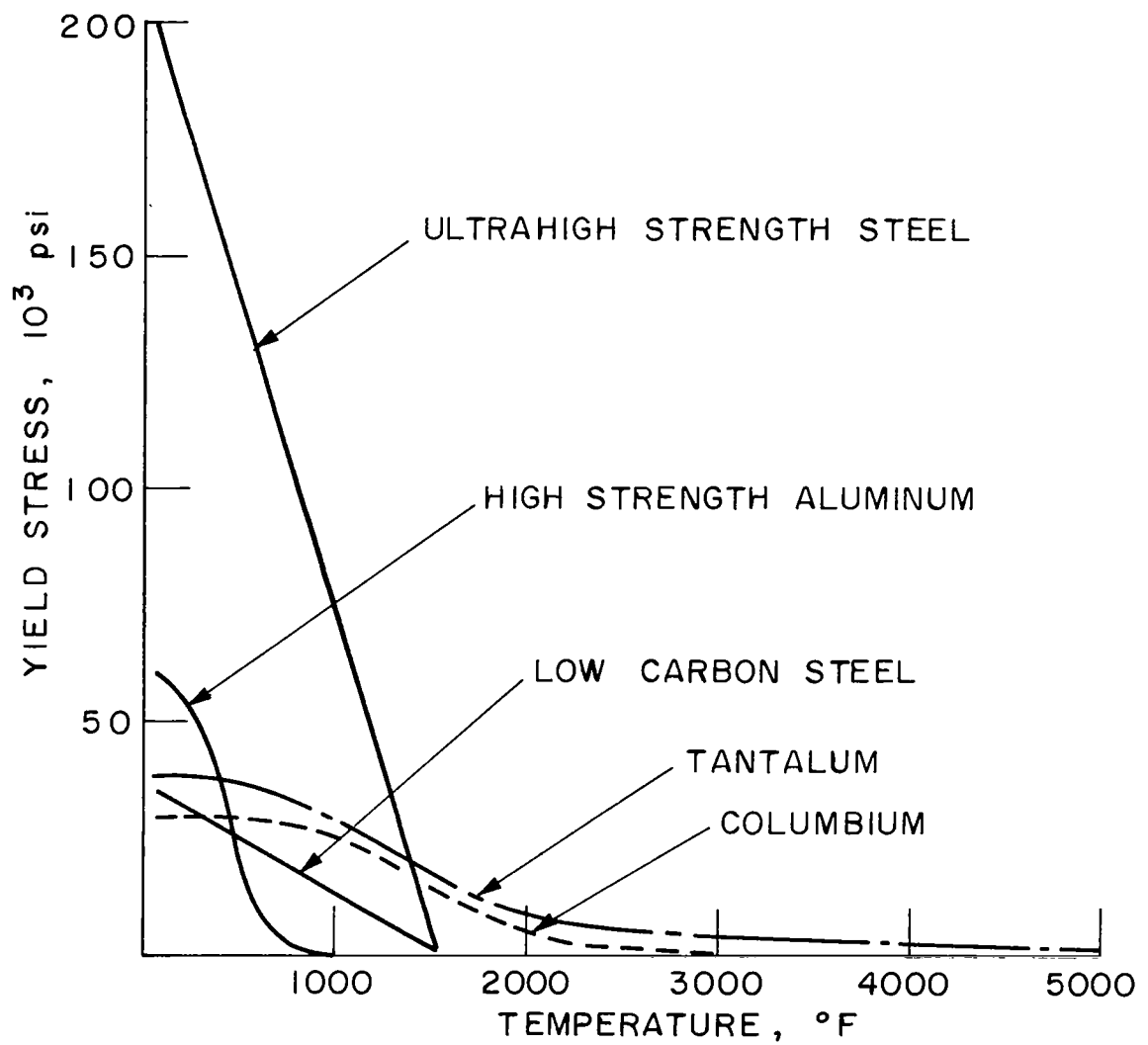


Figure 7-11. Yield strength vs. temperature curves for several materials studied.

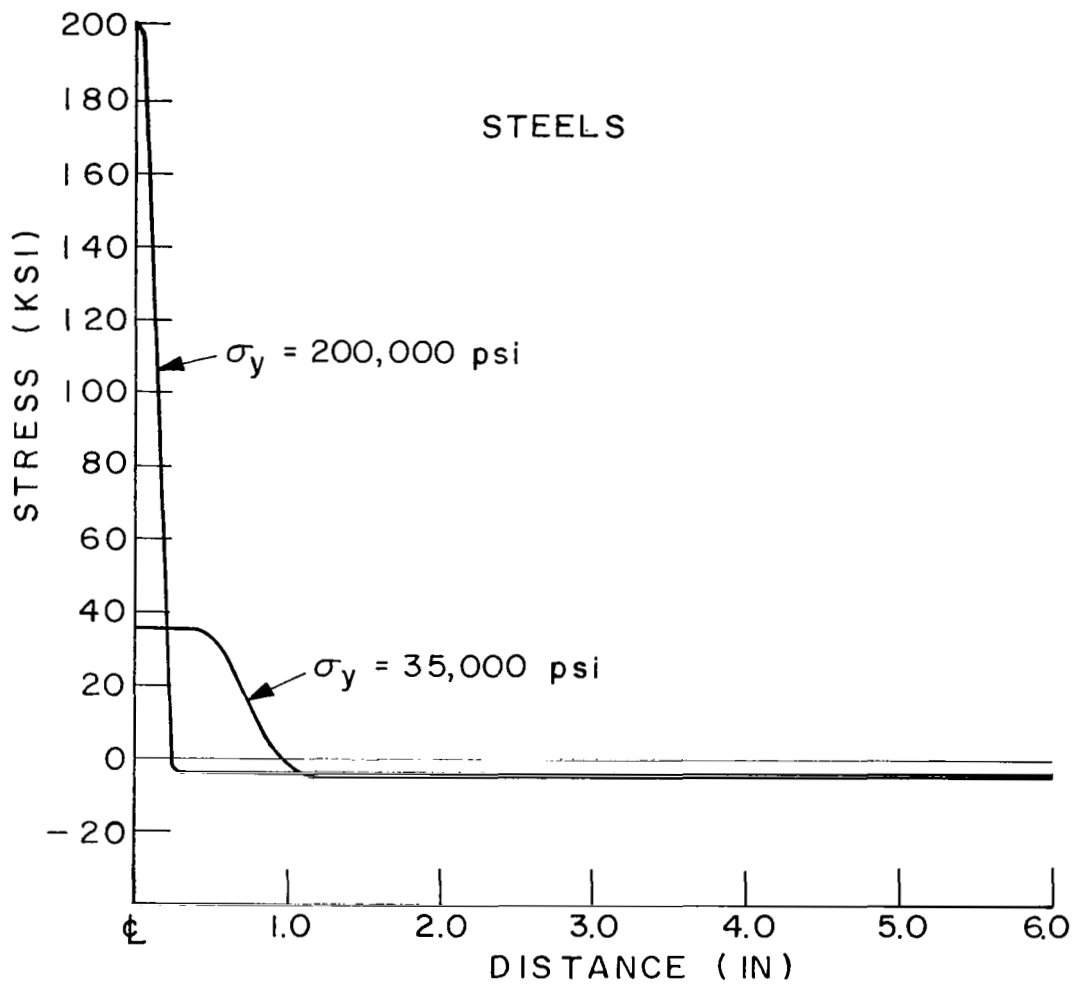


Figure 7-12. Residual Stress Distributions for Low-Carbon Steel and Ultrahigh-strength Steel

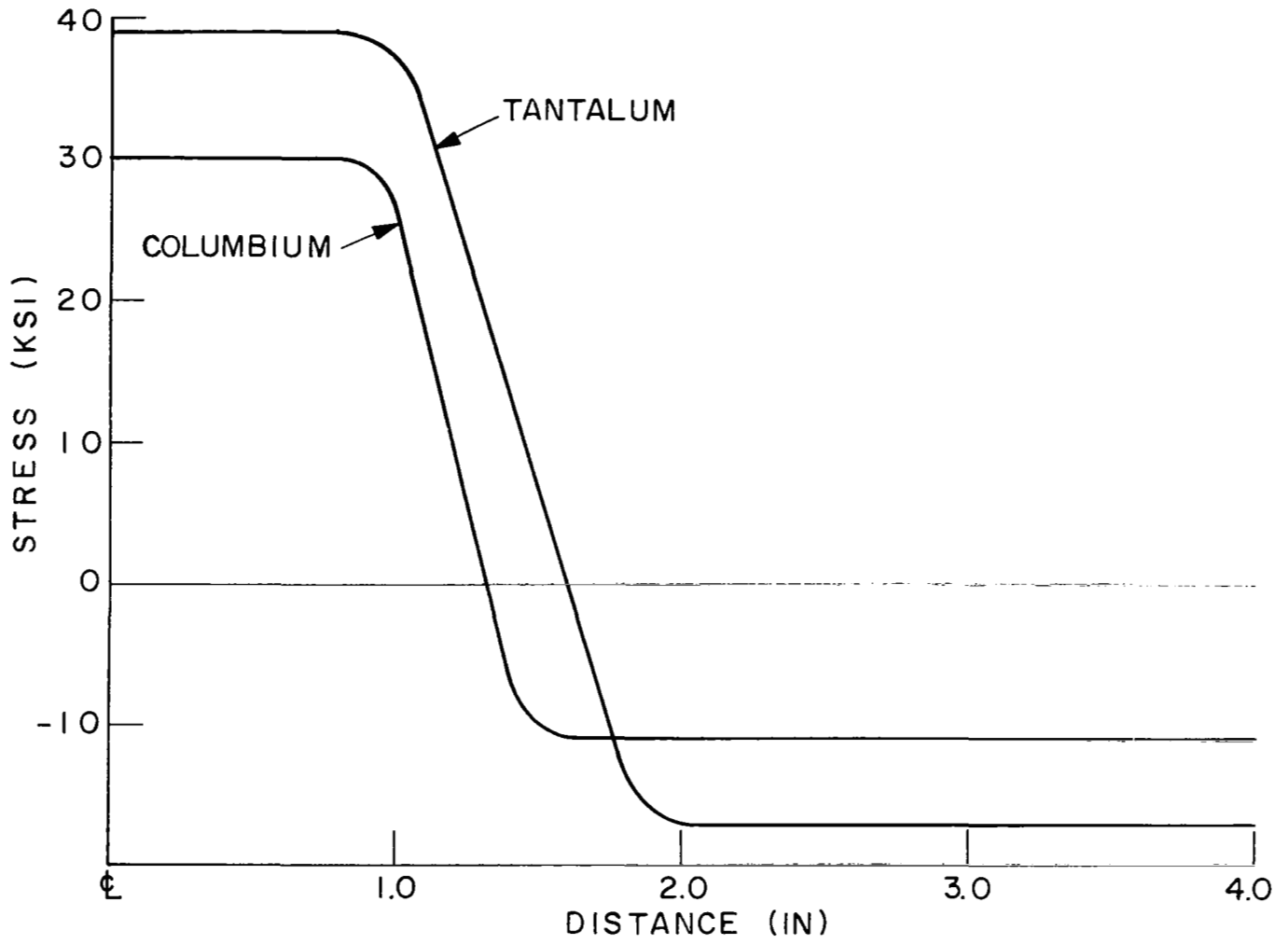


Figure 7-13. Residual stress for columbium and tantalum.

## Experimental Investigation

An experienced investigation was made at M.I.T. to evaluate the accuracy of the mathematical analysis.

Experimental Procedures. To simplify the investigation, experiments were conducted on bead-on-plate welds made in 2219-0 aluminum alloy. Temperature changes during welding were measured by thermocouples, while strain changes were measured by strain gages mounted on specimen surfaces.

Figure 7-14 shows the specimen, which was 30 inches long, 18 inches wide, and 1/4 inch thick. On the particular specimen shown here, which was used for the first series tests, one three-axis rosette strain gage and one thermocouple were mounted. Types and characteristics of the gage and the thermocouple are as follows:

Strain Gage: BLH Type FAER-18RB-12S13ET

Gage length: 0.12 inch

Gage factor: 2.0 at room temperature

Thermocouple: BLH Type GTM-CA (chromel/alumel)

They were manufactured by BLH Electronics, Inc., Waltham, Massachusetts.

The strain gage was mounted with the BLH EPY-600 cement. BLH Barrier C was also used to protect strain gages from high temperatures and other environment.

At the first test (number PR-T1), a weld bead of gas metal arc with argon shielding was laid along a line near the center line of the plate, as shown in Figure 5-1. The lateral distance between the measuring point and the weld line was 2.9 inches. Changes of temperature and strain during welding and subsequent cooling were recorded on an oscillograph paper using a 4-channel recorder.

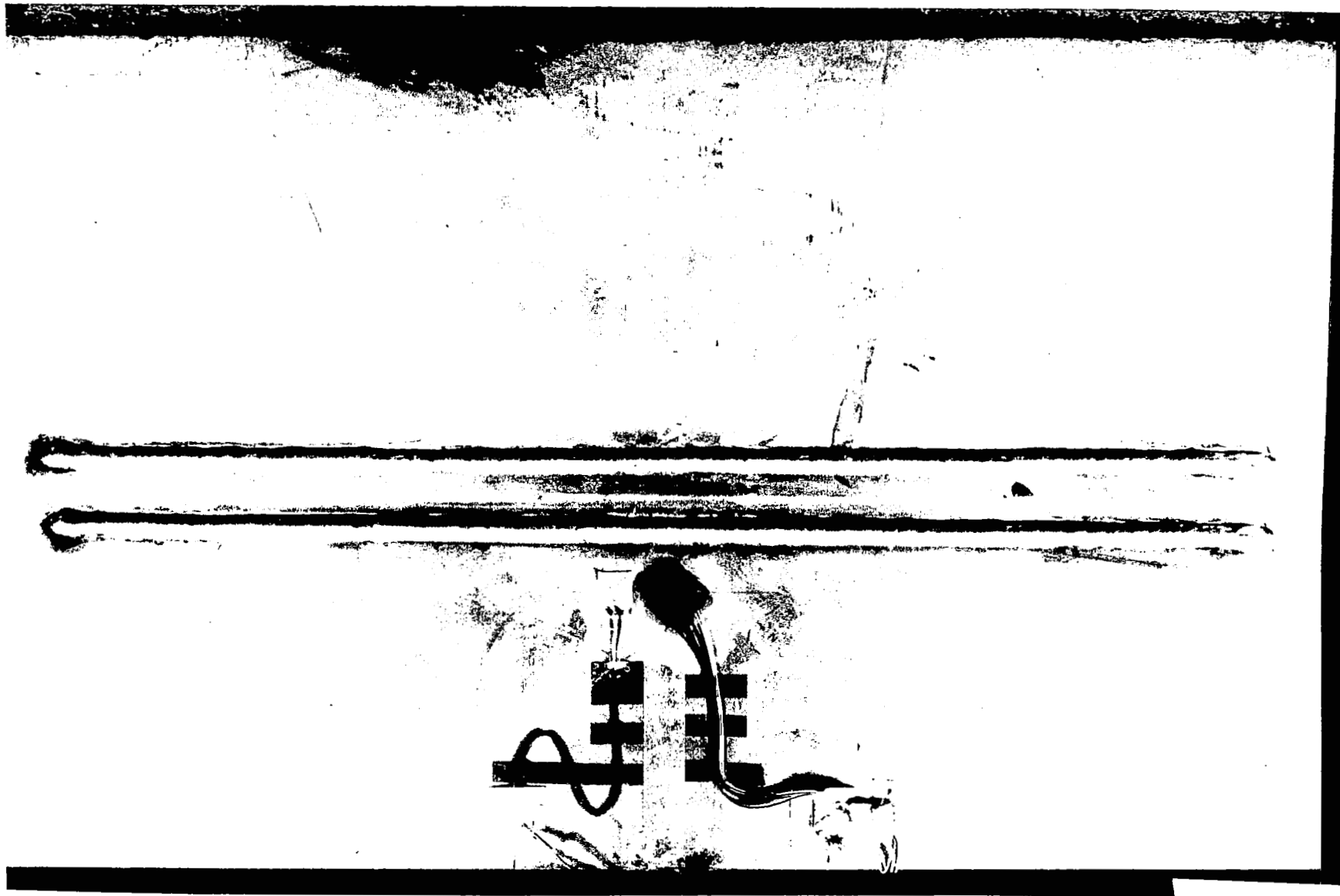


Figure 7-14. Top surface of the specimen used in the series 1 experiment.



After the first test was completed and the specimen cooled to room temperature, the second weld bead was laid along a line closer to the gage. The lateral distance between the measuring point and the weld line under test number PR-T2 was 1.3 inches.

In the third test (number PR-T3), a weld bead was laid on the back surface of the specimen along a line 2.1 inches away from the measuring point.

All of the three bead-on-plate welds were made under the same conditions as follows:

Welding current:	260 amperes
Arc voltage:	23 volts
Arc travel speed:	28 ipm
Linear heat input, h:	51,200 joules/in <sup>2</sup>
Filler wire:	Alloy 4043, 0.062 inch in diameter.

Experiments were conducted on three more specimens. On these specimens three sets of strain gages and thermocouples were mounted at different distances from the weld line. The welding was done by gas tungsten arc process using helium shielding gas, but no filler metal was supplied.

Analysis of Experimental Results. Using the computer programs developed in this study, temperature and strain changes were calculated. Measured values of welding current, arc voltage, and arc travel speed were used for input data of computation.

One unknown quantity in the analysis is the arc efficiency,  $\eta$ , given in Equation (7-1). After comparing measured and calculated temperature and strain changes, it was found that the adequate value of  $\eta$  is 0.7.

Figures 7-15 and 7-16 show changes of temperature and longitudinal strains, respectively, observed during the three test welds on the first specimen. As shown in the figures, measured and computed results coincided fairly well.

On the basis of comparison between experimental and analytical results, it has been concluded that the one-dimensional stress analysis developed in this study can be used as an approximate analysis to investigate general trend of stress changes during welding and resulting residual stresses. However, the current analysis is not adequate to study complex stress changes in areas near the welding arc. Experimental results generated in this study should be useful for developing a two-dimensional stress analysis.

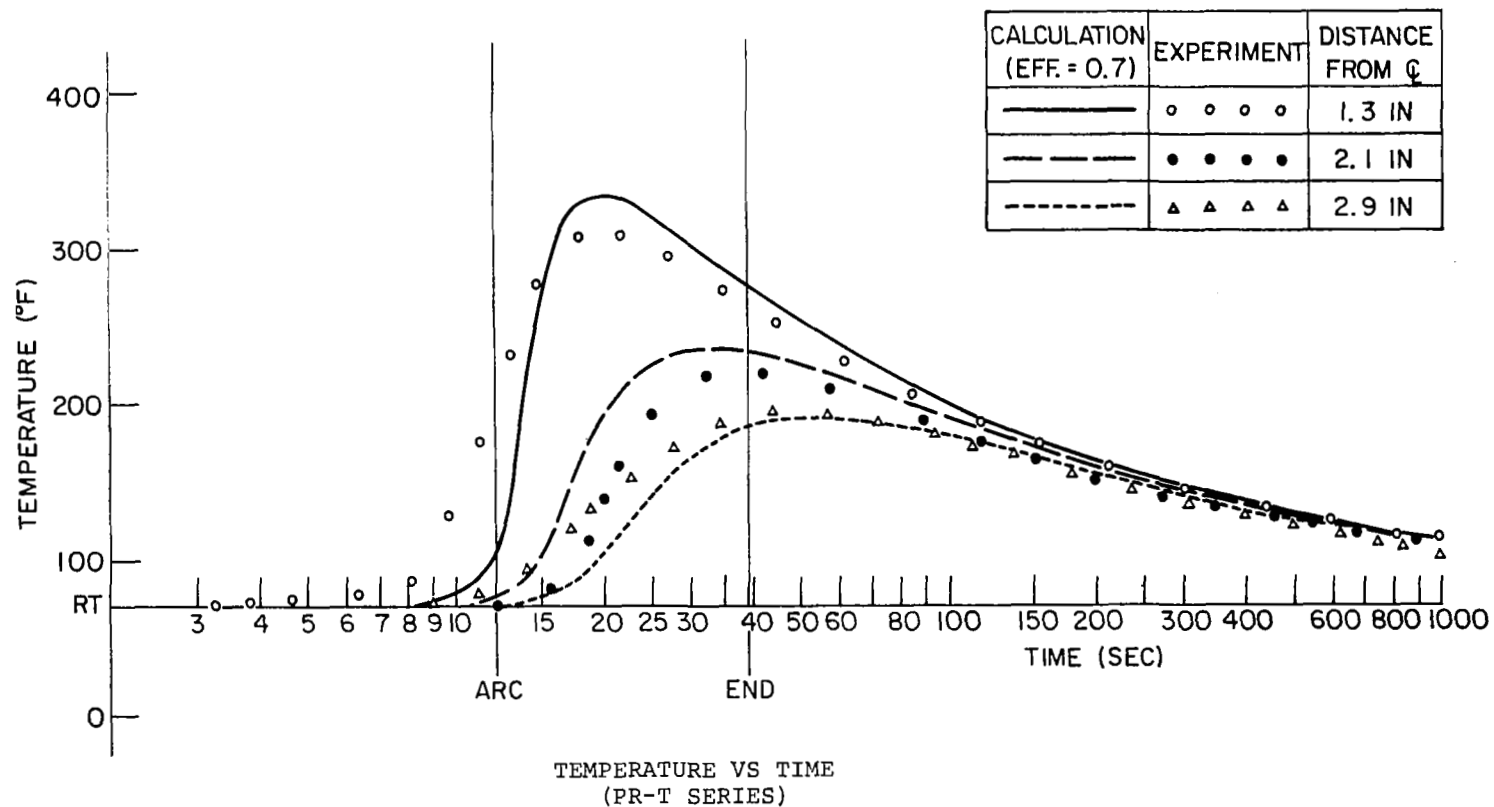


Figure 7-15. Measured and computed temperature changes for the series 1 experiments.

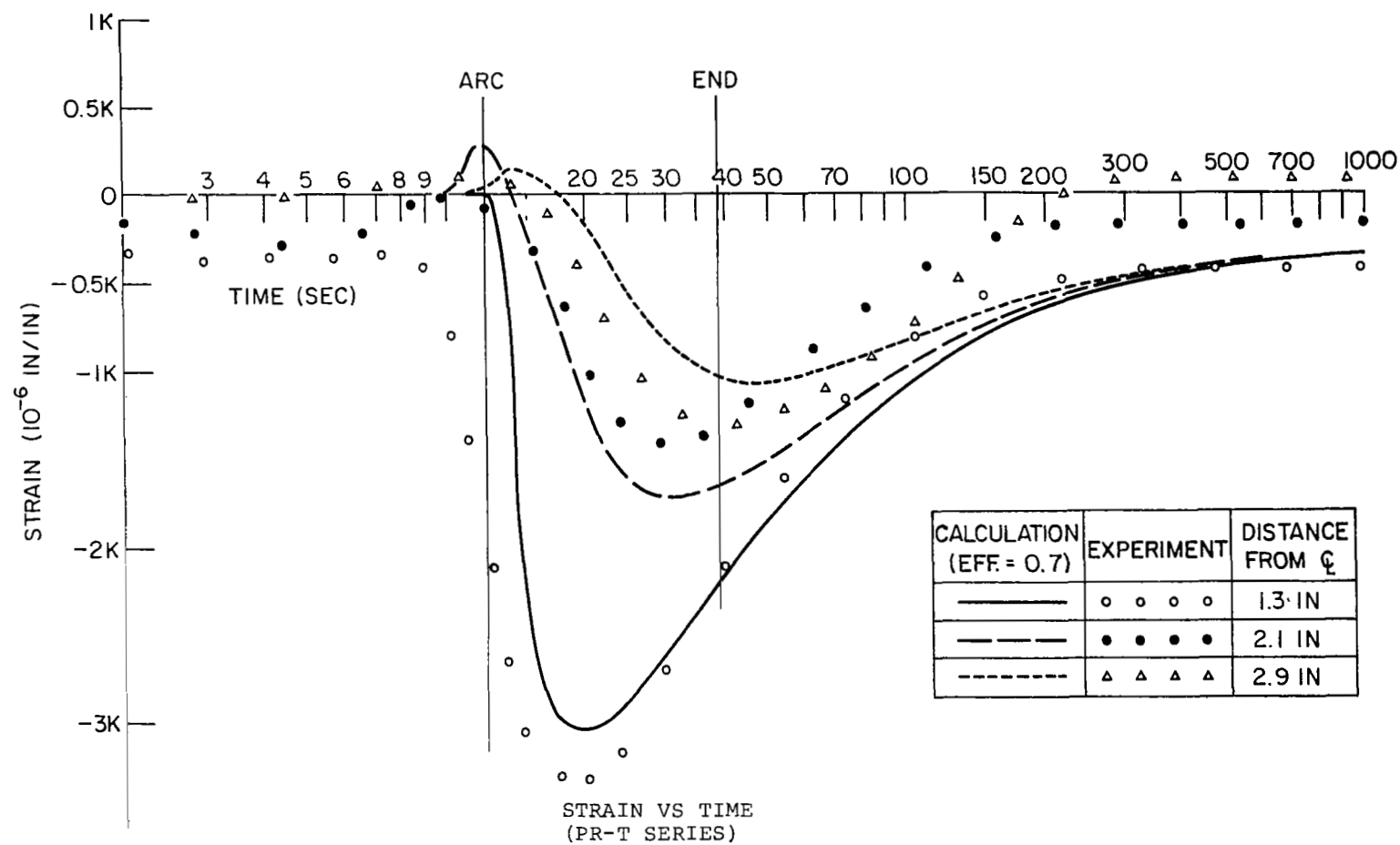


Figure 7-16. Measured and computed longitudinal strains for the series 1 experiments.

## 7.2 Reduction of Warpage and Residual Stresses by Controlling Thermal Pattern during Welding

A study was conducted at the Harvey Aluminum to investigate the feasibility of reducing warpage and residual stresses in aluminum weldments by controlling the thermal pattern during welding. <sup>(24)</sup> The concept involves the use of cryogenic liquids and auxiliary heat sources to produce contraction and expansion of metal in the vicinity of the weld in such a manner as to counterbalance expansion and contraction caused by welding.

### Background and Phases of Study

In the previous study conducted at the Harvey Aluminum, it was found that the tensile strength of welds in 2219-T87 and 2014-T6 plate could be increased approximately 10 percent by using liquid carbon dioxide to extract heat to shorten the time-temperature cycle for the weldment (refer to Chapter 6.3). It was also observed that warpage appeared to be reduced as compared to unchilled welds.

It was decided to continue the study with emphasis on the reduction of residual stresses and distortion. The study covered the following three phases:

Initial phase: analytical study to establish a theoretical thermal pattern which could counterbalance expansion and contraction due to welding

Phase 1 experiment: tests on small samples to determine basic data

Phase 2 experiment: development of beneficial thermal patterns in 12 by 48 by 5/16-inch 2014-T6 welded panels by application of the concept.

## Analytical Study

The analytical study was concerned with heat extraction by means of liquid CO<sub>2</sub> to produce elastic deformation equivalent to the thermal expansion and contraction as well as the weld shrinkage (liquid-to-solid) which occurs during welding. The calculations were based on parameters observed during the performance of the previous study for producing liquid CO<sub>2</sub> chilled weld panels 12 by 48 by 5/16-inch thick in 2014-T6 aluminum alloy.

Results of the mathematical study indicated that the thermal stresses would be counterbalanced if the portion of the plate heated by the arc could be contained within a 2-inch diameter circle with this circle surrounded by an area of approximately 45 square inches cooled to -100° F. It was estimated that approximately 0.8-lb of liquid CO<sub>2</sub> per inch of weld, in addition to that dissipated by the heat of welding in formation of the weld, would be required.

On the basis of the analytical results obtained, the jet system was modified in accordance with the schematic drawing shown in Figure 7-17. This jet system would provide chilling to the front side of the weld using a fine wire brush as a sliding shield to keep CO<sub>2</sub> out of the arc. Actual design of the new jet system and shielding device included provisions for making adjustments to change the thermal pattern as required to accomplish the objectives of the program. Redesign for stability during operation and reproducibility of chilling parameters was also performed.

## Experimental Work

The experimental work to develop controls for warpage and residual stresses consisted of the following principal

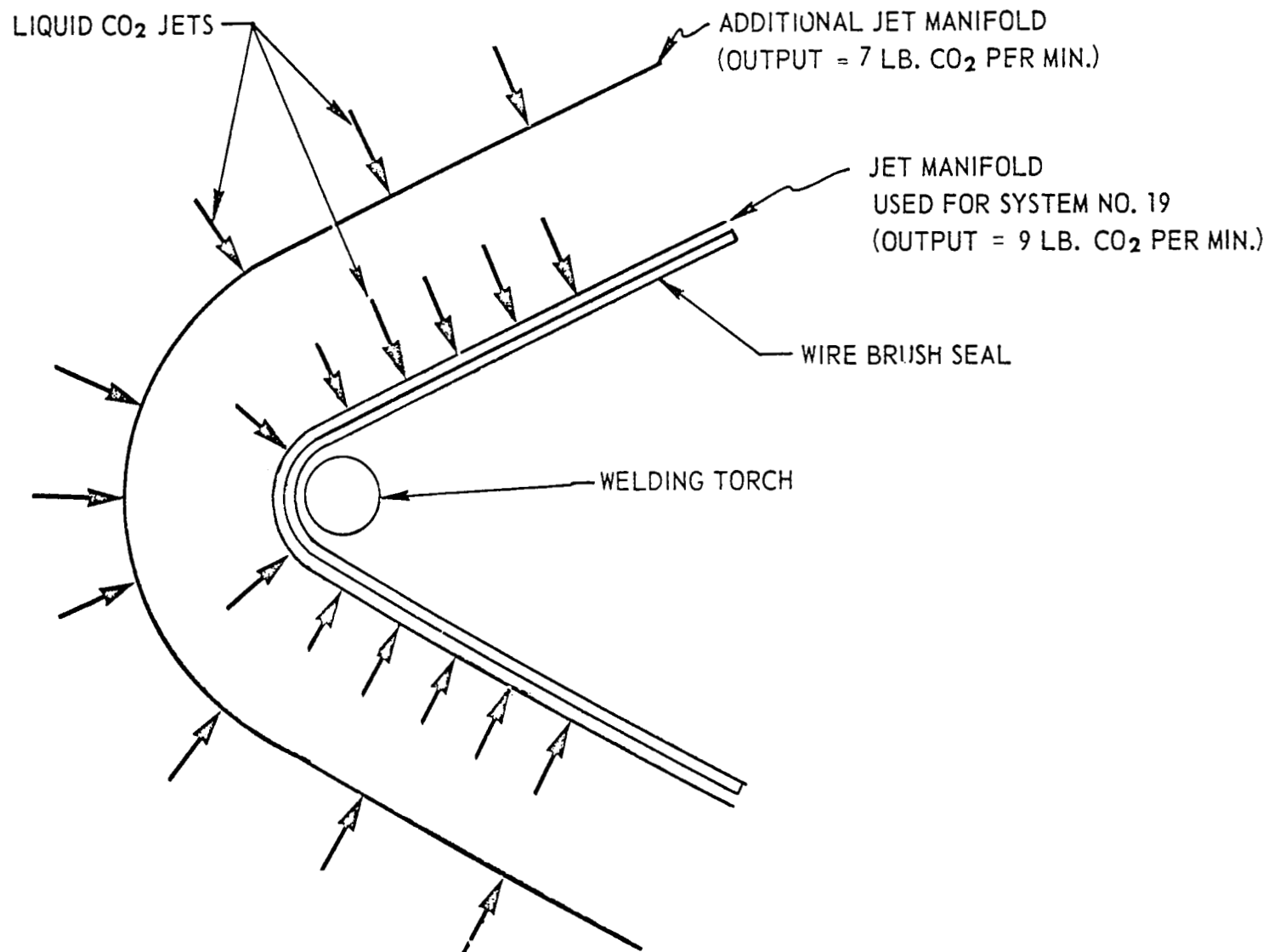


Figure 7-17. Modified jet system no. 19.

efforts: (1) procurement and preparation of materials, (2) setup of welding equipment with instrumentation, (3) development of chilling systems and techniques, (4) development of techniques for measurement of temperatures and residual stresses, (5) development of basic data on thermal stresses, and (6) development of thermal patterns for controlling warpage and residual stresses.

Four major systems were developed for altering the thermal pattern during welding. All employed jet spraying of liquid CO<sub>2</sub> with or without the application of auxiliary heat. The basic systems included the following:

- 1) V-shaped cryogenic jet systems for cooling the front side of the weld.
- 2) Trailing cryogenic jet systems for cooling the front side of the weld.
- 3) Circular cryogenic jet systems for cooling the back side of the weld.
- 4) Auxiliary heating with trailing cryogenic jet systems for cooling the front side of the weld.

A V-shaped system was designed to concentrate the chilling around the welding torch on the front side of the panel. A circular system was designed for concentrating the chilling around the molten puddle on the back side of the panel. A trailing system was designed for use on the front side (but could be used on either side) with the chilling at various distances behind the welding torch. Thirty variations of these systems were used during the experimental welding program.

The experimental portion of the program was performed in two phases. The first phase consisted of tests on small samples to determine basic data on the feasibility of counterbalancing weld expansion and contraction by using liquid cryogenics. In the second phase, experiments were conducted on large panels.



Welding Techniques. All welding was performed with the panels in horizontal position. The GTA process was used with dc straight polarity using helium as the shielding gas. In most cases, welds were made at 250 amperes with travel speed adjusted from 5 to 14 inches per minute as needed to effect optimum penetration.

Temperature Measurement. Six platinum resistance thermocouples were held by spring wire clips against the surface of the panel. The thermocouples were connected to a six-channel recorder.

Warpage Measurement. Warpage was measured using the center at the top of the panel as the reference point. Linear measurements were converted to angular units for convenience.

Residual Stress Measurement. Two techniques were used for measuring residual stresses. Both involved the use of wire or foil strain gages in conjunction with a manually operated strain indicator. Mechanical trepanning, with CO<sub>2</sub> coolant to prevent overheating, was initially used for relaxing the residual stress. However, there was some indication that this technique affected the actual residual stress slightly. Therefore, the slicing technique was used for most residual stress measurements.

### Typical Thermal Patterns

Unchilled Weld Panels. In order to establish a basis for comparison, several 48 by 12-inch panels were welded without chilling. Measurements of warpage, residual stress and tensile properties indicated that warpage is extremely sensitive to the time-temperature cycle, degree of restraint, and shape of the cast weld structure. A typical thermal pattern for unchilled weld panels is shown in Figure 7-18.

Front-side Chilling. Various chilling patterns were used in an effort to select those that would produce the most beneficial effects on warpage and residual stresses. A total of 14 variations of the V-shaped systems were used to weld 48 by 12-inch panels. Fourteen variations of the trailing systems were also used to weld 48 by 12-inch panels. A total of more than 50 panels were welded to investigate the 28 variations of the front side chilling systems. Typical thermal patterns for weld panels chilled from the front side with the V-shaped and trailing manifold systems are shown in Figures 7-19 and 7-20.

Back-side Chilling Systems. During the course of the experimental work with the front side chilling systems, a cursory stress analysis was made in an effort to determine the reason these systems did not effect more pronounced reductions in warpage and residual stresses. The result of this analysis indicated that thermal contraction was non-uniform since liquid  $\text{CO}_2$  could not be applied to the plate ahead of the welding torch without interfering with the welding operation. On this basis, a system was designed and fabricated for chilling in a circular pattern.

The first system was designed for use on the front side but failed to keep  $\text{CO}_2$  out of the arc and was therefore abandoned. The second system was designed for use on the back side and was effective in producing the desired chilling pattern. A typical thermal pattern is shown in Figure 7-21. However, this system caused excessive porosity in the weld.

It is believed that the porosity resulted from water condensed on the cold aluminum becoming trapped between the butting edges ahead of the arc. Inasmuch as this system also did not effect the desired degree of warpage or residual stress reduction, it was postulated that the necessary

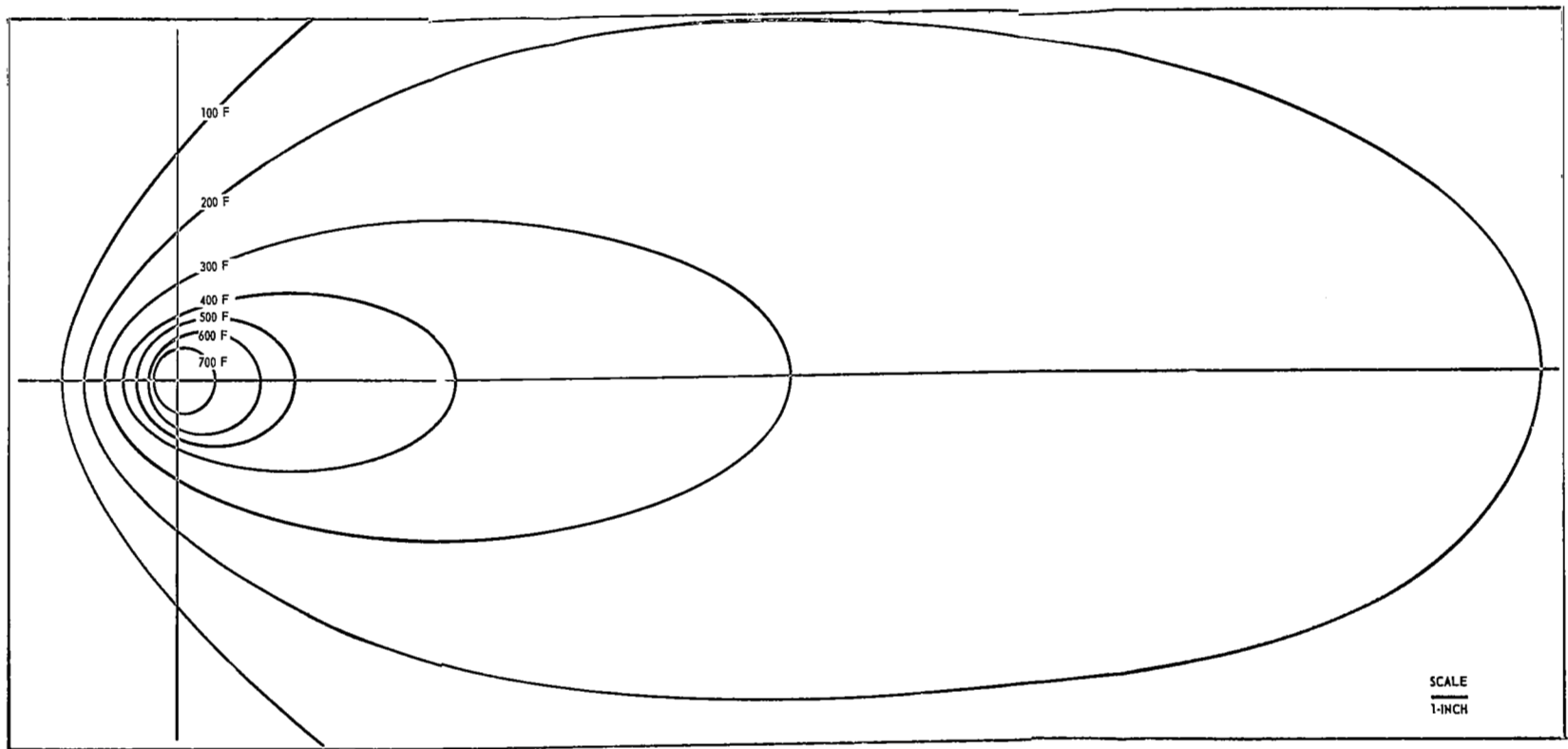


Figure 7-18. Typical thermal pattern for unchilled weld panels.

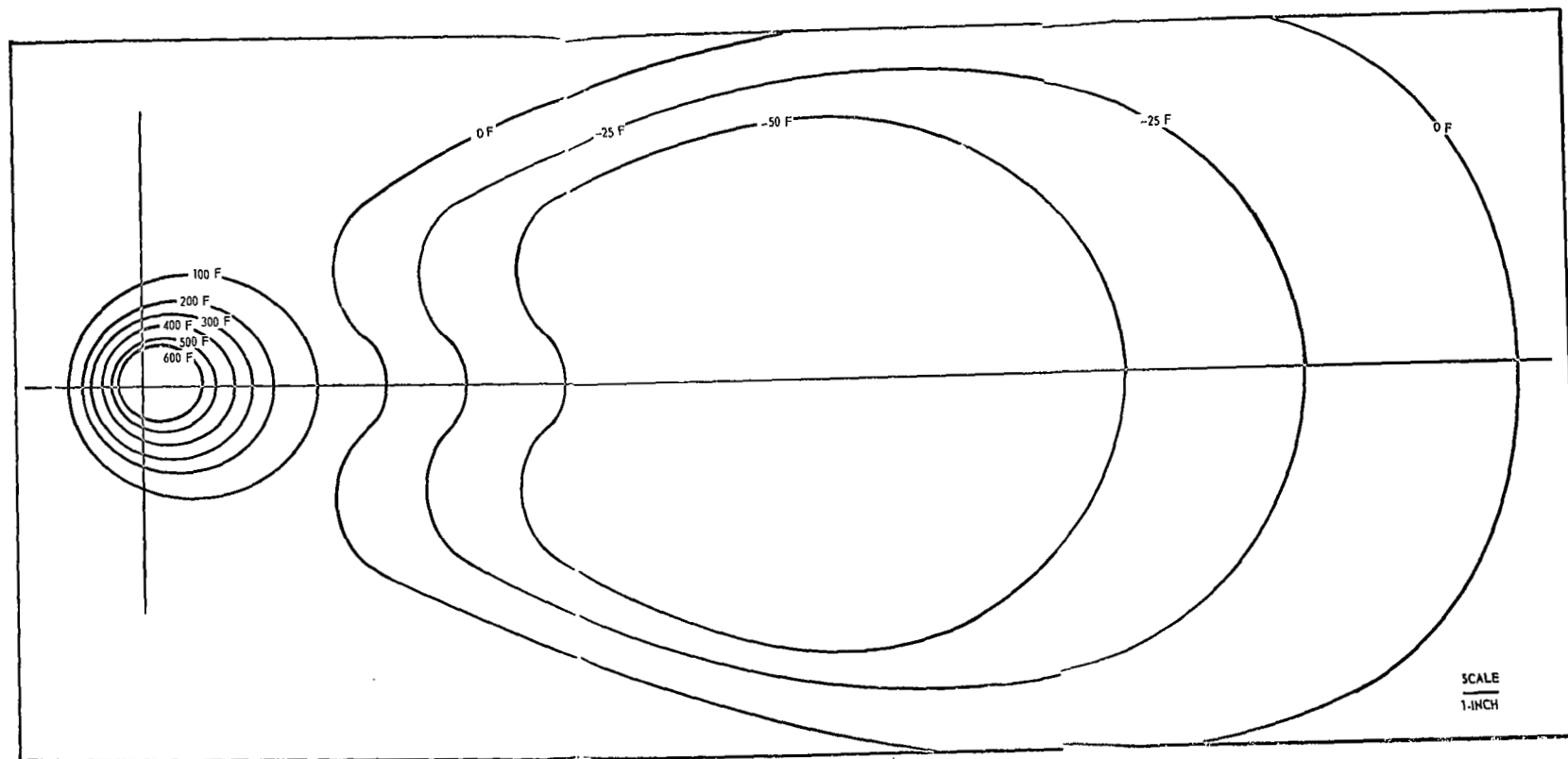


Figure 7-19. Typical thermal pattern for panels welded with V-shaped CO<sub>2</sub> chilling system.

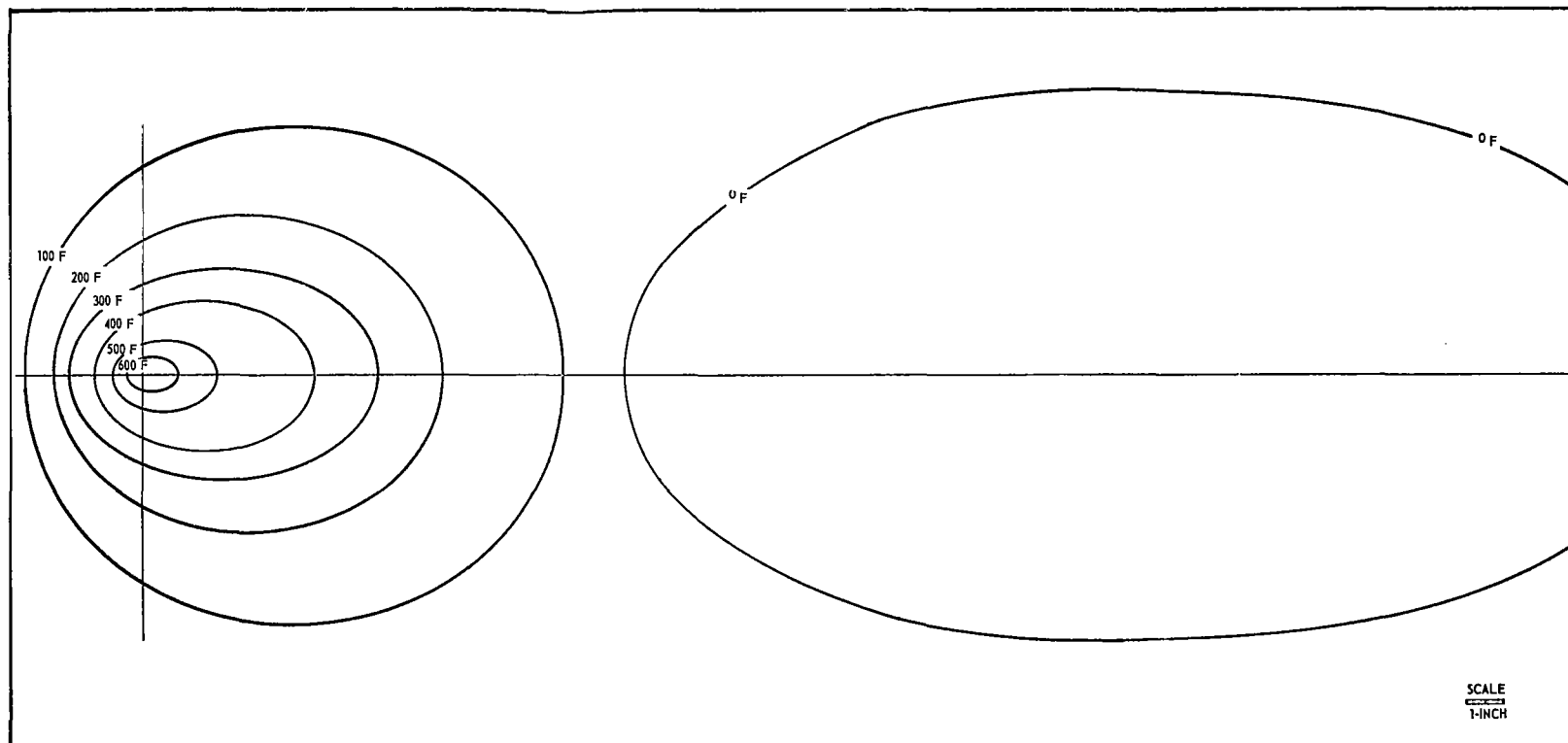


Figure 7-20. Typical thermal pattern for panels welded with trailing CO<sub>2</sub> chilling system.

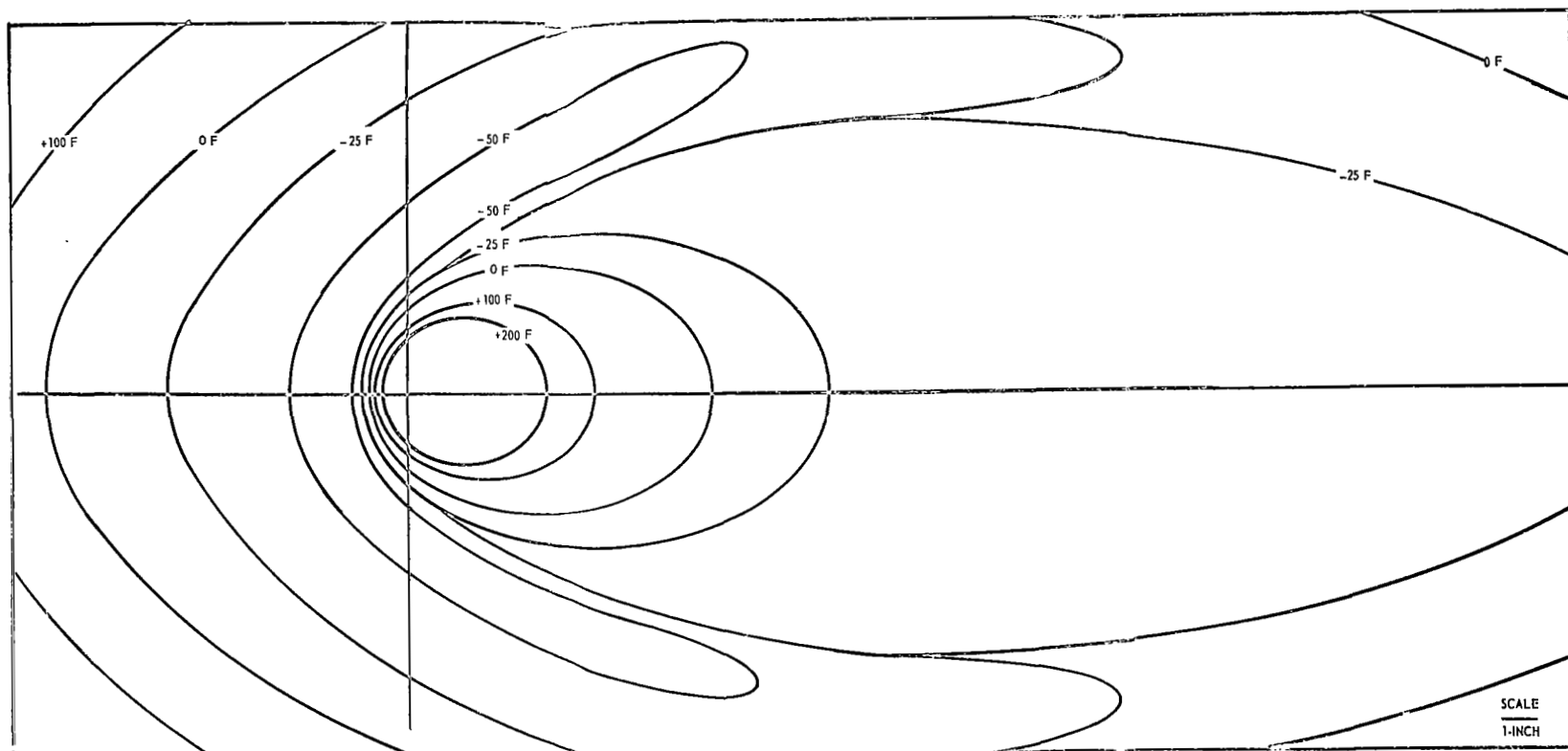


Figure 7-21. Typical thermal pattern for panels welded with circular CO<sub>2</sub> chilling system.

elastic-plastic relationships were not being produced by chilling alone as the expansion after chilling takes place too slowly to be effective. In order to cause the proper relationship to take place, it would be necessary to use auxiliary heat.

Combined Chilling and Auxiliary Heating Systems. The first system utilized one of the front side trailing manifolds for chilling and an acetylene flame behind the chilling manifold to cause more rapid expansion. This system caused the warpage to reverse from normal, but the acetylene flame was difficult to control. Therefore, in the remaining experiments, the flame was positioned manually. It was found that the most effective combined system was a general preheat of the plate of 200° F with approximately 1.5 lbs of CO<sub>2</sub> per inch of weld impinged on the weld seam 10 inches behind the torch. A typical thermal pattern for this system is shown in Figure 7-22. This pattern repeatedly produced panels with low warpage and with longitudinal residual stresses of less than one-third of the normal. Work for further refinement of this combined system could not be accomplished within the limits on this project.

### Experimental Results

Experimental results can be summarized as follows:

Effect of Thermal Pattern on Warpage. As shown in Table 7-3, it was possible to produce unwarped panels either with or without the use of any of the systems for changing the thermal pattern; however, repeatability was extremely low for all except the combined chilling and heating systems as indicated by the variation from maximum to minimum. It is concluded that the degree of warpage is extremely sensitive to minor variations in welding parameters, and in order to "de-sensitize" it is necessary to distribute plastic yielding

TABLE 7-3. EFFECT OF THERMAL PATTERN ON WARPAGE.

Principal Factors Producing Thermal Pattern	Warpage in Degrees (1)					
	Maximum		Minimum		Typical	
	Bow	Peak	Bow	Peak	Bow	Peak
Unchilled	-.08	+1.6	0	0	-0.4	+1.2
Chilled only-front side	-1.2	+3.5	0	0	-0.8	+1.2
Chilled only-back side	-0.8	+0.6	0	0	-0.8	+0.6
Chilled and auxiliary heat	+0.3	-0.3	0	0	+0.2	0

NOTE:

(1) Minus sign (-) indicates direction of bow or peak is away from face of weld; plus sign (+) indicates bow or peak is toward face of weld. Note that the bow is reversed when combined cooling and auxiliary heating are used to change thermal pattern.



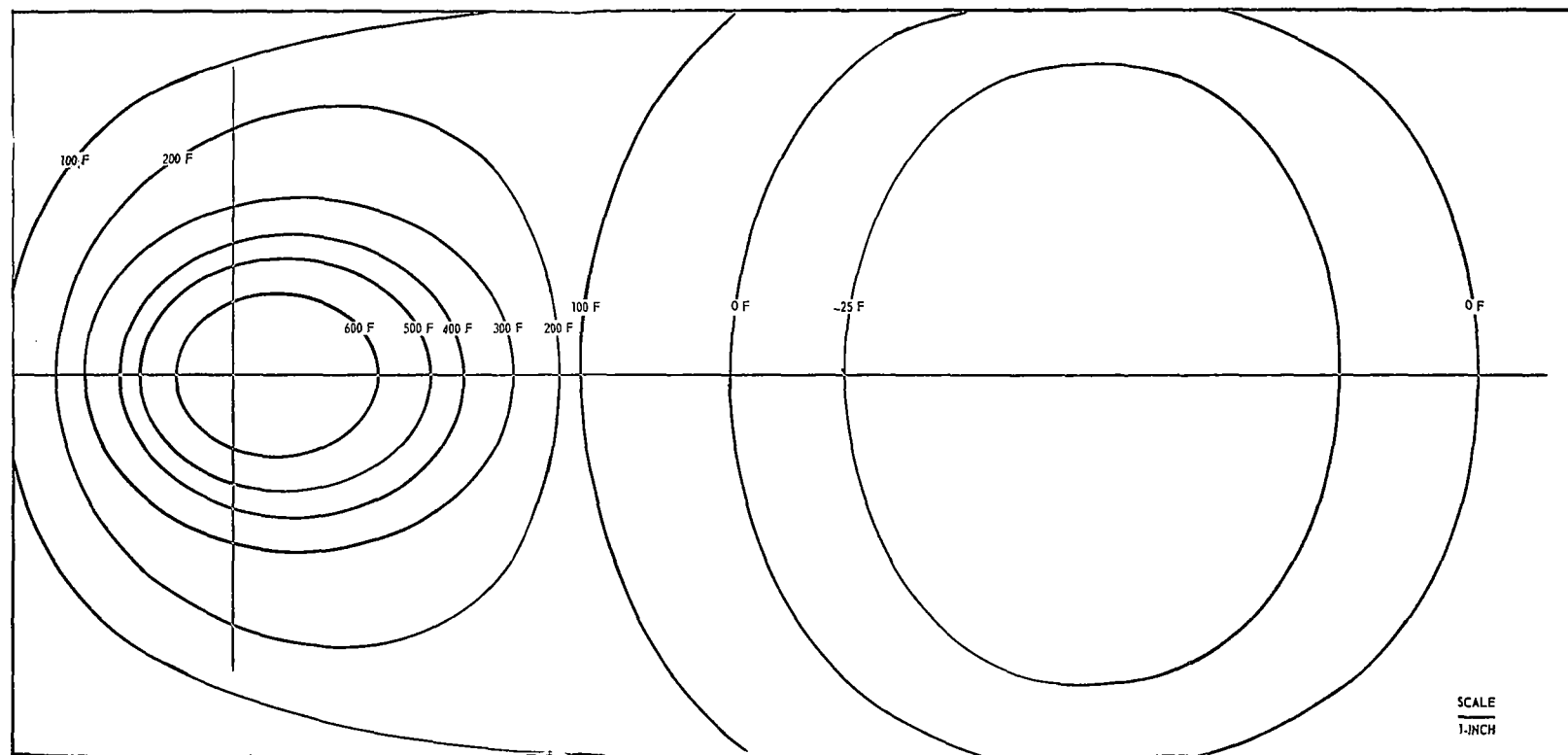


Figure 7-22. Typical thermal pattern for panels welded with trailing CO<sub>2</sub> chilling system and auxiliary heat.

over a wider area of the weldment by spreading the isotherms around the weld puddle while creating elastic strains in such locations as to counteract the thermal strains created by the welding operation.

Effect of Thermal Pattern on Residual Stresses. All of the systems for altering the thermal pattern were effective to some degree in reducing the residual stresses as compared to those present in unchilled weld panels. However, chilling alone produced a maximum of 50 percent reduction in the longitudinal residual stress, while chilling combined with auxiliary heating reduced these stresses as much as 95 percent as shown in Table 7-4.

Effects of Thermal Pattern on Mechanical Properties and Porosity. Although only limited testing was performed, it was indicated that tensile yield strengths were improved through chilling by amounts ranging between 10 and 20 percent. This is in agreement with the findings of work performed in the previous study (refer to Chapter 6.3).

It was observed that porosity in chilled welds was smaller in quantity and size than that in unchilled welds (refer to Chapter 5.5).

## Discussion of Results

The elastic-plastic strain relationship during welding are extremely complex inasmuch as they are influenced by a great many variables, most of which are dependent. In spite of this complexity, the results of the work performed under this contract proved the feasibility of applying the concept of balancing thermal stresses during welding to control distortion and residual stresses. The optimum thermal pattern for a specific weldment can be developed through a combination of theoretical and empirical methods. Computer programs developed at M.I.T. can be useful for determining the optimum thermal pattern.

TABLE 7-4. EFFECT OF THERMAL PATTERN ON RESIDUAL STRESSES.

Principal Thermal Pattern Factors	RESIDUAL STRESS (PSI) (1)					
	Maximum		Minimum		Typical	
	Long.	Trans.	Long.	Trans.	Long.	Trans.
Unchilled	+22,500	-12,300	+17,600	-3,000	+21,000	-7,000
Chilled only- Front side	+20,500	- 8,000	+12,200	-1,600	+12,000	-7,500
Chilled only- Back side	+20,300	- 7,800	+11,900	-4,000	+15,000	-5,000
Chilled and Auxiliary heat	+ 9,200	-12,600	+ 1,100	+ 800	+ 3,000	-2,000

NOTE:

(1) Plus sign (+) indicates residual stress in tension; minus sign (-) indicates residual stress in compression. Strain gages placed in the center of the weld seam.

### 7.3 Development of Non-Destructive Methods for Determining Residual Stresses

Many techniques have been proposed and used for measuring residual stresses in metal. RSIC-410 prepared by Masubuchi<sup>(61)</sup> covers the present state-of-the-art of measurement of residual stress in metals in metal structures, especially in aluminum structures. Masubuchi discusses over 20 methods for measuring residual stresses. These methods are classified into the following groups:

1. Stress-relaxation techniques using electric and mechanical strain gages
2. X-ray diffraction techniques
3. Techniques by use of stress sensitive properties (ultrasonic techniques and hardness techniques)
4. Cracking techniques (for estimating residual stresses by use of hydrogen induced cracking and stress corrosion cracking.)

Stress-relaxation techniques using strain gages, especially resistance wire (or foil) gages, are most widely used for measuring residual stresses in weldments. However, the stress-relaxation techniques are destructive. Therefore, their applications to actual structures have been limited to very rare cases. Obviously, there is a strong need for developing better means for non-destructively measuring residual stresses.

MSFC sponsored a study at the Benson and Associates for developing non-destructive methods for determining residual stress and fatigue damage in metals.

## Ultrasonic Stress Measuring Techniques (27,62)

Ultrasonic methods of stress analysis were first demonstrated in 1957, when it was shown that ultrasonic shear waves may be used in a manner similar to the photoelastic method using polarized light beams with optically transparent models. Exploratory work demonstrated that the change of shear wave velocity was proportional to the applied stress even beyond the elastic limit of certain materials.

Later studies demonstrated that the velocity of ultrasonic surface waves was also affected by stresses, indicating that the stress near the surface may be measured. Further work showed the possible application of ultrasonic methods to dynamic stress analysis.

After evaluating the current status of various ultrasonic systems, researchers at the Benson and Associates decided to use the following two systems:

- 1) Modified time of flight system
- 2) Frequency null system

Modified Time of Flight System. A block diagram of the modified time of flight system is shown in Figure 7-23. Ultrasonic waves are produced by an R. F. pulse generator and travel on through the sample to be read by an oscilloscope.

A delay line signal by-passing the sample is also sent to the scope for comparison. As stress is placed on the sample the velocity of the ultrasonic wave changes. This is equivalent to a change in time it takes for the wave to traverse the sample. When this occurs a phase shift between the sample signal and the delay line signal can be seen on the oscilloscope. Then the internal oscilloscope trigger is adjusted to bring the signals in phase again. This corresponds to a change in time of travel of the wave through the specimen. For example, if the internal trigger must be delayed by

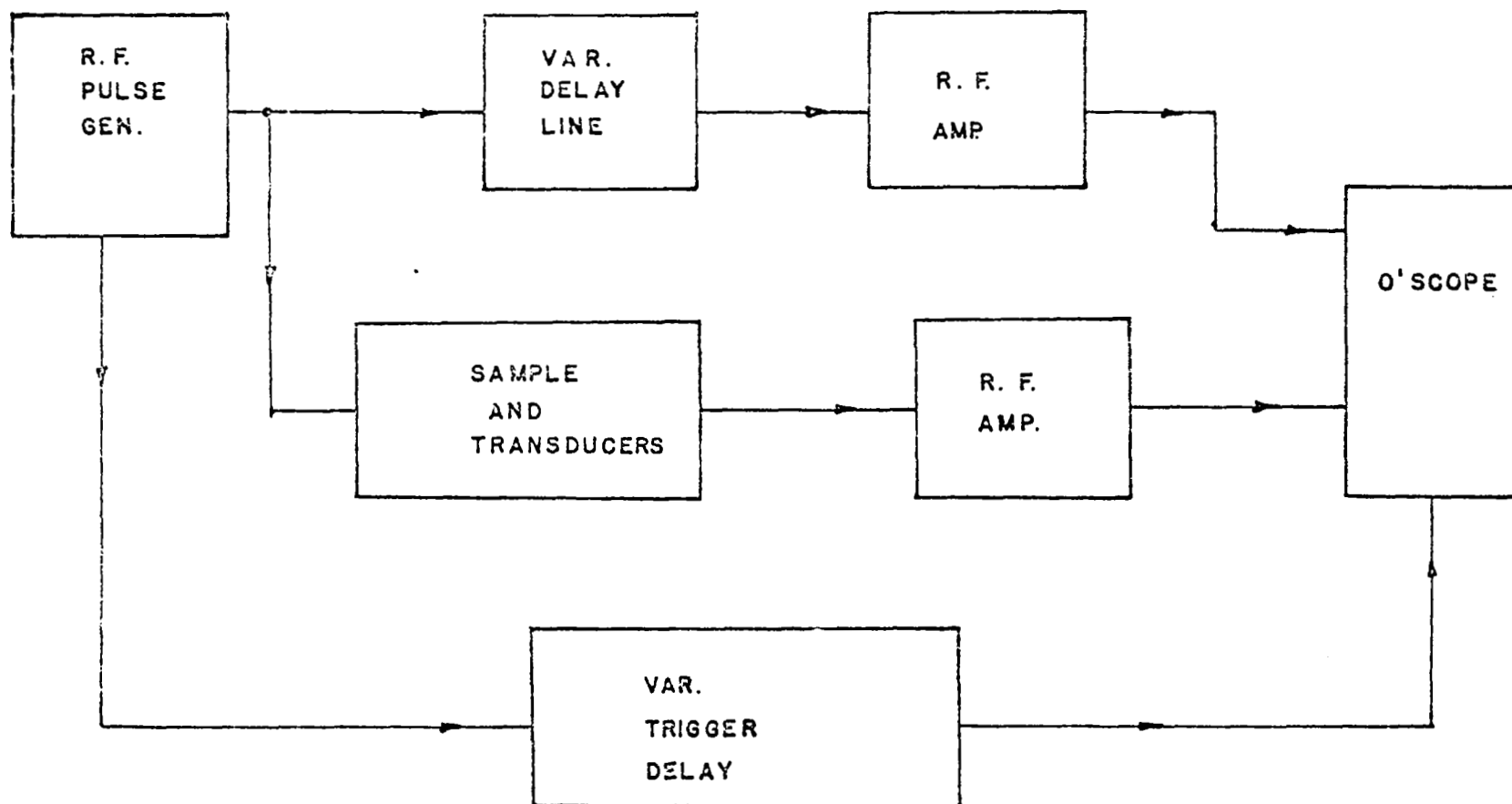


Figure 7-23 Block diagram showing the modified time of flight system used in measuring the change in velocity of ultrasonic surface waves.

$2 \times 10^{-8}$  seconds, this means that this same amount constituted the change in travel time of the ultrasonic wave.

Frequency Null System. The modified time of flight system directly measures the percentage change in velocity of an ultrasonic wave by comparing the change in travel time to the total travel time. A similar measurement can be obtained by the use of the frequency null system as long as there is a fixed path length provided by a transducer (see Figure 7-24). Conditions necessary for the reference pulse to cancel or null a portion of the received pulse are that they be  $180^\circ$  out of phase and have equal amplitudes. This phase condition can be brought about by frequency adjustment of the R. F. oscillator while the amplitude condition is obtained by varying the gain in one channel of the oscilloscope (see Figure 7-25).

In order to utilize this system to measure the change in ultrasonic velocity, the following relationship exists:

$$N_\lambda = \frac{L}{V} f$$

where  $N_\lambda$  is the number of wave lengths,  $L$  is the path length of the surface wave,  $V$  is the velocity of the surface wave, and  $f$  is the frequency of the driving signal. Considering the equation we see that if either driving frequency or surface wave velocity changes the number of wave lengths will change accordingly. Therefore, when the sample is put into compression the velocity would increase and for the same number of wave lengths to occur in a given path length  $L$ , the frequency must increase.

The relationship between change in frequency  $\Delta f$ , and change in travel time  $\Delta t$ , can be obtained under stressed and unstressed conditions as follows:

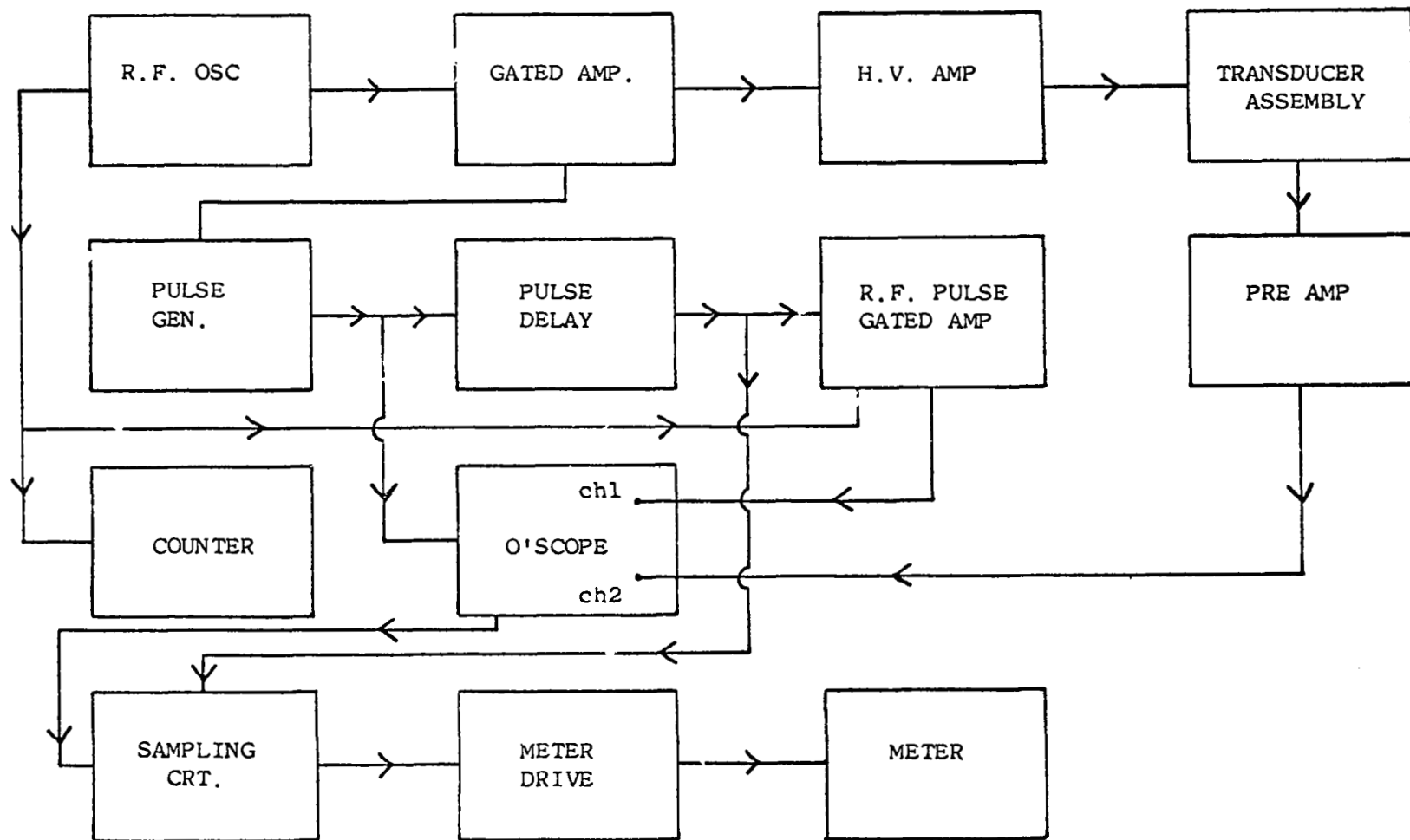


Figure 7-24. Block diagram of the frequency null system



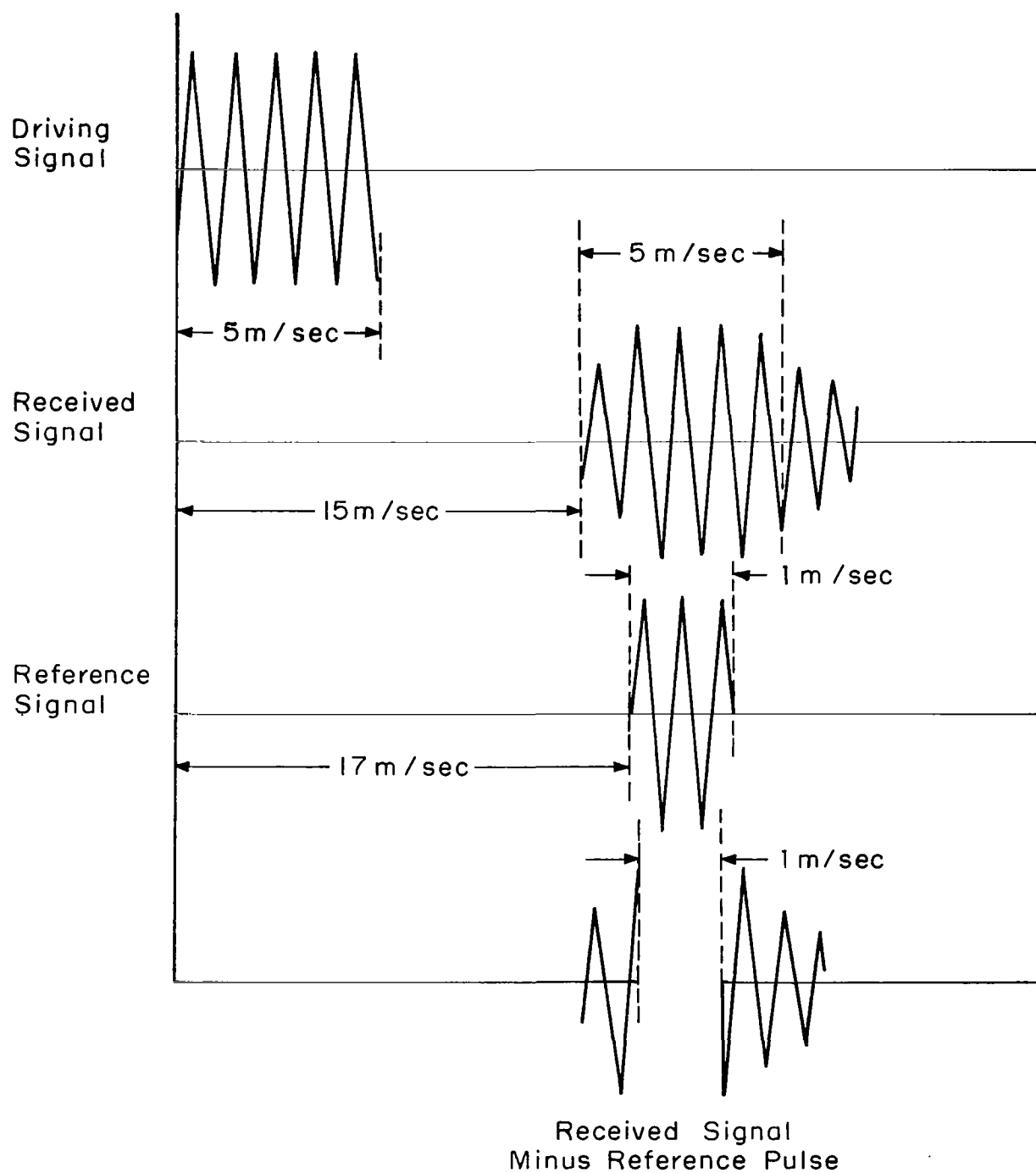


Figure 7-25. Time relationships between the driving signal, received signal, and the reference pulse.

$$N_{\lambda} = \frac{L}{V_0} f_0 = \frac{L}{V_0 + \Delta V} (f_0 + \Delta f)$$

$$\frac{\Delta f}{f_0} = \frac{\Delta V}{V_0}$$

$$\Delta f = \frac{L\Delta V}{LV_0} f_0 = \frac{T\Delta V}{L}$$

is the travel time for the surface wave in unstressed condition and is called T. The stressed condition is:

$$\frac{L}{V_0 + \Delta V} = T - \Delta t$$

By rearranging and substitution we get:

$$\Delta f = \frac{\Delta t \cdot f_0}{T - \Delta t} \approx \frac{\Delta t \cdot f_0}{T}$$

since  $\Delta t \ll T$ .

This technique can also be used to make absolute velocity measurements.

### Investigation on Welded Plates

In the study conducted at the Benson and Associates, a comprehensive investigation was made on fundamentals of the ultrasonic stress-measurement techniques. After conducting the fundamental investigation using specimens with known stress values, an investigation also was made to apply the ultrasonic technique on weldments. Since the major interest of this report is on residual stresses in weldments, the following pages cover results obtained on weldments.

The stress distribution in plates containing weldments had been the subject of previous investigation using both destructive type tests and tests involving the use of strain gages.

The techniques employed by Hasemeyer, et al,<sup>(63)</sup> were followed on a test specimen one-half inch thick and of aluminum alloy 2014-T6. The weldment was in the center of the 9 inch length dimension with two and one half inches of material each side of the weldment. The procedure was to measure the change in length of the weld as succeeding 1/4 inch wide segments were removed symmetrically about the weld. From these measurements it was possible to compute the average stress existing along the weld. The results of the initial measurements were in close agreement with Hasemeyer.

The procedure was then varied to allow for a determination of the actual stress that existed throughout the plate so that a check of ultrasonic measurements could be performed. The new procedure involved the measurement of the deformation of plates containing weldments which were either along the length of the plate or transverse to the plate. Measurements were made of the length of each 1/4 inch wide segment of the plate before and after each pair of 1/4 inch wide segments were removed from the plate. In this manner a complete history of the stress change in the plate was obtained. The results of these measurements are given in Figures 7-26 and 7-27. In Figure 7-26 the plate contained a weldment along the length of the plate and in Figure 7-27, the weldment was along the width of the plate.

It is seen that there is a tensile stress along the weldment extending approximately 1/2 inch to each side of the weldment. The remainder of the plate is in a state of compression along the length dimension. There is also a state of tension in the central portion of the plate transverse to the weld. Again the outer portions of the plate are in compression. It is further noted that the tensile stress is more concentrated along the length of the weld than it is transverse to the weld. The true stress

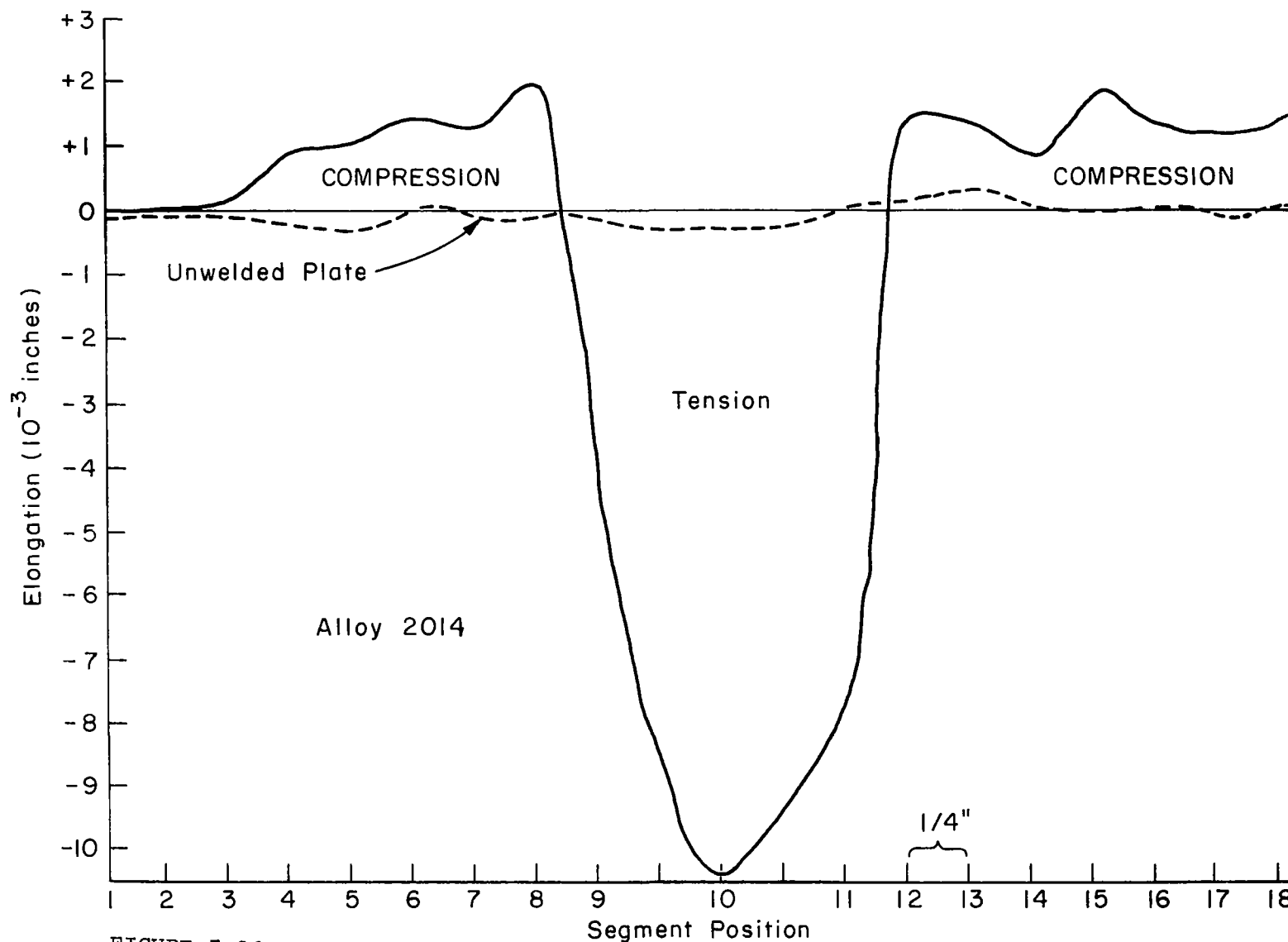


FIGURE 7-26 ELONGATION CHANGE IN  $1/4''$  SEGMENTS VS SEGMENT LOCATION ALONG LENGTH OF PLATE

Figure 7-26. Elongation change in  $1/4$  inch segments Versus segment location along length of plate.

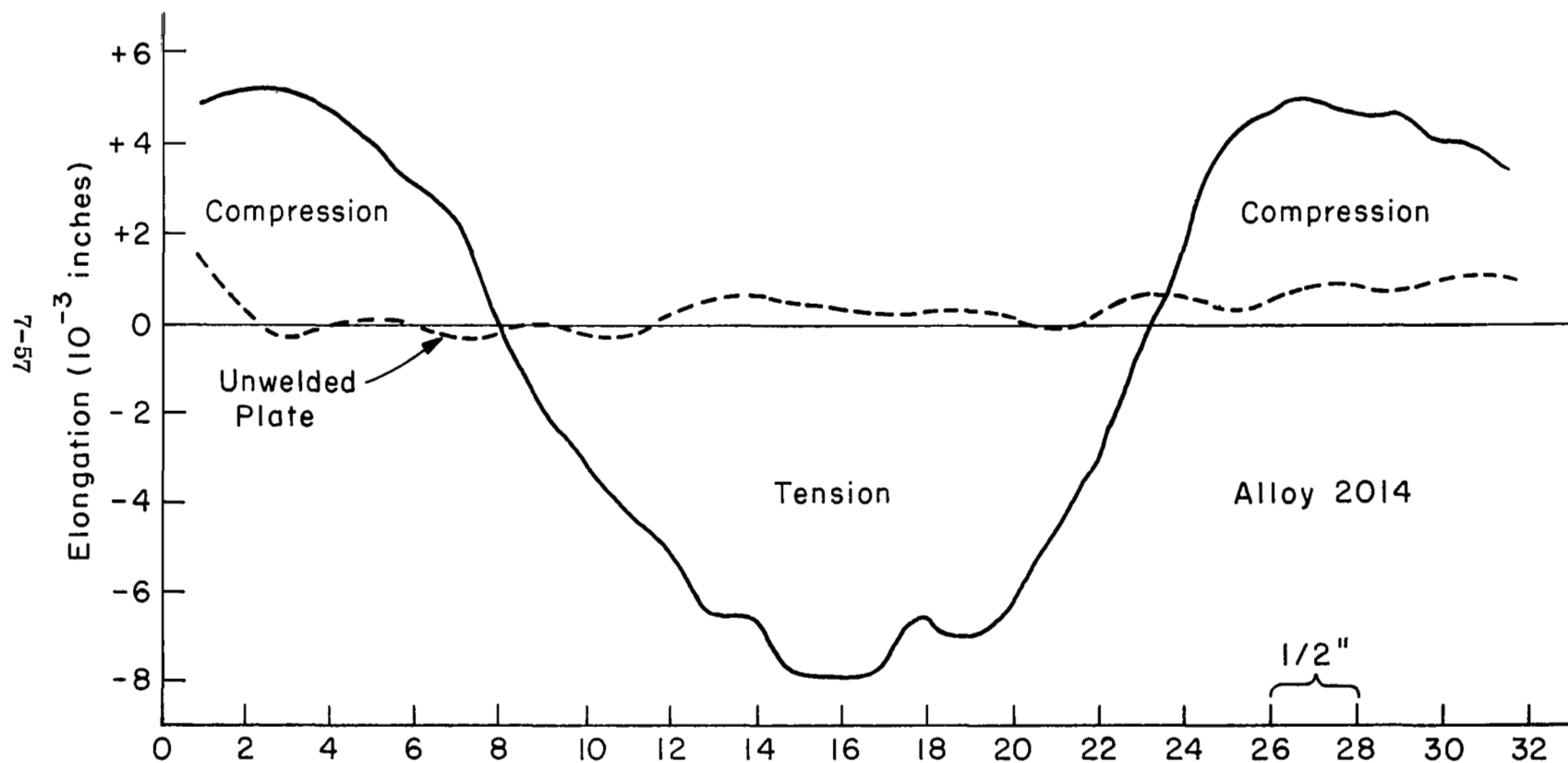


Figure 7-27. Elongation change in  $1/4$  inch segments Versus segment location along width of the plate.

distribution in the plate must therefore consist of the contours of constant stress being somewhat elliptical and oriented about the weld as illustrated in Figure 7-28.

The results of these destructive tests appear reasonable since the welding process involves the melting of the material along the weld, which subsequently cools to room temperature. During the cooling process the material in and near the weldment should shrink in both dimensions resulting in a state of tension, while the surrounding material will oppose the shrinking by exerting a compressive force. It would further be expected that variation in the temperature of the weldment would cause local variations in the stress.

Such a condition would be emphasized at the beginning and end of the weld. If we re-examine the data in Figure 7-27, it is seen that the tensile stress along the weld is a maximum at the beginning of the weld and only the average of the measured stress corresponds to that of the destructive data which inherently measures the average stress along the portion of material removed.

Both types of NDT methods were used on welded specimens and gave the identical tensile-compressive results with destructive tests.

#### Application Technique Considerations

To apply the knowledge and techniques learned from this investigation to specific applications requires careful consideration of all factors involved. It has been demonstrated that both ultrasonic surface and shear waves may be used to measure the stress resulting from an applied load. For residual stresses it is possible to determine the magnitude and major axes of the stress, however, it is difficult to

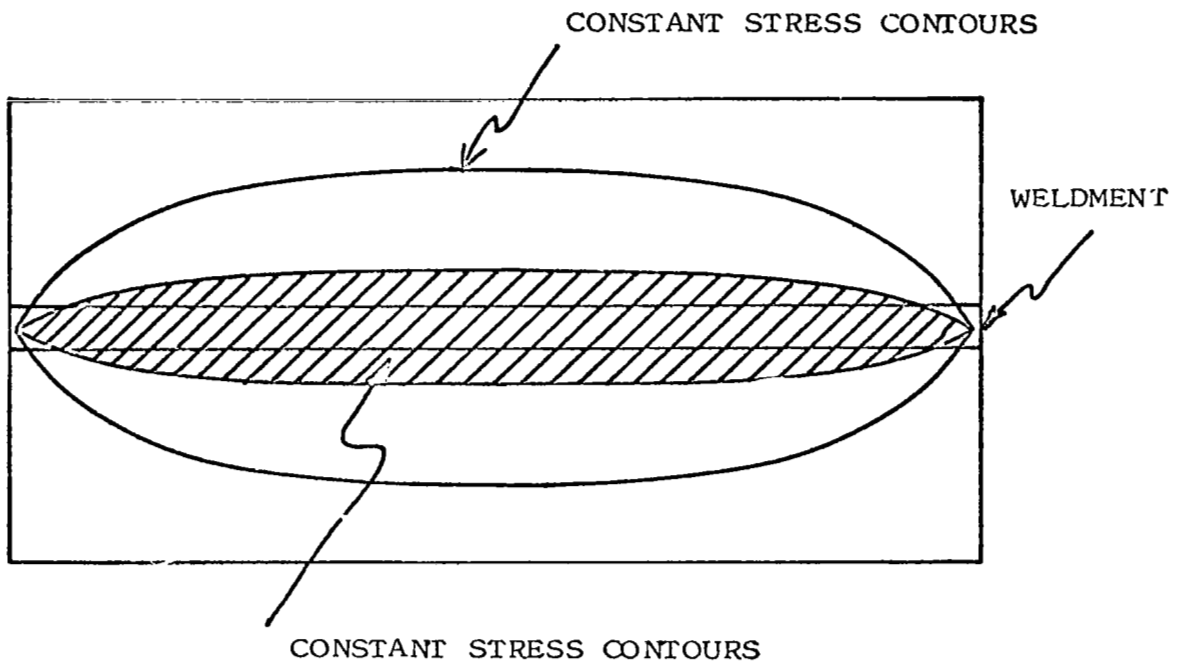


Figure 7-28. Contours of constant stress

determine whether one axis is in compression or the other axis is in tension. The question still remains of whether a uniaxial compressive stress exists transverse to the welded side or a uniaxial tensile stress parallel to the weldment side.

Another possibility would be a biaxial type of loading along these axes. This question cannot be resolved without a standard of comparison.

In measurements such as those made concerning the welded plates where the effect of welding was studied, the destructive tests furnished the necessary standard of comparison. Applications using surface and shear waves, where before and after type measurements are not made need an absolute standard. Such a standard would have to be found for each alloy and would carry the requirement of being stress free. Grain orientation temperature effects, and inconsistencies in the alloy surface composition are a few of the factors which could effect the absolute velocity of every sample tested.

The application of stress analysis with the shear wave technique offers a method of determining the tensile vs compressive direction providing both before and after measurements are possible. This requirement is similar for strain gages, but has the additional merit that stress is measured directly and the element may be removed during processing of the material. The key to the solution of this problem is the ultrasonic longitudinal wave. Since the longitudinal wave is insensitive to stress, it can be used as a reference in the sample.

The X-cut crystal is placed on top of a Y-cut crystal. Each of the crystals are fed from two diode switches in conjunction with the modified time of flight system. The ultrasonic waves will then be generated and received by separate crystals. Note that the longitudinal velocity in aluminum is approximately twice that of the shear wave. Therefore,



the shear wave can be phase compared to the second received longitudinal pulse. In making the actual stress measurement, the same procedure described earlier is used. The absolute numbers read from the delayed trigger dial of the oscilloscope are recorded. As before the difference between these numbers gives the stress magnitude. The sample under investigation is then subjected to the particular process to be studied, for example, welding.

The ultrasonic measurements are again repeated. Since the absolute numbers were recorded during the first measurement, it can now be determined as to how the shear wave velocity along each axis has changed relative to the longitudinal velocity.

#### Detection of Fatigue Damage

A limited study also was made to establish relationships between electrical surface resistance and fatigue damage.

The formation of microcracks due to fatigue damage at the surface of a metal may be thought of as a localized increase in surface roughness and hence, should be measurable as an increase in surface resistivity. An experiment to measure the increase in surface resistivity must be designed in such a manner that surface resistance is measured without also measuring the bulk properties of the material.

By taking advantage of the skin effect of high frequency wave propagation, the depth to which the surface is measured may be controlled by selecting the frequency at which measurements will be made.

Aluminum plates subjected to flexural fatigue damage were investigated at wave length of 3 centimeters. An increase in surface resistance was found to precede any visual evidence of fatigue damage and impending fatigue.

## Summary

A study of the stress distribution in plates containing a weldment was used to illustrate the practical application of the methods. The magnitude of the stresses as determined ultrasonically was correlated against destructive measurements. Agreement was obtained when the stress was averaged over the length of sample included in the destructive tests. The ultrasonic measurements indicated that the maximum stresses occurred near a weld and furthermore, the stresses were greatest near the start and stop of the weldment.

It was further determined that grain orientation imposes limitations on the ultrasonic methods of stress analysis. The ultrasonic waves are sensitive to grain orientation producing effects corresponding to as much as 15,000 pounds per square inch of equivalent stress. For this reason it is necessary to make measurements both before and after processing in a similar manner to that used with strain gages.

Although the methods have been developed to a useful state for application to practical problems of stress analysis, further study is warranted to improve the spatial resolution of the measurement as well as to further define the effects of grain orientation, and extend the methods for use with more complicated welded joints. The ultrasonic methods of stress analysis can be a valuable addition to the methods of analysis already available.

## CHAPTER 8

### Manufacturing Process System Control

As discussed in the introduction of this report, the ultimate purpose of the NASA welding research program is to improve the performance and reliability of space vehicles.

Process control is the final objective. A number of quantitative limits of the major variables generated in the NASA-sponsored studies on welding aluminum can be incorporated in various manufacturing specifications. Chapters 3 through 7 present important findings obtained in these studies. However, some of the findings are useful for an improved control of the manufacturing process system.

This chapter covers the following subjects:

- (1) Transferability of welding parameters
- (2) Development of welding process control systems.

## 8.1 Transferability of Welding Parameters

It is recognized that there are a number of quality-control problems in welding. Consider, for example, the size and shape of the weld. The depth of penetration is not always uniform; it fluctuates along the weld, especially when the weld is made with certain types of welding equipment. When welds are made with machines having different characteristics, the sizes and shapes of welds may differ to some extent, even though the welds are made with the same welding parameters, including welding current, arc voltage, and travel speed.

Ideally, welds should have the same configuration (depth of penetration, weld area, etc.) and quality no matter where or when they are made (by different fabricators at different times); provided the same type of equipment, tooling, and joint design, and the same welding parameters are used. To attain this objective, the following problems are being investigated or considered for future investigation;

- 1) What type of welding equipment (with what types of voltage, current, and electrode-position control systems) is most suitable to obtain consistent welds?
- 2) What weld-quality characteristics are likely to fluctuate--depth of penetration, size and shape of weld, metallurgical and mechanical properties of welds? How are they affected by different welding parameters?
- 3) How are weld-quality characteristics changed when welding equipment is changed? How should we transfer welding parameters from one welding setup to another to obtain welds with the same quality?

The objective at Lockheed-Georgia was to study the transferability of setup parameters for inert gas welding.<sup>(17)</sup> To accomplish this, attempts were made to determine (1) the significant variables and (2) the degree of control that can be achieved.

Analysis was made of GTA and GMA welds made in the horizontal position. The work was thermally insulated from the holding fixture to simulate the minimum tooling, tack-up welding technique very often used in the aerospace industry. No hard tooling or inert gas back-up was used. Welds were made in 1/4- and 3/4-inch thick, 2219-T87 aluminum alloy. All joints were prepared with square-butt edges. The shielding gas was helium.

#### Phases and Experimental Design

The welding test program included two phases. In Phase I, GTA welding parameters and their effect on the response variables were evaluated. The welding setup parameters investigated were current, voltage, weld travel speed, wire deposit, gas purity, gas flow, temperature of the weldment, joint design, and electrode tip diameter. These setup parameters were referred to as the independent variables for the GTA welding process. Table 8-1 lists symbols and units used for independent and dependent variables by the Lockheed investigators.<sup>(17)</sup> Figure 8-1 defines by illustration those variables related to weld cross section and penetration.

A complete factorial for these nine independent variables at two levels requires  $2^9 = 512$  test conditions. In this study, a 1/16-fractional factorial requiring 32 test conditions was used. Four additional test conditions were used to improve the accuracy of statistical analysis. The effects of the independent variables on various weld characteristics were

TABLE 8-1. SYMBOLS AND UNITS FOR VARIABLES USED  
BY THE LOCKHEED INVESTIGATORS.

Symbols	Description and Units for Computer Use	
C	Welding arc current	(amp/100)
V	Welding arc voltage	(v)
T	Travel speed of the arc	(ipm)
Wd	Volume of filler wire deposited per inch of weld	(in. <sup>3</sup> × 100/in.)
Gp	Gas purity - total ppm contamination	(ppm/100)
Gf	Gas flow - cubic feet per hour	(cfh/100)
°F	Work temperature before welding	(°F/100)
J	Joint gap	(in.)
D	Diameter of electrode at the tip	(in.)
M	Cross section area total of melt zone	(in. <sup>2</sup> )
Mc	Cross section area of crown	(in. <sup>2</sup> )
Mf	Cross section area of fall through	(in. <sup>2</sup> )
H	Cross section area of heat-affected zone	(in. <sup>2</sup> )
P	Penetration of melt zone from part surface	(in.)
B	Height of the crown	(in.)
Ep	Electrode position from part surface	(in.)
X	Percent of porosity reading	(%)
Mt	Maximum temperature reading	(°F/100)

TABLE 8-1. (Concluded)

Symbols	Description and Units for Computer Use	
Tt	Time temperature exceeded 450° F	(sec)
At	Area under temperature curve above 450° F	(in. <sup>2</sup> )
Ftu	Ultimate tensile strength	(ksi)
Fty	Yield tensile strength	(ksi)
E	Elongation	(%)
Q	Overlap of welds from both sides	(in.)
A	Angle of GMA torch	(deg)
CP	Distance from contact tube to work	(in.)

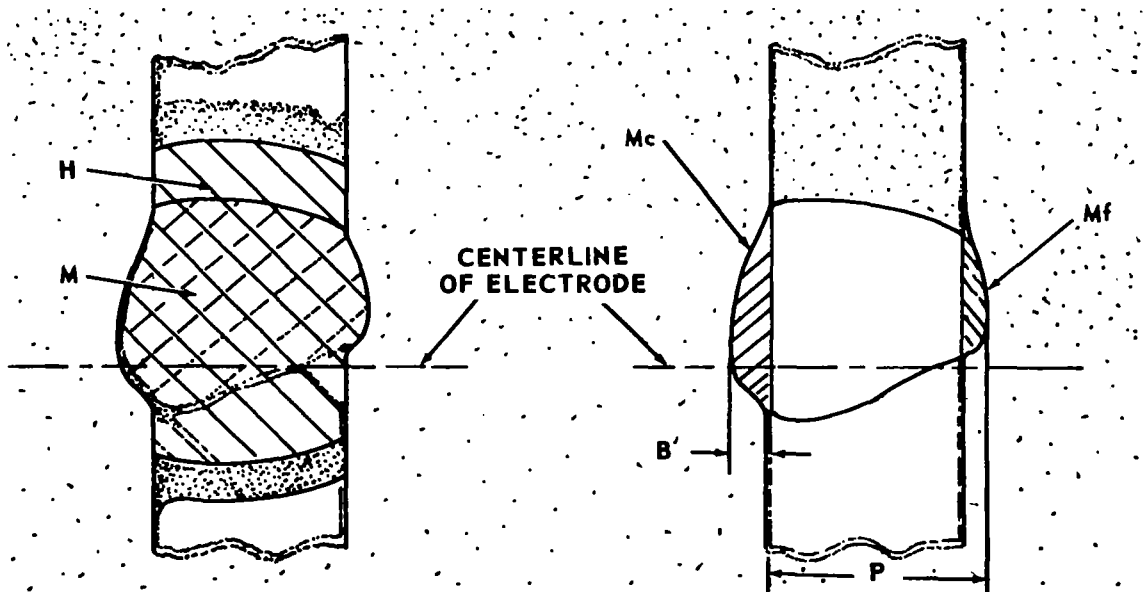


Figure 8-1. Illustrated definitions of variables related to weld cross section and penetration.

studied by statistical analysis using regression equations. Phase II of the project dealt with the GMA welding process. The design principles were the same as for GTA, except that fewer setup parameters were required. There were only five basic parameters investigated for the GMA process, current, voltage, weld travel speed, angle of torch, and the distance from the contact tube to work. A one-half replication of the five variables with all two-variable interaction being measurable was used for the GMA study.

### Welding Test Procedure

Facilities and Equipment. The following two welding units were used in the program:

1) Welding Unit No. 1

Power:	Sciaky Model S-6, functional control, D-C welding power source
Head:	Airco Model HME-E, automatic head
Carriage:	Lockheed-developed carriage controlled by a Servo-Tech techometer feedback governor
Wire feed:	Airco Model AHF-B feedrolls with Airco Model AHC-B feedback type governor control
Instrumentation:	Texas Instrument "Servo/riter" 4 channel potentiometric recorder

2) Welding Unit No. 2

Power:	Sciaky Model S-6, functional control, D-C welding power source
Head:	Precision Sciaky (GTA-GMA) welding head with proximity head control
Carriage:	Servo-Tech control system to operate a Lockheed designed carriage



Wire feed:	Airco AHC-B wire feed control with tachometer feedback governor
Instrumentation:	Minneapolis-Honeywell "Electronic 17" four-channel potentiometric recorder

Electrode Proximity Recording System. It was necessary to better understand the relationship between the welding voltage or arc-length control of the GTA process and the proximity of the torch to the work. A new system developed by Lockheed was used to continuously monitor the electrode proximity. This system operated independently of the arc voltage. The electrode position was measured by the potentiometric recorder, and charted with the welding voltage.

#### Welding Parameter Control Development

Welding Control Studies. During many tests, the electrode position was held constant. With this condition, both the voltage was held constant with an automatic voltage-control head, the electrode position was erratic and equally erratic penetration measurements resulted. It was concluded that neither present automatic voltage control nor constant electrode-position control by themselves maintain adequate process control of the welding arc and molten puddle. Another control system had to be applied to hold a constant electrode position ( $E_p$ ) in addition to a constant current ( $C$ ), constant voltage ( $V$ ), constant carriage travel speed ( $T$ ), and constant filler-wire deposit rate ( $W_d$ ). The wire-feed system used was reasonably accurate and reliable; therefore, no attempt was made to couple this system to the other systems influencing the welding arc process. All of the systems used, in various ways, incorporated the other four welding variables. All of the systems were designed to be regulated by equipment settings and still maintain process control of the

welding arc and the molten puddle. Cross-coupled feedback controls were defined as controls used for measuring the response of one variable and to simultaneously change the settings of another variable. For example, a change in  $E_p$  causes a change in  $C$ . Self-coupled feedback controls were defined as controls used to measure the response of a variable and to adjust the controls of that same variable until the response agrees with the desired set point. For example, if  $E_p$  deviated from the set point, the error was measured on the recorder, amplified, and used to operate a servo system bringing  $E_p$  back to the set point. The basic difference in these two feedback systems was the source of the feedback information. The cross-coupled system depended upon the response of another variable caused by a change in the welding process, while the self-coupled system was a direct measure of the response, independent of all other variables necessary to make up the welding process.

The following six welding control systems were examined:

- 1) Automatic voltage control
- 2) Automatic electrode-position control
- 3) Carriage control coupled to electrode position
- 4) Current control coupled to electrode position
- 5) Current control coupled to voltage
- 6) Self-coupled feedback.

The first three systems were evaluated and considered inadequate for accurate control of the welding process. Tests with the last three systems indicated that they might be capable of maintaining process control of the arc and the molten puddle.

#### Electrode Position Alignment and Distance from Work.

During the first 1/4-inch test series of horizontal welds, the electrode was centered over the joint; however, in the welded

cross section the melt zone was not symmetrical about the centerline of the electrode. In fact, the point of maximum penetration was approximately 0.075 inch above the electrode centerline, as shown in Figure 8-2.<sup>(17)</sup> Although Figure 8-2 shows cross sections of welds 3/4 inch thick, similar phenomena were observed in welds 1/4 inch thick. In several specimens, although penetration was complete, the melt zone did not cover the entire joint. New specimens were welded to replace these joints. During all further welding of 1/4-inch thick material the electrode was centered 0.075 inch below the joint. Additional tests were conducted to further evaluate this phenomenon.

Welds in the 3/4-inch thick plate were made from both sides. As in the 1/4-inch welds, a nonsymmetrical melt zone often caused lack of penetration. For example, Weld No. U154 ST, shown in Figure 8-2, had sufficient penetration to indicate overlap, but again the melt zone did not cover the joint. This condition could not be detected in X-ray inspection, nor was it observed during fixed 3X photographic examination of the cross section. It became apparent in the fracture surface of the tensile-test specimen for which tensile strength was very low.

Another phenomenon observed during the experiments that will require additional investigation is the relationship of electrode position and depth of penetration. Some specimens had considerably deeper penetration on one side than on the other side, as shown in Figure 8-2b and 8-2c. The welds on each side of the plate were set up with identical weld parameters and examination of recordings confirmed that these setups were actually established. In some cases the second weld had less penetration than the first weld, while the reverse was indicated in other tests. It was found that in almost all cases with less penetration, the electrode position

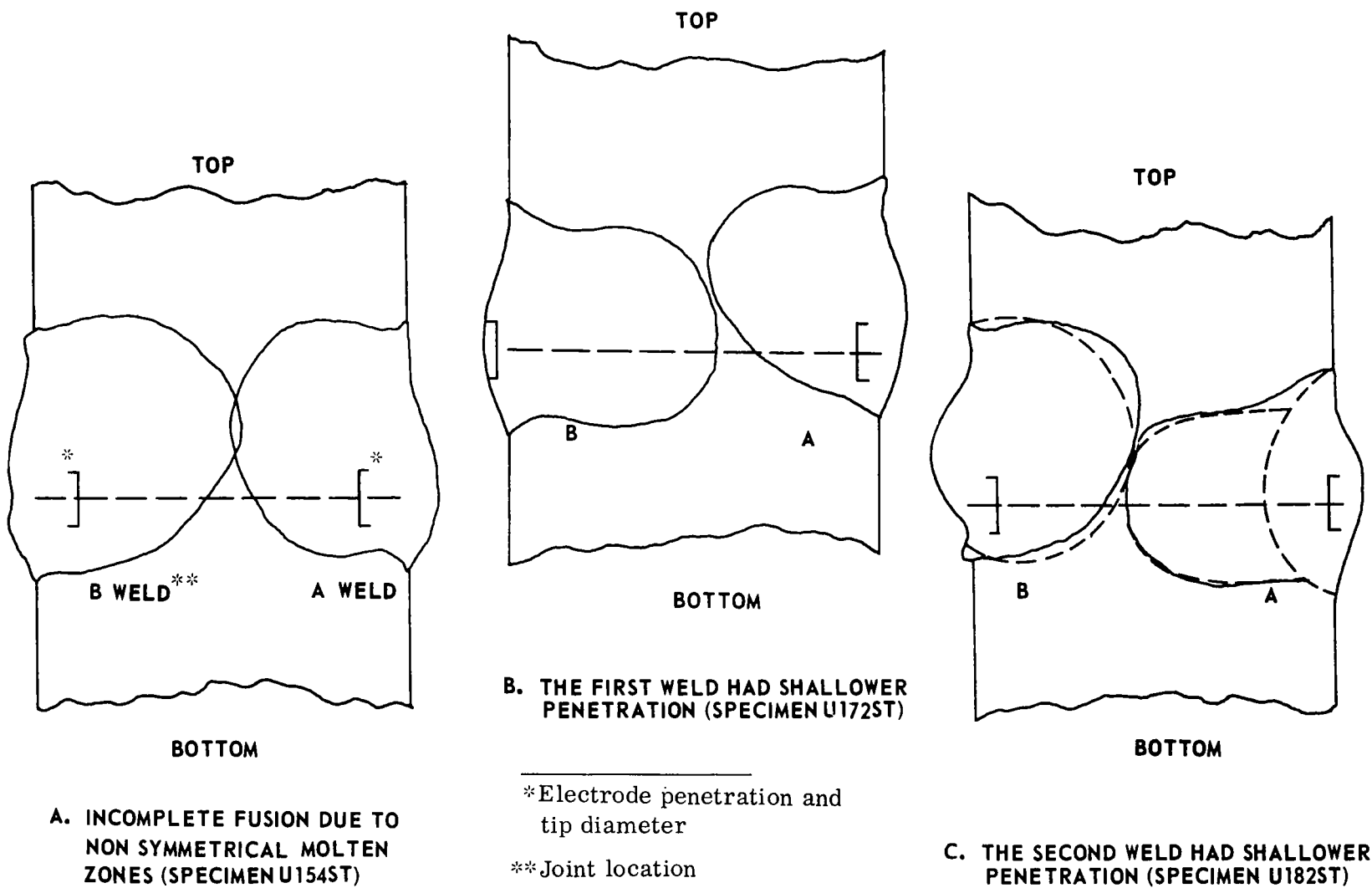


Figure 8-2. Examples of welds having incomplete fusion and irregular nugget shapes.

was deeper. The electrode position for these welds was controlled by the automatic head to maintain a constant arc voltage. In every case, the arc voltage readings were stable and accurately controlled at the correct settings. However, the electrode position recording was erratic in most cases.

The Lockheed investigators concluded that (1) with a given welding setup and with automatic voltage control, the deeper electrode position indicates that a hemispherical arc cavity has developed that will result in a reduction of penetration and (2) variation in penetration due to changes in electrode position is as great as that due to changes resulting from the classic parameters.

Other Problems. Investigations also were made of various other problems including:

- 1) Accuracy of inert-gas flowmeter
- 2) Variation in tungsten-electrode resistance
- 3) Variation in torch resistance
- 4) Shielding gas contamination
- 5) Effect of tungsten electrode on welding parameters.

#### Statistical Analysis of Effects on Welding Parameters on Weld Qualities

Procedures. Table 8-2 shows three values for each of nine independent parameters used for GTA welds in 1/4- and 3/4-inch plate. A constant-current, voltage-control GTA system was used. Table 8-3 shows how the nine parameters were changed in the experimental design for each of 36 specimens. The letters H (high), M (medium), and L (low) are used to represent the value for each parameter as shown in Table 8-2.

TABLE 8-2. PARAMETERS FOR GTA WELDING 2219-T87 ALLOY PLATES 1/4 AND 3/4 IN. THICK.

	Code Letter	1/4-in. Thick Welds*			3/4-in. Thick Welds**		
		High	Medium	Low	High	Medium	Low
Arc current	C	2.85	2.73	2.60	4.40	4.20	4.00
Arc voltage	V	12.75	12.5	12.25	11.5	11.35	11.2
Travel speed	T	23	21	19	10	9	8
Wire deposit per inch of weld	Wd	1.228	0.955	0.682	0.3835	0.1817	0
Shielding-gas purity	Gp	1.50	0.90	0.30	1.50	0.90	0.30
Shielding-gas flow	Gf	1.25	1.00	0.75	1.25	1.00	0.75
Work temperature	°F	1.50	1.13	0.75	1.50	1.13	0.75
Joint gap	J	0.020	0.010	0	0.020	0.010	0
Electrode tip diameter	D	0.125	0.108	0.090	0.135	0.122	0.108

\*One-pass weld

\*\*Two-pass weld (one pass from both surfaces)

TABLE 8-3. EXPERIMENTAL DESIGNS FOR GTA WELDS 1/4 AND 3/4 IN. THICK.

Weld Sequences	C	V	T	Wd	GP	Gf	°F	J	D
1	L	L	L	H	L	H	L	L	H
2	H	L	L	H	L	H	H	H	L
3	M	M	M	M	M	M	M	M	M
4	L	L	L	L	H	H	L	H	L
5	L	H	L	L	H	L	L	L	H
6	L	L	H	H	H	L	L	H	H
7	H	L	L	L	H	H	H	L	H
8	L	H	H	L	L	H	L	H	H
9	H	H	L	H	L	L	H	L	H
10	M	M	M	M	M	M	M	M	M
11	L	H	L	H	H	H	H	H	H
12	L	H	H	L	H	L	H	H	L
13	H	L	L	L	L	L	L	L	L
14	L	L	L	H	H	L	H	L	L
15	L	H	L	L	L	H	H	L	L
16	H	H	H	H	L	L	L	H	L
17	L	H	H	H	L	L	H	L	H
18	L	L	L	L	L	L	L	L	L
19	L	L	H	L	H	H	H	L	H
20	M	M	M	M	M	M	M	M	M
21	H	H	H	L	L	H	H	L	L
22	H	H	L	H	H	H	L	L	L
23	L	H	H	H	H	H	L	L	L
24	H	L	H	L	L	L	H	H	H
25	L	L	H	H	L	H	H	H	L
26	M	M	M	M	M	M	M	M	M
27	L	L	H	L	L	L	L	L	L
28	H	H	H	L	H	L	L	L	H
29	H	L	H	H	L	H	L	L	H
30	H	L	H	H	H	L	H	L	L

TABLE 8-3. (Concluded)

Weld Sequences	C	V	T	Wd	GP	Gf	°F	J	D
31	L	L	L	L	L	L	H	H	H
32	H	L	L	H	H	L	L	H	H
33	H	L	L	H	H	L	H	H	L
34	H	L	H	L	H	H	L	H	L
35	L	L	L	H	H	L	L	H	L
36	H	H	L	L	L	H	L	H	H

TABLE 8-4. PARAMETERS FOR GMA WELDING 2219-T87 ALLOY ¼ IN. THICK.

	Code Letter	High	Medium	Low
Arc current	C	210	200	190
Arc voltage	V	24.5	23.5	22.5
Travel speed	T	26	24	22
Torch angle	A	20	10	0
Distance from contact tube to work	CP	0.500	0.450	0.400



Table 8-4 shows values of parameters used for GMA welds in 1/4-inch plate. The variables were changed in the three levels shown so that welds were made under 21 different conditions.

Figure 8-3 shows how specimens were prepared from both GTA and GMA welds. (16) Three tensile-test specimens, one cross-section specimen, and one longitudinal-section specimen, were prepared from each weld. On all weldments the following 14 responses were measured: ultimate tensile strength (FTV), yield strength (FTY), elongation (E), melt area (M), melt crown area (Mc), melt fall-through area (Mf), heat-affected area (H), penetration (P), build up (B), electrode position (Ep), porosity (X), maximum temperature of back bead (Mt), time above 450° F (Tt), and area under temperature curve above 450° F (At).

A multiple stepwise regressive analysis was made, using an IBM 7094 computer to determine the correlation between the independent variables and each of the responses.

Results of Statistical Analyses. Table 8-5 summarizes results of the regression analyses. Regression equations and the coefficient of determination, which is the square of the multiple coefficient, are shown. For example, the ultimate tensile strength, Ftu, of the 1/4-inch welds is

$$\begin{aligned} F_{tu} = & 446.1 - 21.62 (T) + 9.247 (C \cdot T) - 172.9 (C) \\ & - 60.02 (T \cdot D) + 1138 (D) - 0.2276 (T \cdot Wd) \end{aligned} \quad (8-1)$$

where,

Ftu = Ultimate tensile strength, ksi

T = Travel speed, ipm

C = Arc current, amp/100

D = Electrode tip diameter, inch

Wd = Volume of filler wire deposited per inch of weld,  
inch<sup>3</sup> × 100/inch

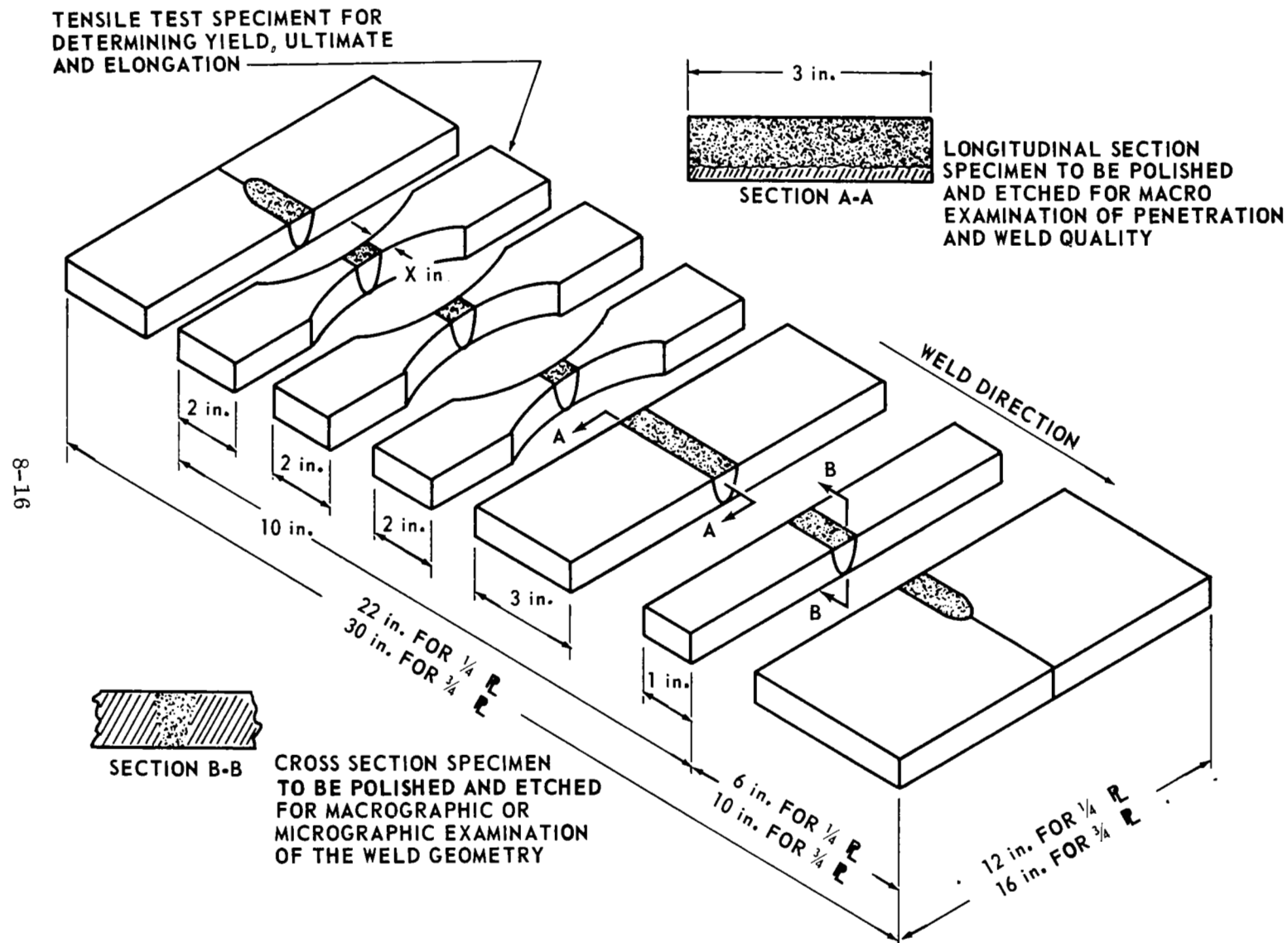


Figure 8-3. Weld test specimen of  $\frac{1}{4}$  and  $\frac{3}{4}$  in. thick 2219-T87 aluminum alloy.

TABLE 8-5. RESULTS OF STATISTICAL ANALYSES OF THE EFFECTS OF WELDING PARAMETERS ON WELD QUALITIES.

Regression Equations Determined		Coefficient of Determination, percent
1) <u>1/4-in. GTA weld</u>		
$F_{tu} = 446.13854 - 21.61667 (T) + 9.24738 (C \cdot T) - 172.85070 (C) - 60.01508 (T \cdot D) + 1138.0066 (D) - 0.22755 (T \cdot Wd)$		86
$F_{ty} = 29.75927 - 10.05339 (T \cdot D) + 62.75876 (C \cdot D) + 0.68234 (T \cdot Gp) - 4.74571 (C \cdot Gp) - 2.89151 (Gf)$		55
$M = 0.05805 - 0.00597 (T) + 0.00480 (C \cdot D) + 0.00040 (T \cdot ^\circ F) - 0.00060 (T \cdot Wd) - 0.00047 (T \cdot Gf)$		86
$H = 0.07413 - 0.00495 (T) + 0.00526 (C \cdot V)$		57
$P = 3.94197 - 0.19187 (T) + 0.07597 (C \cdot T) - 1.25753 (C)$		61
$B = 0.09253 + 0.00138 (T \cdot Wd) - 0.00309 (C \cdot V) + 0.01063 (T \cdot D)$		54

TABLE 8-5. (Continued)

Regression Equations Determined	Coefficient of Determination, percent
<p>2) <u>3/4-in. GTA weld</u></p> <p><math>F_{tu} = 173.89012 - 4.53235 (T) + 78.89110 (Ep) - 8.37078 (V) - 2.18180 (Gp)</math></p> <p><math>F_{ty} = 118.32079 + 68.89160 (Ep) - 2.47662 (T) - 5.53961 (V)</math></p> <p><math>E = 17.68104 - 0.68521 (T) + 16.18741 (Ep) - 1.08126 (V) + 1.53388 (C)</math></p> <p><math>M = 0.11159 - 0.01110 (T) + 0.06422 (C) + 0.30611 (Ep) - 0.38142 (D) + 0.00959 (°F) + 0.01059 (V)</math></p> <p><math>Q = 0.75779 - 0.07020 (T) + 0.03589 (Gp) + 1.37834 (Ep) + 0.17712 (C) - 0.05904 (V) - 1.32220 (D)</math></p> <p><math>H = -0.63726 - 0.02646 (T) + 0.16348 (C) + 0.66632 (Ep) + 0.94564 (V) - 0.87501 (D) + 0.02070 (°F)</math></p> <p><math>P = 0.28945 - 0.03090 (T) + 1.19985 (Ep) + 0.13459 (C) - 1.48151 (D) + 0.01139 (Gp)</math></p> <p><math>B = -0.03320 + 0.02956 (Wd) + 0.02293 (C) - 0.00375 (T) + 0.00446 (Gp) + 0.00570 (°F)</math></p>	<p>74</p> <p>56</p> <p>64</p> <p>82</p> <p>87</p> <p>85</p> <p>82</p> <p>65</p>

TABLE 8-5. (Concluded)

Regression Equations Determined	Coefficient of Determination, percent
<p>3) <u>1/4-in. GMA weld</u></p> <p><math>F_{ty} = 49.18872 - 3.42473 (A \cdot Cp) + 0.02603 (A^2) + 0.16532 (V \cdot A) - 0.03485 (V^2) - 2.39324 (A) - 0.01963 (T \cdot A)</math></p> <p><math>M = -0.06014 + 0.08260 (C) - 0.00006 (T^2)</math></p> <p><math>Q = -0.83123 + 0.40188 (C) - 0.00021 (V \cdot T) + 0.07513 (A) - 0.00034 (A^2) - 0.00115 (V \cdot A) + 0.35249 (Cp) - 0.1747 (A \cdot Cp) - 0.00032 (T \cdot A)</math></p> <p><math>P = -0.28764 + 0.25248 (C) - 0.00038 (V \cdot T) + 0.03060 (A) - 0.00020 (A^2) - 0.00917 (C \cdot A) + 0.01113 (T \cdot Cp) - 0.01714 (A \cdot Cp)</math></p>	<p>71</p> <p>53</p> <p>88</p> <p>70</p>

The coefficient of determination in this case was 86 percent; that is, the variables expressed in the regression equation accounted for 86 percent of the variation observed in  $F_{tu}$ . Regression equations are not given in Table 8-5 for those items with less than 50 percent coefficient of determination.

In reviewing the regression equations, it was noticed that travel speed (T) is a significant parameter for many responses, especially for GTA welds. Table 8-6 shows the most significant parameter for each response and the percentage of response explained by that parameter. Travel speed was the most significant parameter for 5 of the 6 responses listed for 1/4-inch thick welds and 6 of the 8 responses listed for 3/4-inch thick welds. For example,  $F_{tu}$  decreased as T increased, and the change in T was responsible for over 40 percent of the changes in  $F_{tu}$ .

On GMA welds, the coefficient of determination was more than 50 percent for only 4 responses, as shown in Table 8-5. The accuracy of the three equations which had coefficients of determination better than 70 percent,  $F_{ty}$ , Q, and P, are questionable because many terms are involved. For this reason, the regression analysis for GMA welds are not considered reliable, as pointed out by the Lockheed investigations.

#### Analysis and Evaluation of the Lockheed Study on Transferability of Setup Parameters

Summary of the Lockheed Study. It has been found that in order to transfer weld quality in the GTA process good instrumentation must be provided for the six basic GTA welding variables, travel speed, electrode position, current, voltage, gas purity, and electrode tip diameter, listed in their order of importance. The instrumentation should have high resolution, with trace-type potentiometric recorders

TABLE 8-6. PERCENTAGE OF VARIATION IN RESPONSE EXPLAINED BY THE INDICATED PARAMETER IN REGRESSION ANALYSIS FOR WELDS 1/4 AND 3/4 IN. THICK.

Responses	1/4-in. Thick Welds		3/4-in. Thick Welds	
	Parameter	Percentage of Response Explained	Parameter	Percentage of Response Explained
F <sub>tu</sub>	T	43	T	44
F <sub>ty</sub>	T	14	E <sub>p</sub>	41
E	-	-	T	43
M	T	53	T	51
Q	-	-	T	58
H	T	29	T	48
P	T	30	T	47
B	W <sub>d</sub>	25	W <sub>d</sub>	30
Linear effects only are included.				

preferred. Where the conditions above are met, along with duplicate conditions of weld-joint preparation, tooling, and welding position, duplicate trace recordings indicate duplicate welds.

No definite conclusions have been drawn by the Lockheed investigators regarding parameters which need to be duplicate for a successful transfer of GMA welds.

#### Integrator's Comments on the Statistical Analysis.

Welding engineers have always needed a reliable, rational means of selecting proper welding parameters. There are many variables such as welding current, arc voltage, travel speed, etc., and there are many factors to be considered including penetration, weld shape, mechanical properties of the joint, etc. So far, the selection of proper parameters has been made primarily on the basis of past experience and empirical data. It is very important to develop a scientific technique for this selection.

There is no doubt that statistical analysis would be useful for analyzing experimental data. The attempts in this direction by Lockheed investigations are worthwhile. However, their results are not completely satisfactory.

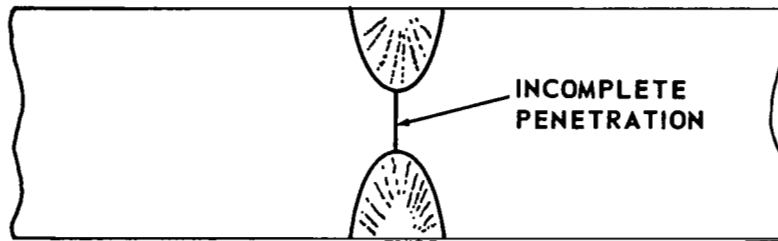
First of all, results of the statistical analysis are not consistent. This is shown in the regression equations in Table 8-4. For example, the ultimate tensile strength,  $F_{tu}$ , was a function of  $T$ ,  $C \times T$  (interaction between  $C$  and  $T$ ),  $C$ ,  $T \times D$ ,  $D$ , and  $T \times W_d$  for 1/4-inch GTA welds; while it was a function of  $T$ ,  $E_p$ ,  $V$ , and  $G_p$  for 3/4-inch GTA welds. No significant correlation existed between  $F_{tu}$  and independent variables for 1/4-inch GMA welds. The yield strengths of welds were functions of the following parameters:



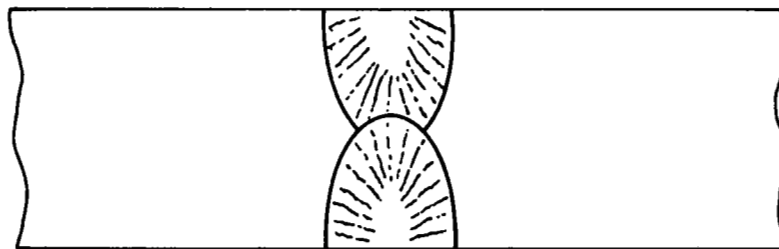
1/4-in. GTA Welds	3/4-in. GTA Welds	1/4-in. GMA Welds
$T \times D$	$E_p$	$A \times C_p$
$C \times D$	$T$	$A^2$
$T \times G_p$	$V$	$V \times A$
$C \times G_p$		$V^2$
$G_t$		$A$
		$T \times A$

A second shortcoming in the statistical analysis is the fact that little attention was paid to the physics of the problems studied. As an example, let us discuss problems related to the ultimate tensile strength of a weld. In the Lockheed study, tensile tests were made on transverse specimens, as shown in Figure 8-4. Many welds contained various degrees of incomplete fusion, as shown in Figure 8-3. Mechanical properties of such welds should be determined by the amount of incomplete fusion, which is a mechanical factor, as well as by properties of the weld metal, heat-affected zone, and the bare metal, which are material or metallurgical factors. The ultimate tensile strength of the well will decrease as the amount of incomplete fusion increases. It is also known that weld strength in 2219-T87 aluminum alloy decreases as the weld heat input increases, as shown in Figure 3-2. These mechanical and metallurgical factors affect the strength of welds prepared under various conditions.

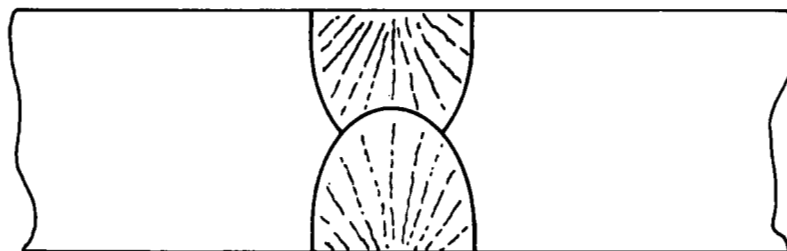
Figure 8-4 shows schematically how welding conditions could affect the strength of a weldment. When a square butt joint is welded with very low heat input, low arc current and high travel speed, the penetration is shallow, as shown in Figure 8-4a and weld strength would be very low. When a joint is welded with medium heat input to obtain complete



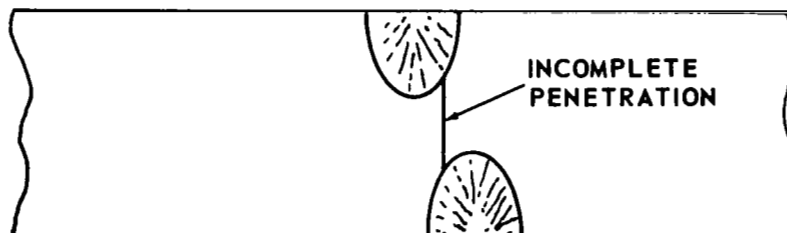
**a. WELD WITH LARGE AMOUNT OF INCOMPLETE FUSION, VERY LOW STRENGTH**



**b. WELD WITH COMPLETE PENETRATION, HIGH STRENGTH**



**c. WELD WITH EXCESSIVE HEAT INPUT, NOT VERY HIGH STRENGTH**



**d. WELD WITH MISMATCH, VERY LOW STRENGTH**

Figure 8-4. Effects of welding parameters on cross section and strength of weldments.

penetration, as shown in Figure 8-4b, weld strength would be high. When a joint is welded with high heat input, excessive penetration results, as shown in Figure 8-4c, and weld strength would not be very high, because of metallurgical damages due to the excessive heat. When welds made from either side are mismatched, as shown in Figure 8-4d, weld strength would be very low.

In analyzing effects of welding parameters on the strength of welds, it is important to separate the mechanical effect and the metallurgical effect. Since the strength of welds with incomplete penetration has, in this case, no practical meaning, the analysis should be limited to welds with complete penetration. However, many welds included in the Lockheed study contained various amounts of incomplete penetration. Consequently, the usefulness of the regression equations, shown in Table 8-5, on mechanical properties is questionable. For example, consider the regression analysis of ultimate tensile strength. The equation indicates that travel speed had the greatest effect on ultimate strength and that strength decreased as travel speed increased. The results might actually be due primarily to the fact that the sectional area of the specimen decreased as the travel speed increased. Further studies need to be made of physical meanings of regression equations for this and other responses.

## 8.2 Development of Welding Process Control Systems

When we evaluate the current welding practice, we find that we have very little control during welding. For example, let us take a case of preventing weld porosity. By conducting various studies, we have found that shielding gas must be pure and the metal surface must be clean in order to produce porosity-free welds. What do we usually do after that?

First, we buy pure shielding gas and make sure that all joints between tubes leading to the welding torch are tight. However, we have no way of knowing how pure shielding gas is as it comes from the torch. We do the best we can to clean the surface. We may even decide to machine the metal surface just before welding, perhaps using such a tool developed at IITRI (refer to Chapter 5.3). However, again, we do not know whether or not the surface is sufficiently clean.

It would be very desirable if we could determine the purity of shielding gas and the cleanliness of metal surface just before welding, or even monitor them during welding operation. Although no such system has not been fully developed, the recent development at the Boeing Company is a significant advancement toward that direction. Since results of the Boeing study have been covered in Chapter 5, the following pages describe briefly subjects which are directly related to manufacturing process system control.

### Prevention of Porosity by Monitoring Shielding-Gas Purity and Surface Cleanliness

Investigations at Boeing<sup>(28)</sup> have designed a probe which could continuously sample a very small portion of gas

and deliver it to a mass spectrometer for analysis. Such a monitoring device, when it is perfected, can be used during actual fabrication of space vehicles.

Investigators at IITRI<sup>(20)</sup> and Boeing<sup>(28)</sup> have developed techniques for analyzing surface contaminants on metal surfaces. A device can further be developed which is capable of determining whether or not a metal surface is clean enough for welding. When the surface is not clean enough, a surface cleaning device, such as that developed by IITRI, can then be used to clean the surface on the spot.

#### Computer Simulation of Welding Processes to Predict Thermal Effects

Computer programs developed at Battelle and M.I.T. have proved to be useful in analyzing thermal stresses during residual stresses and resulting residual stresses. Without a computer, such calculations would need months of engineers time.

By using computers it should be possible to simulate welding processes to predict various thermal effects: material degradation due to metallurgical changes as well as residual stresses.



## CHAPTER 9

### Summary and Practical Recommendations

This chapter summarizes important findings obtained during the NASA-sponsored studies on welding aluminum. Also presented here are practical recommendations generated during this integration study. The following subjects are discussed:

1. Effects of porosity level on weld-joint performance
2. Mechanisms of porosity
3. Sources of porosity
4. Methods of controlling and eliminating porosity
5. Weld thermal effects
6. Welding with high density power sources
7. Time-temperature control by cryogenic cooling
8. Analysis of thermal stresses during welding and residual stresses
9. Reduction of warpage and residual stresses by controlling thermal pattern during welding
10. Development of nondestructive techniques for determining residual stresses and fatigue damage in metals
11. Transferability of setup parameters
12. Selection of welding parameters
13. Recommendations for weld inspection
14. Recommendations for weld repair
15. Closing comments
16. List of important future work

## 1. Effects of Porosity Level on Weld Joint Performance

Effects of porosity level on weld joint performance were investigated in Study 5 at the Martin Company.<sup>(14)</sup> The subject was also investigated to a limited extent at the Boeing Company.<sup>(8)</sup>

Static Tensile Strength of Transverse-Weld Specimens.  
Theoretically, this loss in strength should be approximately proportional to the loss of sectional area due to porosity *in the plane of the expected fracture.*

In the experiments conducted at the Martin Company, investigators prepared specimens from welds made with shielding gas contaminated with water vapor. They found a marked decrease in strength due to porosity when only pores 1/64 inch in diameter and larger were counted in figuring loss of sectional area. A 5 percent loss of sectional area caused as much as 30 percent reduction in strength.

A close investigation revealed that the specimens had a large number of very fine pores less than 1/64 inch in diameter. In a later investigation all pores were counted, and it was found that the loss of strength due to porosity was proportional to the reduction of sectional area. The theory was further verified in an experiment involving specimens taken from production welds.

Although the conclusion reached after all is simple, these studies have provided interesting results and practical hints as follows:

- 1) Aluminum welds may have a number of small pores, therefore, do not discount small pores in inspection.
- 2) Porosity obtained in horizontal position welding appears to be more damaging to mechanical properties.



than other positions because the pores are not randomly distributed throughout all possible fracture planes. They are instead favorably situated in a given plane which is normal to a transverse load. This becomes a plane of weakness.

- 3) When conducting an experiment on porosity using artificially contaminated shielding gas, be careful about the results. You may be making welds which are radically different from production welds. Shapes and distributions of weld defects may be different and some material degradation may have taken place.

#### Static Tensile Strength of Longitudinal-Weld Specimens.

Results of these studies indicated that mechanical properties of longitudinal weld specimens are much less affected by porosity than are those of a transverse-weld specimen because the weld metal represents only a fraction of the cross section of the specimen.

Fatigue Tests of Transverse-Weld Specimens. It has been found in the two programs that fatigue life decreases with porosity. For example, 10% porosity causes:

- 1) Reduction in fatigue strength for 100,000 cycle life from over 20 ksi to 12 ksi (40% less than that of the sound weld)
- 2) Reduction in the number of cycles to failure  
Under 20 ksi: from over  $10^4$  to around  $10^3$  (1/10 that of the sound weld)  
Under 10 ksi: from over  $10^6$  to around  $5 \times 10^4$  (1/20 that of the sound weld)

## 2. Mechanisms of Porosity

A study was made of welding parameters on the nucleation and growth of porosity.<sup>(11)</sup> However, there appears to be reasons for questioning the reliability of some of the equations used in the statistical analysis. More studies are needed before conclusive statements can be made on the mechanisms of porosity formation.

## 3. Sources of Porosity

Sources of porosity in aluminum weldments can be classified as: (1) contamination of shielding gas, (2) contamination of the joint or filler-metal surfaces, and (3) composition of base plate and filler metal.

Shielding-Gas Contamination. It has been found that shielding-gas contamination can be one of the major sources of porosity in aluminum weldments. However, it also has been found that commercial shielding gas is normally acceptably pure as received. In the NASA-sponsored programs conducted at Boeing,<sup>(8)</sup> Battelle,<sup>(9,10)</sup> Douglas,<sup>(11)</sup> and Martin,<sup>(14)</sup> investigators reported that it was always necessary to intentionally contaminate the shielding gas to produce an appreciable amount of porosity. Welds made in the laboratory did not contain appreciable amounts of porosity when they were made with proper procedures, that is, when plates were cleaned properly and commercially pure shielding gas was used.

The effect of individual gas contaminants were studied by making welds in an atmospheric-control chamber containing various levels of gas contamination.<sup>(8)</sup> The metal studied was 1/4-inch thick, 2219-T87 aluminum alloy, welded in the horizontal position by the GTA process using 1/16-inch

diameter, 2319 aluminum-alloy filler wire. The following results were obtained:

- 1) Increasing hydrogen concentration increased porosity.
- 2) Increasing water vapor increased porosity.
- 3) Increasing oxygen did not increase porosity; in some cases, a slight decrease in porosity was observed.
- 4) Increasing nitrogen had little effect on porosity.

The Boeing investigators presented Figure 5-3 as a guide for controlling shielding-gas contamination.<sup>(8)</sup> The contamination levels shown indicate where occurrence of a weld-quality change is initially observed. The figure indicates that 250 ppm of either hydrogen or water vapor was necessary before significant quality changes were observed. As shown in Figure 5-3, shielding-gas contamination caused various effects including surface discoloration, undercut, and reduction in arc stability. Such phenomena also were observed in other programs.<sup>(9,10,11,14)</sup>

Figure 5-4 gives the calculated relationship, as determined by the Boeing investigators, between percent of water-saturated air in the base gas and resulting hydrogen concentration.<sup>(8)</sup> The figure indicates that at 70° F, for example, an addition of 0.6 percent saturated air to pure helium would result in 250 ppm hydrogen in the shielding gas.

On the basis of experience gained in the current programs, it is believed that there is no reason to change the present NASA specification (MSFC-364A) for shielding gas. Normal commercial gases which meet this specification are believed to have sufficient purity.

However, gas contamination can occur within the bottle, or sometimes between the bottle and the torch nozzle. Contamination could occur in a partially empty bottle, for

instance. Or, it could occur due to defective connections in the tubing system. This subject will be discussed in another part of this report.

Surface Contamination. The Boeing investigators, based upon their finding on shielding-gas contamination, reported that a single fingerprint could cause three times the minimum level of hydrogen necessary to cause porosity (Figure 5-5). A thorough evaluation of surface conditions as a potential source of weld porosity was undertaken at IITRI.<sup>(20)</sup>

Table 5-2 summarizes the surface preparations and a description of defects. All tests welds contained significant porosity except the machined specimens (Figure 5-8) that received no further treatment. Figure 5-9 shows large porosity encountered when the surface was not machined but was solvent degreased. Figures 5-10, 5-11, and 5-12 show photos taken of machined surfaces with a scanning electron microscope; numerous tears and smears are present. Figure 5-13 shows a fractured specimen with a residue of trichloroethylene near the surface. Figure 5-14 shows reaction products from chemical cleaning.

Figure 5-15 presents the finding in a simple manner. Shown here are weld-defect potential of various surface preparations. Figure 5-16 is a similar presentation, but it includes the effect of storage time on defect potential. As-machined surfaces have the lowest defect potential.

Composition of Base Plate and Filler Metal. An investigation was made at Battelle of the effects of four factors on porosity.<sup>(9,10)</sup> The four factors, listed in the order of their influence on porosity level, are:

- 1) Shielding-gas moisture content
- 2) Alloying elements
- 3) Metallic impurities
- 4) Internal hydrogen content.

The program was conducted in two phases, the first phase using experimental base metals and filler metals, and the second phase using commercial materials. The results indicate that base-plate and filler-metal compositions are not likely to be significant sources of porosity as long as (1) shielding gas and surface contamination are controlled at low levels and (2) base plates and filler metals are carefully prepared to meet the present specification with no gross hydrogen contamination. It has been hypothesized that there is a synergistic effect of alloy and metal impurity content, and external contamination (shielding gas and surface), which causes significant porosity. This has not yet been substantiated.

Because of these findings, the integrator recommends no changes in the present NASA specification for base-plate and filler-metal compositions.

#### 4. Methods of Controlling and Eliminating Porosity

In the NASA research program on welding aluminum, several attempts were made to develop methods for controlling and eliminating porosity. Subjects studied include:

1. Surface hydrogen analysis
2. Surface preparation
3. Monitoring shielding gas purity
4. Other methods including (1) use of hydrogen getters, (2) magnetic arc shapes and molten metal stirrer, and (3) cryogenic cooling.

Surface Hydrogen Analysis. Analytical techniques for determining surface contaminants were first studied at IITRI<sup>(20)</sup> and a further study was conducted at the Boeing Company.<sup>(28)</sup>

Three techniques were found to be effective in detecting hydrogen contaminants. The first one was gas chromatography.

It is readily calibratable method which could measure adsorbed surface contaminants. It does not readily lend itself to manufacturing applications since the instrumentation and sampling techniques are quite complex.

The second technique involves radioactive tracers. This method is capable of revealing the complete adsorption/desorption cycle with minimum disturbance of the surface being measured. The radioactive tracer method, however, is mainly a research tool.

The third technique was spark emission spectroscopy. It essentially heats, desorbs, dissociates, and excites certain species which exist on the surface. The method of measurement involves the quantitative determination of relative film densities produced by exposure to spark excited spectra. This spark emission method of surface analysis appears to rate surfaces in accordance with their relative hydrogen-contamination levels.

Surface Preparation. A study was conducted at IITRI to develop new techniques for preparing clean metal surfaces adequate for welding. A practical system for preparing the welding surfaces of aluminum components was developed and demonstrated. The system consists of dry milling the abutting edges and adjacent surfaces of aluminum to remove contaminated surface layers and expose a fresh surface with a low defect potential. A prototype device was designed and fabricated to demonstrate the feasibility of the system.

The prototype device was used to prepare the weld surfaces of flat and curved aluminum plates with a square butt weld joint configuration. These surfaces were evaluated on the bases of gas tungsten-arc spot and seam weld soundness, Proficorder measurements, and scanning electron microscopy. Results from these evaluations proved the technique, system, and prototype device to be satisfactory for the intended application.

An attempt also was made for using electrical discharge techniques for preparing clean metal surfaces. Unfortunately, all of the three techniques investigated failed to produce surfaces with low weld defect potential.

Monitoring Shielding Gas. A study was conducted at the Boeing Company,<sup>(28)</sup> with the following objectives:

1. Define the shielding gas profiles of typical production weld torches.
2. Determine the degree of contamination introduced into the arc region as a result of joint defects.
3. Correlate the above with weld porosity.

A special probe was designed which could continuously sample a very small portion of the gas and deliver it to a mass spectrometer for analysis. By means of the motor driven probe it was possible to scan the gas shield and relate composition to position and to reconstruct the contamination profile. The mass spectrometer was set to continuously monitor oxygen. A typical scan is shown in Figure 5-31. From these scans the distances at which oxygen reached 10, 100, 1000, and 5000 ppm were recorded.

The test results may be summarized as follows:

1. If shielding gas flow rate is adequate, gaps do not perturb the contamination profile but if flow rates are reduced to where gaps may cause contamination, then movement of the torch and other slight drafts disturb the shielding gas enough to completely overshadow any effect of the gap. This condition was also found to exist for misfits (Figure 5-32), that is, either no change in the profile was found or drafts overshadow the effect.

2. A helium flow rate that is adequate for short torch to work distance becomes inadequate at longer distances. When carried to extreme, the region of zero contamination decreases to a small cone. At the shorter torch to work distances the work forces the shield gas out, thus there is adequate coverage. When a gap is encountered, the profile exhibits a transition to that observed with no work present, when the gap is large enough.
3. The above-mentioned transition is dependent upon helium flow rate. At a flow rate high enough to provide adequate coverage the transition occurs at a large gap. At lower flow rates the gas shield is unstable with respect to slight air movement and the transition cannot be seen. These data indicate that joint variations may have very little influence on shielding.
4. The data obtained so far strongly suggests that mechanical joint defects do not lead to porosity. That is, mechanical joint defects do not easily produce poor shielding and if they could, atmospheric contamination, particularly moist air, cannot enter the arc region in sufficient quantities to produce porosity in aluminum even under the most adverse production conditions.

Methods for Reducing Porosity. It has been shown that hydrogen contamination can be reduced or eliminated through proper surface preparation, cleanliness precautions during the handling of the materials, and welding procedures. However, carefully these procedures are observed, though, some hydrogen may still be present in the molten puddle.



Thus, it is desirable to devise a means within the welding process to eliminate or neutralize hydrogen that may be present, and thus reduce porosity. Three separate means of doing this were studied in different programs.

1. Hydrogen Getters. It is known that certain elements will act as scavengers of hydrogen, either eliminating it or combining with it in a harmless form. The problem is how to introduce these elements to the welding process. At Southern Research Institute, experiments were made of studying the use of scavenging elements including Ti, Zr, Ce and Ca. In the work conducted so far, no significant reduction in porosity was obtained through use of powders as scavenger elements, and in some cases the severity of porosity was increased. The results, however, do not necessarily mean that the theory of scavenger elements is wrong. Further work should be done to develop other methods of using these elements.
2. Magnetic Arc Shaper and Molten-Puddle Stirrers. Another possible method of reducing porosity is the use of mechanical devices that either agitate the puddle or oscillate or shape the plasma. Both puddle stirring and plasma oscillation have proved successful in reducing the level of porosity, although the percent reduction was relatively small. However, attaining this reduction requires the addition of complicated equipment to the welding torch.
3. Cryogenic Cooling. The results obtained at Harvey Aluminum have shown that porosity could be reduced

by cryogenic cooling during welding. However, the percentage of porosity reduction was relatively small. The use of this method introduces the risk of contaminating the weld and further complicates the welding process. More study is needed before conclusive statements can be given on this subject.

## 5. Weld Thermal Effects

It is known that the transverse strength of a weldment increases as welding heat input decreases. Figure 3-2 summarizes the experimental results obtained at MSFC on the effects of welding heat input on the ultimate tensile strength of welds in 2219-T81 and 2219-T86 alloys.<sup>(4,6,7)</sup>

When the weld heat input is between 40,000 and 100,000 joules/in<sup>2</sup>, the ultimate strength of a weld is between 37,500 and 42,000 psi. As the heat input decreases, the weld strength increases sharply reaching as high as 57,000 psi with a 10,000 joules/in<sup>2</sup> heat input by electron-beam process. The 2218-T87 base metal has a strength of 69,000 psi, about 10,000 psi of which strength is due to strain hardening. The strength of the alloy in the unstrained condition, T-62, is listed at 59,000 psi, nearly reached in electron-beam welds of 10,000 joules/in.<sup>2</sup>

Time-Temperature Effect. Jackson<sup>(57)</sup> proposed the time-temperature concept to study the effects of heat input on the strength of aluminum welds.<sup>(5)</sup> Figure 6-2 shows the temperature change during welding of a point in a weldment. Maximum temperature is defined as the peak temperature which the material being joined experiences during the welding heat cycle. Time at temperature is defined as the time that the material being joined is above the temperature that

adversely affects strength properties of 2219-T87 aluminum alloy are found to be adversely affected above 450° F.

An investigation was made to develop relationships between weld heat input and strength characteristics of 2219 aluminum welds. By the use of multivariate regression analysis of experimental data, the relationship among maximum temperature, time at temperature, and mechanical property characteristics including yield strength, ultimate tensile strength, and elongation were determined.

The following general conclusions were drawn as a result of this investigation.

1. Maximum temperature and time at temperature were found to be significant in measuring effective weld heat input.
2. Current and travel speed were the only controllable independent variables that significantly affected time at temperature while voltage, current and tungsten length affected maximum temperature.
3. Definite mathematical relationships can be developed describing the interactions between weld heat input and factors that require optimization.

## 6. Welding with High Density Power Sources

As shown in Figure 3-2, higher strengths are obtained with welds made with lower energies. Expressed differently, welds made with high power densities and appropriate parameters will produce higher strengths. Attempts were made to weld with high density power sources.

Experiments to Increase GTA Power Density. A study was conducted at Lockheed-Palo Alto<sup>(25)</sup> to investigate

possibilities to significantly increase the power density of GTA welding. Subjects studied include (1) modification of the electrode (cathode), (2) modification of the workpiece (anode), (3) modification of the shielding gas, and (4) use of magnetic fields to constrict the arc plasma. The important findings obtained in the study are as follows:

- 1) Significant increases in arc power density as measured by narrowing of the continuum, were noted for additions of 20 vol % hydrogen to helium or argon shielding gas. Nitrogen additions to helium also increased power density, particularly in concentrations of 40 vol % or greater. The greatest increase measured, however, was with the addition of 0.5 vol %  $\text{SF}_6$  to helium.
- 2) The improvement in weld penetration and depth-to-width ratio obtained in the bead-on-plate tests is much smaller than suggested by the continuum data; for example, an increase of about 30% compared to a tenfold increase in the continuum power density measured for the  $\text{SF}_6$  addition. Moreover, nitrogen additions, actually resulted in lower depth-to-width ratios in stainless steel.
- 3) The use of materials with high thermionic emission for the electrode (cathode) shows some promise with up to a 60% increase in power density, as measured by the continuum, and about a 30% increase in depth-to-width ratios, for the tip configurations studied.
- 4) The use of a longitudinal magnetic field resulted in a slight narrowing of the current width on the copper anode but caused severe distortion of the weld pool under practical welding conditions in the bead-on-plate tests.

- 5) No improvement in power density was observed in the experiments to modify the anode.
- 6) The depth-to-width ratios attainable by the electron beam welding process are over ten times greater than the best GTA conditions. The total power for each process is of the order of 5 KW yet because of the difference in the size of the heat source as it impinges on the work the maximum electron beam power density is of the order of  $10^9 \text{W/cm}^2$  whereas the GTA the maximum power available is of the order of  $10^5 \text{W/cm}^2$ . The results of this study decreased about 1/2 the difference of power density between the two methods but the power density of electron beam welding will still be about 100 times that of the tungsten arc process.

Electron Beam Welding. In 1963, MSFC made its first effort to use an electron-beam welding system for fabricating large aerospace structures. A "split-chamber" concept as designed by the Sciaky Brothers Company was used. MSFC chose the 33-foot diameter ring that makes the transition from a bulkhead to a cylinder in the Saturn V first stage. The cross section of the ring forms a Y, as shown in Figure 6-7. Three segments were joined with EB system into a complete ring.

Non-Vacuum Electron Beam Welding. A newly developed high-voltage, non-vacuum electron-beam welding system was delivered to MSFC in 1969 by Westinghouse. <sup>(22)</sup>

Powered by 150 KV supply, the welder is of a unique compact design. The power supply and welding gun, complete with all high vacuum pumps and accessories, are assembled into a 210-lb package that can be mounted in either the

downhand or horizontal welding position (Figure 6-9). It is mounted on a conventional side beam carriage. Flexible low vacuum lines permit the welding head to be traversed four feet in a straight line. The complete unit is enclosed in a lead shielded room.

Welding has been done on 1/4-inch thick aluminum and 1/8-inch and 1/2-inch thick steel.

But to obtain non-vacuum EB welds in aluminum that are similar in shape to hard vacuum welds, welding must be done at more than 200 in/min. Narrow welds made at any speed impose strict accuracy requirements. Transverse deviations of the beam from the center of the joint, and joint gaps of more than 0.005 inch can result in lack of fusion. The situation is greatly exaggerated when the gun is moving at 200 in/min. At this speed a seam tracking device would have to move the gun system laterally 0.005 inch in 3 1/3 inches of forward movement per second. In addition, shielding of personnel from x-rays generated by the high voltage means that remote monitoring of welding is necessary.

Much analysis, development, and planning are necessary before the system can be considered applicable and thus versatile.

Plasma Electron Beam Welding. A study was conducted at General Electric to develop a plasma electron-beam (PEB) system.<sup>(26)</sup> PEB is a new kind of electron beam source based on a cold hollow cathode gas discharge (Figure 6-10). With a pressure of about 10 microns of nitrogen, for example, a body of plasma fills the cathode and an electron beam formation takes place.

Capability of this equipment was demonstrated by a narrow penetration weld 1 3/4 inches deep into 5456 material.

Porosity was not present at the root of the weld, indicating good electron beam stability as compared to conventional electron beam welding systems. The principle of operation is discussed in detail in the final report from General Electric. PEB offers the advantages of long cathode life and good performance under poor vacuum conditions where gaseous contaminants may be present. Parts can be welded in an atmosphere of about 75 microns. For welding structures too large to be contained in a vacuum chamber, it would seem feasible to extract the electron beam into a small chamber which moves along the weld seam maintaining a reduced pressure by means of a sliding seal.

#### 7. Time-Temperature Control by Cryogenic Cooling

A study was made at Harvey Aluminum<sup>(15)</sup> of cryogenic cooling as a means of shortening thermal cycles and thus improving tensile properties of aluminum weldments. General increases of 4 to 10 percent in yield strength were obtained by cryogenic cooling. The ultimate tensile strength also increased to some extent by cryogenic cooling. The ultimate tensile strengths of the unchilled welds, as reported by Harvey, were in the vicinity of 40 ksi. This appears to be only the start of the upswing of the heat input-strength curve (Figure 3-2). Much higher strengths are yet available by further reducing heat input. The effectiveness of cryogenic cooling may become greater as the weld heat input decreases.

However, to attain the improvement, a risk is taken of contaminating the weld, either by the cooling jet or by condensation on the surface. Further studies are needed to obtain conclusive results on this subject.

## 8. Analysis of Thermal Stresses during Welding and Residual Stresses

Several aerospace companies have encountered distortion problems during fabrication of the Saturn V components including welded fuel and oxidizer tanks. Although production practices have been developed to temporarily overcome these problems, they are empirical solutions and little is known about the mechanisms causing such distortion. It is essential to understand the mechanisms in order to develop methods for minimizing distortion effects during fabrication of future vehicles.

MSFC recognized the importance of conducting research on mathematical analysis of thermal stresses and metal movement during welding and supported studies at Battelle<sup>(29)</sup> and M.I.T..<sup>(30)</sup> Computer programs have been developed to calculate transient thermal stresses during welding and resulting residual stresses.

Existing One-Dimensional Programs. The Battelle study uses the technique which was originally developed in 1964 by Tall.<sup>(59,60)</sup> The Battelle analysis was one-dimensional. It was assumed that (1) the stress component parallel to the direction of welding,  $\sigma_x$ , is a function of the lateral distance from the weld,  $y$ , only and (2)  $\sigma_y$  and  $\tau_{xy}$  are zero (see Figure 7-1).

The Battelle computer program is written in FORTRAN IV computer language for use on a Control Data Corporation (CDC) 6400 computer system including a Cal-Comp plotter. The program is written for bead-on-plate welds made in any material (provided its mechanical and physical properties with various temperatures are available) under any welding conditions.



The Battelle program was improved during a study at M.I.T. completed in October, 1970. Table 7-1 shows comparison between the Battelle and the M.I.T. programs. Major differences are:

- 1) Strain hardening of the material is considered in the M.I.T. program, while the material is assumed to be perfectly plastic in the Battelle program. In both programs, however, the yield strength,  $\sigma_{ys}$ , changes with temperature.
- 2) The M.I.T. program includes the analysis of stresses and strains, while the Battelle program analyses are on stresses only. The analysis of strain is important in comparing results of the theoretical study with experimental data, because strains are usually measured in an experiment.

The M.I.T. program is written in FORTRAN IV for use on an IBM 360/65 computer.

M.I.T. Two-Dimensional Analysis. Under a current contract for MSFC, a study is being conducted at M.I.T to develop a two-dimensional analysis of thermal stresses during welding. All three components,  $\sigma_x$ ,  $\sigma_y$  and  $\tau_{xy}$  are analyzed as functions of  $x$  and  $y$ . The analysis used the finite-element method.

Examples of Analytical Results. Figures 7-3 through 7-6 show results obtained on a sample weld. Figure 7-6 shows the isostress pattern around the welding arc. There is a high compressive stress area shortly ahead of the heat source; however, values of compressive stresses are very low in high-temperature areas very close to the heat source. There is a narrow tensile-stress zone along the center line behind the heat source, and compressive-stress zone expands outwards in a horse-shoe shape.

From the standpoint of metal movement in the thickness direction during welding, which causes joint mismatch, the compressive stress zone appears to be of particular importance. If the plate is thin, or the compressive-stress zone is large, the plate may buckle during welding. Distortion in the thickness direction also may be caused if the temperature and stress distributions are not uniform in the thickness direction.

Effects of Welding Parameters. M.I.T. researchers studied effects of welding parameters on thermal stresses during welding of 2219-0 aluminum plates and resulting residual stresses. The analysis included effects of welding parameters on:

- 1) High tensile thermal stresses in areas behind the arc
- 2) Compressive thermal stresses in areas ahead of the arc
- 3) Size of plastic zone
- 4) Residual stress distributions

The maximum value of tensile residual stress at the weld center is as high as the yield stress of the material at room temperature, regardless of welding conditions. However, the width of tensile residual stress zone is affected by welding parameters.

As shown in Figures 7-9 and 7-10, linear net heat input,  $h$  joules/in/in, is the most significant factor that affect the width of tensile residual stress zone, and it increases with increasing heat input. The effect of heat input, however, is not linear. The increase in the width of tensile residual stress zone per unit increase in heat input decreases as heat input increases.

From the practical viewpoint, the results clearly show the advantage of using low welding heat input to reduce residual stresses and distortion.

Effects of Material Properties. An analysis was made of effects of material properties on residual stresses. Materials studied include low-carbon steel, ultrahigh strength steel, columbium, and tantalum as well as aluminum alloys.

The width of tensile residual stress for ultrahigh-strength steel is very narrow. This is primarily due to the fact that only a very narrow zone undergoes plastic deformation during welding.

On the other hand, the widths of tensile residual stress zones are very large for welds in columbium and tantalum. Since both columbium and tantalum have relatively low yield stresses at a wide temperature range, very large areas of plastic deformation occur during welding. The results suggest, that residual stresses and distortion can be quite a problem during welding some refractory metals including columbium and tantalum.

Experimental Investigation. An experimental investigation was made at M.I.T. to evaluate the accuracy of the mathematical analysis. To simplify the investigation, experiments were conducted on bead-on-plate welds made in 2219-0 aluminum alloy. Temperature changes during welding were measured by thermocouples, while strain changes were measured by strain gages mounted on specimen surfaces.

On the basis of comparison between experimental and analytical results, it has been concluded that one-dimensional stress analysis developed at M.I.T. can be used as an approximate analysis to investigate general trends of stress changes during welding and resulting residual stresses. However, the current analysis is not adequate to study complex stress changes near the welding arc.

## 9. Reduction of Warpage and Residual Stresses by Controlling Thermal Pattern during Welding

A study was conducted at Harvey Aluminum to investigate the feasibility of reducing warpage and residual stresses in aluminum weldments by controlling the thermal pattern during welding.<sup>(24)</sup> The concept involves the use of cryogenic liquids and auxiliary heat sources to produce contraction and expansion of metal in the vicinity of welds in such a manner as to counterbalance expansion and contraction caused by welding.

As shown in Table 7-3, it was possible to produce unwarped panels either with or without the use of cryogenic cooling. The problem, however, was low repeatability of experimental results. Chilling also was found to reduce residual stresses.

The study at Harvey Aluminum proved the feasibility of applying the concept of balancing thermal stresses during welding to control distortion and residual stresses. The computer programs developed at M.I.T. can be useful for determining the optimum thermal pattern to minimize distortion and residual stresses.

## 10. Development of Non-destructive Techniques for Determining Residual Stresses and Fatigue Damage in Metals

A study was conducted at the Benson and Associates to develop non-destructive techniques for non-destructive measuring residual stresses and fatigue damage.<sup>(27)</sup>

Ultrasonic Stress Measurements. After evaluating the current status of various ultrasonic systems, it was decided that detailed studies be made on the following two systems:

- (1) Modified time of flight system (Figure 7-23)
- (2) Frequency null system (Figure 7-24).

After conducting fundamental investigations using specimens with known stress values, an investigation was made to apply the ultrasonic techniques on weldments.

Although it has been found that the ultrasonic techniques may be used for determining residual stresses, more studies are needed before these techniques could be used for measuring residual stresses in engineering structures.

Detection of Fatigue Damage. A limited study was made to establish relationships between electrical surface resistance and fatigue damage. The formation of microcracks due to fatigue damage at the surface may be thought of as a localized increase in surface roughness. An attempt was made to determine the change of surface roughness by measuring the increase in surface resistivity using high frequency waves.

#### 11. Transferability of Setup Parameters

In the study at Lockheed-Georgia<sup>(17)</sup>, it was found that duplicate trace recordings of six basic GTA welding variables indicate welds, if weld-joint preparation, tooling, and welding position have been duplicated. The six variables, in order of importance, are travel speed, electrode tip position, current, voltage, gas purity, and electrode tip diameter. On the basis of experimental results conducted on GMA welds, the regression analyses used were not considered reliable and no final conclusions have been made.

Experimental data were statistically analyzed to determine analytical relationships among welding parameters and weld properties including penetration, nugget shape, and mechanical properties of the joint. However, these results

are not completely satisfactory. Further study needs to be made of the physical meanings of the equations used.

## 12. Selection of Welding Parameters

Selecting proper welding parameters has been an important problem for welding engineers. When fusion welding high-strength heat-treated aluminum alloys, the following two major problems need to be considered in selecting parameters: (1) mechanical properties of weldments and (2) porosity. Other problems such as susceptibility for weld cracking also need to be considered.

In order to improve the mechanical properties of weldments, it is recommended that welding parameters that produce small heat input be used. A lower welding current and a higher arc travel speed produce smaller heat input. Figure A-4 can be used as a guide for evaluating the effect of heat input on the strength of a welded joint.

The selection of proper welding parameters to control porosity requires more analyses. The use of high heat input with slow cooling tends to cause a small number of large pores; loss of cross-sectional area may be low, but the loss of strength due to welding thermal effect is great. Use of a small heat input with fast cooling tends to cause a large number of fine pores; loss of sectional area due to porosity may be high. More study is needed to develop a technique for scientifically selecting welding parameters.

## 13. Recommendations for Weld Inspection

Recommendations for the revision of the current inspection standards is outside the scope of this report. However, it

seems essential to review some points that are suggested by the current programs and are pertinent to these standards. Only general conclusions are given here.

Small Pores. A large number of fine pores, say less than 0.03 inch in diameter, can cause significant reduction of cross-sectional area, resulting in considerable loss of strength. However, present inspection standards tend to place inadequate emphasis on the importance of the fine pores that are often found in aluminum welds. Further study should be made to determine more exactly the importance of these pores.

Stress State of a Joint. Welds that are loaded parallel to the welding direction are less sensitive in their mechanical behavior to defects than welds that are loaded transverse to the weld direction. Consequently, different acceptance levels of porosity might be used, depending upon the location of a weld and the direction of the weld relative to the direction of load expected during service.

Improved Nondestructive Testing. Improved nondestructive testing techniques should be developed for determining the total cross-sectional area of flaws in the expected fracture plane. Multiple X-ray shots appear to offer the best promise.

#### 14. Recommendations for Weld Repair

It is known that repair welds, unless they are made very carefully, may have properties inferior to normal welds. The repair welds can create high residual stresses and additional distortion. Failures in various structures have been traced directly to repair welds. In many cases, porosity does not cause high stress concentration, and loss of strength due to

porosity is rather minor. It is recommended that weld repairs be kept to a minimum. In some cases where defects are not critical, welds might better be left unrepaired.

## 15. Closing Comments

The NASA efforts have been directed toward taking the black magic out of the art of welding and transform it into a science. It is believed that we have achieved some progress toward the goal.

At the end of this integration report, four practical precautions are presented that should be followed during welding fabrication of aluminum structures:

1. The surface cleanliness is important to assure good weld quality without porosity. A technique which appears to be most effective is to remove a thin surface layer of metal immediately before welding.
2. Commercial shielding gases that meet the present NASA specifications are sufficiently pure.
3. The present NASA specifications on chemical compositions of base metal and filler metal are also adequate, as far as the weld porosity is concerned.
4. It is important to weld with high heat density, because it causes an increase in joint strength, a reduction in distortion, and inhibits the growth of hydrogen porosity.

The above comments are directly applicable to large, critical, aerospace structures. However, basic principles can also be applicable to other aluminum structures.



## 16. List of Important Future Work

From the mistakes of yesterday, from the clarification of problems, and from each bit of progress, come the plans for future research.

To pursue the ultimate purpose of the NASA welding research, that is, to improve the performance and reliability of space vehicles, further research should be conducted on a number of subjects. Some of the current studies should be carried further, and studies on new subjects need to be initiated. The following list shows some of the studies which are important to further improve the quality of welds in high-strength heat-treated aluminum alloys:

1. Develop a way for mechanized removal of a thin layer of metal from surfaces to be welded.
2. Develop a method for measuring the purity of shielding gas at the welding torch.
3. Determine gas shielding adequacy where joints have gaps, offsets, etc.
4. Further correlate weld defects and service performance to establish more rational requirements of the weld quality.
5. Further develop analytical methods for estimating and controlling weld mismatch and distortion.
6. Improve the strength of a weldment by altering mechanisms of strengthening aluminum welds.

The new knowledge obtained in these studies should be useful for aerospace and other industries.



## References

- (1) Falkowski, E., "Saturn Illustrated Chronology," MHR-r, G. C. Marshall Space Flight Center, NASA, May, 1965
- (2) NASA Facts, NF-8/12-67, "Space Launch Vehicles," Office of Public Affairs, NASA, 1967
- (3) Parks, P. G., "New Developments in Aluminum Welding," a paper presented at the National Aeronautic Meeting, New York, April 25-28, 1966, Society of Automotive Engineers
- (4) Hasemeyer, E. A., "Aluminum Welding for Space Vehicles and Welding in Outer Space," a report prepared by Welding Development Branch, Manufacturing Engineering Laboratory, G. C. Marshall Space Flight Center, NASA, August 19, 1970
- (5) Masubuchi, K., "Integration of NASA-Sponsored Studies on Aluminum Welding," RSIC-670, Redstone Scientific Information Center, Redstone Arsenal, Alabama, September, 1967
- (6) Hoppes, R. V., "The Welding of Saturn V," New Scientist, 18 January, 1968-128-131.
- (7) Masubuchi, K., Hoppes, R. V., and Parks, P. G., "Quality Requirements for Weldments in the Saturn V Space Vehicle and Related Welding Studies, Public Session on Quality Requirements in Welded Construction held during the 1970 Annual Assembly of the International Institute of Welding, Lausanne, Switzerland, July, 1970, Vol. C, pp. 119-146
- (8) Strobelt, W. E., "Inert Gas Weldment Effects Study," Phase I Report (July, 1965-November, 1965), Phase II Report (January, 1966-June, 1966), Final Report (January, 1966-June, 1966), under Contract NAS8-20168 from Aerospace Group, Quality Control Research Section, The Boeing Company, Boeing Reports Nos. D2-23647-4, D2-23647-5, and D2-23647-6
- (9) Cheever, D. L., Kammer, P. A., Monroe, R. E., and Martin, D. C., "Weld-Base Metal Investigation," Final Report under Contract NAS8-11445 from Battelle Memorial Institute--Columbus Laboratories, July, 1965
- (10) Cheever, D. L., Mishler, H. W., Monroe, R. E., and Martin, D. C., "Welding Commercial Base-Plate Investigation," Final Report under Contract NAS8-20303 from Battelle Memorial Institute--Columbus Laboratories, September, 1966

- (11) Pollock, D. D., Mixon, W. V., and Reinhardt, W. W., "Mechanisms of Porosity Formation in Aluminum Welds," Final Report under Contract NAS8-11332 from Douglas Missile and Space Systems Divisions, Douglas Aircraft Company, Inc., Douglas Report SM-52039, June, 1966
- (12) A letter dated September 9, 1966, from S. F. Frederick, Section Chief, Research Projects, MR & PM, Douglas Missile and Space Systems Division, Douglas Aircraft Company, Inc., to Earl Hasemeyer, Marshall Space Flight Center, NASA
- (13) Willhelm, A. C., "Study on Development of Saturn Manufacturing Technology for Welding Methods and Techniques to Reduce Hydrogen Porosity," Final Report under Contract NAS8-20307 from Southern Research Institute, October, 1966
- (14) Rupert, E. J., and Rudy, J. F., "Analytical and Statistical Study on the Effects of Porosity Level on Weld Joint Performance," Technical Summary Report under Contract NAS8-11335 from Martin Marietta Corporation, Martin Company, March, 1966
- (15) Cole, D. Q., Davis, L. W., and Anderson, P. E., "Development of Controls for Time-Temperature Characteristics in Aluminum Weldments," Final Report under Contract NAS8-11930 from Harvey Engineering Laboratories, Harvey Aluminum, Inc., October, 1966
- (16) Seay, E. R., and Kilpatrick, R. H., "A Study of Inert-Gas Welding Process Transferability of Set-Up Parameters," Interim Report on Contract NAS8-11435 from Lockheed-Georgia Company, November, 1965
- (17) Gillespie, P. A., Kilpatrick, R. H., and Stewart, R. C., "A Study of Inert-Gas Welding Process Transferability of Set-Up Parameters," Final Report under Contract NAS8-11435 from Lockheed-Georgia Company, January, 1967
- (18) Beischer, P., "Magnetic Arc Shaper and Molten Puddle Stirrer, Phase III, Weld Evaluation," Thirteenth Monthly Report under Contract NAS8-11954 from Air Reduction Company, Inc., January, 1967
- (19) Kizer, D. E., Saperstein, Z. P., and Schwartzbart, H., "Preparation and Instrumentation for Welding S-1C Components," Phase I Report under Contract NAS8-20363 from Illinois Institute of Technology Research Institute, November, 1966
- (20) "Material Preparation and Instrumentation for Welding S-1C Components," Final Report under Contract NAS8-20363 from Illinois Institute of Technology Research Institute, September, 1967

- (21) Cushman, E. H., "Saturn Manufacturing Technology for Welding Methods and Techniques," Final Report under Contract NAS8-20338 from Air Reduction Company, June, 1967
- (22) Schumacher, B. W., Seaman, F. D., Goldberg, D. C., "Qualitative and Quantitative Evaluation of Factors Producing High Efficiency Welds with an Out-of-Vacuum Electron Beam Welder," Report under Contract NAS8-11929/Phase I-Task F from Westinghouse Astro-nuclear Laboratory, April, 1969
- (23) "A Study of Optimum Methods for Preparing Aluminum Surfaces for Welding," Final Report under Contract NAS8-21354 from Illinois Institute of Technology Research Institute, July, 1969
- (24) Cole, D. Q., "Development of Techniques for Controlling Warpage and Residual Stresses in Welded Structures," Final Report under Contract NAS8-21174 from Harvey Engineering Laboratories, July, 1968
- (25) Karlak, R. F., and Pfluger, A. R., "Study of Gas-Tungsten-Arc Welding Power Density," Final Report under Contract NAS8-21373 from Lockheed Palo Alto Research Laboratory, Lockheed Missile and Space Company, June, 1969
- (26) Boring, K. L., Dickinson, T. M., McMurray, W., Stauffer, L. H., Travis, E. F., and Zubal, C., "Plasma Electron Beam Welder for Space Vehicles," Final Report under Contract NAS8-11803 from Research and Development Center, General Electric Company, August, 1968
- (27) "Development of Nondestructive Methods for Determining Residual Stress and Fatigue Damage in Metals," Final Report under Contract NAS8-20208 from R. W. Benson and Associates, Inc., March, 1968
- (28) Lowry, N. M., Strobelt, W. E., and Johnson, C., "Study of Welding Defects Saturn Joint Configuration," Final Report under Contract NAS8-24512 from the Boeing Company, 1970
- (29) Masubuchi, K., Simmons, F. B., and Monroe, R. E., "Analysis of Thermal Stresses and Metal Movement during Welding," Final Report under Contract DA-01-021-AMC-14693(Z) from Battelle Memorial Institute to Redstone Scientific Information Center, RSIC-820, July, 1968
- (30) Andrews, J. B., Arita, M., and Masubuchi, K., "Analysis of Thermal Stress and Metal Movement during Welding," Final Report under Contract NAS8-24365 from Massachusetts Institute of Technology, December, 1970

- (31) Hoppes, R. V., "Welding Study on 2219-T87 Aluminum Alloy," Technical Information Report No. TIR-15-64, R-ME-MW, Manufacturing Engineering Laboratory, Marshall Space Flight Center, NASA, April 27, 1964, plus additional informal communication
- (32) Goodier, J. N., "Concentration of Stress around Spherical and Cylindrical Inclusions and Flaws," Transactions ASME, Volume 55, No. 7, 1933, pp. 39-44
- (33) Sadowsky, M. A., and Sternberg, E., "Stress Concentration around a Triaxial Ellipsoidal Cavity," Journal of Applied Mechanics, Vol. 16, No. 2, 1949, pp. 148-157
- (34) Savin, G. N., Stress Concentration around Holes, Pergamon Press, New York, 1961
- (35) Faerberg, I. I., "Tension Applied to a Plate with a Circular Hole with Stresses Exceeding the Limit of Elasticity," Trudy, Tsent. Aerogidr. Inst., No. 165, 1947
- (36) Kammer, P. A., Masubuchi, K., and Monroe, R. E., "Cracking in High-Strength Steel Weldments--A Critical Review," DMIC Report 197, Defense Metals Information Center, Battelle Memorial Institute, February, 1964
- (37) Masubuchi, K., "Effects of Residual Stresses on Fracture Behavior of Weldments," Weld Imperfections, Proceedings of a Symposium at Lockheed Palo Alto Research Laboratory, Palo Alto, California, September 19-21, 1966, Addison-Wesley Publishing Company, 1968, pp. 567-589
- (38) Parker, E. R., Brittle Fracture of Engineering Structures, John Wiley & Sons, Inc., New York, 1957
- (39) Fracture Toughness Testing and Its Applications, ASTM Special Technical Publication, No. 381, 1965
- (40) Irwin, G. R., and Kies, J. A., "Fracturing and Fracture Dynamics," The Welding Journal, Vol. 31, No. 2, Research Supplement, 1952, pp. 95s-100s
- (41) Irwin, G. R., "Fracture," Encyclopedia of Physics, Vol. VI, Elasticity and Plasticity, Springer-Verlag, Berlin, Goettingen, Heidelberg, 1958, pp. 551-590
- (42) "Fracture Testing of High-Strength Sheet Materials," A Report of a Special ASTM Bulletin, No. 243, June, 1960, pp. 29-40; No. 244, February, 1960, pp. 18-28; and Materials Research and Standards, Vol. 1, No. 11, November, 1961, pp. 877-885

- (43) McClintock, F. A., and Argon, A. S., (editors) Mechanical Behaviors of Metals, Addison-Wesley Publishing Company, 1966
- (44) Kihara, H., Tada, Y., Watanabe, M., and Ishi, Y., Nondestructive Testing of Welds and Their Strength, Volume 7 of the 60th Anniversary Series of the Society of Naval Architects of Japan, Tokyo, 1960
- (45) Pense, A. W., and Stout, R. D., "Influence of Weld Defects on the Mechanical Properties of Aluminum Alloy Weldments," Bulletin 152, Welding Research Council, New York, July, 1970
- (46) Shore, R. J., "Effects of Porosity on High-Strength Aluminum 7039 Welds," Master of Science Thesis, Ohio State University, 1968
- (47) Meister, R. P. and Martin, D. C., "Welding of Aluminum and Aluminum Alloys," DMIC Report 236, Defense Metals Information Center, Battelle Memorial Institute, April, 1967
- (48) Hansen, M., Constitution of Binary Alloys, McGraw-Hill Book Company, New York, 1958
- (49) Saperstein, Z. P., Prescott, G. R., and Monroe, F. H., "Porosity in Aluminum Welds," The Welding Journal, Vol. 43, No. 10, Welding Research Supplement, pp. 443s-453s, 1964
- (50) Rosenthal D. and Schmerber, R., "Thermal Study of Arc Welding--Experimental Verification of Theoretical Formulas," The Welding Journal, Vol. 17, No. 1, Welding Research Supplement, pp. 2s-8s, 1938
- (51) Adams, C. M., Jr., "Cooling Rates and Peak Temperatures in Fusion Welding," The Welding Journal, Vol. 37, No. 5, Welding Research Supplement, pp. 210s-215s, 1958
- (52) Collins, F. R., "Porosity in Aluminum Alloy Welds," The Welding Journal, Vol. 37, No. 6, pp. 589-593, 1958
- (53) Lyons, E. H., Jr., "What Is a Clean Surface," Tran. Electrochem. Society, Vol. 88, pp. 281-290, 1945
- (54) Emeleus, H. J. and Anderson, J. S., Modern Aspects of Inorganic Chemistry, Van Nostrand, New York, pp. 231-262, 1944
- (55) Hurd, D. T., An Introduction to the Chemistry of the Hydrides, J. Wiley, New York, 1952

- (56) Libowitz, G. G., "Nonstoichiometry in Metal Hydrides," Advances in Chemistry Series, Vol. 39, pp. 74-86, 1963
- (57) Jackson, F. L., "Analysis of Time-Temperature Effects in 2219 Aluminum Welding," The Welding Journal, Vol. 45, No. 8, August, 1966
- (58) Masubuchi, K., "Control of Distortion and Shrinkage in Welding," WRC Bulletin 149, Welding Research Council, April, 1970
- (59) Tall, L., "The Strength of Welded Built-up Columns," Lehigh University, Ph.D. Dissertation, 1961
- (60) Tall, L., "Residual Stresses in Welded Plates--A Theoretical Study," Welding Journal, Research Supplement, Vol. 43, No. 1, pp. 10s-23s, 1964
- (61) Masubuchi, K., "Nondestructive Measurement of Residual Stresses in Metals and Metal Structures," RSIC-410, Redstone Scientific Information Center, U. S. Army Missile Command, Redstone Arsenal, Alabama, April, 1965
- (62) Hirsch, A. S., "Development of Nondestructive Methods of Determining Residual Stress and Fatigue Damage in Metals--A Summary," a report to Professor K. Masubuchi as a term paper for the subject 13.39, Analysis of Techniques for Fabricating Structures, Massachusetts Institute of Technology, May 14, 1970
- (63) Private document from E. Hasemeyer entitled "A Method of Estimating Residual Stresses in 0.25 inch Thick 2219-T87 Aluminum Alloy Plate Weldments," September 11, 1967